Understanding the meltdown behavior of frozen dessert: from ice cream to model system

By

Biqing Wu

A dissertation submitted in partial fulfillment of the requirements of the degree of

Doctor of Philosophy

(Food Science)

at the

UNIVERSITY OF WISCONSIN-MADISON

2023

Date of final oral examination: 8/16/2023

This dissertation is approved by the following members of the Final Oral Committee:

Richard W. Hartel, Professor, Food Science

Scott A. Rankin, Professor, Food Science

Jiamian Hu, Assistant Professor, Materials Science and Engineering

Arnoldo Lopez-Hernandez, Lecturer, Food Science

Dedication

In memory of my beloved grandfather, Shiqi Zhang (张世琦). I miss you more than words can express. Thank you for cheering for me with every little success.

Acknowledgment

First and foremost, I would like to express my deepest gratitude to my advisor, Richard Hartel, for your unwavering support, exceptional guidance, and invaluable insights throughout the entire research process. Your dedication and expertise have been instrumental in shaping the direction and quality of this study. I am truly grateful for the freedom you provided, allowing me to explore different research ideas and fostering my growth as an independent researcher. I am also grateful for your continuous encouragement and availability whenever I needed guidance or faced challenges over the years.

I would like to extend my sincere gratitude to my dissertation committee members, Dr. Scott Rankin, Dr. Arnoldo Lopez-Hernandez, and Dr. Jiamian Hu, for their invaluable feedback. Additionally, I would like to thank Dr. Kurt Weiss from the Biochemistry Optical Core for teaching me how to use the equipment at their facility.

My heartfelt gratitude goes to my wonderful labmates whom I had the privilege of meeting in the basement at Babcock Hall. Your constant presence and support have filled my graduate school life with endless laughter and joy. Special thanks to Sam VanWees, Cameron Wicks (CJ), Dieyckson Osvani Freire, Hassan Firoozmand, Yunna Wang, and Ruican Wang for their friendship and engaging science discussions. My graduate school life would not be happier without your constant companion. Thanks also to the awesome lab assistants Elizabeth James, Sami Lefever, and Zoe Atkins for their invaluable help with the research.

A special thanks goes to Zhaoning (April) Yu. Your constant encouragement, support, and even your sense of humor with your bad jokes have been a source of happiness throughout graduate school. I cannot imagine having achieved all of this without your unconditional support. I am truly grateful to have met you in Madison.

Lastly, I would like to express my gratitude to my parents, Xiaofeng Zhang and Shibin Wu, for their unconditional support in every decision I have made. I am especially grateful to my mom, whose constant presence as my greatest pillar of support has made her not only my therapist but also my closest confidant, offering encouragement and solace whenever I need it. Additionally, I would like to thanks to my little fluffy companions, Eric and Alex, for providing delightful distractions from the research.

Getting a Ph.D. is like running a marathon without seeing the finish line at the beginning, but now, here we are! Looking back, I am grateful for every up and down that I have experienced, as they have shaped me into a better person and scientist. If life is made up of moments, getting a Ph.D. undoubtedly be one of the biggest one for me.

Abstract

The ice cream meltdown test has been utilized to comprehend the structural changes in ice cream. While there is broad knowledge regarding the impact of ingredients and processing conditions on meltdown, an understanding of the fundamental mechanisms by which the structure influences the meltdown process remains limited. This study aims to investigate how the structural components of ice cream (fat destabilization, overrun, and mix viscosity) influence the entire meltdown process. Additionally, a sucrose model system was designed to aid in understanding the role of rheological properties, overrun, and phase separation between milk protein-polysaccharides in the meltdown process in both aerated and non-aerated systems.

The induction time, melting rate, final drip-through weight extracted from the meltdown curve as well as the height change rate and final height calculated from the height-change curve offer as parameter to describe the meltdown process. Among all the structural components examined, ice cream mix viscosity was the most important parameter on the meltdown process. Only without the stabilizer, which meant the mix viscosity was the lowest, did the extent of fat destabilization and overrun influence the meltdown process.

In the non-aerated system, it was observed that the type of polysaccharides, rather than rheological properties like mix viscosity or shear-thinning behavior, influenced the melting behavior. Specifically, the anionic polysaccharide exhibited a faster melting rate compared to the neutral ones. In the aerated system, when polysorbate 80 was included, there was a positive correlation between mix viscosity and both the induction time and melting rate. However, this correlation was not observed between shear-thinning behavior and rheological properties. Considering the strong correlation between shear-thinning behavior and apparent viscosity, as well as the relatively insignificant impact of shear-thinning behavior on the meltdown process

compared to the apparent viscosity, the apparent viscosity appeared to be a more suitable parameter for describing the meltdown process.

When the milk protein was introduced into the system, both the phase separation behavior and its correlation with the meltdown were investigated. It was observed that the locust bean gum system prevented of phase separation after freezing-melting, attributed to the formation of cryo-gel by locust bean gum. This cryo-gel structure further contributed to the maintenance of the foam structure during the meltdown test.

Overall, this study provides a deeper insight into each main component's impact on the meltdown process. This knowledge contributes to the design of healthier frozen desserts with enhanced heat resistance.

Table of Contents

List of Tables

List of Figures

1. Introduction

Ice cream is a complex product primarily composed of milk fat, milk solids-non-fat, air, ice, stabilizers, emulsifiers, and sweeteners. The intricate microstructure of ice cream not only influences sensory perception and rheological properties but also affects its meltdown behavior. The meltdown of ice cream is a crucial parameter that indicates the product's ability to withstand heat shock conditions and assesses the structural changes resulting from the alteration of ingredients or processing conditions. Various factors, such as fat destabilization, overrun, air cell size, ice crystal size, and mix viscosity, contribute to ice cream melting. Despite numerous studies investigating the relationship between microstructure and meltdown, several questions still remain to be answered.

This research is structured into four sections, each building upon the previous one. It begins by examining the influence of microstructure on the overall meltdown process of ice cream. While the melting rate is commonly analyzed in meltdown tests, it is equally important to consider the initial melting phase and the completion of the meltdown to gain insights into the structural changes that occur during the test. Therefore, the primary objective of the initial study was to characterize the complete meltdown process by analyzing the entire meltdown curve. This was achieved by manipulating factors such as fat destabilization, overrun, and mix viscosity to create a wide range of ice cream microstructures.

In the second phase of the study, a simplified model system was developed to examine the influence of each structural component on the meltdown process. The structural components were sequentially added to the system from the second phase to the fourth phase. Initially, the focus was on investigating the rheological properties of the non-aerated frozen dessert system, as it was identified as the dominant factor affecting meltdown in the first phase. Subsequently, air was

introduced to assess the combined impact of rheological properties and overrun on the meltdown process.

In the final phase of the study, milk protein was incorporated into the system to gain insights into the interaction between milk protein and hydrocolloids, specifically focusing on their impact on phase separation and its subsequent effect on the meltdown process. Furthermore, κ-carrageenan, known for its ability to prevent phase separation in dairy systems, was also added to compare and contrast how phase separation influenced the meltdown process. This additional experimental setup allowed for a more comprehensive understanding of the intricate dynamics at play and provided valuable insights into the complex interplay between milk protein, hydrocolloids, phase separation, and the resulting impact on the ice cream's meltdown characteristics.

Ultimately, this comprehensive research endeavor contributes to the advancement of knowledge by providing a quantitative understanding of the intricate interplay between various structural components, in addition to milk fat, and their influence on the ice cream's meltdown characteristics.

2. Literature review

2.1 Ice cream composition

Ice cream is a complex frozen food system that is comprised of air, water, milk fat, stabilizers, emulsifiers, sweeteners, and milk solids-non-fat (MSNF) (Goff & Hartel, 2013). It has a restricted composition requirement in the United States. According to the Code of Federal Regulations, finished ice cream products should contain a minimum of 10% MSNF and 10% of milkfat as well as at least 1.6 lbs./gal of total solids and 4.5 lbs./gal of final products (21CFR135.110). On this basis, commercial ice creams are divided into different grades including economy, standard, premium, and super-premium based on different fat content, total solids content, and overrun.

2.1.1 Air

During the ice cream freezing process, the air is whipped into the ice cream mix by the dashers and the air bubbles are dispersed and stabilized in the final products (Goff & Hartel, 2013). Air, one of the main ingredients in ice cream, provides sensory properties such as smoothness, fluffiness, and melting resistance. The amount of air in the ice cream product is defined as the overrun and can be calculated from the following equation 2-1:

$$\%Overrun = \frac{Weight\ of\ mix - Weight\ of\ ice\ cream}{Weight\ of\ ice\ cream} \times 100 \qquad 2\text{-}1$$

2.1.2 Water and ice

Water in ice cream commonly comes from milk, cream, or adding extra water. As a solvent, water dissolves dry ingredients into the milk/cream to help incorporate the ingredients. After the freezing process, some water is in the form of ice crystals and the rest remains unfrozen in the concentrated serum phase.

Ice is an important component in the ice cream product. It can influence both ice cream's physical structure and sensory attributes including hardness, denseness, iciness, and smoothness. In general, a majority of ice crystals for an acceptable smooth ice cream product must be less than 50μm (Goff & Hartel, 2013). Ice creams with large ice crystal sizes have a harder texture compared to those with small ice crystals (Muse & Hartel, 2004; Sakurai et al., 1996).

2.1.3 Milk fat

Milk fat in ice cream commonly comes from fresh or frozen cream, unsalted butter, and/ or anhydrous milk fat. Milk fat is one of the most important components in ice cream, which contributes to the richness, smoothness, and creaminess of the sensory properties (Roland et al., 1999). Also, fat helps to stabilize the air cells in ice cream, holds ice cream structure, and gives ice cream slow-melting properties in the presence of a large number of fat globule clusters.

2.1.4 Stabilizers

Hydrocolloids are widely used as stabilizers in ice cream and frozen dessert products. The common stabilizers used are sodium alginate, carboxymethyl cellulose, carrageenan, gelatin, guar gum, locust bean gum, microcrystalline cellulose, and xanthan gum. These hydrocolloids increase ice cream mix viscosity by hydrating and swelling in the aqueous phase and taking up a large

volume in the solution (Goff & Hartel, 2013). Different hydrocolloids show different abilities to increase viscosity and affect non-Newtonian behavior. Generally, neutral hydrocolloids show a greater increase in non-Newtonian behavior compared to anionic hydrocolloids in the ice cream mix (Cottrell et al., 1980). Even though stabilizers have a limited impact on freezing point depression and initial ice crystal size during freezing and hardening (Flores & Goff, 1999a), they retard the rate of ice recrystallization (Hagiwara & Hartel, 1996), especially during temperature fluctuation (Bolliger et al., 2000).

2.1.5 Milk solids-non-fat

Milk solids-non-fat (MSNF) provides ice cream with a specific flavor and texture. The traditional and best sources of MSNF come from concentrated skim milk and spray-dried skim milk powder. MSNF in ice cream includes whey proteins, caseins, lactose, minerals, vitamins, and enzymes. Excess use of lactose contributes to the problems of extreme freezing point depression and lactose crystallization, which gives the ice cream an unpleasant sandiness defect (Nickerson, 1962).

Proteins provide three different functions to ice cream texture, including emulsification, aeration, and viscosity. Proteins prevent individual fat globules from partial coalescence by absorbing into the fat membrane to create a stable surface. They can increase the steric stability between fat globules, which decrease fat destabilization (Goff et al., 1989). When whey protein is the only protein source in the ice cream, the fat globules are too stable to undergo fat destabilization (Zhang & Goff, 2005). Milk proteins also act as surfactants that stabilize the air cells by absorption to the air-serum membrane during the whipping process. Without sufficient functional protein, ice

cream can exhibit a shrinkage defect (VanWees et al., 2022). By interacting with water, milk proteins also increase the viscosity of serum phase (Alvarez et al., 2005).

2.1.5.1 Milk protein-polysaccharide interaction

Milk protein and stabilizers are typically incorporated into ice cream formulations to enhance their functionalities, such as texture and structure. Nevertheless, these two types of polymers may exhibit non-covalent interactions that could result in undesirable outcomes like phase separation in the ice cream mix, or after severe temperature fluctuations in the ice cream. The nature of the protein and hydrocolloids, as well as their concentrations, can influence the type of interaction that takes place. Additionally, environmental factors such as temperature, ionic strength, and pH can also have an impact on these interactions.

There are two types of interactions between proteins and hydrocolloids: attractive and repulsive. Opposite charges on proteins and hydrocolloids result in attractive interaction, which leads to the formation of either a soluble complex or a two-phase system through associative separation. Segregative separation occurs when both biopolymers are either uncharged or have the same charges. The concentration of biopolymers in the system determines the type of system formed. At low concentrations, they can be cosoluble in the solution, resulting in a one-phase system. However, at concentrations above a certain level, phase separation occurs, resulting in one phase enriched in protein and the other phase enriched in hydrocolloids (McClements, 2006).

Two mechanisms, thermodynamic incompatibility, and depletion flocculation, are responsible for segregative separation. Thermodynamic incompatibility arises when the mixing enthalpy is greater than the difference in entropy, leading to biopolymers having a greater affinity for the same type of molecules. It can also occur due to differences in their solvent affinity, where

the solvent-protein (or solvent-polysaccharide) interaction is more favorable than protein-polysaccharide or solvent-solvent interactions (Doublier et al., 2000; Goh et al., 2019). Depletion flocculation is commonly observed in large colloidal particles such as casein micelles. In such cases, the osmotic pressure of the biopolymer acts as the driving force, generating an additional attractive force between the colloidal particles. As a result, the depletion layer of the particles overlaps, leaving a depletion region between them (Goh et al., 2019). A schematic diagram of depletion flocculation mechanism is shown in **Figure 2.1**.

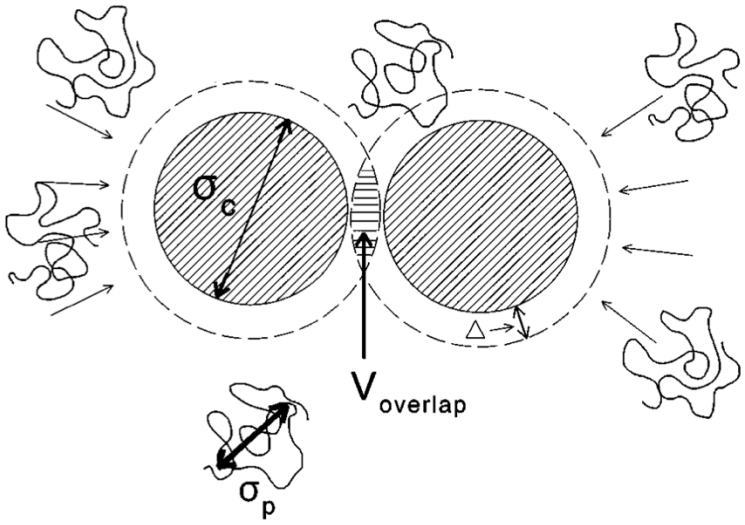

Figure 2.1 Schematic diagram of depletion flocculation mechanism. The colloidal spheres with diameter σ_c have attractive interaction by the osmotic pressure gradient from the polymer molecule with diameter σ_p (from Tuinier & Kruif, 1999).

2.1.6 Emulsifiers

Emulsifiers are commonly used to produce a uniform emulsion in food products by reducing the interfacial tension between oil and water, and stabilizing the droplets. In ice cream products, emulsifiers are mainly used for increasing fat destabilization to provide dryness and stiffness as well as a smooth mouthfeel. By lowering interfacial tension between fat and water in the ice cream mix, emulsifiers help to displace protein from the fat globule surface, which results

in active fat globule surfaces that can be partially coalesced during whipping and freezing (Goff & Hartel, 2013). Emulsifiers blended with stabilizers can promote fat agglomeration to provide ice cream with better texture and sensory properties (Cropper et al., 2013).

Two common types of emulsifiers in ice cream products are mono- and diglycerides and sorbitan esters. The usage levels of mono- and diglycerides (MDG) and polysorbate 80 (PS80), a common type of sorbitan ester in ice cream products, are 0.1-0.2% and 0.02-0.04%, respectively. A blend of these two emulsifiers is commonly used in commercial products because the mono- and diglycerides are more effective at stabilizing air bubbles whereas sorbitan ester is more functional at the fat interface to promote fat destabilization (Goff & Hartel, 2013; Warren & Hartel, 2018).

2.1.7 Sweeteners

The function of sweeteners in ice cream is mainly to provide an acceptable sweet flavor as well as to enhance subtle fruit flavors (Goff & Hartel, 2013). Besides sucrose, common sweeteners are high fructose corn syrup (HFCS), corn syrup (CS), high maltose corn syrup, and other mono- and disaccharides. Sweeteners also influence ice cream's physical properties and may decrease the ice crystallization rate by restricting the mass transfer rate. The most prominent effect on ice crystallization is by affecting freezing point depression. A lower freezing point means less ice phase at a particular temperature, which in turn produces soft ice cream because of a low amount of ice crystals. Also, sweeteners can interact with water to increase the viscosity of the unfrozen serum phase (Hagiwara & Hartel, 1996; Livney & Hartel, 1997).

2.2 Processing

The manufacture of ice cream starts with mixing ice cream ingredients, including dry and liquid ingredients. The mixed ingredients then go through pasteurization and homogenization to kill all the pathogens and break down fat globules. After storage at 4˚C for 4 to 24 hr, the ice cream mix is frozen in a continuous or batch freezer, followed by the packaging and hardening process.

2.2.1 Mixing and pasteurization

The liquid ingredients (milk, cream, water, syrup, etc.) and dry ingredients (MSNF, crystalline sugar, skim milk powder, stabilizers, etc.) are blended separately before combining them into the vat and agitating to 50˚C (122˚F). Generally, dry ingredients are slowly poured into a vat and mixed with liquid ingredients to prevent lumpiness. Mixing ingredients at 50˚C ensures the complete dissolution of dry ingredients and assists mixing by melting the fat globules and decreasing viscosity (Goff & Hartel, 2013).

Pasteurization aims to kill all the pathogens in the ice cream mix. According to the Code of Federal Regulations, ice cream should contain a maximum of 50,000 bacteria per gram and 10 coliform organisms per gram for plain flavor. The two common approaches to pasteurize ice cream mix are low-temperature long-time (LTLT) pasteurization, 69˚C (155˚F) for at least 30 minutes, and high-temperature short-time (HTST) pasteurization, 80˚C (175˚F) for 25 seconds.

2.2.2 Homogenization

Homogenization decreases fat globule size and creates more interfacial area by breaking down large globules into small globules. **Figure 2.2** illustrates the decrease in size of the initial emulsion (second peak) after homogenization.

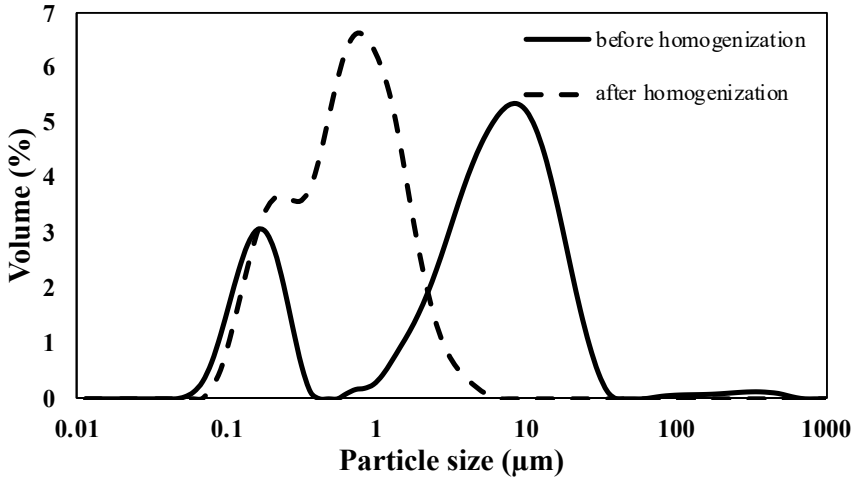

Figure 2.2 Example of ice cream mix particle size comparison before and after homogenization. The first peak is protein (casein micelles) and the second peak is initial emulsion (individual fat globules).

Pressure and temperature are two important parameters during homogenization to increase efficiency (Goff & Hartel, 2013). Homogenization pressure applied to ice cream products commonly ranges from 6 to 20 MPa. Raising the pressure to 200 MPa can greatly decrease fat particle size and enhance viscoelastic properties as well as apparent viscosity (Innocente et al., 2009). High-pressure homogenization not only has an impact on the fat droplet sizes but also has a greater structural impact on proteins that cause a firmer gel-like network compared to conventional-pressure homogenization (Biasutti et al., 2013; Innocente et al., 2009).

2.2.3 Cooling and aging

After homogenization, the ice cream mix is cooled and aged. Ice cream mix cannot directly go into the freezer after homogenization because it takes time for the stabilizers to hydrate and increase the viscosity as well as for the fat globules to complete crystallization. Commonly, ice cream mix is placed in the refrigerator at 2 to 4˚C for 4 to 24 hr (Goff & Hartel, 2013). The aging time is crucial to the color, texture, and taste of the final products (Caniyilmaz et al., 2016).

2.2.4 Freezing

Freezing transforms ice cream mix into ice cream products. When the ice cream mix enters the freezer, whether batch or continuous, three changes occur: ice crystallization, fat destabilization, and aeration. After ice cream exits the freezer, it contains partially-frozen water (the rest remains in the unfrozen serum phase), air cells, fat globules and clusters, and unfrozen serum phase (including sweeteners, salts, partial proteins, and stabilizers) (Goff & Hartel, 2013).

Batch freezers target small-scale production or laboratory use. They are less expensive but also less efficient to make a large batch compared with continuous freezers. Batch freezer capacities range from 15 to 57 L. As for continuous freezers, they target large-scale production where ice cream is made continuously without changing the ice cream mix from batch to batch. The capacities of continuous freezers range from 114 to 4542 L/hr. The main difference between the two freezers is the way air is incorporated into the ice cream mix. The air is whipped into the mix from the chamber in the batch freezers, whereas air is injected into the mix in the continuous freezers, which is more controllable. Generally, the draw temperature for the ice cream ranges from -5 to -6˚C targeting 50%-60% of the water to freeze.

2.2.5 Hardening and storage

After ice cream is extruded from the freezer, it is in a semisolid state, which needs hardening to freeze additional water and form a firm structure. Hardening and storage freezers are commonly at -18˚C and preferably at -25 to -30˚C (Goff & Hartel, 2013). Hardening is considered complete when the temperature at the center of the ice cream product reaches -18˚C. Forced convection cooling is more effective than natural convection, which takes 3 hr to cool to -28˚C compared to 8-10 hr in natural convection (Chang & Hartel, 2002c).

Ice cream is later sent to retail stores and stored at a large temperature variability, between -9˚C and -26˚C (Ben-Yoseph & Hartel, 1998). The temperature fluctuation may cause product defects such as sandiness from lactose crystallization (Livney et al., 1995), iciness from ice recrystallization (Donhowe & Hartel, 1996), and shrinkage from foam destabilization (VanWees et al., 2022).

Two main components change during the hardening and storage process, the air cells and the ice crystals. Air cells go through three different changes during the hardening and storage time: Ostwald ripening, coalescence, and drainage. These three changes contribute to the increasing size of air cells in the hardening process at the temperature above -28˚C (Chang & Hartel, 2002c). The ice crystals also go through ripening/recrystallization, partially because of temperature fluctuation (Goff and Hartel 2013). The number of ice crystals decreases during hardening and storage since no new ice crystals form, and small ice crystals grow at the expense of others.

2.3 Physical microstructure of ice cream

Ice cream has a complex microstructure with three phases interacting with each other: liquid (serum phase), gas (air cells), and solid (fat clusters and ice crystals). During aging, some proteins on the surface of fat globules are partially displaced by the low molecular weight surfactants, destabilizing the fat globules, and forming partially-coalesced clusters. When the ice cream mix is frozen into ice cream, fat globule clusters are formed by the whipping force. Air is injected and stabilized in the form of small air cells by the fat clusters. Meanwhile, ice nuclei form on the barrel and are scraped into the mix while the remaining unfrozen concentrated serum forms the lamella between air cells and fat clusters. This microstructure can greatly influence ice cream

macroscopic properties, such as meltdown behavior and rheological properties, which further affect sensory properties.

2.3.1 Air cells

Air provides ice cream with a fluffy and scoopable texture as well as resistance to meltdown. The range of air cell size is broad, ranging from a few microns up to 100 μm. Shear force, dasher speed and overrun affect air cell size during the manufacturing process. Warren and Hartel (2018) found that increased dasher speed significantly decreased air cell sizes with the presence of polysorbate 80, but no effect was found in absence of emulsifiers or when only MDG was added. Additionally, the mean air cell size decreased with the increase of overrun since more air was incorporated into the ice cream slurry. Higher apparent viscosity with more air increases the breakdown of air cells (Chang & Hartel, 2002a; Sofjan & Hartel, 2004; Warren & Hartel, 2018). Eisner et al. (2005) found that higher shear forces from cooling ice cream to -12˚C through a twin-screw extruder significantly decreased air cell size. The maximum air cell diameter decreased from 52 to 19 μm, resulting in a narrower size distribution.

Air cells are stabilized by individual fat globules, fat clusters, and proteins. The stability of air cells during hardening and storage is related to three mechanisms: disproportionation, coalescence, and drainage (Chang & Hartel, 2002c). Disproportionation is comparable to Ostwald ripening in ice crystals where the larger air cells expand at the expense of smaller air cells. Air cells with different surface tension as well as principal radii of curvature have different Laplace pressure, which causes air to diffuse from the small one to the large one and results in disproportionation. Coalescence mainly results from Brownian motion among air cells where the interfacial films merge when air cells come into contact. Drainage is the result of buoyancy where

the less dense air cells move upwards based on Stokes law. The high viscosity of the serum phase inhibits drainage by reducing air cell mobility (Chang & Hartel, 2002b; Sofjan & Hartel, 2004; Wilson, 1989).

2.3.2 Ice crystals

About 50% of water is frozen after coming out from the freezer and 75% of water is frozen after the hardening process (Cook & Hartel, 2010). While there is an increasing volume of water frozen during the hardening process, the ice crystal size also increases. The mean ice crystal size of the fresh ice cream product from the freezer is 15 to 30 μm and that grows to 35 to 45 μm after hardening (Goff & Hartel, 2013). Ice crystal size distribution varies with formulation and process conditions.

2.3.2.1 Ice crystal formation

Ice crystal nuclei only form during the dynamic freezing process. Nuclei grow on the inner surface of the freezing barrel where the temperature is the coolest inside the barrel. The ice crystal is formed in a dendritic shape. As they grow on the freezer surface, the dashers scrape the ice crystals into the center of the barrel at a higher temperature causing some of the crystals to melt

and regrow again (**Figure 2.3**). About half the water is frozen after the dynamic freezing process (Cook & Hartel, 2010).

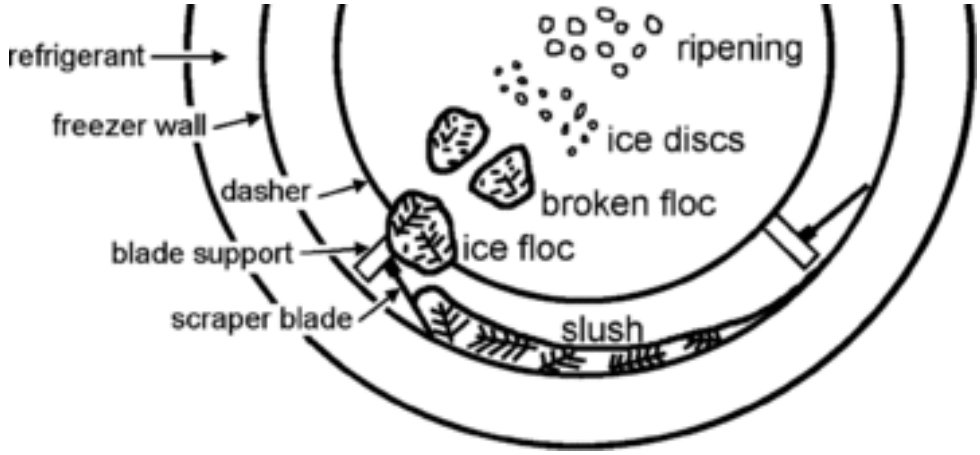

Figure 2.3 Schematic diagram of ice crystal formation inside the freezer barrel (from Cook & Hartel, 2010).

2.3.2.2 Ice recrystallization mechanism

The recrystallization of ice crystals during hardening and storage is related to four mechanisms: accretion, melt-refreeze mechanism, migratory recrystallization (Ostwald ripening), and isomass recrystallization (Donhowe & Hartel, 1996). Accretion occurs between two adjacent crystals, where they share a boundary, and a neck forms in between until a single larger crystal is formed. Melt-refreeze recrystallization mainly happens during the temperature cycling in the freezer, where small ice crystals melt as temperature increases and refreeze as the temperature drops down. Isomass recrystallization involves the transformation of ice crystals from irregular to smooth shapes to lower the specific energy caused by the surface curvature. Migratory recrystallization (Ostwald ripening) refers to the large ice crystals growing at the expense of small ones, which has been rarely observed in the ice cream system (Donhowe & Hartel, 1996). The ripening rate is found to be negatively related to the concentration of solutes, which may account

for a rare observation of Ostwald ripening in ice cream stored at a lower temperature with a high unfrozen serum phase (Pronk et al., 2005).

2.3.2.3 Effect of formulation on ice crystal size

The effect of ingredients on the initial ice crystal size distribution is mainly through the effect on the freezing point of the mix. Trgo et al. (1999) and Donhowe et al. (1991) found that increasing total solids content gave smaller ice crystals because of the decreasing amount of water in the ice cream mix. No effects of stabilizers are found on the initial ice crystal distribution during the batch freezing process (Flores & Goff, 1999).

The effect of ingredients on ice recrystallization is mainly by affecting accretion and melt-refreeze recrystallization. Sweeteners are used in ice cream to adjust the freezing point and the amount of frozen water, which further affect the ice recrystallization rate. A higher freezing point or a higher percentage of frozen water generally leads to a slower recrystallization rate (Hagiwara & Hartel, 1996). Different sweeteners have various abilities to decrease the freezing point and adjust the percentage of frozen water because of their distinct molecular weight, consequently, affecting the ice recrystallization. Livney and Hartel (1997) found that ice cream made with high fructose corn syrup had the highest ice recrystallization rate whereas ice cream with 20 dextrose equivalent corn syrup had the slowest recrystallization rate.

Ice cream made with stabilizers generally has a slow recrystallization rate through the steric hindrance effect and the increases in microviscosity in the unfrozen phase from the addition of polysaccharides, which restricts water mobility or hinders the ice crystal growth (Hagiwara & Hartel, 1996; Livney & Hartel, 1997). Some stabilizers, such as locust bean gum and κ-carrageenan, retard the ice crystal growth by forming a gel-like network, facilitating the melt-

regrow instead of melt-diffuse-grow mechanism of recrystallization within the local region (Brigham et al., 1994; Regand & Goff, 2002). Antifreeze proteins, also known as ice-binding proteins (IBPs), inhibit ice recrystallization by binding to the crystal surface. These ice-binding sites are commonly extensive, flat, hydrophobic, and regular planes on the ice crystals (Davies, 2014).

2.3.2.4 Effect of freezing on ice crystal size

Ice crystallization in the freezer goes through four steps: supercooling, nucleation at the wall surface of the barrel, growth, and recrystallization. Ice crystal size is influenced by residence time in the freezer, draw temperature, and dasher speed (Drewett & Hartel, 2007; Russell et al., 1999). A decrease in the residence time of the ice cream mix in the freezer results in faster recrystallization as well as a smaller mean ice crystal size. Ice crystal growth and recrystallization occur in the freezer when the dasher blade scrapes the nuclei into the warmer slurry in the center of the freezer and the nuclei partially melt, which accelerates ice crystal growth and recrystallization. A longer residence time for the ice cream within the freezer means a longer time that ice crystals are exposed to the warmer temperature, thus contributing to the increased size of ice crystals (Drewett & Hartel, 2007).

Draw temperature influences both latent heat generation, which is related to ice crystal content, and the rate of heat removal. Thus, lowering the draw temperature leads to smaller ice crystal size as well as reduces the recrystallization rate (Amador et al., 2017; Drewett & Hartel, 2007). Also, Russell et al. (1999) and Drewett and Hartel (2007) found increasing dasher speed resulted in increasing mean ice crystal size because the temperature inside the freezer increased in the high dasher speed owing to fractional heat liberation, which resulted in ice crystal growth and

recrystallization. In contrast, Warren and Hartel (2018) found the effect of dasher speed on ice crystal size to be minimal, accounting for the production of the ice cream at same draw temperature by reducing the evaporator pressure, which counteracted the heat generation from the increased dasher speed.

2.3.2.5 Effect of hardening and storage on ice crystal size

Ice crystals grow during hardening mainly because lower temperature causes more water to be frozen, consequently ice crystals go through the ripening process and continue to grow. Temperature fluctuations during storage can promote recrystallization and increase crystal size. Generally, the mean size of ice crystals linearly increases with storage time to one-third power (Donhowe & Hartel, 1996; Hagiwara & Hartel, 1996).

Ice crystals grow and the number of ice crystals decreases during the hardening period caused by the Ostwald ripening (Russell et al., 1999). A similar trend is found during ice cream storage (Donhowe & Hartel, 1996). Flores and Goff (1999b) found that a constant -30˚C storage temperature did not significantly affect ice crystal distribution while ice cream storage at -16˚C led to larger ice crystal size. The temperature cycle during storage also affects ice recrystallization as well as ice crystal shape. A constant storage temperature significantly reduces the ice recrystallization rate and provides more rounded ice crystals compared to an oscillating storage condition (Donhowe & Hartel, 1996). By comparing two walk-in freezers with the different operation and defrost cycle but the same time interval between each defrost, the ice recrystallization rate is significantly reduced in the freezer with a lower defrost temperature and shorter defrost time (Sharqawy & Goff, 2022).

2.3.3 Serum phase

The continuous aqueous phase in ice cream, also called the unfrozen serum phase, holds the microstructure together. The serum phase contains all the ingredients that can be dissolved in the water, including proteins, sweeteners, and stabilizers. The proportion of the serum phase gradually decreases and becomes more concentrated as temperature goes down, which is called freeze concentration.

The viscosity of the serum phase is an important property. It not only affects ice cream's physical properties such as melting rate, but also sensory attributes such as iciness and greasiness (Amador et al., 2017). The viscosity of the ice cream mix is often used to represent the viscosity of the serum phase, which can be adjusted by adding stabilizers and proteins. The freeze-concentrated unfrozen phase is simulated by reducing the corresponding frozen water at a given temperature from the original mix and maintaining the same ratio of solids as in the mix (Goff et al., 1995a; Masselot et al., 2020). The serum phase goes through a transition from dilute to concentrated solution during freeze concentration, and polymer helical coil overlap or entanglement may occur, resulting in a significant increase in the apparent viscosity (Goff et al., 1995a).

Milk protein and polysaccharide phase separation occurs in the freeze-concentrated serum phase. Goff et al. (1999) reported that the addition of guar gum or locust bean gum in the presence of milk protein facilitated the formation of a protein-enriched region surrounding the ice crystals in the frozen solution, likely due to increased self-association and entanglements. Additionally, locust bean gum, which acts as a gelling stabilizer, can undergo cryo-gel formation during the freezing-thawing process (Tanaka et al., 1998). This cryo-gel retains its structure even after all the ice crystals have melted.

2.3.4 Fat destabilization/partially coalesced fat

After the homogenization process, milk proteins are covered on the fat droplet surface to provide steric stabilization between droplets. If the low-molecular-weight surfactants, such as mono- and di-glycerides and polysorbate 80, are present in addition to proteins, they can displace the protein from the surface and promote destabilization of the fat droplets. These destabilized fat globules go through partial coalescence during the freezing and churning process, which is also called fat destabilization.

The partial coalescence mechanism was first noted by van Boekel and Walstra (1981). Recent studies unveil that partial coalescence is mainly affected by Laplace pressure and elastic energy between two fat droplets (Thiel et al., 2016). Laplace pressure drives the two droplets to coalesce whereas the elastic energy of crystalline structure prevents two droplets from complete coalescence. The fat globules are either fully coalesced or stable remaining as two droplets when either the interfacial energy or the elastic energy is dominant, respectively. Solid fat formed during the aging process provides structural rigidity and high elastic energy within the globule. Depending on the solid fat content, the coalescence degree varies from complete coalescence to full stability (**Figure 2.4**).

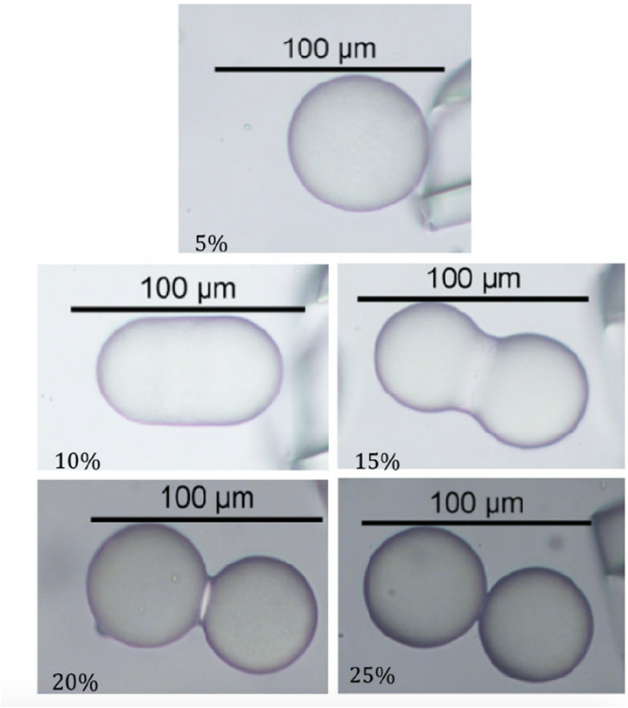

Figure 2.4 Fat coalescence between two tristearin/triolein droplets containing 5%, 10%, 15%, 20%, and 25% solid fat content (from Thiel et al., 2016).

The degree of fat destabilization is affected by both formulation and processing conditions. In terms of formulation, the type and amount of emulsifiers, the type of protein, the ratio of solid fat to liquid fat as well as overrun contribute to the extent of fat destabilization (Amador et al., 2017; Chang & Hartel, 2002a; Méndez-Velasco & Goff, 2012; Muse & Hartel, 2004; Sung & Goff, 2010; Warren & Hartel, 2018). The fat destabilization level increases with the increasing emulsifiers added, where more proteins are displaced by emulsifiers and fat globules become less stable (Amador et al., 2017; Chang & Hartel, 2002a; Muse & Hartel, 2004; Warren & Hartel, 2018). Polysorbate notably causes a higher degree of fat destabilization than mono- and diglyceride, potentially from a greater reduction in interfacial tension. The saturation degree of monoglyceride has an impact on the extent of fat destabilization (Méndez-Velasco & Goff, 2012).

Unsaturated monoglyceride tends to form larger fat clusters and retain a portion of intact individual fat globules whereas saturated monoglyceride tends to form smaller fat clusters with limited size.

Whey protein and casein are the two main proteins influencing fat stabilization. In particular, casein is better at stabilizing fat compared to whey protein. Whey protein tends to form a monolayer and covers more surface area whereas casein forms a thicker layer, making it hard for emulsifiers displaced to lower the surface tension (Daw & Hartel, 2015; Segall & Goff, 1999). Generally, the degree of fat destabilization decreases as protein content increases due to a thicker absorbed protein layer. Ice cream made with 10% protein forms an extremely stable emulsion with no fat destabilization observed (Daw & Hartel, 2015).

Increasing overrun leads to increased fat destabilization extent (Sofjan & Hartel, 2004; Warren & Hartel, 2018). There are two possible mechanisms to explain this trend. First, the introduction of air in the ice cream causes a higher apparent viscosity and higher shear stress in the freezing process, which promotes fat destabilization. Second, the additional air surface area created contributes to the repeated adsorption and desorption of fat to the air/water interface, which increases the collision rate between fat globules (Warren & Hartel, 2018).

The processing conditions also affect fat destabilization mainly by influencing shear force during freezing. Either increasing the dasher speed (Inoue et al., 2008; Warren & Hartel, 2018) or decreasing the draw temperature (Bolliger et al., 2000) promotes fat destabilization by enhancing the shearing effect in the freezing process. With an increase in shear force and longer shear time, the collision rate among fat globules increases, and thus further accelerates partial coalescence.

2.4 Ice cream meltdown

Ice cream melting in the mouth and at room temperature are used for evaluating product quality. Meltdown at room temperature is one of the most important attributes in ice cream for both industry and research. In the industry, slow-melting ice cream with good shape retention is considered to have better heat resistance without sacrificing the foamy structure during heat fluctuation. The meltdown test is also a simple and visual test in research to differentiate ice creams with different microstructures, either by adjusting processing conditions or formulation.

2.4.1 Meltdown process

The meltdown process can be divided into three phases: the lag phase, the fast-melting phase, and the stationary phase. In the lag phase, heat penetrates the ice cream, and ice crystals start melting and diluting the serum phase, causing a reduction in viscosity. With increasing flowability of the diluted serum phase, ice cream meltdown reaches the second stage, the fast-melting phase, where the melted ice cream starts dripping through the wire mesh by the force of gravity. During this phase, ice cream collapses at a rate and to an extent, depending on the remaining structures including air cells and fat clusters/globules. If there are numerous fat clusters around the air cells, the fat clusters collide with each other and jam to form a three-dimensional network with air cells. Subsequently, meltdown slows down and comes to the stationary phase leaving melted ice cream foam on the mesh. If there are few fat clusters, ice cream can totally drip through in a short time (< 2 hr). The meltdown curve constructed from the meltdown test is a sigmoidal shape. Generally, the rate at the fast-melting stage is defined as the ice cream meltdown rate (**Figure 2.5**), but the information at the lag phase and stationary phase has been rarely investigated.

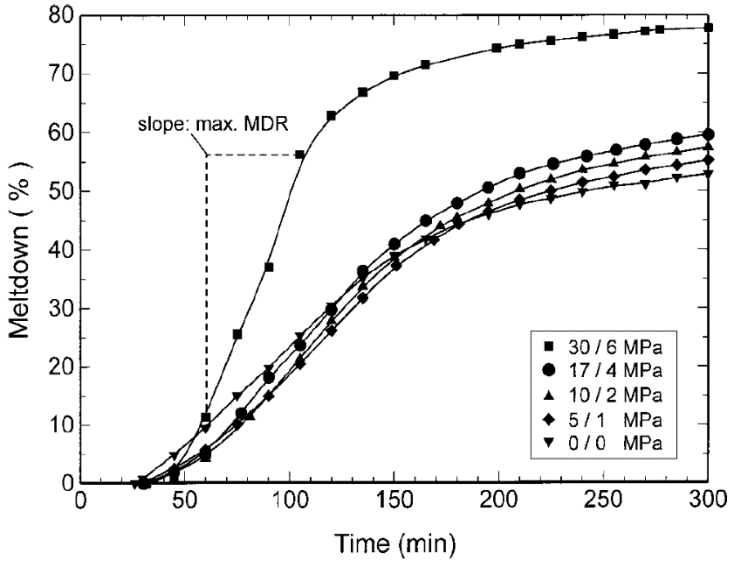

Figure 2.5 The illustration of ice cream maximum meltdown rate (MDR) is defined as ice cream meltdown rate (from Koxholt et al., 2001).

2.4.2 Meltdown behavior

Ice cream has two types of meltdown behavior during the meltdown test: complete meltdown and foam retention (**Table 2.1**). For the ice cream that completely melts and drips, the melting and dripping process start from the surface, where the temperature increases fastest by heat convection with air. Melted liquid drips layer by layer, and the sample gradually shrinks to a hemispherical shape until the entire sample drips through the mesh. Ice cream with complex microstructure has a good capability to hold the melted liquid within its structure. Melted liquid travels through the lamella between air cells and drips from the bottom of the sample, contributing to partial structural collapse. After the melting process comes to an end, a large quantity of stable remnant foam remains that can maintain its shape without further collapse for up to 6 hr.

Table 2.1 Example of two types of meltdown behaviors with the same formulation in the ice creams. The complete meltdown sample contains 50% overrun and the foam retention sample has 100% overrun.

Time (min)	Complete meltdown	Foam retention
0	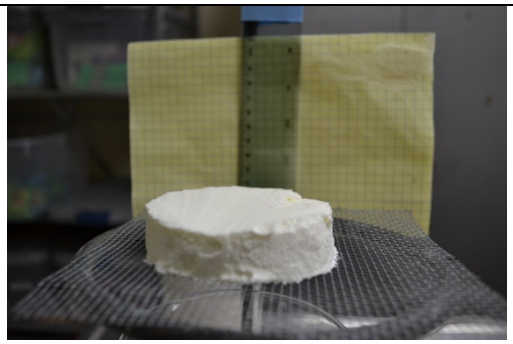	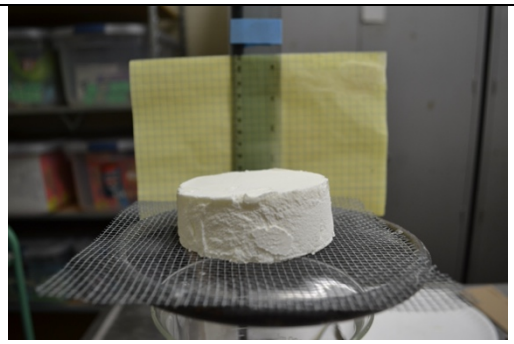
40	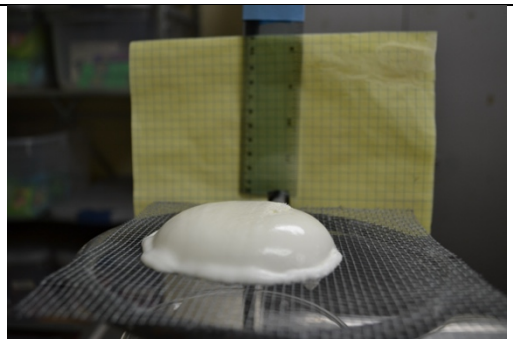	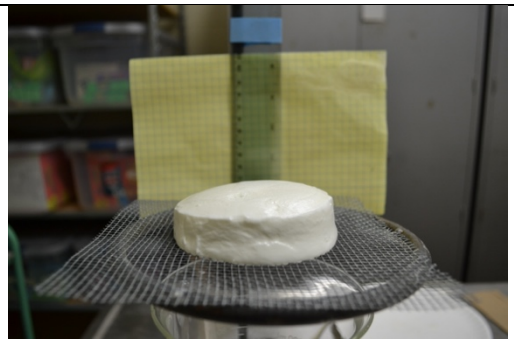
60	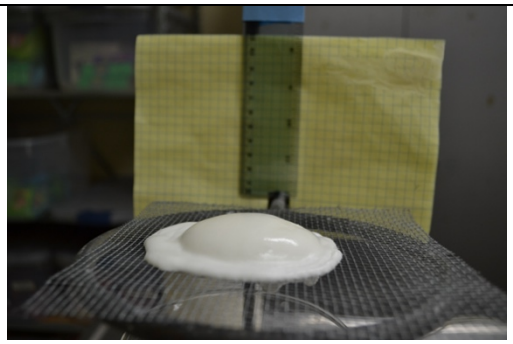	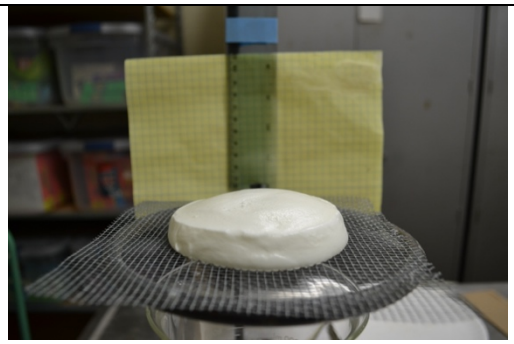
100	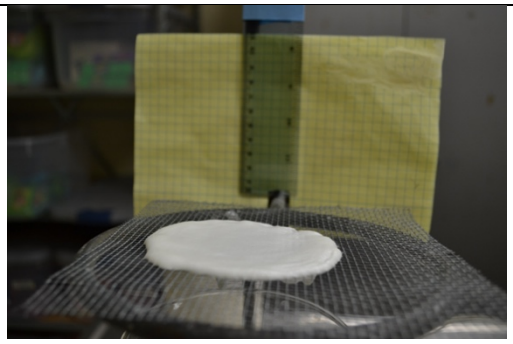	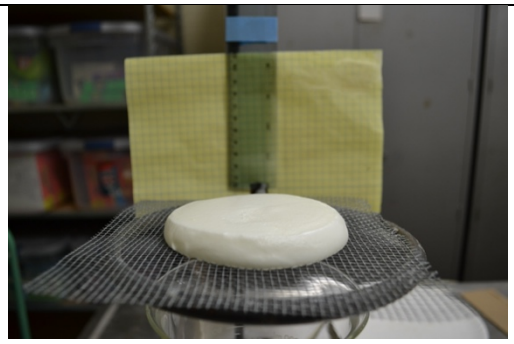

2.4.3 Structural elements affect meltdown

The ice cream microstructure formation, whether by manipulating formulation or changing production parameters, is associated with meltdown rate and meltdown behavior. A strong structure with a large amount of air and fat clusters, viscous serum phase, and small ice crystals contributes to a slow meltdown rate and better shape retention.

2.4.3.1 Fat

Fat not only provides a smooth mouthfeel but also plays a critical role in meltdown by providing a rigid structure in the lamella and obstructing the drainage of the serum phase. Fat content, the degree of fat destabilization, and fat cluster size have been found to influence the meltdown rate and the meltdown behavior.

Increasing fat content leads to a slower meltdown rate, longer induction time, and less melted liquid drainage, which ultimately leads to better shape retention of melted foam after the meltdown test (Liu et al., 2022; Roland et al., 1999). In general, increasing fat content contributes to a higher amount of fat destabilization and more fat globules dispersed in the serum phase. These large fat clusters and globules form a three-dimensional fat network in the serum phase to provide rigidity and resistance to drainage. The ice cream mix viscosity increases with the addition of fat content, which may indirectly slow the drainage of the melted ice cream (Li et al., 1997).

The emulsifier types and levels contribute to the change in fat destabilization, which in turn influence the ice cream meltdown rate. Polysorbate 80, mono-and diglycerides, and glycerol monooleate are found to effectively reduce melting rate by promoting the formation of fat destabilization (Bolliger et al., 2000; Cropper et al., 2013; Méndez-Velasco & Goff, 2011; Muse & Hartel, 2004). Adding additional emulsifiers leads to a higher fat destabilization level due to a

greater protein displacement at the fat-water interface (Davies et al., 2000), and results in a slow meltdown process and better shape retention. As mentioned, the destabilized fat clusters form a network and block the liquid drainage channel in the lamella to prevent the melted ice cream from expelling and provide a good stand-up property.

Fat globule size manipulated during homogenization is also found to affect the meltdown rate (Biasutti et al., 2013; Koxholt et al., 2001). A larger fat size contributes to a slower meltdown rate. As shown in **Figure 2.6**, fat globules size in the drip-through part is correlated with the maximum meltdown rate, which indicates that fat globules larger than a critical diameter tended to be trapped in the foam matrix and retained the shape, whereas smaller fat globules easily flowed through the lamellae. Liu et al. (2022) found that the fat aggregate size mainly affected the initial melting stage, and a longer induction time was seen in the system with larger fat aggregates. The large fat aggregates provide a rigid initial structure, and may also change the ice crystal connectivity and result in a different flow path of the serum phase.

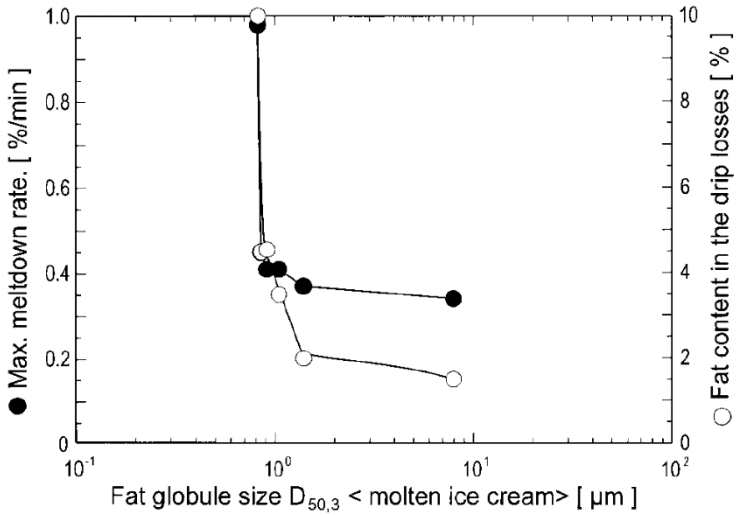

Figure 2.6 Effect of fat globule size on the maximum meltdown rate and fat content in the drip through portion (%) (from Koxholt et al., 2001).

Solid fat content affects the meltdown rate mainly by changing the degree of fat destabilization. The adjustment of the ratio between unsaturated and saturated fat achieves various solid fat content in the ice cream. Sung and Goff (2010) used palm kernel oil (PKO) as saturated fat and high-oleic sunflower oil as unsaturated fat to adjust the solid fat content in the ice cream. They found that a slower meltdown rate was observed when the palm kernel oil content of the fat phase was in the range of 50%-80%. Ice cream melted faster when PKO was either above or below this range.

Applying different melting fractions of milk fat can also change the fat destabilization and ultimately affect the meltdown behavior. Ice cream made with low-melting milk fat fraction forms a higher degree of fat destabilization than the one made with high-melting milk fat fraction throughout freezing (Adleman, 1998), which may potentially result in a slower meltdown rate in the ice cream. On the other hand, El-Rahman et al. (1997) noted that ice cream made with very high melting milk fat fraction (VHMF) had a longer induction time, a slower melting rate, and better shape retention compared to the ones with anhydrous milk fat (AMF) or low melting milk fat fraction (LMF). The VHMF with 44.9˚C melting point still had solidified fat when melting at room temperature, which was accounted for providing the structure and reducing melting rate during melting.

2.4.3.2 Protein

Milk protein is found to affect the ice cream meltdown behavior through two main mechanisms. First, as a macromolecule, protein increases the viscosity and the shear-thinning behavior of the ice cream mix, which is related to the increased voluminosity of the colloidal particle (Alvarez et al., 2005; Daw & Hartel, 2015). Particularly, micellar casein has a better

capability to improve viscosity than whey protein on account of its larger molecular size. Second, an increase in protein content in the mix leads to a reduction in fat destabilization. During the formation of fat globules clusters, emulsifiers such as polysorbate 80 and mono- and diglyceride displace proteins at the fat globule interface, leading to destabilized fat droplets that are readily coalesced with each other (Goff & Hartel, 2013). With a high amount of protein present in the mix, a dense and thick protein film is expected to form at the fat interface, providing a strong steric barrier against fat coalescence. Because of the difference in size and structure between whey protein and micellar casein, whey protein more readily destabilizes fat than casein at a low concentration (<6%) in ice cream (Daw & Hartel, 2015). However, no general relationship was found in the literature about the influence of protein on meltdown rate. For example, Daw and Hartel (2015) found a moderate correlation between melting rate and viscosity, flow index, and fat destabilization level from different protein sources in the ice cream, which did not simply account for the viscosity or fat destabilization changes by the proteins. The type and the structure of the protein, whether it is in a native or hydrolysate form (Chen et al., 2019), are also found to result in the difference in melting rate and shape retention. Beyond that, the role of protein-polysaccharide interaction (e.g., phase separation) in meltdown has been barely discussed.

2.4.3.3 Air

Air bubbles in the ice cream are stabilized by fat droplets/clusters, proteins, and emulsifiers at the interface (Goff & Hartel, 2013). Sakurai et al. (1996) and Warren and Hartel (2018) unveiled a negative correlation between overrun and meltdown rate, attributing this to the good insulation of air to prevent heat penetration during the meltdown. In addition, air bubbles surrounded by fat globules and clusters are trapped by the fat network. A high overrun ice cream contains more air

cells trapped and stacked in the process of ice cream foam collapse, which in turn may account for the slower melting rate and more residual melted foam (VanWees et al., 2020). If the overrun is controlled within a narrow range (around 50%-60%), the effect of overrun on the meltdown is less significant (Muse & Hartel, 2004).

2.4.3.4 Ice

Frozen water is in the form of small ice crystals in ice cream. Ice crystals in the serum phase can provide a tortuous flow path through which melted liquid may flow, and further affect the ice cream meltdown rate. Muse and Hartel (2004) found that increasing ice crystal size in the range of 40 to 65 μm contributed to an increased meltdown rate. Small ice crystals may be more scattered and dispersed and create a more tortuousness to slow the drainage compared to large crystals. In contrast, Warren (2015) and Daw and Hartel (2015) found that ice crystal size had minimal effect on the meltdown rate when it was controlled in a limited range from 20 to 40 μm. Besides ice crystal, the ice phase volume may also affect meltdown. Ice cream made with high total solids and low water content is found to have a faster meltdown rate (Li et al., 1997). The increase in total solids decreases the freezing point. In the same hardening and storage condition, ice cream with a lower freezing point has less ice phase volume available to melt.

2.4.3.5 Serum phase

The viscosity of the serum phase in ice cream can be adjusted by the inclusion of polymers such as polysaccharides and proteins. The inclusion of probiotics or prebiotics, such as dietary fiber (Akalın et al., 2018), polyphenols (Ahmad et al., 2020), and probiotic strains (Goktas et al., 2022), can also influence the viscosity. Enhancing viscosity generally increases shear-thinning

behavior. A slow meltdown process can be achieved by a viscous serum phase, which allows restricted mobility of ice cream structural elements and a slow drainage rate in melted liquid (Amador et al., 2017; Muse & Hartel, 2004).

In the presence of protein and polysaccharide in the serum phase, water holding capacity increases and the cryo-gelation effect occurs, which provides steric hindrance and limits water mobility. This effect decreases the recrystallization rate of ice crystals, leading to slower ice crystal growth and potentially reducing the meltdown rate (Fernández et al., 2007; Regand & Goff, 2003). Previous studies have suggested that the presence of milk protein can enhance the strength of the cryo-gel formed by locust bean gum (Patmore et al., 2003), which may help to slow down the melting process by retaining the liquid within the gel network.

2.4.4 Other ice cream meltdown analyses

The ice cream meltdown test is one of the most common tests in the literature due to its convenience and low-cost operation. In addition to the meltdown test, researchers have also used various techniques to analyze the phase transition of ice cream to better characterize the microstructure, and provide additional information.

2.4.4.1 Rheology

Dynamic rheological measurement can be used for the characterization of structure in food foam (Smith et al., 2000). The structural rigidity, scoopability, and creaminess of ice cream are correlated with storage and loss moduli at different temperature ranges by running the oscillatory thermo-rheometry (OTR) test (Wildmoser et al., 2004). The oscillation test measured between -20 and 10˚C can be divided into three zones (**Figure 2.7**):

- *Zone I*: the lower temperature range between -20 and -10˚C. Storage modulus decreases as temperature increases on account of the reduction in ice fraction. The rheological property in this region is associated with the rigidity and scoopability of ice cream from the sensory aspect.
- *Zone II*: the temperature range between -10 to 0˚C. Both storage and loss moduli dramatically decrease due to the ice crystal melting. The steeper slope is correlated with a more prominent sensory coldness.
- *Zone III*: the higher temperature range between 0 to 10˚C. All ice crystals have melted and the storage and loss moduli are governed by the air phase and the fat phase. The incorporation of air and the formation of the fat aggregates contribute to an increase in loss modulus, which is correlated with the sensory creaminess of ice cream.

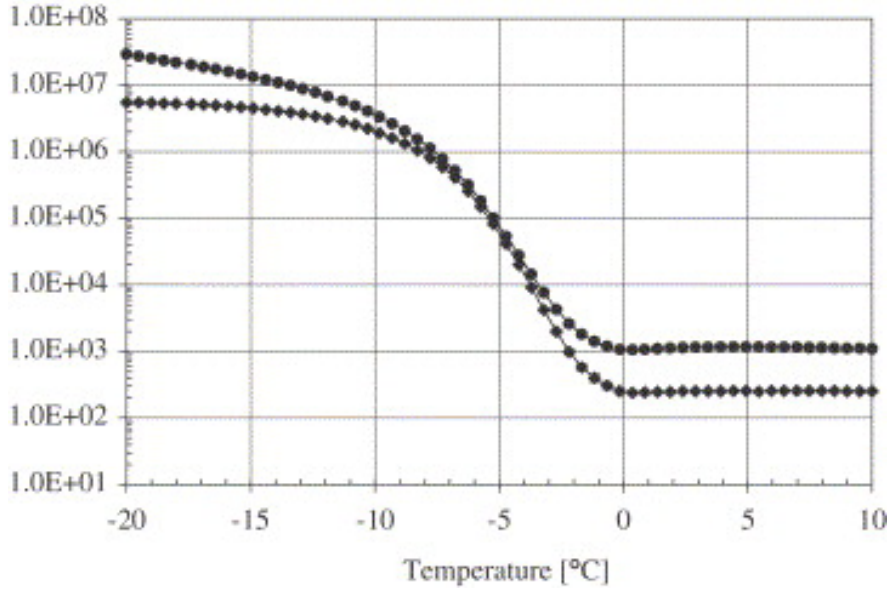

Figure 2.7 The storage (circles) and loss (diamonds) moduli behavior of ice cream in the OTR measurement (from Wildmoser et al., 2004).

2.4.4.2 Differential scanning calorimetry

Differential scanning calorimetry (DSC) is a potent tool to characterize the thermal property of food products. Particularly, it has been widely used to determine the glass transition, ice fraction, the amount of unfrozen water, and melting enthalpy in ice cream (Hwang et al., 2009; Jardines et al., 2018; Yan et al., 2021).

Glass transition temperature (T_g) indirectly indicates the thermodynamic stability of ice cream. Ice cream is in a rubbery state at temperatures above T_g, where greater mobility of molecules is achieved causing less stability of the sample. Below T_g, ice cream is in a glassy state with limited water diffusion activity, and its stability is dominant by the viscosity. Water content, the concentration of the serum phase, the molecular weight of solutes, and the cooling rate can all affect the glass transition (Hagiwara & Hartel, 1996).

Ice fraction and the amount of unfrozen water calculated from DSC can estimate the ice formation and crystallization. Sample with a higher amount of unfrozen water tends to form larger crystals and higher ice volume. The enthalpy of the ice-melting transition is also found to have a positive relationship with the amount of freezable water in the sample, and the sample with the decreased amount of freezable water shows a faster melting rate (Hwang et al., 2009).

2.4.4.3 X-ray microtomography

X-ray tomography is an imaging tool to visually observe a three-dimensional structural evolution of ice cream during heat fluctuations, which is not easy to achieve by conducting the meltdown test. Beyond that, it can track the evolution of ice crystals and air bubbles respectively (**Figure 2.8**). Interestingly, the air bubbles are in the rugged shape at -14˚C, and the interface does not relax during the measurement, which infers the Ostwald ripening driven by surface tension

may not play an important role at a cold temperature storage condition (Pinzer et al., 2012). This inference could not be drawn without this novel analysis technique.

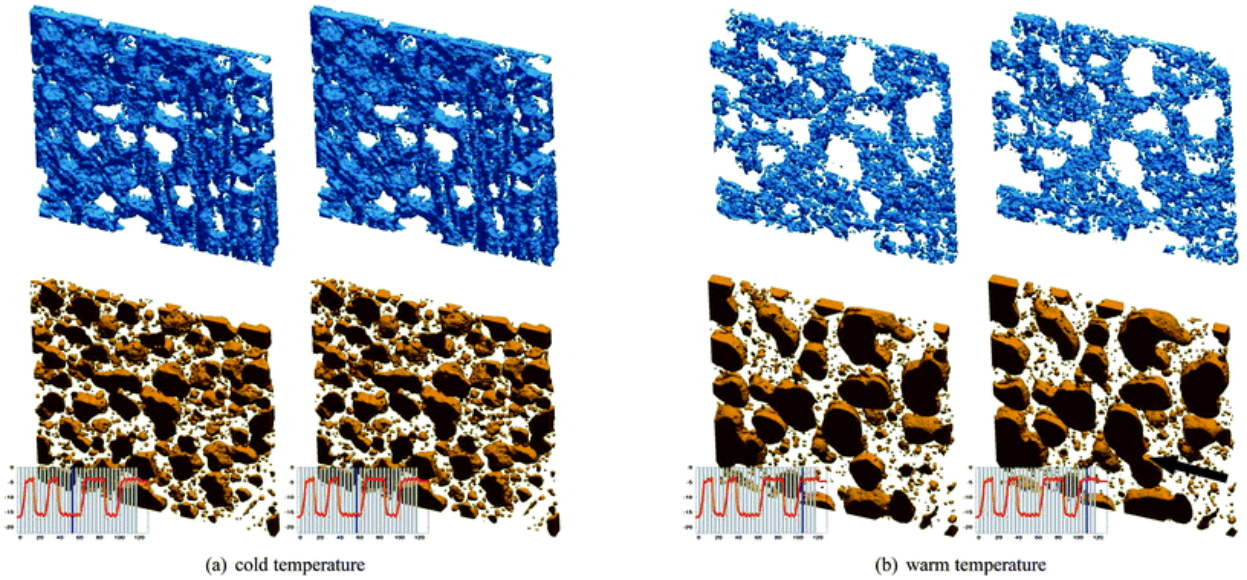

Figure 2.8 Three-dimensional computational rendering of ice phase (top) and air phase (bottom) at cold (-16˚C) and warm (-4˚C) temperature. The black arrow at (b) showed where the coalescence between two air bubbles happened (from Pinzer et al., 2012).

2.4.4.4 Laser speckles

Laser speckle is a novel tool to investigate structural change during phase transition and has been rarely applied to the food field. The first attempt to perform the laser speckle technique to monitor ice cream surface deformation and activity was conducted by Silva et al. (2010). A laser beam illuminates the ice cream surface and the intensity momentum as the function of time is

collected by a detector. The deformation and surface activity are indicated by calculating the inertia moment during the 50-minute meltdown. High inertia moment indicates fast activity or deformation on the ice cream surface. When ice cream melts at 20˚C or 25˚C, two peaks occur in the inertia moment versus time graph. The first peak is related to the dispersed ice crystal melting when warming up ice cream and the second peak correlates to the migration of air cells. Ice cream melted at 30˚C results in random peaks instead of two peaks, which is possibly explained by the thermal effects (**Figure 2.9**). As an efficient and simple method, it is promising to use laser speckles to track the particle motion of the ice cream during melting by comparing the speckle pattern at a given time interval.

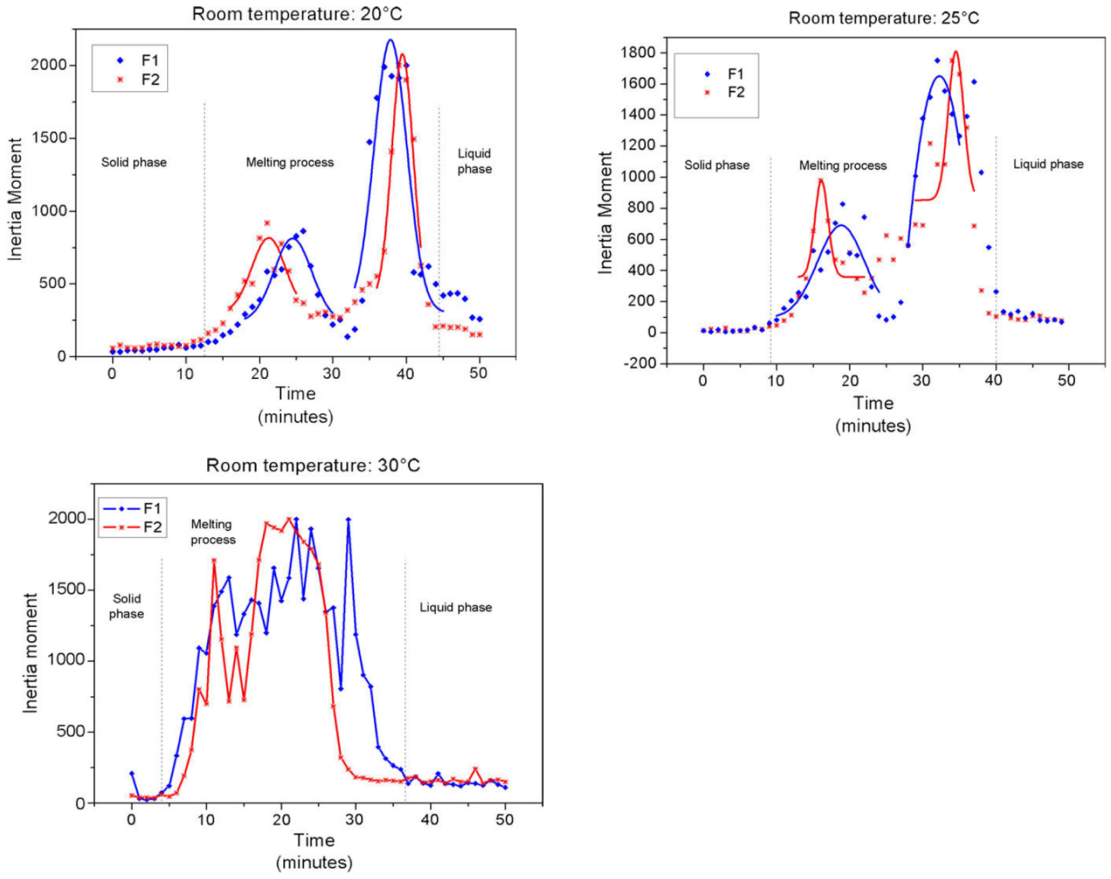

Figure 2.9 Performing laser speckle acquisitions to understand the inertia moment change during the ice cream meltdown process at different temperature (from Silva et al., 2010).

2.5 Summary

The melting properties of ice cream can provide additional information of ice cream such as thermal properties, heat resistance, and foam stability. Given lots of attempts on studying meltdown with different techniques, the meltdown test is still one of the most widely used tests in ice cream research. It is not only important to understand how the structural elements affect melting rate and melting behavior, but what is more crucial and needs more research is to understand the interaction between phases and interaction between particles during melting and liquid flowing.

3. Materials and methods

The materials and methods section are divided into four parts, corresponding to the four studies conducted in this research. Section **3.1** discussed the materials and methods employed to investigate the impact of structural components (fat destabilization, overrun, and mix viscosity) on the overall ice cream meltdown behavior. In section **3.2** and **3.3**, model systems were designed to examine the influence of rheological properties of mix on the meltdown process. The analytical methods used to measure the rheological properties of the mix, the analysis of structural components such as ice and air, as well as meltdown test, are outlined in sections **3.2** and **3.3**. Section **3.4** provided an overview of the analytical methods employed for understanding the role of phase separation between hydrocolloids and milk protein, and structural elements on meltdown of frozen desserts.

3.1 Effect of overrun, fat destabilization, and ice cream mix viscosity on the entire meltdown behavior

This section outlines the materials and methods employed for the effects of ice cream structural components on meltdown. A 3x3x3 factorial experiment was designed to achieve a wide range of microstructures in the ice cream. The analysis methods, including fat destabilization, mix viscosity, and meltdown test, were discussed in detail.

3.1.1 Materials

Cream, sugar (United Sugars, Edina, MN, USA), and nonfat dry milk (Dairy America, Fresno, CA, USA) were purchased from the dairy plant at the University of Wisconsin-Madison (Madison, WI, USA). Germantown Premium I.C blended stabilizers in a combination of locust

bean gum, guar gum, and carrageenan, as well as Grinsted® mono- and diglyceride (MDG) were purchased from Danisco USA (New Century, KS, USA). Avapol™ 80K sorbitan Ester (Polysorbate 80/PS80) was acquired from Avatar® (University Park, IL, USA).

3.1.2 Experimental design

Ice cream mix was made with 12% milk fat, 16.9% sucrose, 11.3% milk solids nonfat, and 0.15% MDG consistently throughout different formulations. A 3×3×3 factorial design was conducted on three levels of blended stabilizer, polysorbate 80, and overrun to achieve a broad range of microstructure (**Table 3.1**). Stabilizer and polysorbate 80 were added to the base mix. The ice cream mix had approximately 41% total solids and the freezing point was -2.76 ± 0.06˚C.

Table 3.1 The 3x3 factorial design of ice cream with three levels of stabilizer, polysorbate 80 and overrun.

Stabilizer	Polysorbate 80	Overrun
0.0%	0.000%	50%
0.2%	0.015%	75%
0.4%	0.030%	100%

3.1.3 Ice cream making process

Dry and liquid ingredients were mixed, blended, and heated to 85˚C in a batch-jacketed pasteurization Stephan Mixer (Stephan Food Processing Machinery, Hamelin, Germany), followed by the homogenization process. Pasteurized mix went through a two-stage homogenizer (Manton-Gaulin MFG, Co. Inc., Everett, MA, USA). The homogenized ice cream mix was later transferred back to the Stephan Mixer to cool to 10˚C. The ice cream mix was aged at 4˚C for 24hr.

Ice cream mix was frozen in a Hoyer Frigus KF 80 F continuous freezer (Tetra Pak Hoyer Inc., Aarhus, Denmark). The Hoyer freezer was manipulated in manual mode to control the processing parameter for the experimental design. The pump ratio was set to 1 to have the same residence time in the barrel for all ice cream mix, and the air system was set to 2, 3, and 4 gal/hr to reach the target overrun of 50%, 75%, and 100%, respectively. The dasher speed was set at 500 RPM and the draw temperature was targeted at -6˚C. Ice cream was collected in 473.2 ml containers, stored in a small blast freezer at -29˚C for 1 hr and then transferred to a walk-in freezer at -29˚C for further storage. Ice cream samples were made in duplicate, and all samples mixed were made and frozen in random order.

3.1.4 Analyses

3.1.4.1 Overrun

The measurement of overrun involved separately weighing the ice cream mix and ice cream in a fixed-volume container (around 177.4 mL). For each batch, the overrun was taken every other sample throughout the ice cream production, controlling the error within ±3%. Overrun measurement was carried out in triplicate.

3.1.4.2 Meltdown test

The method of the ice cream meltdown test was described by Bolliger et al. (2000) and the method of drip-through rate calculation was described by Koxholt et al. (2001). Ice cream containers were placed in the -20˚C freezer to temper for 24 hr before conducting the meltdown test at ambient temperature (22 ± 1˚C). An 80 g slice of ice cream (with approximately 8.0 cm diameter) was cut in the middle of the pint-size container and placed on a wire mesh (3 holes/cm).

Samples with higher overrun had increased volume due to the lower density. A beaker was placed on a scale underneath the ice cream to collect the drip-through part. The time when the first drop dripped was recorded as the induction time. The weight of the drip-through part was recorded every 5 min for 360 min. Height (in cm) was recorded by ruler every 5 min in the first 120 min and at the end of the meltdown test. The meltdown test was carried out in triplicate.

3.1.4.3 Partially coalesced milkfat size distribution

Milkfat particle size distribution was measured by Malvern Mastersizer 2000 (Malvern Instruments Ltd., Worcestershire, United Kingdom), which uses light scattering to determine the relative volume in each size increment. Samples of melted ice cream and ice cream mix were stored at 4˚C before measurement. Two to four drops of the sample were added to the chamber for dilution and measurement. Milkfat was the dispersed phase with a refractive index set to 1.47 and absorbance set to 0.01. Deionized water was used as a dispersant with a 1.33 refractive index, and the measurement was conducted within the range of 13% to 15% obscuration values. The size distribution of the ice cream mix was used to compare with the melted ice cream curve to determine the extent of partial coalescence, which was calculated as the ratio of the third peak volume in melted ice cream to the initial emulsion peak (the second peak) in the ice cream mix (Warren & Hartel, 2018). In addition, images were taken through optical microscopy to further confirm the fat destabilization extent. Fat destabilization measurement was carried out in triplicate.

3.1.4.4 Mix viscosity

Ice cream mix viscosity was measured by a Discovery DHR-2 hybrid rheometer (TA Instrument, New Castle, DE, USA) with cup and bob geometry as described by Amador et al. (2017). Ice cream mix was loaded in the temperature-controlled cell to equilibrate to 0˚C. Flow sweep test was conducted from 100 to 1 s^{-1} shear rate and the apparent viscosity at 50 s^{-1} shear rate in the curve was selected to represent mix viscosity. The flow sweep test and the calculated apparent viscosity at 50 s^{-1} were carried out in triplicate.

3.1.4.5 Ice crystal size distribution

A refrigerated glove box was used for ice crystal size analysis as described by Donhowe et al. (1991). A light microscope (model FX-35DX, Nikon, Inc., Garden City, NY, USA) was set inside the glove box at -15˚C for image capture. After samples were tempered to equilibrate at -15˚C, a thin slice of ice cream was loaded on a chilled cover slide. Ice crystals were spread out by gently tapping the cover slide with chilled tweezers. Ice crystal images were taken at 40× magnification to obtain 300 to 400 ice crystals per container and traced by using Microsoft Softonic Paintbrush. The traced images were analyzed by using Image Pro Plus software (Version 7.0, Media Cybernetics, Inc., Rockville, MD, USA) and results were gathered in the Microsoft Excel software. Ice crystal size measurement was carried out in triplicate.

3.1.4.6 Air cell size distribution

A method of measuring air cell size by using the same refrigerated glove box mentioned above was described by Chang and Hartel (2002). The ice cream sample was placed in the glove box for 30 min for tempering at -15˚C. To analyze, a small ice cream slice was scooped from the

center of the sample by a chilled metal spatula and loaded on a glass slide. The ice cream slice was placed in a well (roughly 100 to 200 μm depth) created by two glued cover slides (25 × 25 mm). Then, the temperature was adjusted to -6˚C to allow the air cells to rise to the top of the slice. Approximately, six images were captured by the light microscope at 40× magnification to obtain 300 to 400 air cells per container. The air cells were traced manually, sizes were calculated by Image Pro Plus software, and the results were gathered in Microsoft Excel software. Air cell size measurement was carried out in triplicate.

3.1.4.7 Statistical analyses

Data analysis was performed on JMP Pro 13.0 software (SAS, Cary, NC, USA). The effects of the respective variables on the ice cream meltdown response were determined by performing one-way ANOVA and Tukey's HSD tests ($\alpha<0.05$). The correlations between the variables and responses were determined by performing multivariate analysis.

3.2 Effect of apparent mix viscosity and flow index on meltdown in the non-aerated frozen sucrose model system

In this section, a 30% sucrose model system was developed, along with seven hydrocolloid formulations, to manipulate rheological properties such as apparent viscosity and shear-thinning behavior, referred to as flow rate index.

3.2.1 Materials

Granulated sucrose was purchased from Domino Foods (Domino Foods, Yonkers, NY, USA). Xanthan, pectin, guar gum, locust bean gum, and sodium alginate used as stabilizers were donated by Ingredion (Ingredion, Westchester, IL, USA).

3.2.2 Experimental design

To study apparent mix viscosity and flow index separately, two experiments were designed, one with the same apparent mix viscosity and the other with the same flow index. Sucrose was added to both systems to match the freezing point in the ice cream. **Table 3.2** and **Table 3.3** show the formulations of the 30% sucrose model system with three levels of apparent mix viscosity and four levels of flow rate index. The flow rate index was calculated from the power law equation shown below:

$$\tau = K\gamma^n \qquad 3\text{-}1$$

where τ is shear stress, K is the consistency factor, γ is the shear rate, and n is the flow rate index.

Table 3.2 Same flow index where the flow index was controlled within the range of 0.74 ± 0.01

Sample	Apparent viscosity at 5 s^{-1} (Pa•s)*
0.22% guar gum (GG)	0.10 ± 0.00^{a}
0.3% locust bean gum (LBG)	0.15 ± 0.00^{b}
0.3% sodium alginate (SA)	0.26 ± 0.00^{c}

* Tukey's HSD test was performed for the significant difference at $P<0.05$
$^{a, b, c}$ denote significant differences among samples with different hydrocolloids

Table 3.3 Same apparent viscosity at 5 s^{-1} shear rate, where the apparent mix viscosity was controlled in the range of 0.19 ± 0.01 Pa•s

Sample	Flow rate index*
0.11% xanthan (XAN)	0.47 ± 0.00^{a}
0.28% guar gum (GG)	0.66 ± 0.00^{b}
0.25% sodium alginate (SA)	0.76 ± 0.00^{c}
0.7% pectin (PEC)	0.86 ± 0.01^{d}

* Tukey's HSD test was performed for the significant difference at $P<0.05$
$^{a, b, c, d}$ denote significant differences among samples with different hydrocolloids

3.2.3 Preparation of non-aerated frozen sucrose system

Sucrose and stabilizers were mixed with deionized water and vigorously stirred on a stirrer/hot plate (Corning, NY USA) for 20 min to break up any large particles. The solution was heated to 70˚C to fully dissolve and hydrate, then cooled down to room temperature, and stored at 4˚C overnight. The solution was subsequently frozen using the Musso L2 ice cream maker (Musso S.R.L., Mortara, Italy) at a draw temperature of -6˚C. The frozen sample was transferred to 177.4 mL containers and stored in a freezer at -20˚C for further analysis. Samples were prepared in triplicate.

3.2.4 Preparation of unfrozen phase solution

The formulation of the unfrozen phase solution was designed with the assumption that 80% of the water in the frozen sample would undergo conversion to ice at -20°C, as determined by the freezing curve (Goff & Hartel, 2013). To achieve this, 80% of the water was removed from the model system before mixing. Sucrose and hydrocolloids were fully mixed before being added to the remaining water. The mixture was stirred at a 300 RPM shear rate using an overhead stirrer (Reliance Motion Control INC, OH, USA) to ensure fully hydration and heated to 70°C. The

sample was then cooled to room temperature and stored at 4˚C overnight for rheological analysis. Samples were prepared in triplicate.

3.2.5 Freezing point

The freezing point was determined using an osmometer model 3250 (Advanced Instruments, Norwood, MA, USA). A standard curve correlating the freezing point with osmolality was constructed using a known osmolality standard solution. The sample tube, coated with 3 mg of talcum powder, was loaded with a 25 µl sample solution and inserted into the osmometer. The osmolality of the sample was measured by the instrument, and the corresponding freezing point was determined using the standard curve. The freezing point was measured in triplicate.

3.2.6 Surface tension

To determine the surface tension of the sample solution at the air-water interface, pendant drop tensiometry was conducted using the Kruss DSA 30R Drop Shape Analyzer (Kruss, Hamburg, Germany). Samples were tempered to room temperature (22 ± 1˚C) prior to the measurements. A 20 µl of droplet was suspended for 2 hr at the tip of the capillary needle inside a closed humid cuvette to minimize evaporation. The contour of the droplet was analyzed using the Young-Laplace equation to calculate the surface tension using the ADVANCE software. The surface tension measurement was taken in triplicate.

3.2.7 Ice crystal size analysis

To capture ice crystal images, an optical microscope (Accu-Scope 3000-LED Microscope, Microscope Central, Feasterville, PA, USA) was installed in a refrigerated glove box set at -15˚C.

The sample was equilibrated at -15˚C in the glove box, and a thin layer of frozen sample was placed on a glass slide, dispersed by 1:1 kerosene: pentanol solution, and covered with a cover glass. Images were captured at 40X magnification to obtain 300 to 400 ice crystals for tracing and analysis. The ice crystal size measurement was taken in triplicate.

3.2.8 Overrun

The overrun of the sample was determined by calculating the difference in weight between the solution and frozen sample in a fixed container using the following equation:

$$Overrun\ (\%) = \frac{m_{mix} - m_{frozen}}{m_{frozen}} \times 100\% \qquad 3\text{-}2$$

where m_{mix} is the mass of the model solution, and m_{frozen} is the mass of the frozen sample. The overrun was measured in triplicate.

3.2.9 Meltdown test

The meltdown test was conducted at room temperature (22 ± 1˚C). The sample with same volume (around 177.4 cm^3) was directly taken out of the -20˚C freezer, carefully removed from its packaging, and placed on a wire mesh screen (3 holes/cm). A beaker was placed underneath the screen on a scale to collect the melting liquid portion, and its mass was recorded by the scale every 5 min for 150 min. The time when the first melted liquid dripped through the mesh was recorded as the induction time. The meltdown curve was constructed, and the melting rate was calculated from the slope on the linear-melting phase of the curve. Meltdown test was conducted in triplicate.

3.2.10 Rheology

The rheological properties were measured using a Discovery DHR-2 hybrid rheometer (TA Instrument, New Castle, DE, USA) with a cup and bob geometry. The rheological test was performed to select the hydrocolloids with same flow rate index or same apparent viscosity in both set of experiments. The solution was injected into the cup and measured at 0˚C. Flow sweep test was conducted from 100 to 1 s^{-1} shear rate, and apparent viscosity at 5 s^{-1} shear rate was selected as solution viscosity to better represent the gravity drainage. The power law model was applied to fit the shear stress curve and determine the flow rate index.

The same rheometer as mentioned in the previous paragraph was used to measure the apparent viscosity and viscoelastic properties of the unfrozen phase system, with parallel plate (40mm diameter) geometry. Both tests were conducted at -19.6˚C to measure the rheological properties without freezing the samples. A flow sweep test was performed from 100 to 1 s^{-1} shear rate, and the apparent viscosity at 5 s^{-1} shear rate was selected. To generate other rheological properties, such as the flow rate index, yield stress, and consistency, the Herschel-Bulkley model shown below (equation 3-3) was selected.

$$\tau = \tau_0 + k\dot{\gamma}^n \qquad 3\text{-}3$$

where τ is shear stress, τ_0 is the yield stress, k is the consistency factor, $\dot{\gamma}$ is the shear rate, and n is the flow rate index. In addition, a frequency sweep test was conducted at 1% strain, with an angular frequency range of 0.5 to 100 rad/s.

3.2.11 Statistical analyses

Data analysis was conducted using JMP Pro 15.0 software (SAS, Cary, NC, USA). ANOVA and Tukey's HSD tests ($\alpha<0.05$) were performed to compare surface tension, rheological properties, ice crystal size, and meltdown parameters across conditions. Multivariate analysis was conducted to assess the correlations between variables and responses.

3.3 Effect of apparent mix viscosity and flow index on meltdown in the aerated frozen sucrose system

In this section, air was introduced into the system to examine the impact of rheological properties on meltdown in the aerated frozen sucrose system. The materials, sample preparation, and analytical measurements, including rheological properties, structural component analysis, and meltdown test, were discussed.

3.3.1 Materials

Granulated sucrose was acquired from Domino Foods (Domino Foods, Yonkers, NY, USA). Xanthan and guar gum were donated by Ingredion (Ingredion, Westchester, IL, USA). Avapol^{TM} 80K sorbitan ester (Polysorbate 80) was obtained from Avatar® (University Park, IL, USA).

3.3.2 Experimental design

Two experiments were designed to study the effect of apparent viscosity and flow rate index in the aerated frozen sucrose system. Polysorbate 80 was added to better incorporate air

during the freezing process. Two levels of polysorbate 80 were selected to achieve two overrun levels. The experimental design was shown in **Table 3.4**.

Table 3.4 The experimental design with the same flow rate index (0.75±0.01) and the same apparent viscosity at 5 s^{-1} (0.19±0.01 Pa•s).

Control factor	Sample	Polysorbate 80 in the system (%)	Target overrun	Flow index	Apparent viscosity at 5 s^{-1} shear rate
Same flow rate index	0.014% xanthan	0.04	45%	0.76 ± 0.01	0.02 ± 0.00
		0.15	75%	0.76 ± 0.01	0.02 ± 0.00
	0.22% guar gum	0.04	45%	0.74 ± 0.00	0.10 ± 0.00
		0.15	75%	0.74 ± 0.00	0.10 ± 0.00
Same apparent viscosity	0.11% xanthan	0.04	45%	0.47 ± 0.00	0.20 ± 0.00
		0.15	75%	0.47 ± 0.00	0.20 ± 0.00
	0.28% guar gum	0.04	45%	0.67 ± 0.00	0.18 ± 0.00
		0.15	75%	0.67 ± 0.00	0.19 ± 0.00

3.3.3 Preparation of aerated frozen sucrose system

Sucrose, stabilizers, and polysorbate 80 were mixed with deionized water and stirred vigorously on a stirrer/hot plate (Corning, NY USA) for 20 min to break up any large particles. The solution was then heated to 70˚C to fully dissolve and hydrate, followed by cooling down to room temperature. The solution was stored at 4˚C overnight. All solutions were frozen in the Musso L2 ice cream maker (Musso S.R.L., Mortara, Italy) at -5˚C draw temperature to reach the target overrun. For samples containing 0.014% xanthan, freezing was conducted at -6˚C to reach the target overrun. The frozen samples were filled into 177.4 mL containers and placed in a -20˚C freezer for further analysis. Samples were prepared in triplicate.

3.3.4 Freezing point

The freezing point was measured using an osmometer model 3250 (Advanced Instruments, Norwood, MA, USA). A standard curve correlating osmolality with the corresponding freezing point was created using a known osmolality standard solution. To measure the freezing point, a 25µl sample of the solution was injected into a sample tube that was coated with 3 mg of talcum powder. The osmolality was recorded, and the freezing point was calculated using the standard curve. The freezing point was measured in triplicate.

3.3.5 Rheology

The apparent viscosity for the solution was measured by a Discovery DHR-2 hybrid rheometer (TA Instrument, New Castle, DE, USA) with a cup and bob geometry. The solution was injected into the cup and measured at 0˚C. Flow sweep test was performed from 100 to 1 s^{-1} shear rate and apparent viscosity at 5 s^{-1} shear rate was selected to represent solution apparent viscosity. The power law model was fit with the shear stress curve to obtain the flow rate index. The rheological measurement was measured in triplicate.

3.3.6 Surface tension

Pendant drop tensiometry was used to measure surface tension with the Kruss DSA 30R Drop Shape Analyzer (Kruss, Hamburg, Germany). Samples were equilibrated to room temperature (22 ± 1˚C) before measurements were taken. A 12 µl droplet was suspended from the tip of the capillary needle for 30 min and placed into a closed humid cuvette to minimize evaporation. The droplet contour was analyzed using the Young-Laplace equation, and the surface tension was calculated by ADVANCE software. The surface tension was measured in triplicate.

3.3.7 Surface dilatational rheology

Surface dilatational rheology was measured using the same drop shape analyzer mentioned previously. An amplitude sweep was carried out from 1.5% to 40% at a frequency of 0.1 Hz. A frequency sweep was performed from 0.01 to 0.1 Hz on a logarithmic scale at an amplitude of 35% in order to achieve a 2-3% area change. The viscoelastic modulus obtained from the frequency sweep test was plotted as a function of frequency on a double logarithmic scale, and the slope of the curve was calculated to determine the interfacial viscoelasticity. The surface dilatational rheology was measured in triplicate.

3.3.8 Meltdown test

The melting test was conducted under controlled humidity conditions of 33% RH at room temperature (22 ± 1˚C) in a sealed chamber. Frozen samples with same volume (around 177.4 cm^3) were taken out of the -20˚C freezer, carefully removed from their packages, and placed on a wire mesh screen with 3 holes/cm. A beaker was positioned beneath the screen on a scale to collect the melted liquid, and its mass was recorded every 5 min for 120 min. The time when the first liquid melted and dripped through the mesh was noted as the induction time. A melting curve was constructed, and the melting rate was calculated from the slope during the linear-melting phase. The meltdown test was conducted in triplicate.

3.3.9 Ice crystal size analysis

To capture images of ice crystals, an optical microscope (Accu-Scope 3000-LED Microscope, Microscope Central, Feasterville, PA, USA) was installed in a refrigerated glove box set at -15°C. The sample was equilibrated at -15°C in the glove box, and a thin layer of frozen

sample was placed on a glass slide, dispersed with a 1:1 kerosene:pentanol solution, and covered with a cover glass. Images were captured at 10X magnification instead of 40X in section **3.2** to obtain large ice crystals that were out of view under 40X magnification. Images were traced and analyzed using Image Pro Plus software (Media Cybernetics, Inc., Rockville, MD, USA). Ice crystal analysis was carried out in replicate.

3.3.10 Air cell size analysis

The same optical microscope mentioned above was used to capture images of air cells in the refrigerated glove box. The sample was tempered at -15˚C for 30 min in the glove box. A small slice was then scooped from the center of the sample using a chilled metal spatula and placed onto a glass slide. The sample was loaded into a well created by two glued cover slides (25x25 mm) with a depth of roughly 100-200 μm, and covered by the cover slide. The temperature was then adjusted to -6˚C to allow the air cells to rise to the top of the slice. Images were captured at 10X magnification to obtain 300 to 400 air cells for tracing and analysis. Air cell analysis was carried out in replicate.

3.3.11 Statistical analyses

Data analysis was conducted using JMP Pro 15.0 software (SAS, Cary, NC, USA). One-way ANOVA and Tukey's HSD tests ($\alpha<0.05$) were performed to compare surface tension, rheological properties, interfacial rheological properties, and meltdown parameters across conditions. Multivariate analysis was conducted to assess the correlations between variables and responses.

3.4 Effect of milk protein-galactomannans interaction on meltdown in the aerated frozen sucrose system

In this section, the study focused on investigating the interaction between milk protein and hydrocolloids in relation to meltdown. The materials, sample preparations, and analytical methods, including phase separation analysis, frozen sample structural component analysis, and meltdown test, were outlined.

3.4.1 Materials

Granulated sucrose was purchased from Domino Foods (Domino Foods, Yonkers, NY, USA). Guar gum, locust bean gum, and κ-carrageenan, used as stabilizers, were donated by Ingredion (Ingredion, Westchester, IL, USA). High-heat nonfat dry milk was purchased from Associated Milk Producers, Inc (New Ulm, MN, USA). Rhodamine B was purchased from Santa Cruz Biotechnology, Inc (Dallas, TX, USA). Sodium azide was purchased from Sigma-Aldrich Co. LLC (St. Louis, MO, USA).

3.4.2 Experimental design

The experimental design is shown in **Table 3.5**, where two typical galactomannans, guar gum and locust bean gum, were selected to investigate the interaction between milk protein and galactomannans during the meltdown of ice cream. The study involved three levels of milk protein content (4%, 6%, and 8%) and two levels of galactomannans (0.05% and 0.15%) to create systems with and without phase separation behavior. Additionally, κ-carrageenan, a commonly used polysaccharide in ice cream to prevent phase separation, was included in all the systems to explore

its effect on phase separation and meltdown. The sucrose content was adjusted in different protein content systems to achieve the same freezing point at -2.7˚C.

3.4.3 Sample preparation

Sucrose, hydrocolloids, and nonfat dry milk were vigorously mixed with deionized water on a hot plate (Corning, NY USA) for 30 min to break up any large particles. The solution was then heated to 83˚C (the temperature required to dissolve κ-carrageenan) to ensure complete dissolution and hydration of any hydrocolloids. Afterward, the solution was cooled down to room temperature and stored at 4˚C overnight. All solutions were frozen using the Musso L2 ice cream maker (Musso S.R.L., Mortara, Italy) at a constant shear rate of 108 RPM and a draw temperature of -6˚C. The frozen samples were filled into 177.4 mL containers and placed in a -20˚C freezer for further analysis. Samples were prepared in triplicate.

3.4.4 Rheology

The mix apparent viscosity was determined using a cup and bob geometry on a Discovery DHR-2 hybrid rheometer (TA Instrument, New Castle, DE, USA). The measurement was conducted at 0˚C after injecting the solution into the cup. A flow sweep test was conducted across shear rates ranging from 100 to 1 s^{-1}, and the apparent viscosity at a shear rate of 5 s^{-1} was chosen as the representative viscosity value. The power law model was then applied to fit the shear stress curve and obtain the flow rate index and consistency. The rheological properties were measured in triplicate.

Table 3.5 Experimental design of samples with three levels of protein content, two levels of galactomannans and with and without κ-carrageenan. NFDM: nonfat dry milk; LBG: locust bean gum; GG: guar gum.

	NFDM	Sucrose	LBG	GG	κ-carrageenan	Water
4% protein						
0.05% LBG	11.06	20.76	0.05		0	68.13
0.15% LBG	11.06	20.76	0.15		0	68.03
0.05% GG	11.06	20.76		0.05	0	68.13
0.15% GG	11.06	20.76		0.15	0	68.03
4% protein with κ-carrageenan						
0.05% LBG	11.06	20.76	0.05		0.015	68.12
0.15% LBG	11.06	20.76	0.15		0.015	68.02
0.05% GG	11.06	20.76		0.05	0.015	68.12
0.15% GG	11.06	20.76		0.15	0.015	68.02
6% protein						
0.05% LBG	16.59	15.84	0.05		0	67.52
0.15% LBG	16.59	15.84	0.15		0	67.42
0.05% GG	16.59	15.84		0.05	0	67.52
0.15% GG	16.59	15.84		0.15	0	67.42
6% protein with κ-carrageenan						
0.05% LBG	16.59	15.84	0.05		0.015	67.51
0.15% LBG	16.59	15.84	0.15		0.015	67.41
0.05% GG	16.59	15.84		0.05	0.015	67.51
0.15% GG	16.59	15.84		0.15	0.015	67.41
8% protein						
0.05% LBG	22.12	10.90	0.05		0	66.93
0.15% LBG	22.12	10.90	0.15		0	66.83
0.05% GG	22.12	10.90		0.05	0	66.93
0.15% GG	22.12	10.90		0.15	0	66.83
8% protein with κ-carrageenan						
0.05% LBG	22.12	10.90	0.05		0.015	66.92
0.15% LBG	22.12	10.90	0.15		0.015	66.82
0.05% GG	22.12	10.90		0.05	0.015	66.92
0.15% GG	22.12	10.90		0.15	0.015	66.82

3.4.5 Particle size analysis

The particle size distribution of milk protein was determined using the Malvern Mastersizer 3000 (Malvern Instruments Ltd., Worcestershire, United Kingdom), which utilizes light scattering to assess the relative volume within each size increment. To facilitate measurement, samples were added into the chamber for dilution. The test was configured with a particle refractive index of 1.456 and a dispersant refractive index, in this case deionized water, set to 1.33. Measurements were performed within the obscuration value range of 10% to 15%. The volume-weighted mean diameter ($D_{[4,3]}$) value was determined to characterize the particle size of the milk protein. Particle size analysis was carried out in triplicate.

3.4.6 Overrun

The overrun of the sample was determined by measuring the weight difference between the solution and frozen sample in a standardized container. The calculation was performed using the equation 3-2. The overrun was measured in triplicate.

3.4.7 Ice crystal size analysis

Images of ice crystals were captured using an optical microscope (Microscope Central, Feasterville, PA, USA), which was installed inside a refrigerated glove box maintained at -15°C. The frozen sample was equilibrated to -15°C within the glove box and a thin layer of the sample was carefully placed on a glass slide. To disperse the sample, a 1:1 kerosene:pentanol solution was applied, followed by covering it with a cover glass. Image capture was performed at a magnification of 10X to ensure clear visualization of larger ice crystals that might not be easily discernible at 40X magnification. A comprehensive analysis was carried out on 300 to 400 ice

crystals using Image Pro Plus software (Media Cybernetics, Inc., Rockville, MD, USA). Ice crystal analysis was carried out in replicate.

3.4.8 Air cell size analysis

Using the same optical microscope mentioned above, images of air cells in the refrigerated glove box were captured. The sample was tempered for 30 min at -15°C inside the glove box. Subsequently, a small slice was scooped from the center of the sample using a chilled metal spatula and placed onto a glass slide. The sample was loaded into a well created by two glued cover slides (25x25 mm) with a depth of approximately 100-200 μm and covered with another cover slide. The temperature was then adjusted to -6°C to allow the air cells to rise to the top of the slice. Images were captured at 10X magnification, resulting in the acquisition of 300 to 400 air cells for subsequent tracing and analysis by using Image Pro Plus software (Media Cybernetics, Inc., Rockville, MD, USA). Air cell size was measured in replicate.

3.4.9 Phase separation analyses

3.4.9.1 Microscope phase separation

Confocal laser scanning microscopy (CLSM) was employed to investigate the microscopic phase separation. Around 1.5 mL samples were stained with 10 μL of Rhodamine B dye (0.2%, w/v) to label the milk protein. Subsequently, a drop of the stained samples was transferred onto a glass slide for imaging. The observations encompassed both the overnight aging solution and the drip-through liquid collected from the beaker after the meltdown test. Confocal imaging was carried out using a Nikon A1R-Si+ confocal microscope (Nikon Instruments Inc., Melville, NY, USA). Images were captured using a 20x objective, with an excitation wavelength of 560 nm and

an emission wavelength of 595 nm. At least six images were acquired per sample for each replicate, and the representative images were presented.

3.4.10 Macroscopic phase separation

Macroscopic phase separation was observed in both the original mix and drip-through liquid after being kept at 4˚C for 7 days. To collect the drip-through liquid, care was taken to pour it without including the protein foam layer that floated above. The volume of top phase and bottom phase was recorded. The addition of sodium azide was for preservation purposes. Images were taken in replicate, and the volume was recorded in replicate.

3.4.11 Meltdown

The melting test was conducted in a sealed chamber at a controlled humidity of 33% RH and room temperature (22 ± 1˚C). Frozen samples with around 177.4 cm^3 volume (at -20˚C) were carefully removed from their packages and placed on a wire mesh screen with 3 holes/cm. A beaker was positioned below the screen on a scale to collect the melted liquid, and its mass was recorded every 5 min for 120 min. The induction time was noted as the time when the first liquid melted and dripped through the mesh. A melting curve was generated, and the melting rate was calculated from the slope during the linear-melting phase.

Images of the melted samples were obtained by scraping a slice of frozen sample onto a glass slide, covering it with a cover slide, and allowing it to sit at room temperature until the sample had completely melted on the glass slide. The samples were observed using a Nikon Eclipse FN1 microscope (Melville, NY, USA) equipped with a 20x objective. Meltdown test was conducted in triplicate and images were taken in replicate.

3.4.12 Statistical analyses

Data analysis was performed using JMP Pro 15.0 software (SAS, Cary, NC, USA). Particle size, rheological properties, overrun, and meltdown parameters were compared across conditions through one-way ANOVA and Tukey's HSD tests ($\alpha<0.05$). Furthermore, the correlations between variables and responses were assessed through multivariate analysis.

4. Results and Discussion

This dissertation aims to investigate the effects of microstructural elements on the meltdown process of ice cream and frozen desserts. Section **4.1** examined various microstructures, including overrun, fat globule clusters, and mix viscosity, to gain a better understanding of how these structural elements affect the meltdown behavior. To build up complexity, a sucrose model system was used to investigate how the addition of polysaccharides (section **4.2**), polysorbate 80 (section **4.3**), and milk proteins (section **4.4**) affect the meltdown process. In section **4.2**, the rheological properties of the system, particularly non-Newtonian behavior and apparent viscosity, altered by the polysaccharides were studied. Section **4.3** investigated the effect of air and overrun on meltdown by adding polysorbate 80 to the system. In section **4.4**, nonfat dry milk was added as a milk protein source to study the effect of milk protein-polysaccharide phase separation on the meltdown process. Ultimately, a better understanding of how the meltdown process is affected by structural elements in the absence of milk fat will be gained, and it will provide guidance for the production of low-fat or nonfat frozen desserts with good heat resistance.

4.1 The effect of ice cream microstructure on the entire meltdown behavior

To investigate the relationship between ice cream microstructure and its entire meltdown behavior, a wide range of microstructures was obtained through a series of ice cream formulations. This range varied from the weakest structure containing the least amount of air, the lowest mix viscosity, and the lowest amount of fat destabilization, to the strongest structure with the highest amount of air, the highest mix viscosity, and the highest level of fat destabilization. By covering this wide range of structural elements in ice cream, it was possible to draw a relationship between ice cream microstructure and the entire meltdown behavior.

This study utilized the meltdown curve and height change curve to comprehensively describe the meltdown behavior. Specifically, the lag phase, linear-melting phase, and stationary phase of the meltdown curve were characterized using the induction time, drip-through rate, and final drip-through weight, respectively. Additionally, the height change measured during the melting process enabled better differentiation between the two types of melting behavior.

4.1.1 Effect of stabilizer, emulsifier and overrun on ice cream microstructure

The microstructure of ice cream was manipulated by altering the amount of stabilizer, emulsifier, and overrun. Increasing the amount of stabilizer augmented the ice cream mix viscosity, affecting not only the flow properties of the ice cream serum phase but also providing higher shear force during the freezing process to alter other structural elements such as fat destabilization. Polysorbate 80 was used as an emulsifier at three levels to manipulate the extent of fat destabilization. Overrun was adjusted during freezing to incorporate air cells into the matrix. Although several studies have investigated how mix viscosity, fat destabilization, and overrun affect meltdown, few have combined all three factors to achieve a broad range of structures, as proposed in this study.

4.1.1.1 Ice cream mix viscosity

Ice cream mix viscosity is a crucial factor affecting ice cream quality, such as whipping quality, melting resistance, and smoothness. Stabilizers and other large macromolecules are added to the ice cream mix to increase the viscosity and modify the texture of the ice cream. As a thickening agent in the ice cream mix, the concentration of stabilizer plays a critical role. The solution exhibits Newtonian fluid behavior at concentrations below a specific threshold known as

the overlap concentration (C*). However, at concentrations above this threshold, the solution shows non-Newtonian behavior, with a notable increase in viscosity (Williams & Phillips, 2009). The amount of stabilizer added in this study was above the critical concentration. As a result, increasing amount of stabilizer increased apparent mix viscosity (**Figure 4.1**). As the concentration of stabilizers increase, the entanglement and interpenetration among stabilizers occurs, which leads to an increase in viscosity.

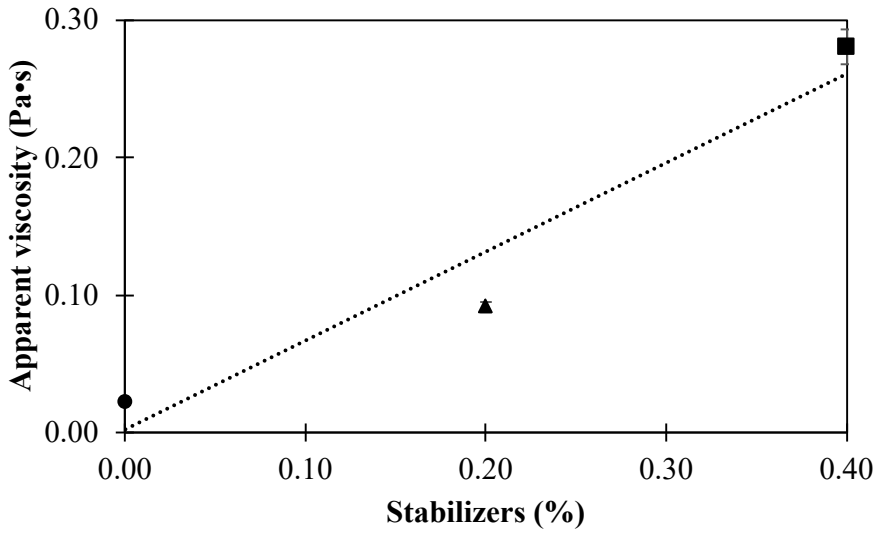

Figure 4.1 The correlation between stabilizer levels and apparent mix viscosity (at $50s^{-1}$ shear rate). The error bars refer to the standard variation among samples with different polysorbate 80 levels.

4.1.1.2 Mean ice crystal size

The mean ice crystal size fell in a narrow range from 28.5 to 38.2 μm regardless of various formulas as shown in **Table 4.1**. Even though the mean size of ice crystal varied slightly among different formulations, no specific trend was observed regardless of different levels of stabilizer, polysorbate 80, and overrun, which agrees with previous findings (Amador et al., 2017; Warren & Hartel, 2018).

Table 4.1 Mean and standard deviation of ice crystal size. The standard deviation (±) refers to the variation between duplicate mean ice crystal size of the ice cream with different stabilizers, overrun, or polysorbate 80 levels.

Mean ice crystal size (μm)*				
Stabilizer	Overrun	Polysorbate 80		
		0%	0.015%	0.03%
0%	50%	$28.5 \pm 2.9^{x,X,A}$	$33.9 \pm 0.3^{y,X,A}$	$32.3 \pm 0.8^{xy,X,A}$
	75%	$31.6 \pm 0.9^{x,X,A}$	$35.8 \pm 0.1^{y,Y,A}$	$35.4 \pm 1.0^{y,Y,A}$
	100%	$31.0 \pm 0.5^{xy,X,A}$	$33.4 \pm 1.1^{x,X,A}$	$29.8 \pm 1.7^{y,X,A}$
0.2%	50%	$31.9 \pm 0.9^{x,X,A}$	$37.7 \pm 1.3^{y,X,B}$	$33.1 \pm 0.9^{x,X,A}$
	75%	$32.6 \pm 1.9^{x,X,A}$	$38.2 \pm 0.4^{y,X,B}$	$33.2 \pm 1.8^{x,X,A}$
	100%	$32.1 \pm 0.9^{x,X,A}$	$33.0 \pm 1.2^{x,Y,A}$	$33.4 \pm 0.4^{x,X,AB}$
0.4%	50%	$32.9 \pm 0.3^{x,X,A}$	$31.9 \pm 0.4^{x,X,A}$	$37.1 \pm 1.5^{y,X,B}$
	75%	$30.7 \pm 0.6^{x,Y,A}$	$29.5 \pm 0.7^{x,Y,C}$	$35.3 \pm 1.2^{y,X,A}$
	100%	$32.0 \pm 0.6^{x,X,A}$	$37.0 \pm 0.4^{y,Z,B}$	$36.6 \pm 2.3^{y,X,B}$

* Tukey's HSD test was performed for the significant difference at $P<0.05$

$^{x, y, z}$ denote significant differences among ice cream with different polysorbate 80 levels

$^{X, Y, Z}$ denote significant differences among ice cream with different overrun levels

$^{A, B, C}$ denote significant differences among ice cream with different stabilizer levels

Overrun has been found to affect ice crystal size. An increase in overrun may result in a thinner lamella and impede the collision rate among ice crystals, leading to a decrease in the ice crystal size (Flores & Goff, 1999a). A lower heat transfer rate resulting from a higher amount of air may also lead to a difference in ice crystal size (Sofjan & Hartel, 2004). Despite these effects, the change in ice crystal size due to overrun was relatively small in this study, owing to a constant draw temperature across all samples. Examples of ice crystal size distribution and the microscope image of ice crystals of ice cream samples with three levels of overrun are shown in **Figure 4.2**.

a.

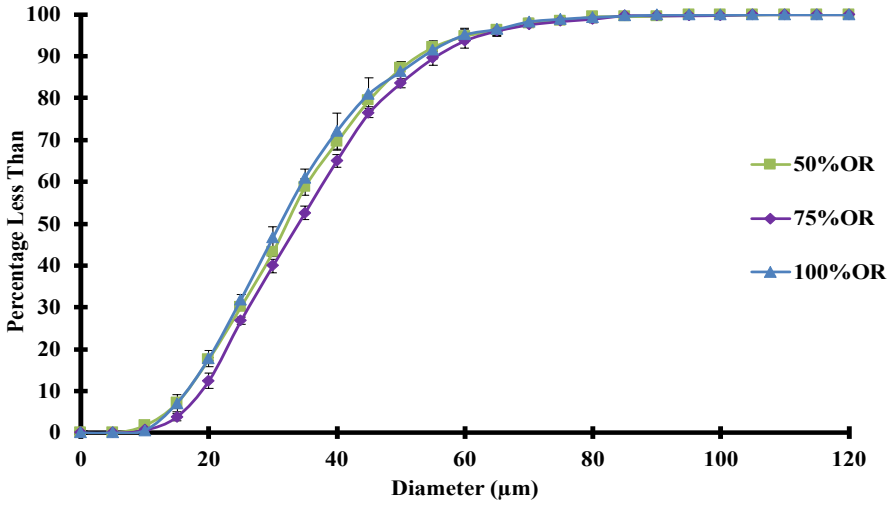

b.

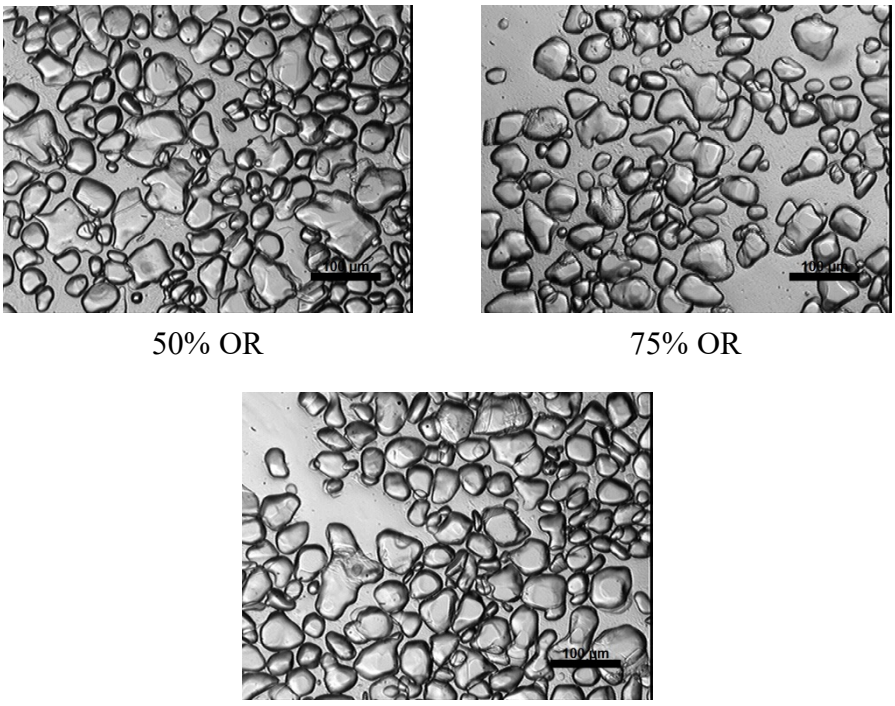

50% OR

75% OR

100% OR

Figure 4.2 Ice crystal size distribution (a) and the microscope image of ice crystals (b) of ice cream made with 0% stabilizer, 0.015% polysorbate 80 and different overrun (OR). The error bars in (a) represents the standard deviation of mean ice crystal size measured in triplicate.

Stabilizers are known to slow ice recrystallization rates and decrease changes in ice crystal size, but do not have a direct effect on initial ice crystal size (Flores & Goff, 1999a). Increased viscosity due to additional stabilizers inhibits mobility and thus minimize ice crystal coalescence or Ostwald ripening. The ability of stabilizers to reduce ice crystal size greatly depends on the type of sweetener and storage temperature. When the storage temperature is set at -30˚C, ice crystal size distribution does not differ between ice cream with and without stabilizers (Flores & Goff, 1999b). In this study, ice creams were stored at -29˚C prior to ice crystal analysis to prevent any structure change caused by temperature fluctuation. As a result, no significant difference in the ice crystal size caused by the stabilizers was found among all the samples (**Table 4.1**). Examples of ice crystal size distribution and the microscope image of ice crystals of ice cream samples with three levels of stabilizer are shown in **Figure 4.3**.

a.

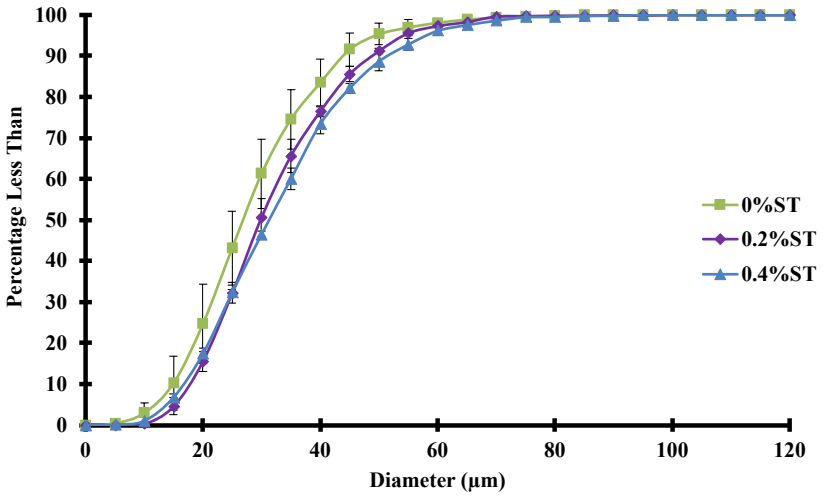

b.

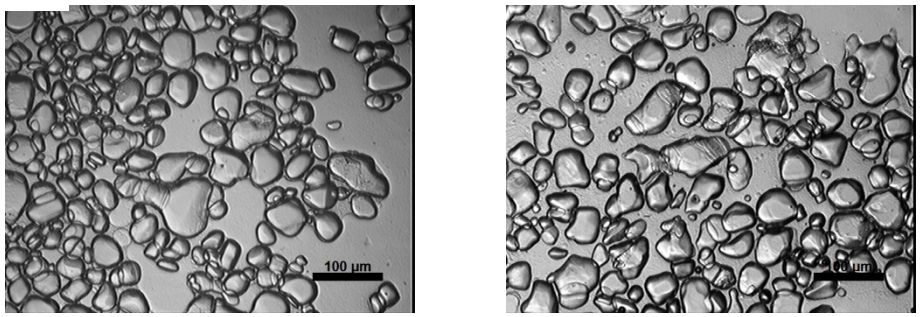

0% ST 0.2% ST

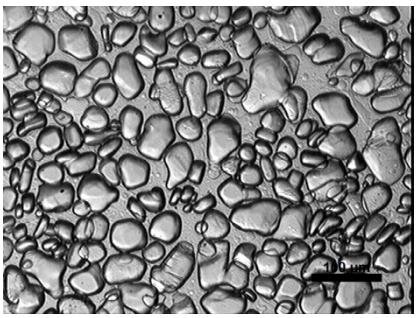

0.4% ST

Figure 4.3 Ice crystal size distribution (a) and the microscope image of ice crystals (b) of ice cream made with 0% polysorbate 80, 50% overrun and different stabilizer levels (ST). The error bars in (a) represents the standard deviation of mean ice crystal size measured in triplicate.

4.1.1.3 Fat destabilization

Table 4.2 shows that the fat destabilization extent in the ice cream samples varied widely, ranging from 8.8% to 73.2%, depending on the levels of stabilizer, polysorbate 80, and overrun. The ice cream with the highest overrun (100%), polysorbate 80 level (0.03%), and stabilizer level (0.4%) had the greatest fat destabilization, whereas ice cream with the lowest overrun (50%), and no added polysorbate 80 or stabilizer had the least. Typically, fat destabilization increased as overrun increased, though this trend was not seen in the ice cream samples with 0.4% stabilizer and 0.015% polysorbate 80. Furthermore, increased stabilizer levels enhanced fat destabilization throughout all samples. The additional polysorbate 80 increased fat destabilization extent in the sample without stabilizers. By adding stabilizers at 0.2% level, the lowest fat destabilization occurred when polysorbate 80 was 0.015%. When the stabilizer level increased to 0.4% level, a general trend of increasing polysorbate 80 enhanced fat destabilizations was seen, except in samples with 100% overrun.

Previous studies (Warren & Hartel, 2018; Wildmoser et al., 2004) reported that increasing overrun leads to greater fat destabilization. Fat destabilization is promoted with the presence of air incorporation during freezing. In high overrun ice cream, the narrow lamellae between air cells increases the possibility of collisions between fat globules/clusters, resulting in their adsorption to the surface of air cells and promoting partial coalescence. **Figure 4.4** shows examples of particle size distribution and microscope images of fat globules and clusters in ice cream samples with three levels of overrun. A linear correlation between overrun and fat destabilization regardless stabilizer and polysorbate 80 levels is shown in **Figure 4.4b**.

Table 4.2 Mean and standard deviation of the degree of fat destabilization. The standard deviation (±) refers to the variation between duplicate of the fat destabilization of the ice cream with different stabilizers, overrun, or polysorbate 80 levels.

Fat destabilization (%)*				
Stabilizer	Overrun	Polysorbate 80		
		0.000%	0.015%	0.030%
0.0%	50%	$8.8 \pm 5.0^{x,X,A}$	$11.8 \pm 5.0^{x,X,A}$	$22.3 \pm 4.8^{y,X,A}$
	75%	$18.7 \pm 3.0^{x,Y,A}$	$22.7 \pm 4.6^{x,Y,A}$	$46.2 \pm 8.1^{y,Y,A}$
	100%	$30.0 \pm 2.9^{x,Z,A}$	$29.1 \pm 6.2^{x,Y,A}$	$58.0 \pm 9.2^{y,Z,A}$
0.2%	50%	$20.3 \pm 3.4^{x,X,B}$	$15.1 \pm 8.7^{x,X,A}$	$46.6 \pm 14.5^{y,X,B}$
	75%	$34.8 \pm 11.9^{x,X,B}$	$24.0 \pm 11.6^{x,X,A}$	$57.2 \pm 8.4^{y,XY,AB}$
	100%	$51.6 \pm 12.6^{x,Y,B}$	$45.5 \pm 8.8^{x,Y,B}$	$69.5 \pm 7.2^{y,Y,B}$
0.4%	50%	$39.8 \pm 7.7^{x,X,C}$	$49.4 \pm 5.7^{xy,X,B}$	$56.8 \pm 10.8^{y,X,B}$
	75%	$55.4 \pm 5.0^{x,Y,C}$	$57.0 \pm 4.2^{x,X,B}$	$63.2 \pm 8.7^{x,XY,B}$
	100%	$68.5 \pm 4.6^{x,Z,C}$	$55.9 \pm 8.7^{y,X,B}$	$73.2 \pm 4.3^{x,Y,B}$

* Tukey's HSD test was performed for the significant difference at $P<0.05$
$^{x, y, z}$ denote significant differences among ice cream with different polysorbate 80 levels
$^{X, Y, Z}$ denote significant differences among ice cream with different overrun levels
$^{A, B, C}$ denote significant differences among ice cream with different stabilizer levels

A higher apparent mix viscosity from additional stabilizers generally promotes fat destabilization during freezing. The higher viscosity generates greater shear force in the ice cream mix, which promotes interaction among fat globules and clusters (Stanley et al., 1996). In this study, ice cream without stabilizers had the lowest fat destabilization compared to ice cream with 0.2% and 0.4% stabilizer. **Figure 4.5** shows examples of particle size distribution and microscope images of fat globules and clusters in ice cream samples with three levels of stabilizer. A linear correlation between mix viscosity and fat destabilization is also shown in **Figure 4.5b**.

Generally, samples with 0% and 0.015% levels of polysorbate 80 did not show a statistical difference in fat destabilization extent compared to 0.03% level. The increase of polysorbate 80 resulted in higher fat destabilization levels across all overruns in the absence of stabilizer, consistent with the previous finding by Tharp et al. (1997). The additional polysorbate 80 enhances

the displacement of protein on the fat globule surface and promotes fat partial coalescence (Goff & Hartel, 2013). However, this same trend was not seen with the inclusions of stabilizers. As previously mentioned, the shear stress generated by the viscous mix promotes fat destabilization, which appears to be the dominant factor affecting fat destabilization level in this study, more so even than additional polysorbate 80. Therefore, the addition of polysorbate 80 did not significantly influence fat destabilization extent in ice creams with 0.2% or 0.4% stabilizer. **Figure 4.6** shows examples of particle size distribution and microscope images of fat globules and clusters in ice cream samples with three levels of polysorbate 80.

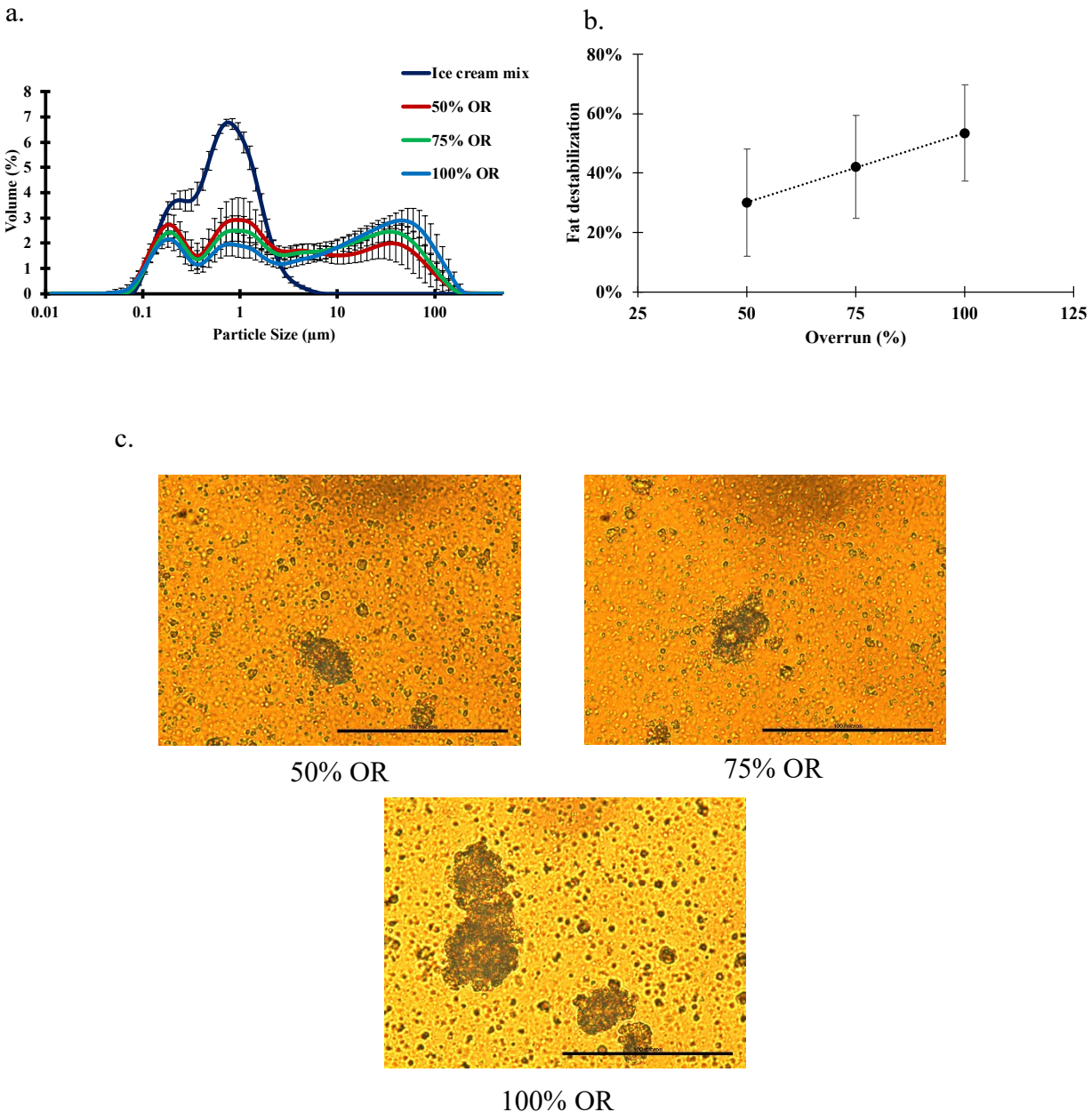

Figure 4.4 Particle size distribution (a), correlation between overrun and fat destabilization (b), and the microscope image of fat globules and clusters (c) of ice cream. (a) and (b) are ice cream made with 0.2% stabilizer, 0.03% polysorbate 80 and different overrun (OR) levels. The error bars in (a) represents the standard deviation of distribution measured in triplicate. The error bar in (b) represents the standard deviation of ice cream made with different stabilizer and polysorbate 80 levels.

a.

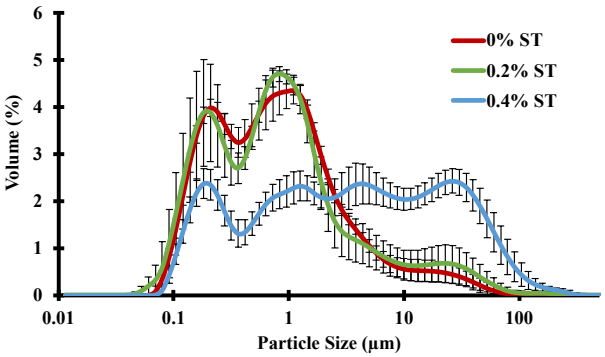

b.

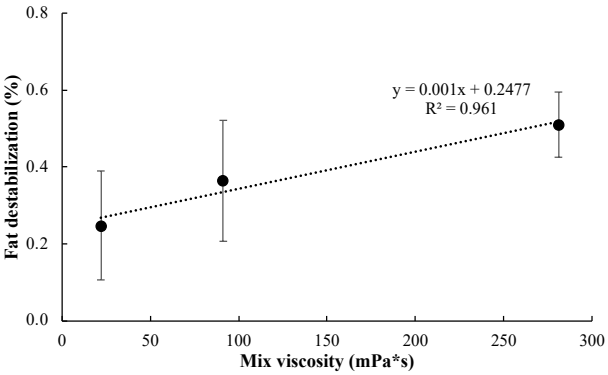

c.

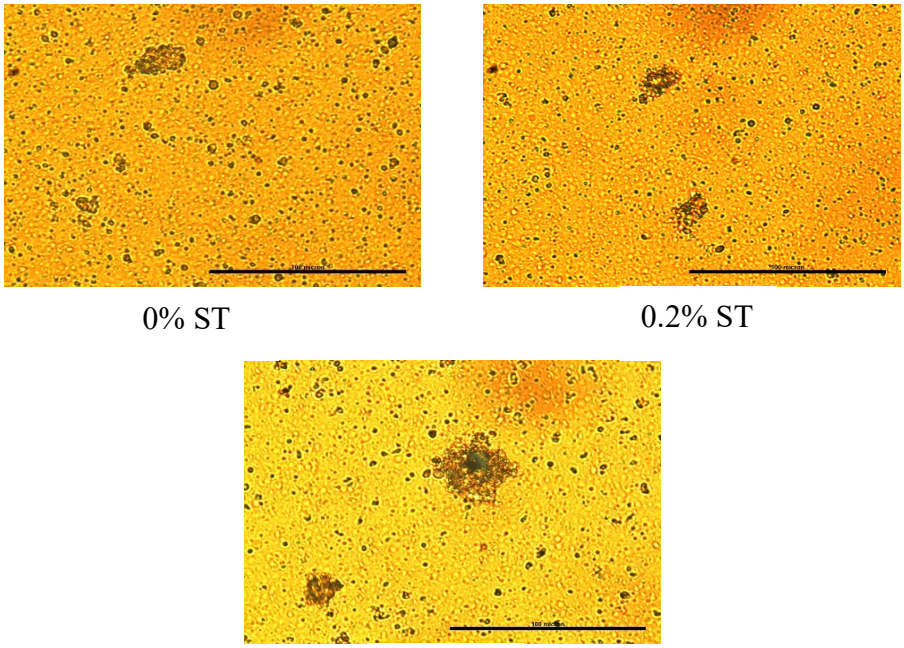

Figure 4.5 Particle size distribution (a), correlation between mix viscosity and fat destabilization (b), and the microscope image of fat globules and clusters (c) of ice cream. (a) and (c) are ice cream made with 0.03% polysorbate 80, 50% overrun and different stabilizer (ST) levels. The error bars in (a) represents the standard deviation of distribution measured in triplicate. The error bars in (b) represents the standard deviation of ice cream with different overrun and polysorbate 80 levels.

a.

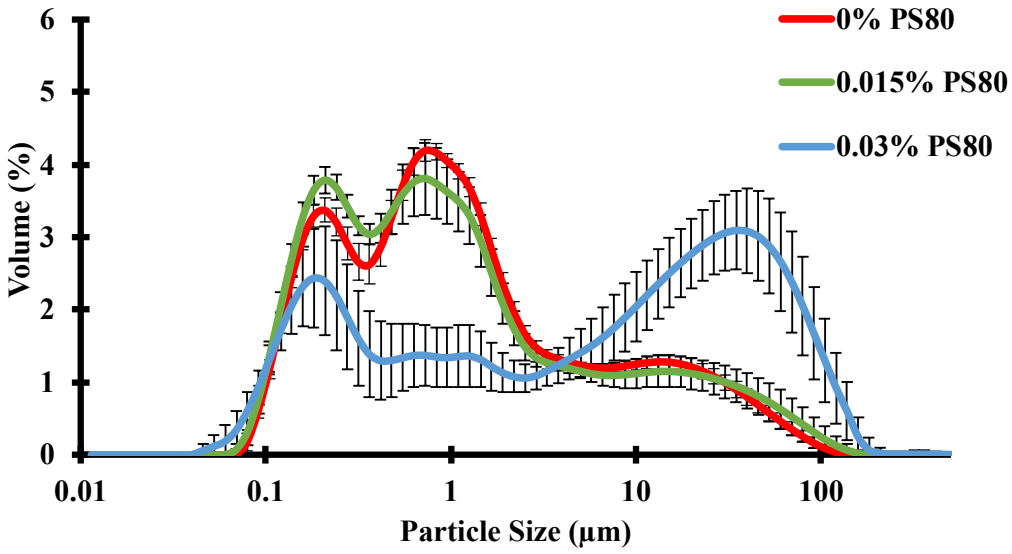

b.

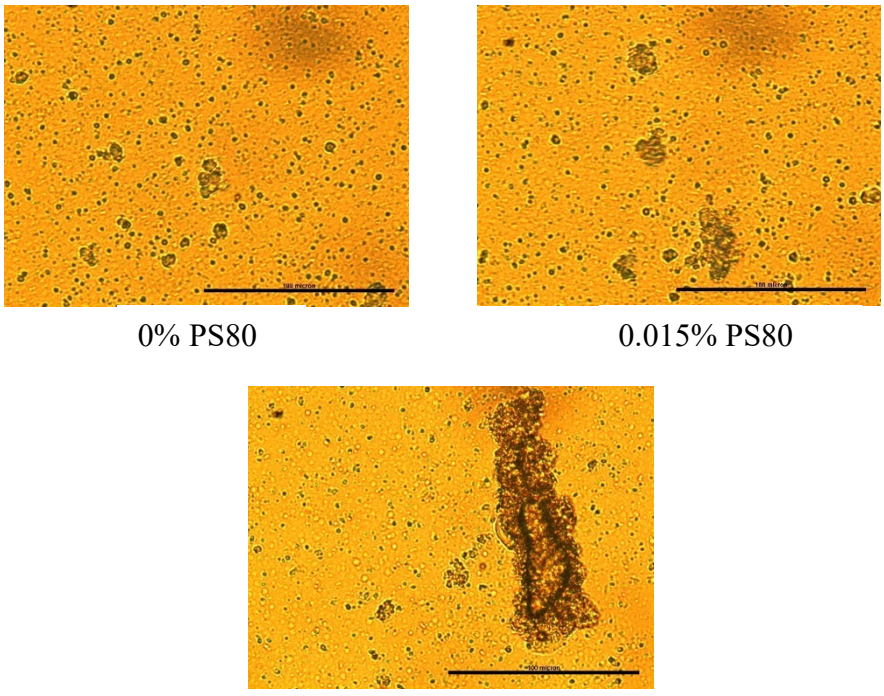

0% PS80 0.015% PS80

0.03% PS80

Figure 4.6 Particle size distribution (a) and the microscope image of fat globules and clusters (b) of ice cream made with 0% stabilizer, 100% overrun and different polysorbate 80 (PS80) levels. The error bars in (a) represents the standard deviation of distribution measured in triplicate.

4.1.1.4 Mean air cell size

The mean air cell size ranged from 11.8 to 30.1μm across the different formulas as shown in **Table 4.3**. An increase in overrun generally resulted in a decrease in mean air cell size ($p<0.05$), which aligned with previous studies (Sofjan & Hartel, 2004; Warren & Hartel, 2018). **Figure 4.7** shows examples of air cell size distribution and microscope images of air cells in ice cream samples with varying overrun levels. The freezing process leads to an increase in apparent viscosity in the ice cream slurry with higher overrun (Chang & Hartel, 2002a). During churning, a more viscous fluid generates a higher shear force, breaking down the air cells into smaller sizes. This effect is particularly pronounced in ice cream with high overrun (Sofjan & Hartel, 2004).

Table 4.3 Mean and standard deviation of air cell size. The standard deviation (±) refers to the variation between duplicate mean air cell size of the ice cream with different stabilizers, overrun, or polysorbate 80 levels.

Mean air cell size (μm)*				
Stabilizer	Overrun	Polysorbate 80		
		0%	0.015%	0.03%
0%	50%	$22.4 \pm 1.9^{xy,X,A}$	$24.3 \pm 2.5^{x,X,A}$	$18.1 \pm 1.7^{y,X,A}$
	75%	$18.3 \pm 2.7^{x,XY,A}$	$20.1 \pm 1.9^{x,XY,A}$	$16.1 \pm 0.9^{x,XY,A}$
	100%	$16.0 \pm 1.7^{x,Y,A}$	$16.2 \pm 1.9^{x,Y,A}$	$11.8 \pm 2.9^{x,Y,A}$
0.2%	50%	$30.1 \pm 0.4^{x,X,B}$	$24.8 \pm 0.5^{y,X,A}$	$24.4 \pm 0.5^{y,X,B}$
	75%	$24.6 \pm 0.6^{x,Y,B}$	$20.5 \pm 1.2^{y,Y,A}$	$18.8 \pm 1.2^{y,Y,B}$
	100%	$26.9 \pm 0.7^{x,Z,B}$	$18.3 \pm 1.7^{y,Y,A}$	$13.9 \pm 1.1^{z,Z,A}$
0.4%	50%	$26.8 \pm 0.8^{x,X,C}$	$25.3 \pm 1.2^{x,X,A}$	$25.3 \pm 1.2^{x,X,B}$
	75%	$23.2 \pm 0.7^{x,Y,B}$	$22.8 \pm 0.7^{x,Y,A}$	$23.0 \pm 0.9^{x,X,C}$
	100%	$21.1 \pm 0.7^{x,Z,C}$	$24.4 \pm 0.5^{y,XY,B}$	$22.4 \pm 1.7^{xy,X,B}$

* Tukey's HSD test was performed for the significant difference at $P<0.05$

$^{x, y, z}$ denote significant differences among ice cream with different polysorbate 80 levels

$^{X, Y, Z}$ denote significant differences among ice cream with different overrun levels

$^{A, B, C}$ denote significant differences among ice cream with different stabilizer levels

a.

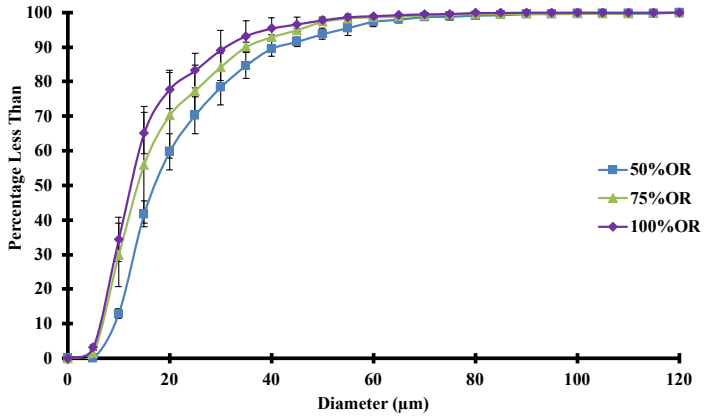

b.

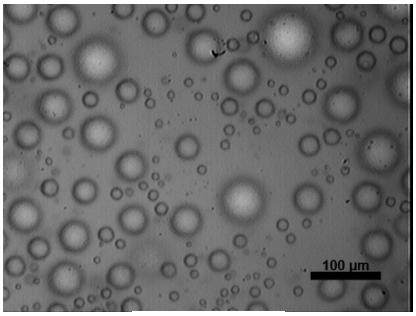

50% OR

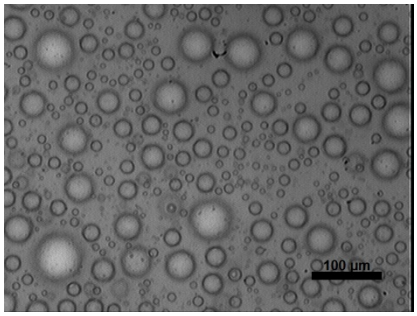

75% OR

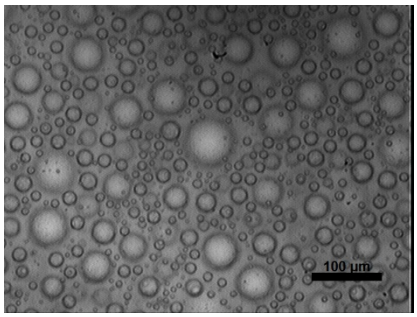

100% OR

Figure 4.7 Air cell size distribution (a) and the microscope image of air cells (b) of ice cream made with 0% polysorbate 80, 0% stabilizer and different overrun (OR). The error bars in (a) represents the standard deviation of mean ice crystal size measured in triplicate.

According to Amador et al. (2017), the additional stabilizers result in a decrease in mean air cell size at -3˚C draw temperature, as the high shear stress caused by the viscosity breaking down the air cells. However, no specific trend was observed in air cell size at -6˚C draw temperature (**Table 4.3**). Some statistical differences were found in mean air cell size, but the differences were very subtle. **Figure 4.8** shows examples of air cell size distribution and microscope images of air cells in ice cream samples with three levels of fat destabilization. Nonetheless, further research is necessary to better understand the effect of processing conditions and stabilizers on air cell size.

Ice cream with a high degree of fat destabilization generally exhibits smaller air cell sizes (Chang & Hartel, 2002c; Warren & Hartel, 2018). The fat network formed by the destabilized fat clusters impedes the growth of air cells. In this study, a strong negative relationship was seen between the degree of fat destabilization and mean air cell size in ice cream samples containing 0% ($p<0.05$) and 0.4% stabilizer ($p<0.05$) (**Figure 4.9b**). However, the effect of fat destabilization on air cell size was less pronounced in the ice cream with 0.2% stabilizer ($p=0.0664$). Examples of air cell size distribution and the microscope image of air cells of ice cream samples with three levels of fat destabilization are shown in **Figure 4.9**.

a.

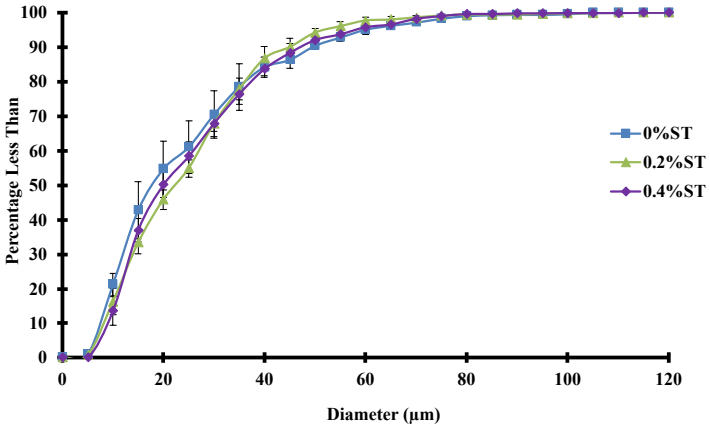

b.

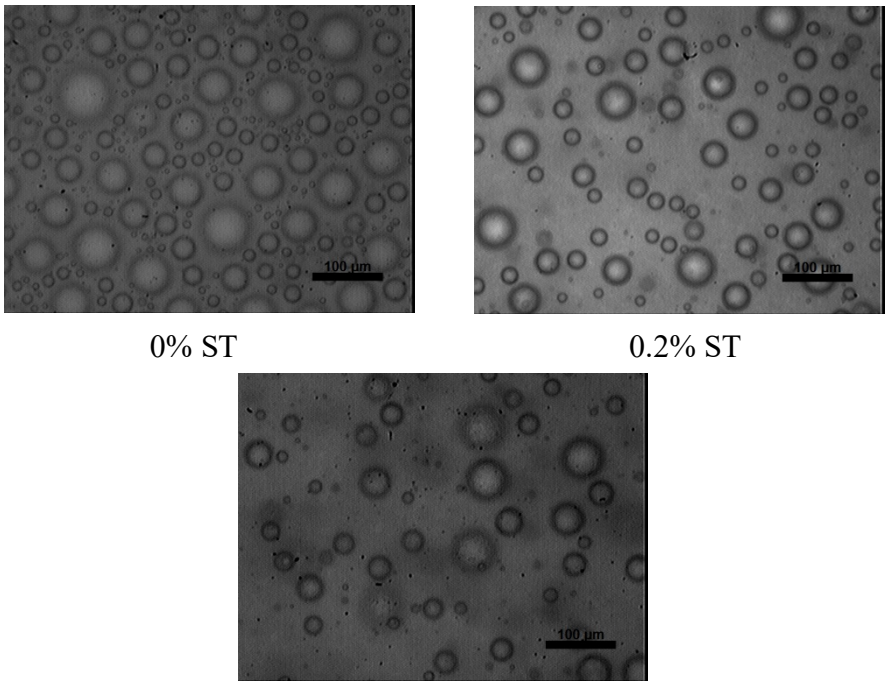

0% ST 0.2% ST

0.4% ST

Figure 4.8 Air cell size distribution (a) and the microscope image of air cells (b) of ice cream made with 0.015 polysorbate 80, 50% overrun and different stabilizer (ST) levels. The error bars in (a) represents the standard deviation of mean ice crystal size measured in triplicate.

a.

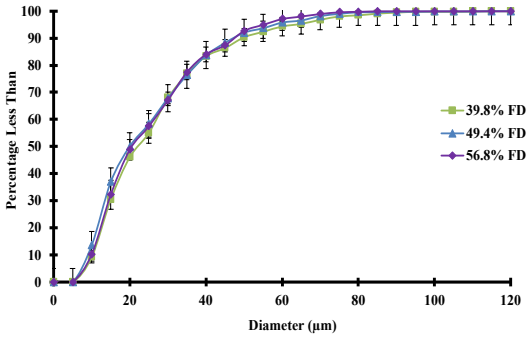

b.

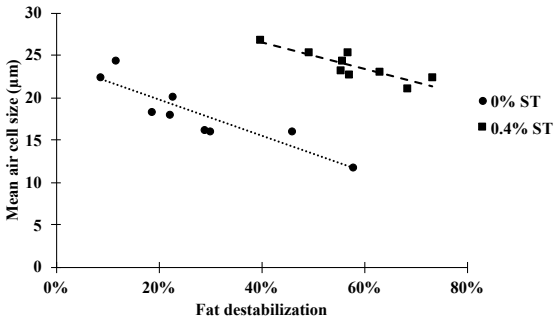

c.

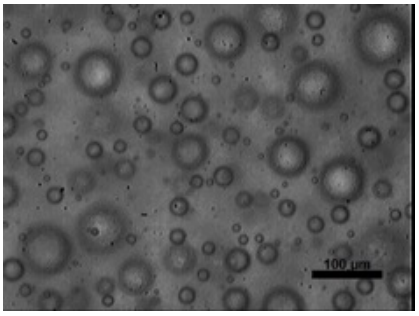

39.8% FD (0%PS80)

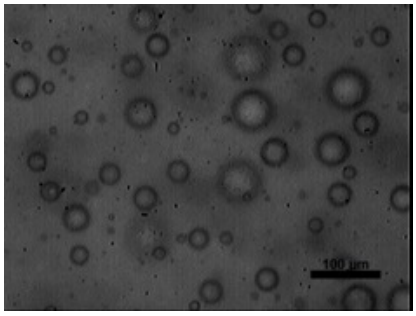

49.4% FD (0.015%PS80)

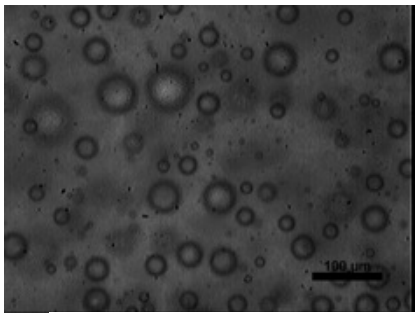

56.8% FD (0.03%PS80)

Figure 4.9 Air cell size distribution (a), the correlation between fat destabilization and mean air cell size (b), and the microscope image of air cells (c) of ice cream. (a) and (c) are ice cream made with 0.4% stabilizer, 50% overrun and different fat destabilization (FD) levels by adjusting the amount of polysorbate 80 (PS80). The error bars in (a) represents the standard deviation of mean ice crystal size measured in triplicate.

4.1.2 Characterization of ice cream meltdown behavior

This study described the ice cream meltdown behavior using two measures: the change of drip-through weight and the height change. The meltdown curve was used to describe the change of drip-through weight, while the height curve was used to describe changes in the height of ice cream as it melted. The meltdown curve was divided into three phases: lag phase, linear melting phase and stationary phase. Lag phase was described using the induction time, which is the time between the start of experiment and the first drop of melted ice cream. The slope of the linear region of the curve was used to describe the linear melting phase. The stationary phase is described using the amount of remnant foam. For the height curve, height change rate and final height were used to describe the change in the height of ice cream during melting. As with the meltdown curve, the slope of linear region of the height curve was calculated to describe the height change rate, and the final height was determined by measuring the height of the remnant foam at the end of the experiment.

The composition of ice cream was found to influence the shape of the meltdown curve, as presented in **Figure 4.10**, where three curves were selected to exhibit the range of behaviors observed. The sample with 50% overrun, 0% stabilizer and polysorbate 80 had the weakest structure of all the samples tested, resulting in the lowest fat destabilization, and melted completely within 1-2 hr. Conversely, the sample with 100% overrun, 0.4% stabilizer, and 0.03% polysorbate 80 had the most complex structure and the highest fat destabilization, retaining nearly 85% of the original mass in the remnant foam after the meltdown test. The intermediate structure was observed for the sample with 75% overrun, 0.2% stabilizer, and 0.015% polysorbate 80.

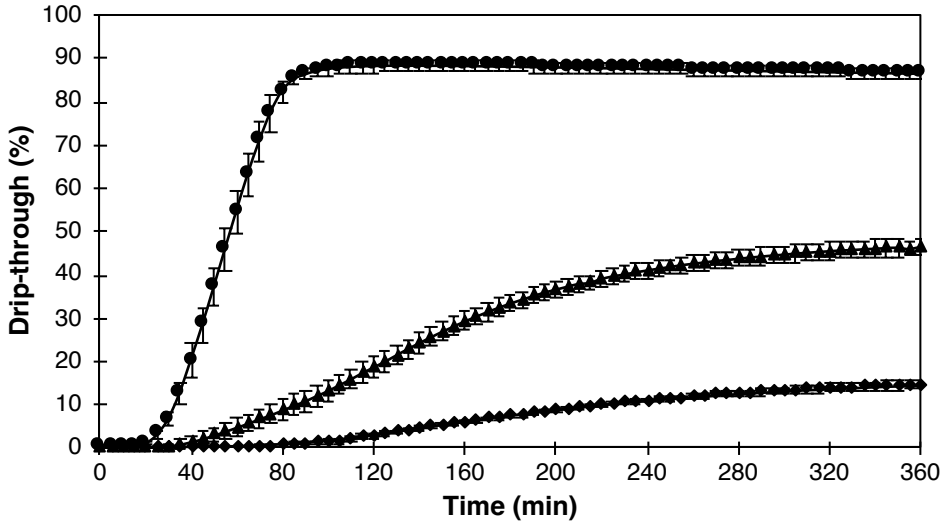

Figure 4.10 Example of different shapes of ice cream meltdown curves. The error bars stand for standard deviation of mean values among six samples. Circle, ice cream with 0% stabilizer (ST), 0% polysorbate 80 (PS80) and 50% overrun (OR); triangle, ice cream with 0.2% ST, 0.015% PS80 and 75% OR; diamond, ice cream with 0.4% ST, 0.03% PS80 and 100% OR.

Researchers have explored the impact of ice cream microstructure on its meltdown behavior in recent years. Studies have shown that manipulating ice cream formulas to modify its structure can result in different melting rate. Factors such as the extent of fat destabilization, mix viscosity, and overrun have been found to be the major impact on this process (Amador et al., 2017; Daw & Hartel, 2015; Muse & Hartel, 2004; Sakurai et al., 1996; Sofjan & Hartel, 2004; Warren & Hartel, 2018). For instance, adding polysorbate 80 increases the extent of fat destabilization by lowering the surface tension of fat globules (Goff & Hartel, 2013), which causes larger fat clusters to collide and jam with each other during the meltdown process, thereby impeding further melted ice cream drainage (Muse & Hartel, 2004; Warren & Hartel, 2018). In addition, the addition of stabilizers increases the viscosity of the serum phase. As the ice crystals melt, water dilutes the serum phase, causing the melted ice cream to drain due to gravitational force. When the serum phase is viscous, the drainage process slows down, resulting in a low rate of meltdown (Amador

et al., 2017; Muse & Hartel, 2004). Furthermore, the amount of air present in ice cream affects heat conduction and thus the rate of meltdown, as air acts as an insulator that prevents heat penetration (Sakurai et al., 1996; Sofjan & Hartel, 2004; Warren & Hartel, 2018). In the following sections, the effects of these three structural elements on the ice cream meltdown will be further discussed.

4.1.2.1 The effect of major structural elements on lag phase on meltdown curve

Table 4.4 presents the induction time for meltdown of ice cream, ranging from 14.2 to 55.6min, which varied based on the levels of polysorbate 80, overrun, and stabilizer. Notably, the induction time is associated with the surface layer of the ice cream rather than the entire structure. When ice cream is placed at room temperature, the outer layer is exposed to the surrounding heat, which causes the ice crystals on the surface to melt first. This melted ice cream layer then flows around to generate a large enough drop for dripping.

A multivariate analysis of the data demonstrated a significant positive correlation between fat destabilization and induction time ($r=0.7726$, $p<0.0001$), indicating that increasing the extent of fat destabilization led to a longer induction time to the first drop. In other words, ice cream with higher levels of fat destabilization exhibited a higher yield stress, which in turn increased the resistance of water to flow against gravitational force.

Table 4.4 Mean and standard deviation of induction time for meltdown of ice cream. The standard deviation (±) refers to the variation between duplicate induction time of the ice cream with different stabilizers, overrun, or polysorbate 80 levels.

Induction time (min)*				
Stabilizer	Overrun	Polysorbate 80		
		0.000%	0.015%	0.030%
0.0%	50%	$14.2 \pm 1.4^{x,X,A}$	$14.9 \pm 3.0^{xy,X,A}$	$19.8 \pm 5.3^{y,X,A}$
	75%	$17.7 \pm 2.9^{x,X,A}$	$18.0 \pm 5.4^{xy,X,A}$	$25.5 \pm 6.3^{y,XY,A}$
	100%	$17.0 \pm 3.1^{x,X,A}$	$20.3 \pm 2.8^{x,X,A}$	$31.2 \pm 6.1^{y,Y,A}$
0.2%	50%	$31.0 \pm 5.1^{xy,X,B}$	$29.0 \pm 0.8^{x,X,B}$	$36.1 \pm 4.2^{y,X,B}$
	75%	$29.1 \pm 4.0^{x,X,B}$	$26.5 \pm 4.9^{x,X,B}$	$31.8 \pm 4.2^{x,X,A}$
	100%	$32.5 \pm 5.2^{x,X,B}$	$37.6 \pm 3.8^{x,Y,B}$	$33.0 \pm 3.7^{x,X,A}$
0.4%	50%	$43.3 \pm 4.2^{x,X,C}$	$46.4 \pm 6.7^{x,X,C}$	$47.1 \pm 10.7^{x,X,C}$
	75%	$36.5 \pm 7.4^{x,X,B}$	$34.8 \pm 2.5^{x,Y,C}$	$49.6 \pm 11.9^{y,X,B}$
	100%	$42.9 \pm 6.1^{x,X,C}$	$55.6 \pm 11.1^{x,X,C}$	$54.5 \pm 12.9^{x,X,B}$

* Tukey's HSD test was performed for the significant difference at $P<0.05$
$^{x, y, z}$ denote significant differences among ice cream with different polysorbate 80 levels
$^{X, Y, Z}$ denote significant differences among ice cream with different overrun levels
$^{A, B, C}$ denote significant differences among ice cream with different stabilizer levels

A strong positive correlation ($r=0.8806$, $p<0.0001$) was observed between ice cream mix viscosity and induction time, as depicted in **Figure 4.11**. Increasing the amount of stabilizer in the ice cream increases the apparent viscosity of the mix, thereby extending the time taken for the first drop to drip through the mesh. Notably, this relationship was independent of the levels of polysorbate 80 or overrun. As ice crystals begin to melt and dilute the serum phase, the induction time is associated with the viscosity of the melted ice cream on the surface, which has to counteract the gravitational force. Thus, the more viscous the serum phase, the longer it takes to flow along the surface of the ice cream and drip through the screen.

Kurultay et al. (2010) noted that when the total solid level was held constant at 30%, overrun and induction time in the drip-through test were inversely correlated. However, no

significant correlation between overrun and induction time was found in this study (r=0.1639, p=0.4141). Upon careful observation of the melting process, the outer surface of the samples melted and dripped first, indicating that minimal heat had penetrated into the sample before the initial drip. Therefore, thermal diffusivity did not appear to be the primary factor governing the induction time for the first drip.

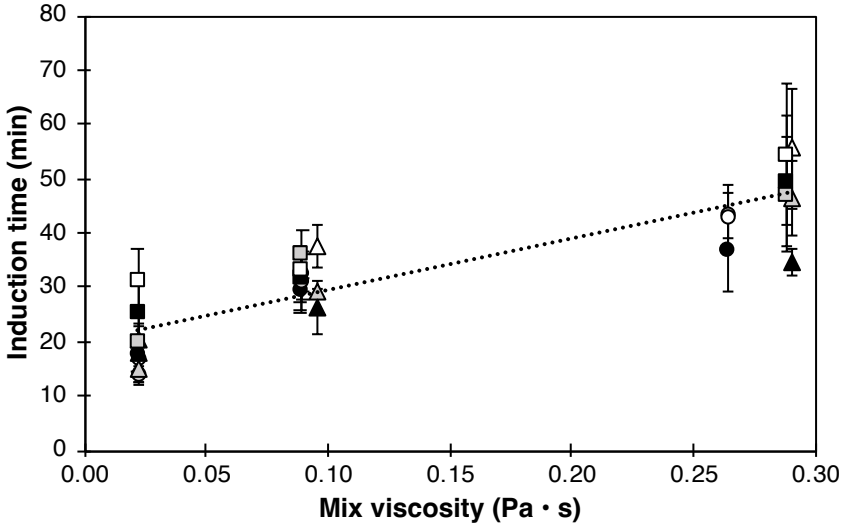

Figure 4.11 The correlation between mix viscosity (at 50 s^{-1} shear rate) and induction time. The error bars stand for standard deviation of mean values among six samples. Grey, 50% overrun; black, 75% overrun; hollow, 100% overrun. Circle, 0% polysorbate 80 (PS80); triangle, 0.015 PS80; square, 0.03% PS80.

4.1.2.2 The effect of major structural elements on linear melting phase on meltdown curve

The drip-through rate (g/min) is determined by calculating the slope of the linear part of the melting curve. As shown in **Table 4.5**, drip-through rates of ice cream varied from 1.79 to 0.08g/min, depending on the levels of polysorbate 80, stabilizer, and overrun. The ice cream with 50% overrun and no stabilizer had the highest drip-through rate, whereas the ice cream with 0.4% stabilizer had the lowest.

Table 4.5 Mean and standard deviation of drip-through rate. The standard deviation (±) refers to the variation between duplicate drip-through rate of the ice cream with different stabilizers, overrun, or polysorbate 80 levels.

Drip-through rate (g/min)*				
Stabilizer	Overrun	Polysorbate 80		
		0.000%	0.015%	0.030%
0.0%	50%	$1.63 \pm 0.06^{x,X,A}$	$1.79 \pm 0.17^{x,X,A}$	$1.00 \pm 0.26^{y,X,A}$
	75%	$0.82 \pm 0.03^{x,Y,A}$	$0.82 \pm 0.05^{x,Y,A}$	$0.60 \pm 0.11^{y,Y,A}$
	100%	$0.73 \pm 0.06^{x,Z,A}$	$0.65 \pm 0.03^{x,Z,A}$	$0.47 \pm 0.09^{y,Y,A}$
0.2%	50%	$0.21 \pm 0.02^{x,X,B}$	$0.19 \pm 0.02^{x,X,B}$	$0.22 \pm 0.02^{x,X,B}$
	75%	$0.25 \pm 0.01^{x,Y,B}$	$0.25 \pm 0.01^{x,Y,B}$	$0.24 \pm 0.01^{x,Y,B}$
	100%	$0.25 \pm 0.01^{x,Y,B}$	$0.24 \pm 0.01^{x,Y,B}$	$0.24 \pm 0.01^{x,Y,B}$
0.4%	50%	$0.10 \pm 0.02^{x,X,C}$	$0.07 \pm 0.01^{y,X,B}$	$0.08 \pm 0.01^{y,X,B}$
	75%	$0.14 \pm 0.03^{x,X,C}$	$0.09 \pm 0.00^{y,Y,C}$	$0.09 \pm 0.01^{y,X,C}$
	100%	$0.13 \pm 0.05^{x,X,C}$	$0.07 \pm 0.02^{y,X,C}$	$0.08 \pm 0.01^{y,X,C}$

* Tukey's HSD test was performed for the significant difference at $P<0.05$
$^{x, y, z}$ denote significant differences among ice cream with different polysorbate 80 levels
$^{X, Y, Z}$ denote significant differences among ice cream with different overrun levels
$^{A, B, C}$ denote significant differences among ice cream with different stabilizer levels

Increasing the amount of polysorbate 80 in ice cream without stabilizer led to a decrease in drip-through rates, which can be attributed to fat destabilization. This observation is consistent with previous studies (Bolliger et al., 2000; Muse & Hartel, 2004; Tharp et al., 1997; Warren & Hartel, 2014, 2018), which have shown an inverse correlation between fat destabilization and drip-

through rate. This effect was particularly pronounced under specific conditions, such as low stabilizer levels. **Figure 4.12** shows that an increase in fat destabilization extent in ice cream without stabilizer significantly reduced the drip-through rate. Ice cream with 0.03% polysorbate 80 showed a significantly lower drip-through rate compared to 0% and 0.015% polysorbate 80 levels, due to a higher extent of fat destabilization. However, for ice creams with 0.2% and 0.4% stabilizer, the change in drip-through rate was not affected by the change in fat destabilization (**Figure 4.12**). The increase in fat destabilization did not significantly decrease the drip-through rate when the mix viscosity was high. For ice creams with 0.2% stabilizer, the drip-through rate mostly fell within the narrow range of 0.19-0.25 g/min, whereas for ice creams with 0.4% stabilizer, it was within the range of 0.07-0.14 g/min. Without stabilizer, the drip-through rate was greatly dependent on how the large fat clusters collided with each other and resisted the drainage of the serum phase. In contrast, ice cream with high mix viscosity had a high yield stress for the serum phase to flow and drip through. Therefore, when the mix viscosity increased to a certain degree, it became the dominant factor affecting the drip-through rate instead of fat destabilization extent.

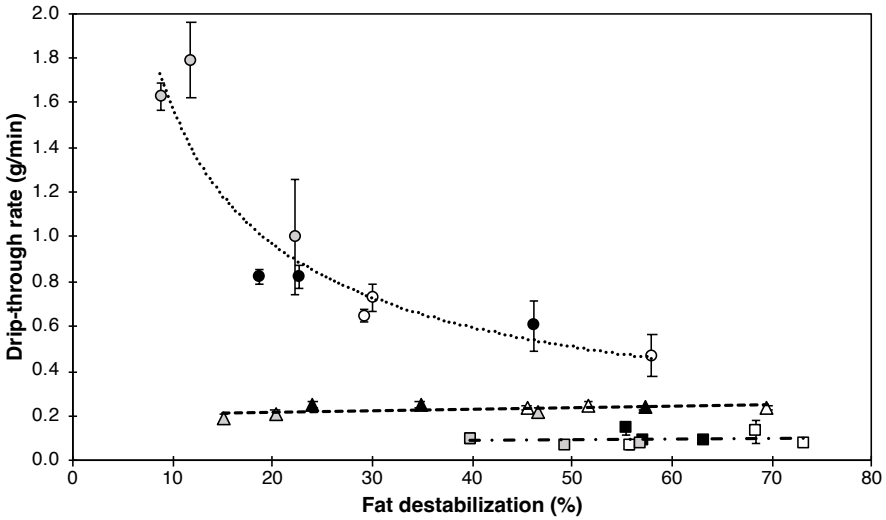

Figure 4.12 The correlation between drip-through rate and fat destabilization. The error bars stand for standard deviation of mean values among six samples. Grey, 50% overrun; black, 75% overrun; hollow, 100% overrun. Circle, 0% stabilizer; triangle, 0.2% stabilizer; square, 0.4% stabilizer.

The dominant factor affecting drip-through rate in this study was the mix viscosity, which was determined by the concentration of stabilizer. An increase in stabilizer concentration led to a decrease in drip-through rate, which was consistent across all samples ($r=-0.6679$, $p<0.0001$). These findings are consistent with previous research by Amador et al. (2017) and Muse and Hartel (2004). As shown in **Table 4.5**, ice creams with no added stabilizer had the highest drip-through rate, while those with 0.4% stabilizer had the lowest. It should be noted that the decrease in drip-through rate with an increase in mix viscosity was independent of overrun and fat destabilization levels, as illustrated in **Figure 4.13**. Notably, low fat destabilization levels (8.8% and 11.8%) in ice creams without stabilizers resulted in relatively high drip-through rates (1.63 g/min and 1.79g/min, respectively) due to the low viscosity of the serum phase during meltdown, allowing for rapid drainage through the lamella. On the other hand, ice creams with high mix viscosity (above 0.8 Pa•s at a 50 s^{-1} shear rate) had limited mobility for drainage, resulting in a low drip-through rate.

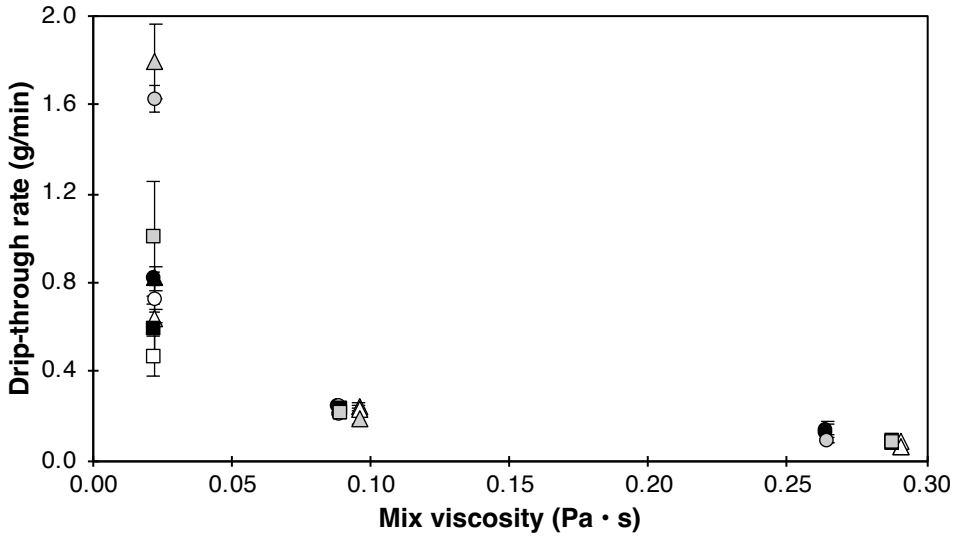

Figure 4.13 The correlation between mix viscosity (50 s^{-1} shear rate) and drip-through rate. The error bars stand for standard deviation of mean values among six samples. Grey, 50% overrun; black, 75% overrun; hollow, 100% overrun. Circle, 0% polysorbate 80 (PS80); triangle, 0.015% PS80; square, 0.03% PS80.

The negative correlation between high overrun and low drip-through rate was observed only in samples without stabilizer (r=-0.8058, p=0.0087), while no trend was observed when stabilizer was added at 0.2% or 0.4%, as shown in **Figure 4.14**. When the mix viscosity exceeded 0.08 Ps•s, drip-through rate remained below 0.4 g/min, regardless of the levels of overrun and polysorbate 80. Within this limited range of drip-through rate, overrun did not have any effect. However, previous studies by Sofjan and Hartel (2004) and Sakurai et al. (1996) reported that high overrun ice cream (without polysorbate 80) exhibited lower melting rates and better shape retention during the meltdown test. Additionally, Warren and Hartel (2018) found that the relationship between high overrun and decreased drip-through rate was predominantly observed in ice cream without polysorbate 80. While the finding in this study partially aligns with Warren and Hartel (2018), further investigation is necessary to fully understand the impact of overrun on drip-through rate.

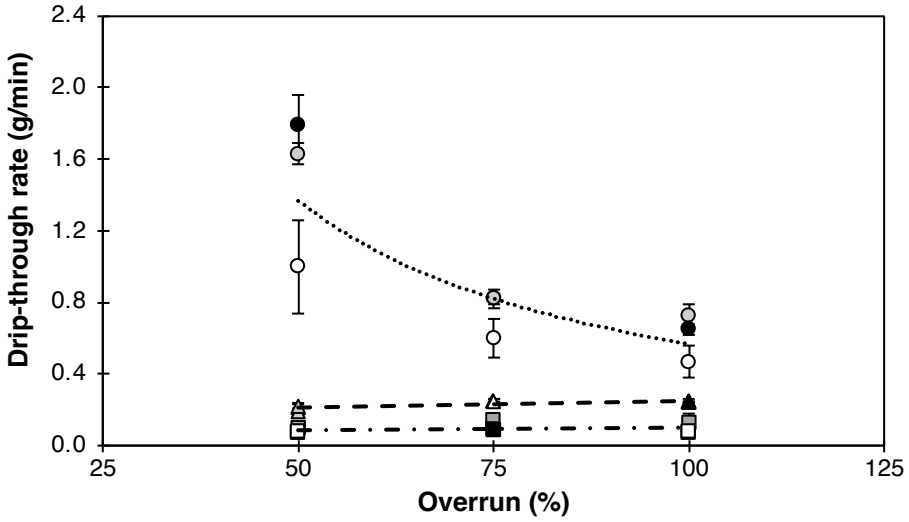

Figure 4.14 The correlation between drip-through rate and overrun. The error bars stand for standard deviation of mean values among six samples. Grey, 0% PS80; black, 0.015% PS80; hollow, 0.03% PS80. Circle, 0% stabilizer; triangle, 0.2% stabilizer; square, 0.4% stabilizer.

4.1.2.3 The effect of major structural elements on stationary phase on meltdown curve

The final drip-through weight (%) is calculated by dividing the weight of the remnant foam by the weight of the original sample. **Table 4.6** shows that the final drip-through weight of ice cream ranged from 14.9 to 97.6%, which varied based on the levels of polysorbate 80, stabilizer, and overrun. A higher final drip-through weight corresponds to greater collapse when the ice cream melts. Among the samples tested, the ice cream with 50% overrun and no stabilizer exhibited the highest final drip-through weight, whereas the ice cream with 0.4% stabilizer had the lowest.

Table 4.6 Mean and standard deviation of final drip-through weight. The standard deviation (±) refers to the variation between duplicate drip-through rate of the ice cream with different stabilizers, overrun, or polysorbate 80 levels.

Final drip-through weight (%)*				
Stabilizer	Overrun	Polysorbate 80		
		0.000%	0.015%	0.030%
0.0%	50%	$97.6 \pm 2.4^{x,X,A}$	$96.8 \pm 2.0^{x,X,A}$	$81.8 \pm 6.4^{y,X,A}$
	75%	$85.1 \pm 2.4^{x,Y,A}$	$81.7 \pm 3.0^{x,Y,A}$	$67.4 \pm 9.1^{y,Y,A}$
	100%	$79.0 \pm 1.9^{x,Z,A}$	$78.1 \pm 4.0^{x,Y,A}$	$57.8 \pm 10.5^{y,Y,A}$
0.2%	50%	$48.0 \pm 1.2^{x,X,B}$	$50.6 \pm 2.4^{x,XY,B}$	$44.5 \pm 1.8^{y,X,B}$
	75%	$50.6 \pm 1.4^{xy,Y,B}$	$53.5 \pm 2.6^{x,X,B}$	$47.8 \pm 3.7^{y,X,B}$
	100%	$51.0 \pm 1.8^{x,Y,B}$	$48.0 \pm 1.8^{xy,Y,B}$	$46.4 \pm 3.1^{y,X,B}$
0.4%	50%	$23.6 \pm 4.3^{x,X,C}$	$14.9 \pm 1.9^{y,X,C}$	$15.8 \pm 2.4^{y,X,C}$
	75%	$33.7 \pm 5.7^{x,Y,C}$	$23.3 \pm 1.9^{y,Y,C}$	$18.5 \pm 1.5^{y,Y,C}$
	100%	$29.4 \pm 6.6^{x,XY,C}$	$16.3 \pm 4.4^{y,X,C}$	$17.4 \pm 1.0^{y,XY,C}$

*Tukey's HSD test was performed for the significant difference at $P<0.05$
$^{x, y, z}$ denote significant differences among ice cream with different polysorbate 80 levels
$^{X, Y, Z}$ denote significant differences among ice cream with different overrun levels
$^{A, B, C}$ denote significant differences among ice cream with different stabilizer levels

Tharp et al. (1997) observed that an increase in fat destabilization led to a decrease in melted ice cream drainage. In this study, a similar relationship was observed at 0% stabilizer, as illustrated in **Figure 4.15a**. An example of the remnant foam of melted ice cream with 75% overrun, no stabilizer and varying fat destabilization levels is shown in **Figure 4.15b**. A strong negative correlation was found between fat destabilization and final drip-through weight at 0% stabilizer ($r=-0.9815$, $p<0.0001$). Interestingly, for ice cream containing 0.2% or 0.4% stabilizer, the extent of fat destabilization did not significantly impact the amount of melted ice cream dripping through, as indicated in **Figure 4.15a** (0.2% stabilizer: $r=-0.5250$, $p=0.1467$; 0.4% stabilizer: $r=0.0146$, $p=0.9703$). When the serum phase's apparent viscosity was low, the fat clusters moved freely during drainage, colliding with one another, and maintaining the foam structure on the mesh. However, as the mix viscosity increased to 0.09 Pa•s or even 0.28 Pa•s, the mobility of fat clusters

was restricted by the viscous serum phase. Thus, despite the broad range of fat destabilization levels tested (0.2% stabilizer: 15.1% to 69.5%; 0.4% stabilizer: 39.8% to 73.2%), the final drip-through weight changes were limited at each stabilizer level (0.2% stabilizer: 44.5% to 53.5%; 0.4% stabilizer: 14.9% to 33.7%).

Figure 4.16a displays a strong negative correlation between mix viscosity and final drip-through weight ($r=-0.9121$, $p<0.0001$), demonstrating that ice cream mix viscosity (and, consequently, serum viscosity) is the primary determinant of the amount of ice cream that remains on the screen after 6 hr. Higher viscosity resulted in less melted ice cream dripping through the mesh and more remnant foam being retained on top. An example of melted ice cream with three levels of stabilizer is shown **Figure 4.16b**.

Although no correlation was found between overrun and final drip-through weight for the entire dataset ($r=-0.0896$, $p=0.6569$), a trend of decreased final weight with increasing overrun was observed in ice creams without added stabilizer. An example of melted ice cream with three levels of overrun is shown **Figure 4.17**. This trend can be attributed to the high correlation between final weight and fat destabilization in the absence of stabilizer, as fat clusters stabilize air cells. Ice cream with high overrun increases the level of fat destabilization, leading to the creation of a large fat network that prevents further drainage. As a result, overrun indirectly affected final weight under these conditions. During meltdown, however, the effect of mix viscosity dominates. A high viscosity of the serum phase reduces the mobility of air cells and fat clusters, causing them to become jammed within the lamella and preventing further drainage, regardless of overrun levels. Further study is needed to investigate the effect of air cell size on the remnant foam.

a.

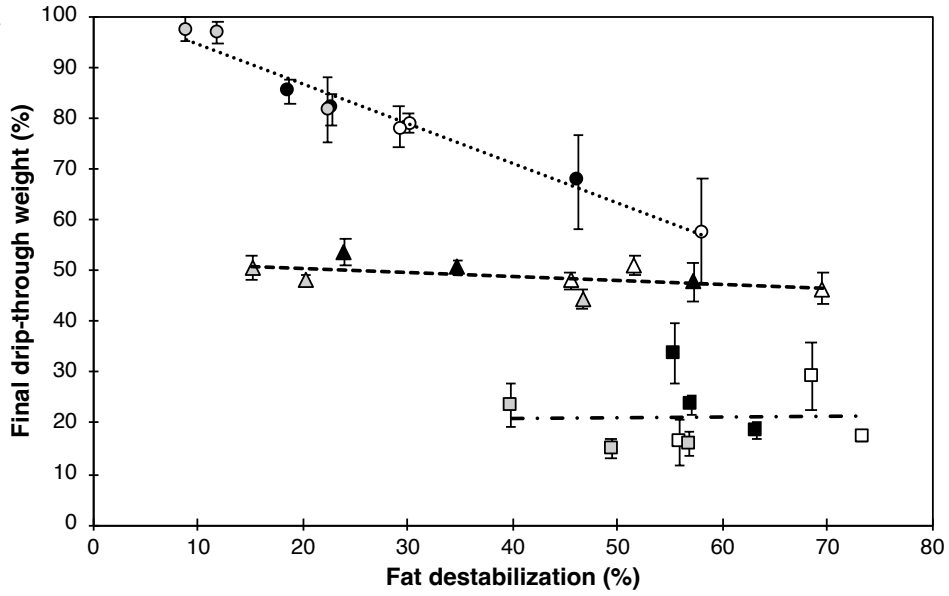

b.

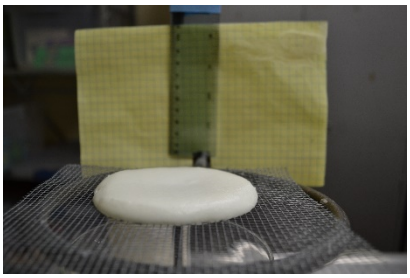

18.7% FD

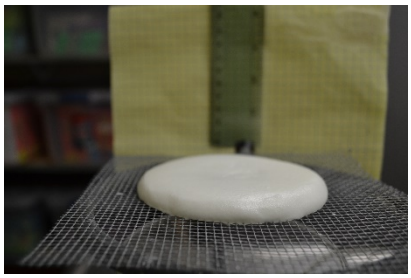

22.7% FD

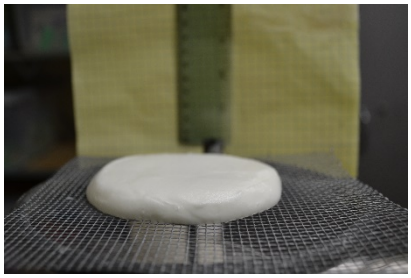

46.2% FD

Figure 4.15 The correlation between fat destabilization (FD) and final drip-through weight (a) and images of melted ice cream remaining on the mesh after 2hr meltdown test with 75% overrun, no stabilizer, and varying levels of fat destabilization adjusted by polysorbate 80 (b). The error bars in (a) stand for standard deviation of mean values among six samples. Grey, 50% overrun; black, 75% overrun; hollow, 100% overrun. Circle, 0% stabilizer; triangle, 0.2% stabilizer; square, 0.4% stabilizer.

a.

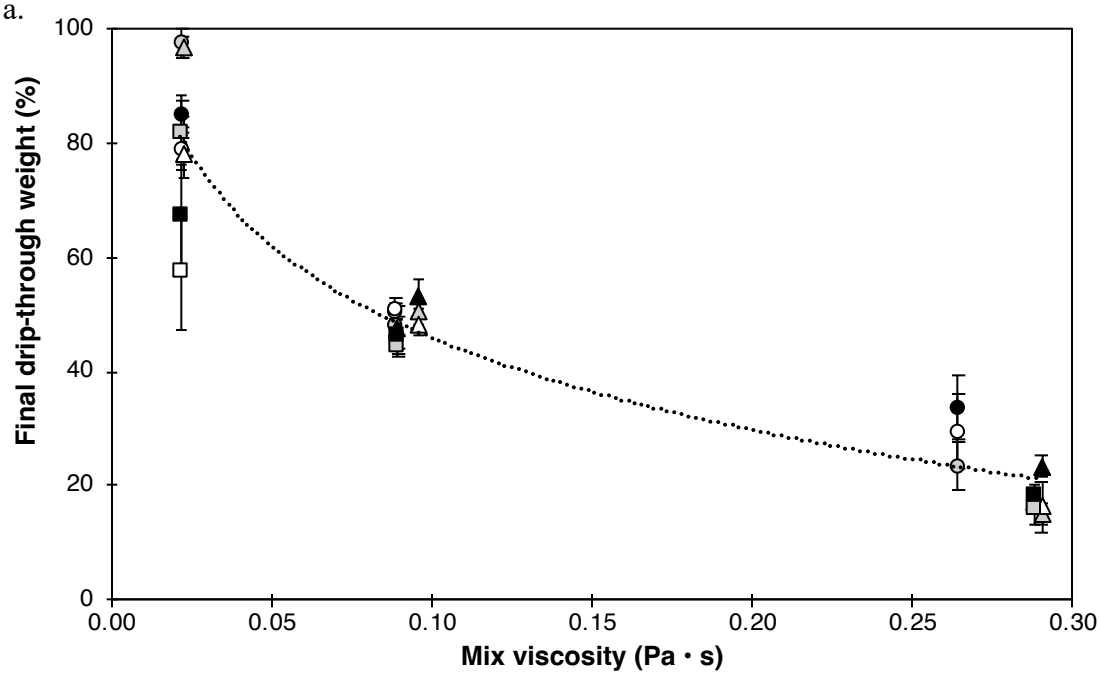

b.

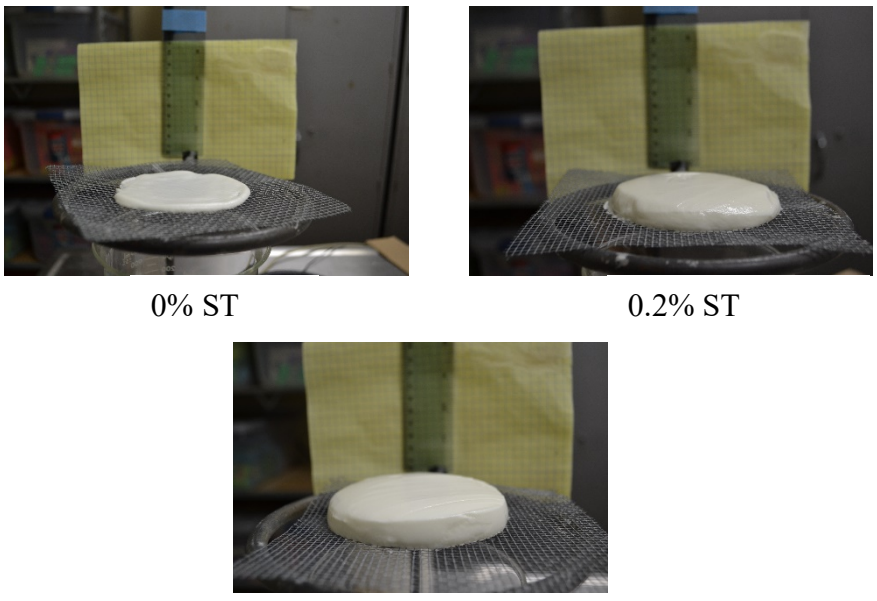

0% ST

0.2% ST

0.4% ST

Figure 4.16 The correlation between mix viscosity (50 s^{-1} shear rate) and final drip-through weight (a) and images of melted ice cream remaining on the mesh after 2 hr meltdown test with 50% overrun, 0% polysorbate 80, and varying levels of stabilizer (ST) (b). The error bars in (a) stand for standard deviation of mean values among six samples. Grey, 50% overrun; black, 75% overrun; hollow, 100% overrun. Circle, 0% stabilizer; triangle, 0.2% stabilizer; square, 0.4% stabilizer.

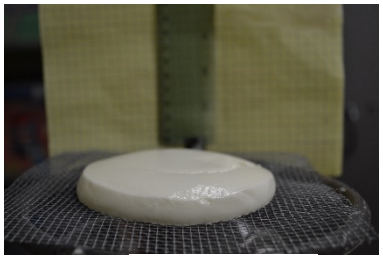

50% OR

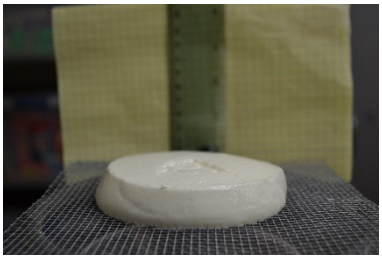

75% OR

100% OR

Figure 4.17 Images of melted ice cream remaining on the mesh after 2 hr meltdown test with 0.2% stabilizer, 0% polysorbate 80, and varying levels of overrun (OR).

4.1.2.4 The effect of major structural elements on height-change rate on height curve

Ice cream height-change during the meltdown test provides valuable information on structure collapse. Since there are two types of meltdown behavior after a certain time, total drip-through and remnant foam, the height changes observed are drastically different. In ice cream that completely drip-through, the height change exhibits a sharp reduction over a short period of time, whereas in ice cream that leaves a remnant foam structure, the height gradually decreases and remains at a relatively constant height with only slight decrease after six hours. An example of the height change curves can be found in **Figure 4.18**, where the curve in the circle symbol represents the height change for the totally drip-through sample, while the curve in the diamond symbol represents the partially collapsed sample, with only 20% height change at the end of the 2 hr drip-through test.

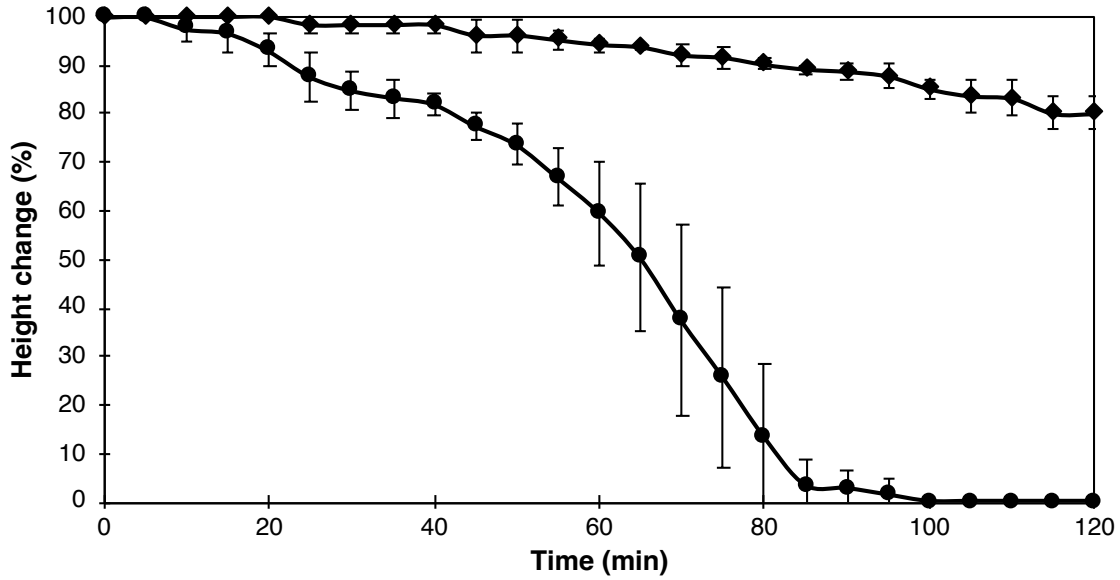

Figure 4.18 Example ice cream height change curves. The error bars represent standard deviation of mean values among six samples. Circle, ice cream with 0% stabilizer (ST), 0% polysorbate 80 (PS80) and 50% overrun (OR); diamond, ice cream with 0.4% ST, 0.03% PS80 and 100% OR.

Table 4.7 displays the height-change rate (cm/min) of ice cream, calculated by determining the slope of the linear region of the height curve. The results indicate that the height-change rate ranged from 0.007 to 0.042 cm/min, depending on the levels of polysorbate 80, stabilizer, and overrun. A higher height-change rate suggests a greater degree of collapse during melting. The ice cream sample with 50% overrun and no stabilizer demonstrated the highest height-change rate among all the samples, while the ice cream containing 0.4% stabilizer generally exhibited the lowest rate. A trend of decreased height-change rate with increasing overrun was observed in ice cream without stabilizer ($r=-0.8060$, $p=0.0087$); however, there was no significant correlation between overrun and height-change rate across all samples ($r=-0.3187$, $p=0.1051$).

Table 4.7 Mean and standard deviation of heigh-change rate. The standard deviation (±) refers to the variation between duplicate drip-through rate of the ice cream with different stabilizers, overrun, or polysorbate 80 levels.

Height-change rate (cm/min)*				
Stabilizer	Overrun	Polysorbate 80		
		0.000%	0.015%	0.030%
0.0%	50%	$0.042 \pm 0.003^{x,X,A}$	$0.029 \pm 0.003^{y,X,A}$	$0.026 \pm 0.006^{y,X,A}$
	75%	$0.024 \pm 0.004^{x,Y,A}$	$0.026 \pm 0.004^{x,X,A}$	$0.019 \pm 0.001^{y,Y,A}$
	100%	$0.019 \pm 0.003^{x,Z,A}$	$0.018 \pm 0.001^{xy,Y,A}$	$0.014 \pm 0.002^{y,Y,A}$
0.2%	50%	$0.017 \pm 0.004^{x,X,B}$	$0.015 \pm 0.006^{x,X,B}$	$0.011 \pm 0.002^{x,X,B}$
	75%	$0.013 \pm 0.002^{x,Y,B}$	$0.008 \pm 0.001^{y,X,B}$	$0.012 \pm 0.002^{x,X,B}$
	100%	$0.013 \pm 0.002^{x,Y,B}$	$0.015 \pm 0.009^{x,X,A}$	$0.007 \pm 0.002^{x,Y,B}$
0.4%	50%	$0.011 \pm 0.004^{x,X.C}$	$0.007 \pm 0.002^{x,X,C}$	$0.010 \pm 0.003^{x,X,B}$
	75%	$0.010 \pm 0.002^{x,X,B}$	$0.009 \pm 0.001^{x,X,B}$	$0.009 \pm 0.005^{x,X,B}$
	100%	$0.010 \pm 0.002^{x,X,B}$	$0.009 \pm 0.002^{x,X,A}$	$0.008 \pm 0.004^{x,X,B}$

* Tukey's HSD test was performed for the significant difference at $P<0.05$

$^{x, y, z}$ denote significant differences among ice cream with different polysorbate 80 levels

$^{X, Y, Z}$ denote significant differences among ice cream with different overrun levels

$^{A, B, C}$ denote significant differences among ice cream with different stabilizer levels

In general, a negative correlation was observed between fat destabilization and height-change rate ($r=-0.7572$, $p<0.0001$); however, stabilizer levels also affected this correlation. **Figure 4.19** displays a strong negative correlation between fat destabilization and height-change rate in ice cream with 0% stabilizer ($r=-0.8187$, $p=0.0070$). Nevertheless, due to the narrow range of height-change rates (0.007% to 0.017% and 0.007% to 0.011%, respectively), only a minor reduction in height-change rate was observed in ice cream with 0.2% ($r=-0.5055$, $p=0.1650$) or 0.4% stabilizer ($r=-0.2841$, $p=0.4588$). When ice cream contained a greater degree of fat destabilization without stabilizer, the foam structure was maintained by the network of fat clusters and air cells, resulting in less variation in height. However, the effect of stabilizer on height-change rate was significant, as the presence of stabilizers slowed the collapse of the melted ice cream structure due to the low mobility of the serum phase, resulting in a gradual change in height.

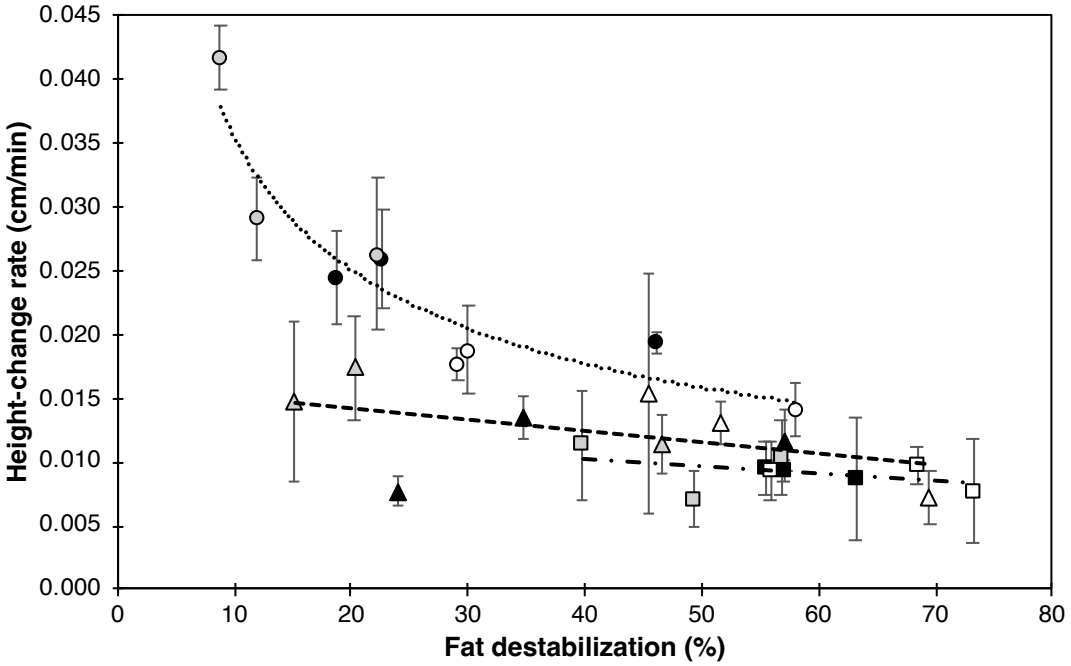

Figure 4.19 The correlation between height-change rate and fat destabilization extent. The error bars stand for standard deviation of mean values among six samples. Grey, 50% overrun; black, 75% overrun; hollow, 100% overrun. Circle, 0% stabilizer; triangle, 0.2% stabilizer; square, 0.4% stabilizer.

Figure 4.20 shows that ice cream mix viscosity was negatively correlated with height-change rate, with an increase in viscosity leading to a decrease in the rate of ice cream collapse. This trend was similar to the effect observed on drip-through rate (**Figure 4.13**). During the meltdown process, ice cream samples with the lowest fat destabilization (8.8% and 11.8%) melted gradually from the outer layer, shrunk to a core, and exhibited a low height-change rate during the first hour of melting (**Figure 4.18**). The rapid height-change rate in these samples was mainly due to the core melting and rapidly dripping through in the latter part of the meltdown (**Figure 4.18**). In contrast, for the remaining ice cream samples, the structure partially collapsed but stopped when the fat globule clusters and air cells became jammed at a certain height, limiting the height-change rate within a narrow range.

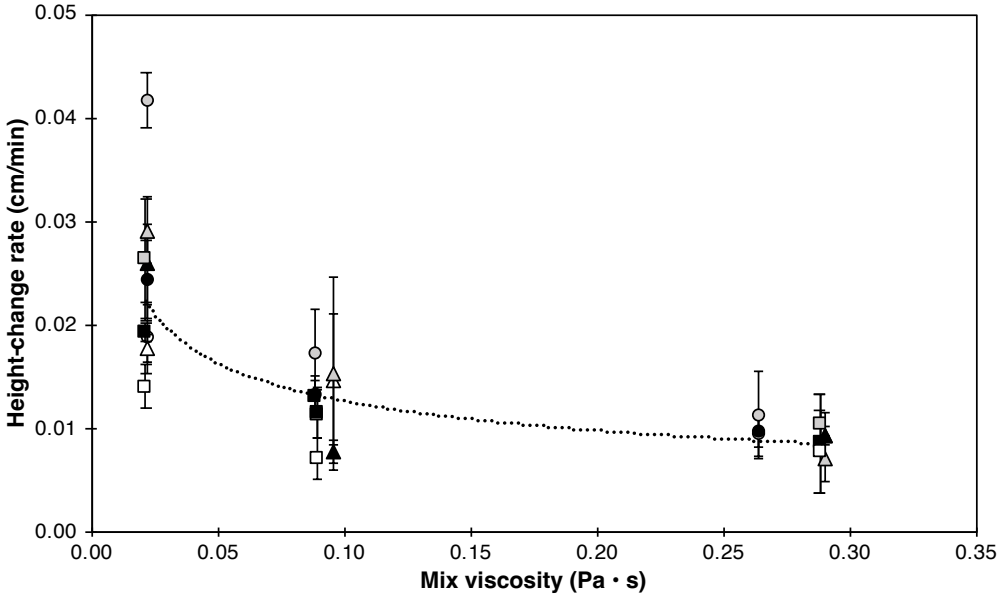

Figure 4.20 The correlation between height-change rate and mix viscosity (50 s^{-1} shear rate). The error bars represent standard deviation of mean values among six samples. Circle, 0% polysorbate 80 (PS80); triangle, 0.015% PS80; square, 0.03% PS80. Grey, 50% overrun; black, 75% overrun; hollow, 100% overrun.

4.1.2.5 The effect of major structural elements on final height on height curve

Table 4.8 presents the final height (%) of ice cream, calculated by dividing the final height by the original height. The results indicate that the final height varied from 0 to 59.9%, depending on the levels of polysorbate 80, stabilizer, and overrun. A higher final height suggests a greater degree of remnant foam left on the mesh. The ice cream sample with 50% overrun and no stabilizer had no foam left after 2 hr, while the ice cream containing 0.4% stabilizer generally showed the highest amount of remnant foam. The correlation between overrun and final height was only seen in ice creams without added stabilizer ($r=0.9518$, $p<0.0001$). Among ice creams with low serum phase viscosity, the 50% overrun samples had the lowest final height (0% to 13%) compared to 75% overrun (16% to 20%) and 100% overrun (34% to 40%). Nonetheless, the effect of mix viscosity was dominant in the drainage process. The extent of fat destabilization has been linked to shape retention in previous studies (Bolliger et al., 2000; Tharp et al., 1997; Warren & Hartel, 2018). In this study, a positive correlation between fat destabilization and final height was also shown in all ice cream samples ($r=0.8571$, $p<0.0001$). This is likely due to the stabilization of the structure provided by the fat clusters and air cells on the mesh after the meltdown test.

A strong correlation between ice cream mix viscosity and final height was observed ($r=0.8051$, $p<0.0001$) as depicted in **Figure 4.21**. A higher viscosity of the serum phase facilitated better shape and structure retention by providing resistance to drainage. Notably, for ice cream with 50% overrun, the final height showed a wider range (0% to 58%) when mix viscosity varied as compared to ice creams with 75% and 100% overrun (ranging from 16% to 60% and from 34% to 59%, respectively). However, when mix viscosity was increased to 0.29 Pa•s, the impact of overrun was minimized.

Table 4.8 Mean and standard deviation of final height. The standard deviation (±) refers to the variation between duplicate drip-through rate of the ice cream with different stabilizers, overrun, or polysorbate 80 levels.

Final height (%)*				
Stabilizer	Overrun	Polysorbate 80		
		0.000%	0.015%	0.030%
0.0%	50%	$0.0 \pm 0.0^{x,X,A}$	$7.7 \pm 2.9^{y,X,A}$	$13.1 \pm 5.8^{y,X,A}$
	75%	$16.4 \pm 2.1^{x,Y,A}$	$17.8 \pm 2.7^{x,Y,A}$	$19.7 \pm 3.6^{x,X,A}$
	100%	$34.4 \pm 2.0^{x,Z,A}$	$38.2 \pm 4.4^{xy,Z,A}$	$40.2 \pm 4.0^{y,Y,A}$
0.2%	50%	$25.5 \pm 3.9^{x,X,B}$	$30.0 \pm 4.8^{x,X,B}$	$42.2 \pm 4.3^{y,X,B}$
	75%	$36.1 \pm 6.4^{x,Y,B}$	$34.0 \pm 15.3^{x,X,B}$	$44.0 \pm 2.5^{x,X,B}$
	100%	$48.2 \pm 4.3^{x,Z,B}$	$34.4 \pm 8.6^{y,X,A}$	$50.6 \pm 3.3^{x,Y,B}$
0.4%	50%	$45.3 \pm 5.2^{x,X,C}$	$57.8 \pm 3.5^{y,X,C}$	$57.7 \pm 6.5^{y,X,C}$
	75%	$52.2 \pm 4.3^{x,Y,C}$	$54.7 \pm 1.5^{x,X,C}$	$59.9 \pm 2.3^{y,X,C}$
	100%	$52.7 \pm 2.4^{x,Y,B}$	$57.0 \pm 4.2^{xy,X,B}$	$59.1 \pm 5.3^{y,X,C}$

* Tukey's HSD test was performed for the significant difference at $P<0.05$

$^{x, y, z}$ denote significant differences among ice cream with different polysorbate 80 levels

$^{X, Y, Z}$ denote significant differences among ice cream with different overrun levels

$^{A, B, C}$ denote significant differences among ice cream with different stabilizer levels

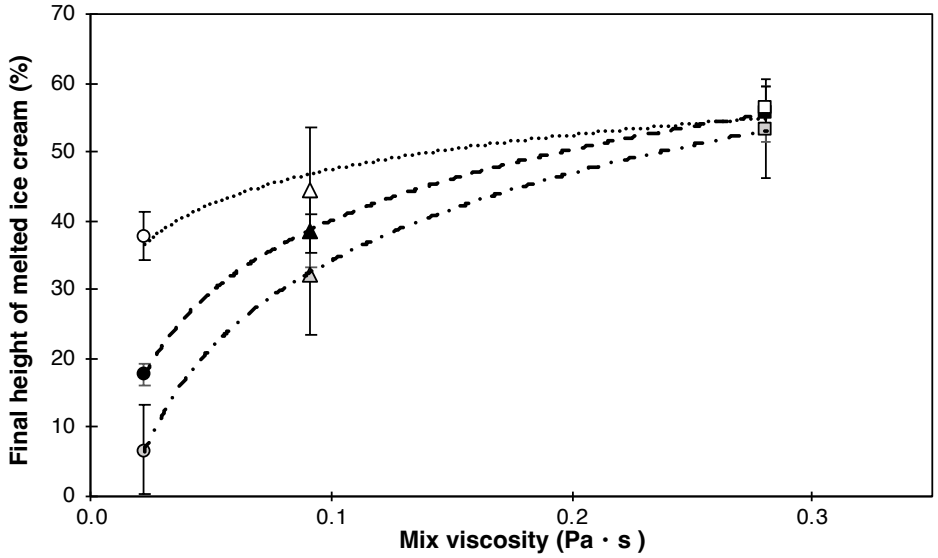

Figure 4.21 The correlation between final height of melted ice cream and mix viscosity (50 s^{-1} shear rate). The error bars represent the standard deviation of mean values among three formulas regardless of polysorbate 80 level. Circle, 0% stabilizer; triangle, 0.2% stabilizer; square, 0.4% stabilizer. Grey, 50% overrun; black, 75% overrun; hollow, 100% overrun.

4.1.3 Summary

In this study, a variety of ice cream structures were achieved through different formulations. The use of three levels of stabilizers, overrun, and polysorbate 80 aimed to primarily adjust the mix viscosity, amount of air, and fat destabilization, respectively. However, it was found that fat destabilization was not solely influenced by the presence of polysorbate 80. An increase in overrun or mix viscosity also led to greater fat destabilization, likely caused by the higher shear force generated during freezing.

This study introduced several additional indicators to describe the melting behavior of ice cream beyond just the drip-through rate. These indicators include the induction time, final drip-through weight, height change rate, and final height. Furthermore, the meltdown curve and height-change curve offer further insights into the melting process of ice cream, including different types of melting behavior and overall structural stability.

Of all the factors examined, ice cream mix viscosity was found to be the most significant in governing the meltdown process. Without stabilizers, ice cream exhibited the least viscous serum phase, and the melting behavior was also influenced by other microstructural elements, such as fat destabilization and overrun. However, in the presence of stabilizers, the viscosity of the serum phase played a dominant role in restricting the mobility of other structural components and limited liquid drainage.

4.2 The effect of rheological properties on meltdown behavior of non-aerated frozen sucrose system

Starting from this section, a sucrose model system was designed to investigate how rheological properties, air, and protein impact the meltdown behavior of ice cream. Each main structural component of ice cream was added to the system successively to gain a better understanding of its effects, excluding milkfat, which was thought to be one of the components responsible for providing rigidity to the structure and slowing down the melting rate during ice cream meltdown (Warren & Hartel, 2018).

In section **4.1**, it was found that the viscosity of the ice cream mix had an important effect on meltdown behavior. As aforementioned, the viscosity was modified by adjusting the amount of stabilizers in the mix. As more stabilizers were added, the viscosity increased, and the ice cream mix exhibited more shear-thinning behavior. It is intriguing to determine whether the apparent viscosity or the shear-thinning behavior plays a more dominant role in the meltdown process. To investigate this, two sets of experiments were designed in this study to observe how the rheological properties affect the meltdown process. One set had the same apparent viscosity (at a shear rate of 5 s^{-1}) but different shear-thinning behavior, while the other set had the same shear-thinning behavior but different apparent viscosity (at a shear rate of 5 s^{-1}). The shear rate for gravitational drainage typically ranges from 0.1 to 10 s^{-1} (Steffe, 1996). The choice of a 5 s^{-1} shear rate is based on its effectiveness as the lowest attainable shear rate in the flow ramp test.

4.2.1 Rheology

As mentioned above, two sets of experiments were designed to separate the effect of apparent viscosity and shear-thinning behavior, as denoted as flow rate index, on meltdown behavior. To separate these two parameters, different polysaccharides were chosen, assuming that the type of polysaccharide affected only rheological properties and had no effect on the meltdown. The flow rate index was calculated using the power law model, and any rheological changes during the freezing-melting process were observed by measuring the rheology of the melted liquid.

Table 4.9 presents the rheological properties of two sets of experiment, including flow rate index, apparent viscosity (at 5 s^{-1} shear rate), and consistency. It is worth noting that, although a statistical difference was detected in the flow rate index within the same experiment, the disparity among the samples was deemed insignificant. In the experiment with identical flow rate index, the selection of polysaccharide systems resulted in a broad range of apparent viscosity, ranging from 0.10 to 0.26 Pa•s. Meanwhile, in the experiment with identical viscosity, the choice of polysaccharide systems yielded a wide range of flow rate index, varying from 0.47 to 0.86. The xanthan gum solution exhibited the most shear-thinning behavior, whereas the pectin displayed the least shear-thinning behavior.

Table 4.9 Flow rate index, apparent viscosity at 5 s^{-1} shear rate, and consistency coefficient of the power law model for samples with same flow rate index and same apparent viscosity. The standard deviation (±) refers to the variation among triplicate samples.

Same flow rate index/shear-thinning behavior*			
Sample	Flow rate index	Apparent viscosity at 5 s^{-1}(Pa•s)	Consistency (Pa•s)
0.22% guar gum (GG)	0.73 ± 0.00^{b}	0.104 ± 0.002^{c}	0.18 ± 0.00^{c}
0.3% locust bean gum (LBG)	0.74 ± 0.00^{a}	0.147 ± 0.003^{b}	0.26 ± 0.01^{b}
0.3% sodium alginate (SA)	0.74 ± 0.00^{a}	0.258 ± 0.002^{a}	0.45 ± 0.01^{a}
Same apparent viscosity at 5 s^{-1} (Pa•s)*			
Sample	Flow index	Apparent viscosity at 5 s^{-1}(Pa•s)	Consistency (Pa•s)
0.11% xanthan (XAN)	0.47 ± 0.00^{d}	0.195 ± 0.007^{a}	0.46 ± 0.02^{a}
0.28% guar gum (GG)	0.66 ± 0.00^{c}	0.194 ± 0.007^{a}	0.37 ± 0.01^{b}
0.25% sodium alginate (SA)	0.76 ± 0.00^{b}	0.192 ± 0.002^{a}	0.33 ± 0.00^{c}
0.7% pectin (PEC)	0.86 ± 0.01^{a}	0.197 ± 0.005^{a}	0.28 ± 0.01^{d}

*Tukey's HSD test was performed for the significant difference at $P<0.05$

^{a,b,c,d} denote significant differences among samples in same set of experiment

4.2.2 Freezing point

The freezing point of different amounts of polysaccharides varied within a narrow range of -2.81 to -2.97 ˚C as shown in **Table 4.10**. Although there may be some statistical differences among samples, these were likely due to slight adjustments made to the water content. Overall, the freezing points fell within a relatively consistent range. Freezing point depression is primarily influenced by low molecular weight solutes like sucrose and salt, which reduce the vapor pressure of water. This reduction in vapor pressure causes the equilibrium between the vapor pressure of pure water and ice to be achieved at a lower temperature. In contrast, large molecules such as polysaccharides are not expected to affect either the freezing point depression or the latent heat of fusion of water (Flores & Goff, 1999a; Livney & Hartel, 1997).

Table 4.10 Freezing point (˚C) of the solution as measured by osmometer. The standard deviation (±) refers to the variation among triplicate samples.

Same flow rate index*	
0.22% GG	-2.84 ± 0.06[a]
0.3% LBG	-2.84 ± 0.01[a]
0.3% SA	-2.86 ± 0.04[a]
Same apparent viscosity*	
0.11% XAN	-2.83 ± 0.02[ab]
0.28% GG	-2.81 ± 0.01[a]
0.25% SA	-2.84 ± 0.01[b]
0.7% PEC	-2.97 ± 0.03[c]

*Tukey's HSD test was performed for the significant difference at $P<0.05$

[a,b,c] denote significant differences among samples in same set of experiment

4.2.3 Surface tension

In this study, all the samples exhibited a gradual decrease in surface tension over time, as illustrated in **Figure 4.22** and **Table 4.11**. A higher concentration of guar gum and sodium alginate resulted in a slight reduction of surface tension, as more polysaccharides were available to migrate to the surface. Notably, pectin and galactomannans such as guar gum and locust bean gum demonstrated a greater surface-active property, reducing surface tension to 54-58.4 mN/m, in comparison to xanthan and sodium alginate (**Table 4.11**). Anionic polysaccharides such as sodium alginate and pectin, which contain diaxial 1-4 glycoside bonds, exhibit surface-active properties due to electrostatic repulsion at the interface (Garti & Leser, 2001). Additionally, the functional groups within pectin, including its protein moieties and ester group, influence its emulsifying properties by altering the hydrophobicity of pectin molecules, ultimately leading to a reduction in surface tension (Schmidt et al., 2015).

Despite the fact that high viscosity generates more viscous force, which might affect surface tension, it is noteworthy that the tensile strength of the surface, also referred to as surface stickiness, has a stronger correlation with surface tension than viscosity (Adhikari et al., 2007). In this study, apparent viscosity measured at 0˚C and surface tension did not exhibit any correlation among all samples (r=0.4185), indicating that the surface-active property of the polysaccharide is related to its nature rather than any changes in viscosity.

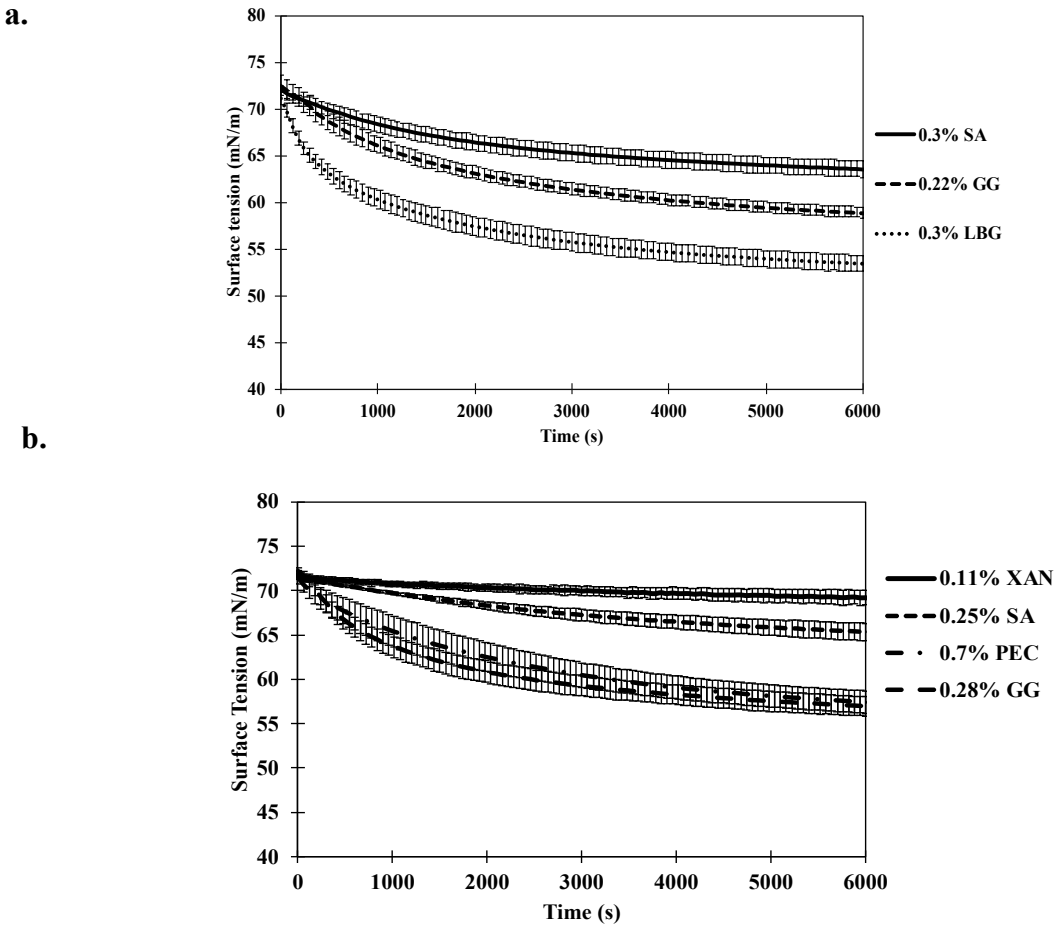

Figure 4.22 Surface tension of samples with same flow rate index (a), and same apparent viscosity at 5 s^{-1} shear rate (b). The error bars represent the standard deviation of surface tension measured in triplicate.

Although polysaccharides are typically hydrophilic and not considered emulsifiers, some polysaccharides containing protein, such as gum arabic (Yadav et al., 2007), certain modified starches (Chanamai & McClements, 2002), and gelatin (Lobo, 2002), exhibit emulsifying activity due to the hydrophobic groups in their protein portion. However, there was no correlation found between the protein content in the ingredients - xanthan (6.64%), sodium alginate (0.3%), locust bean gum (0%), guar gum (4.14%), and pectin (0%) - and surface tension, which is consistent with the findings of Wu et al. (2009).

Table 4.11 Surface tension (mN/m) of the solution at 2 hr. The standard deviation (±) refers to the variation among triplicate samples.

Same flow rate index*	
0.22% GG	58.4 ± 0.8^{b}
0.3% LBG	54.0 ± 0.6^{c}
0.3% SA	63.2 ± 0.9^{a}
Same apparent viscosity*	
0.11% XAN	69.0 ± 1.0^{a}
0.28% GG	56.4 ± 1.0^{c}
0.25% SA	64.9 ± 1.0^{b}
0.7% PEC	56.8 ± 1.2^{c}

*Tukey's HSD test was performed for the significant difference at $P<0.05$
^{a,b,c} denote significant differences among samples in same set of experiment

Docoslis et al. (2000) demonstrated that while monomeric molecules, such as sucrose and glucose, can increase surface tension, their polymer counterparts, such as ficoll and dextran, cause a decrease in surface tension. In their monomeric state, the sugar molecules increase cohesion due to hydrogen bonding and are repelled by the water-air interface, resulting in a thin sugar-depletion zone and an increase in surface tension. However, upon polymerization into polysaccharides, the molecules lose their bipolarity, limit hydrogen-bonding interactions, and decrease liquid cohesion, causing a decrease in the surface tension. Polysaccharides retain their surface-active properties even after protein purification (Garti & Reichman, 1994).

4.2.4 Overrun

While designed as a non-aerated system for study, air was unavoidably incorporated into the system during churning and freezing as a result of shear forces from the viscous fluid. A strong negative correlation was found between apparent viscosity and overrun among the samples with same flow rate index (r=-0.7193), whereas no correlation was found among the samples with same apparent viscosity at 5 s^{-1} shear rate (r=0.0974). Given only three polysaccharide systems were tested in the experiment with the same flow rate index, it is difficult to draw a clear conclusion regarding the relationship between apparent viscosity and overrun. As shown in **Table 4.12**, the percentage of overrun ranged from 9.2% to 17.5%. Despite the polysaccharides exhibiting surface-active properties, no correlation was found between surface tension and overrun (r=-0.4407). Among all the polysaccharide systems, guar gum showed the highest ability to incorporate air bubbles and increase overrun, which may be attributed to the protein it contains.

Table 4.12 Overrun (%) of the frozen samples. The standard deviation (±) refers to the variation among triplicate samples.

Same flow rate index*	
0.22% GG	17.5 ± 1.4^{a}
0.3% LBG	13.7 ± 1.0^{b}
0.3% SA	11.9 ± 2.9^{b}
Same apparent viscosity*	
0.11% XAN	12.4 ± 0.7^{b}
0.28% GG	16.1 ± 0.8^{a}
0.25% SA	9.2 ± 1.5^{c}
0.7% PEC	9.8 ± 1.4^{c}

*Tukey's HSD test was performed for the significant difference at $P<0.05$
^{a,b,c} denote significant differences among samples in same set of experiment

4.2.5 Ice crystal size

The mean ice crystal size falls within a range of 49.7 to 59.2 μm, as presented in **Table 4.13**, which is generally larger than that of normal ice cream. This is attributed to insufficient churning caused by the benchtop freezer. Examples of ice crystal images are shown in **Figure 4.23**. No significant trend was observed between the type of stabilizer and ice crystal size in either experiment, which is consistent with previous studies (Hagiwara & Hartel, 1996). Furthermore, no correlation was found between overrun and ice crystal size in both experiments (same flow rate index: r=-0.1484, same apparent viscosity: r=0.5859), given the narrow range of both overrun and ice crystal size. It should be noted that only ice crystals within the 40X magnification frame were counted, which resulted in the exclusion of some larger ice crystals.

Table 4.13 Mean ice crystal size (μm) of the frozen samples. The standard deviation (±) refers to the variation among triplicate samples.

Same flow rate index*	
0.22% GG	56.0 ± 4.6^{a}
0.3% LBG	55.5 ± 5.6^{a}
0.3% SA	59.2 ± 4.9^{a}
Same apparent viscosity*	
0.11% XAN	53.7 ± 4.6^{ab}
0.28% GG	58.2 ± 3.8^{a}
0.25% SA	53.1 ± 3.7^{ab}
0.7% PEC	49.7 ± 3.2^{b}

*Tukey's HSD test was performed for the significant difference at $P<0.05$
^{a,b,c} denote significant differences among samples in same set of experiment

a.

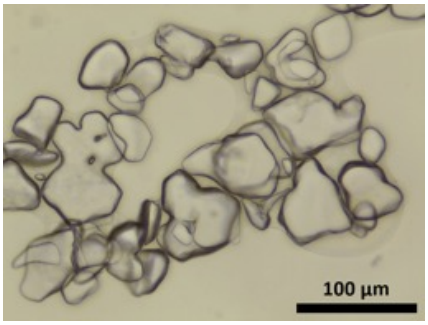

0.22% guar gum

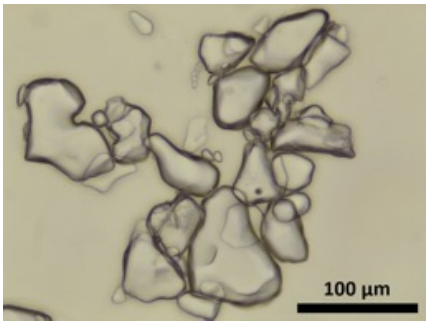

0.3% locust bean gum

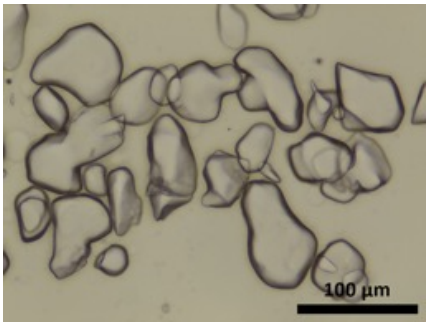

0.3% sodium alginate

b.

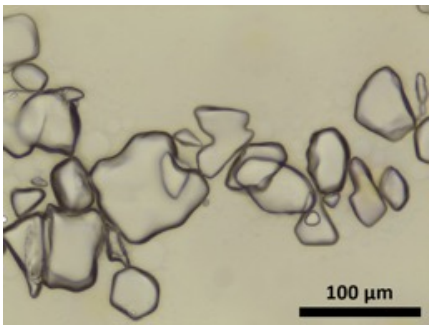

0.11% xanthan

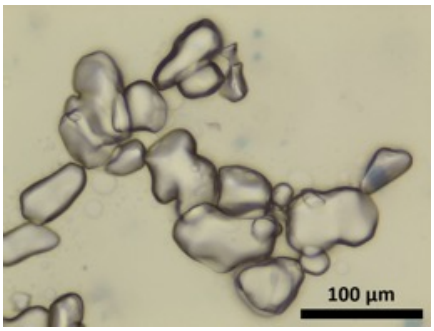

0.25% sodium alginate

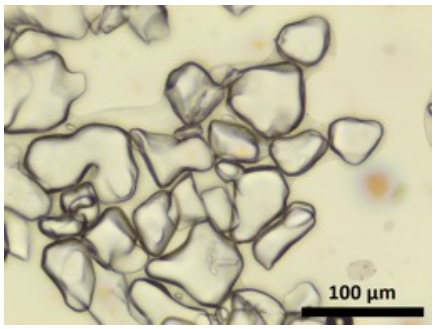

0.28% guar gum

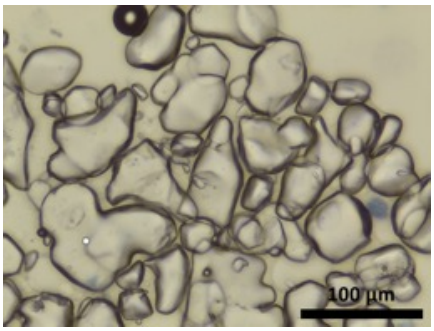

0.7% pectin

Figure 4.23 Example of ice crystals images for samples with the same flow rate index (a), and the same apparent viscosity at 5 s^{-1} shear rate (b).

4.2.6 Meltdown

Little structure was developed in the simple system, resulting in narrow ranges for both induction time and melting rate, ranging from 37.3 to 42.1 min and 1.58 to 1.90 g/min, respectively (**Table 4.14**). There was no statistical difference in induction time among samples, regardless of whether they had the same flow rate index or the same apparent viscosity. Samples with the same apparent viscosity showed a slightly higher induction time. Furthermore, there was no correlation found between induction time and overrun, ice crystal size, viscosity, or flow rate index in either set of experiments.

Samples with either the same flow rate index or the same apparent viscosity exhibited similar meltdown behavior, except for the 0.3% locust bean gum system, which also showed a slowest melting rate (**Figure 4.24** and **Table 4.14**). During the melting process, the melted liquid forms a thin film layer that surrounds the frozen samples and flows on its surface (Iwasaki et al., 2010). The liquid then flows to the bottom of the frozen samples, forming droplets that eventually drip by gravitational force. For samples that melt into a hemispherical shape, the surface thin layer of liquid keeps dripping through the mesh, while the remaining part melts layer by layer. In contrast, samples like locust bean gum take longer to drip because the thin film layer does not drip promptly, and a liquid layer is building up at the bottom of the frozen samples. As time goes by, more liquid accumulates and spreads out on the screen, waiting to form droplets. In such cases, the sample melts/collapses differently and its melting rate decreases.

All the samples completely dripped through the mesh at the end of the meltdown test without leaving a large quantity of remnant foams on the mesh, as seen in the ice cream sample. However, a thin bubble layer was observed in the pectin system both on the mesh, as shown in **Figure 4.24c**, and in the melted liquid. This indicates that the foam layer left on the screen, which

is generally caused by surface-active molecules, can stabilize the air bubbles while waiting to drip. Any samples that were not able to drip, whether due to high viscosity or low surface tension, had the chance to leave a foam layer on the mesh due to the presence of surface-active molecules. Meanwhile, the remaining surface-active molecules drain along with the melted liquid and air bubbles, causing a thin layer of foam floating on the melted liquid.

Table 4.14 The induction time and melting rate of samples with same flow rate index and same apparent viscosity. The standard deviation (±) refers to the variation among triplicate samples.

Same flow rate index/shear-thinning behavior*		
Sample	Induction time (min)	Melting rate (g/min)
0.22% guar gum (GG)	37.3 ± 2.7^{a}	1.70 ± 0.11^{b}
0.3% locust bean gum (LBG)	39.6 ± 2.2^{a}	1.58 ± 0.09^{c}
0.3% sodium alginate (SA)	38.6 ± 2.5^{a}	1.95 ± 0.02^{a}
Same apparent viscosity at 5 s^{-1} (Pa•s)*		
Sample	Induction time (min)	Melting rate (g/min)
0.11% xanthan (XAN)	41.9 ± 2.8^{a}	1.90 ± 0.05^{a}
0.28% guar gum (GG)	42.1 ± 3.5^{a}	1.60 ± 0.16^{c}
0.25% sodium alginate (SA)	41.3 ± 2.9^{a}	1.81 ± 0.10^{ab}
0.7% pectin (PEC)	41.2 ± 3.4^{a}	1.75 ± 0.08^{b}

*Tukey's HSD test was performed for the significant difference at $P<0.05$
^{a,b,c} denote significant differences among samples in same set of experiment

It is interesting to note that despite the simplicity of the system, two distinct meltdown behaviors were observed. During the preliminary study of locust bean gum (LBG), varying the concentration of the LBG led to different meltdown behaviors. At a concentration of 0.15%, the sample displayed the same hemispherical meltdown behavior as other samples in this study. However, when 0.25% or 0.3% locust bean gum was used, the behavior of liquid spreading on the mesh before dripping through was observed (**Figure 4.25**). The latter melting behavior observed at higher concentrations of locust bean gum may be due to the formation of cryo-gel during the

freezing-thawing process. When the sample is frozen, water freezes into ice while the remaining solute, including sugar and polysaccharide, concentrates into unfrozen phase. As ice crystals grow, locust bean gum molecules are displaced, and its mannose chains are of sufficient size to create lateral linkages, resulting in the creation of junction zones via the accumulation of locust bean gum molecules (Hatakeyama et al., 2005; Tanaka et al., 1998). This process results in the creation of a cryo-gel structure that is able to maintain its integrity even after the ice melts (Goff et al., 1999). As a result, during the melting process, the cryo-gel formed by locust bean gum is able to hold its structure, allowing melted liquid to spread on the mesh until it reaches a certain threshold before dripping through.

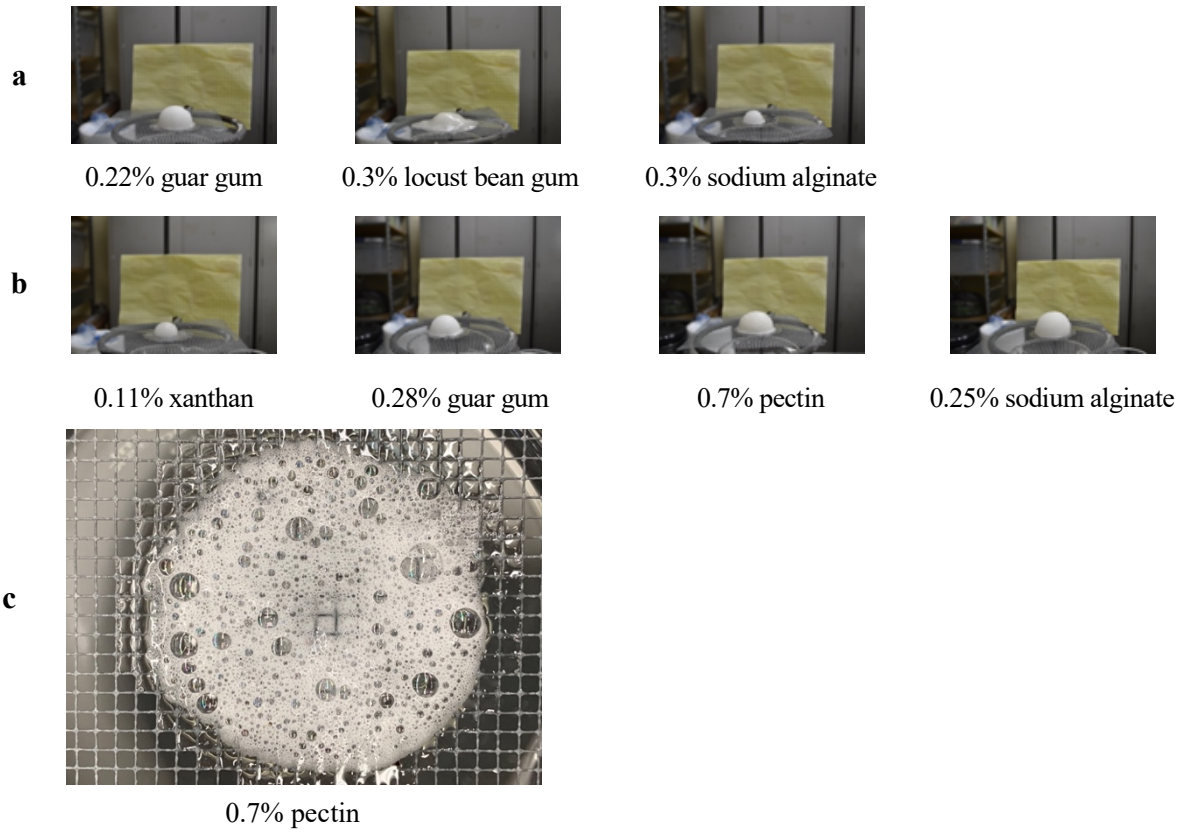

Figure 4.24 Meltdown images of sample on the screen with (a) same flow rate index, and (b) same apparent viscosity at 5 s^{-1} shear rate at 120 min of the meltdown test. (c) displayed the thin bubble layer left on the mesh after the meltdown test of 0.7% pectin sample.

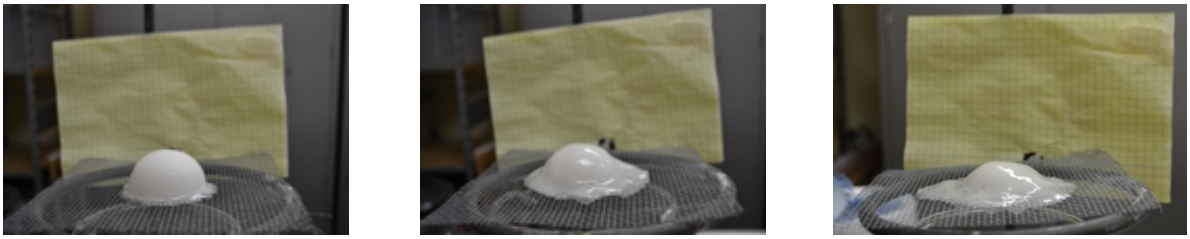

0.15% 0.25% 0.3%

Figure 4.25 Meltdown images of sample on the screen with three levels of locust bean gum at 120 min of the meltdown test.

Although no significant trend in melting rate was observed in either set of experiments related to rheological properties, a noteworthy correlations between surface tension, the type of polysaccharide, and melting rate were discovered when all samples were analyzed together (**Figure 4.26**). Higher surface tension was positively correlated with faster melting rates (r=0.7493), with samples having anionic polysaccharides, such as xanthan and sodium alginate, having higher surface tension. One possible explanation for this observation is that liquids with higher surface tension tend to form larger droplets on the bottom of the screen, resulting in a faster dripping rate. When droplets pass through a wire mesh, their size (D') can be related to the surface tension and density of the liquid, as well as the opening of the mesh, as demonstrated by equation 4-1 (Hung & Yao, 2002):

$$D' = \left[\frac{12\sigma}{\pi\rho_L g}\, D\right]^{1/3} \qquad 4\text{-}1$$

where σ is surface tension, ρ_L is the density of liquid, g is the gravitational acceleration constant, and D is the opening size of the mesh. A positive correlation was found between surface tension and droplet size (r=0.758), as calculated from equation 4-1 (**Table 4.15**).

a.

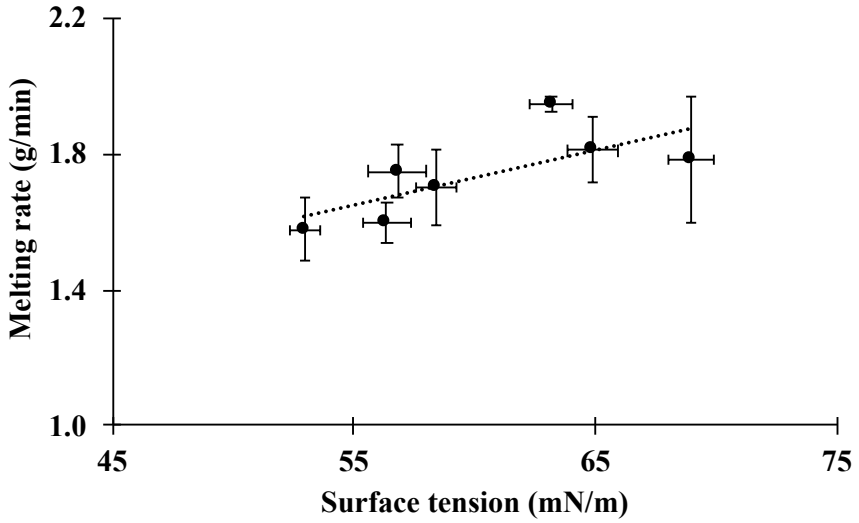

b.

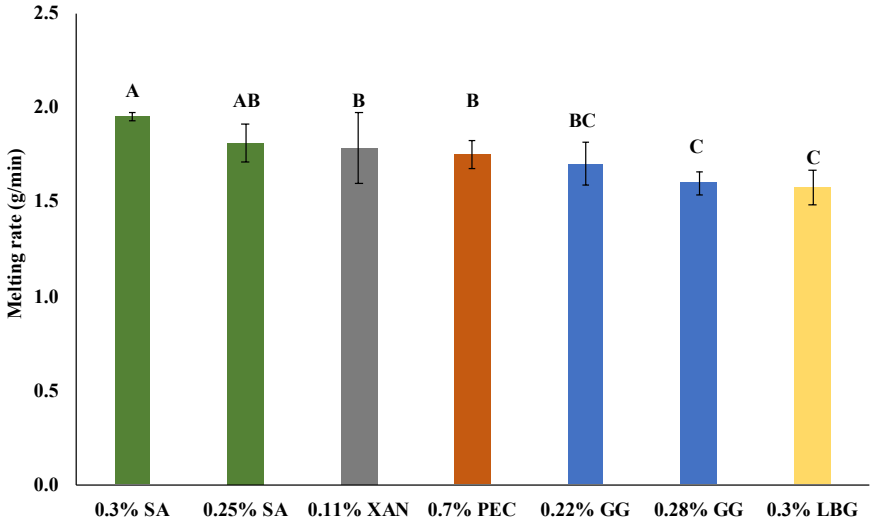

Figure 4.26 (a) The correlation between surface tension and melting rate, and (b) the grouping of melting rate based on the type of polysaccharides. The error bars in (a) and (b) represent the standard deviation of melting rate/surface tension measured in triplicate.

Table 4.15 The calculated droplet size (mm) from equation 4-1 of samples with same flow rate index and same apparent viscosity. The standard deviation (±) refers to the variation among triplicate samples.

Same flow rate index*	
0.22% GG	4.05 ± 0.02^{b}
0.3% LBG	3.93 ± 0.02^{c}
0.3% SA	4.16 ± 0.02^{a}
Same apparent viscosity*	
0.11% XAN	4.29 ± 0.02^{a}
0.28% GG	4.00 ± 0.02^{c}
0.25% SA	4.19 ± 0.03^{b}
0.7% PEC	4.01 ± 0.03^{c}

*Tukey's HSD test was performed for the significant difference at $P<0.05$
^{a,b,c} denote significant differences among samples in same set of experiment

The rheological changes during the freezing and melting process were compared by measuring the apparent viscosity of the drip-through solution. In most samples, a slight decrease in viscosity was observed for the drip-through solution compared to the starting solution, which may be due to residue left on the mesh (**Table 4.16**). However, overall, the changes were minimal.

Table 4.16 Apparent viscosity at 5 s^{-1} shear rate of sample before freezing and after melting. The standard deviation (±) refers to the variation among triplicate samples.

Same flow rate index/shear-thinning behavior*		
Sample	Sample before freezing	Drip-through solution
0.22% guar gum (GG)	0.104 ± 0.002^{A}	0.101 ± 0.004^{A}
0.3% locust bean gum (LBG)	0.147 ± 0.003^{A}	0.099 ± 0.008^{B}
0.3% sodium alginate (SA)	0.258 ± 0.002^{A}	0.231 ± 0.006^{B}
Same apparent viscosity at 5 s^{-1} (Pa•s)*		
Sample	Sample before freezing	Drip-through portion
0.11% xanthan (XAN)	0.195 ± 0.007^{A}	0.185 ± 0.006^{B}
0.28% guar gum (GG)	0.194 ± 0.007^{A}	0.200 ± 0.006^{A}
0.25% sodium alginate (SA)	0.192 ± 0.002^{A}	0.181 ± 0.007^{B}
0.7% pectin (PEC)	0.197 ± 0.005^{A}	0.189 ± 0.004^{B}

*Tukey's HSD test was performed for the significant difference at $P<0.05$
^{A,B} denote significant differences among samples in same set of experiment

4.2.7 Unfrozen phase

To investigate whether the rheological properties of the unfrozen phase, the freeze-concentrated serum in the lamella, have an impact on the start of the melting process, its rheological properties were examined. The unfrozen phase was prepared using the method described by Goff et al. (1995) and Masselot et al. (2020), which assumes that 80% of the water in the original formulation is frozen into ice and directly reducing the remaining 20% of water, resulting in an unfrozen phase.

Table 4.17 shows the rheological properties of unfrozen phase measured at -19.6˚C. All samples exhibited a yield stress, with the pectin system demonstrating the highest yield stress and the locust bean gum system displaying the lowest yield stress. A sharp increase in apparent viscosity and consistency was observed in this concentrated system, with the pectin system

showing the highest viscosity and the locust bean gum system displaying the lowest viscosity. However, the shear-thinning behavior or flow rate index did not follow this trend, possibly due to the significant change in the amount of polysaccharide in the unfrozen phase compared to the original solution, given that different systems are being compared. Although galactomannans, such as guar gum and locust bean gum, exhibited the slowest melting rate, their unfrozen phase viscosity was the lowest among the samples.

No significant correlation was found between the rheological properties of the unfrozen phase and the meltdown rate, except for the flow rate index (apparent viscosity: r=0.3185; yield stress: r=0.2133; consistency: r=0.3627; flow rate index: r=-0.7203). The correlation between flow rate index and melting rate is shown in **Figure 4.27**. It was observed that as the flow rate index increased, indicating a more Newtonian fluid behavior, the melting rate slowed down. This suggests that when the ice crystals melt and dilute the unfrozen serum phase, the apparent viscosity of the unfrozen phase, which is more sensitive to shear, decreases more compared to the one with less shear-thinning behavior. The motion of dilution and mixing with the unfrozen phase, which exhibits a more shear-thinning behavior, results in a faster liquid flow and drainage, as evidenced by the melting rate.

Table 4.17 The rheological properties of unfrozen phase measured at -19.6˚C with same flow rate index and same apparent viscosity in the corresponding solution. The standard deviation (±) refers to the variation among triplicate samples.

Same flow rate index/shear-thinning behavior*				
Sample	Flow index	Apparent viscosity at 5 s^{-1} (Pa•s)	Yield stress (Pa)	Consistency coefficient (Pa•s)
0.22% guar gum (GG)	0.86 ± 0.02^{b}	39.94 ± 0.50^{b}	14.19 ± 2.80^{b}	45.84 ± 2.41^{b}
0.3% locust bean gum (LBG)	0.96 ± 0.02^{a}	25.41 ± 5.46^{c}	5.46 ± 2.37^{c}	25.76 ± 1.83^{c}
0.3% sodium alginate (SA)	0.71 ± 0.00^{c}	126.40 ± 5.12^{a}	114.38 ± 7.13^{a}	166.66 ± 10.06^{a}
Same apparent viscosity at 5 s^{-1} (Pa•s)*				
Sample	Flow index	Apparent viscosity at 5 s^{-1} (Pa•s)	Yield stress (Pa)	Consistency coefficient (Pa•s)
0.11% xanthan (XAN)	0.77 ± 0.01^{b}	55.55 ± 1.86^{c}	18.05 ± 3.09^{c}	74.62 ± 3.36^{c}
0.28% guar gum (GG)	0.83 ± 0.01^{a}	51.50 ± 1.88^{c}	18.62 ± 2.24^{c}	61.84 ± 3.58^{c}
0.25% sodium alginate (SA)	0.72 ± 0.01^{c}	105.92 ± 2.46^{b}	101.44 ± 8.69^{b}	135.41 ± 6.93^{b}
0.7% pectin (PEC)	0.63 ± 0.01^{d}	356.33 ± 8.31^{a}	605.02 ± 25.67^{a}	428.23 ± 14.81^{a}

*Tukey's HSD test was performed for the significant difference at $P<0.05$

^{a,b,c,d} denote significant differences among samples in same set of experiment

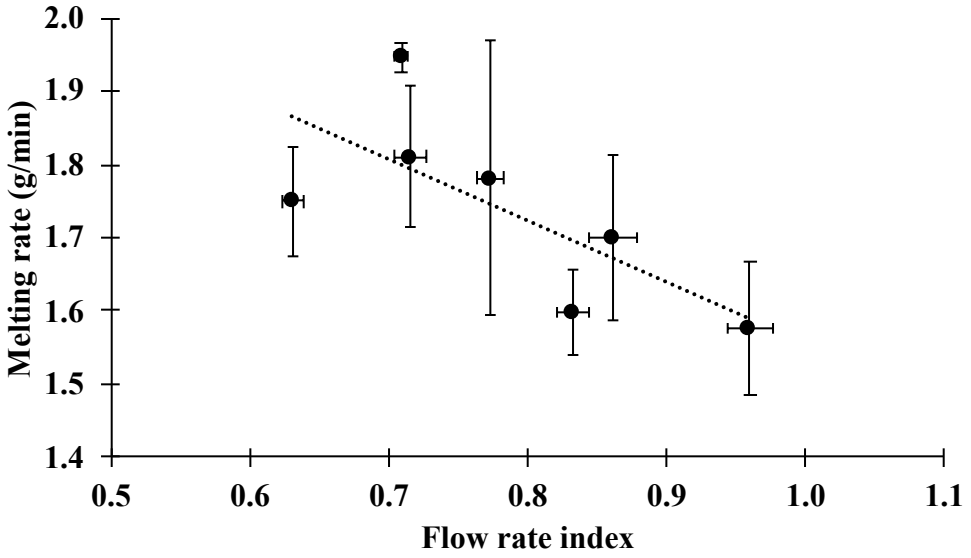

Figure 4.27 The correlation between flow rate index of unfrozen phase measured at -19.6˚C and melting rate. The error bars represent the standard deviation of melting rate and flow rate index measured in triplicate.

The viscoelasticity of the unfrozen phase was explored through a dynamic oscillatory test. G' and G'' indicate the elastic and viscous properties of the samples, respectively. The samples examined in this study can be classified as dilute solutions that exhibit either G'' higher than G' across the entire frequency range (Huang et al., 2016), such as locust bean gum, guar gum, and xanthan, or a crossover at a lower frequency, such as sodium alginate and pectin (**Figure 4.28**).

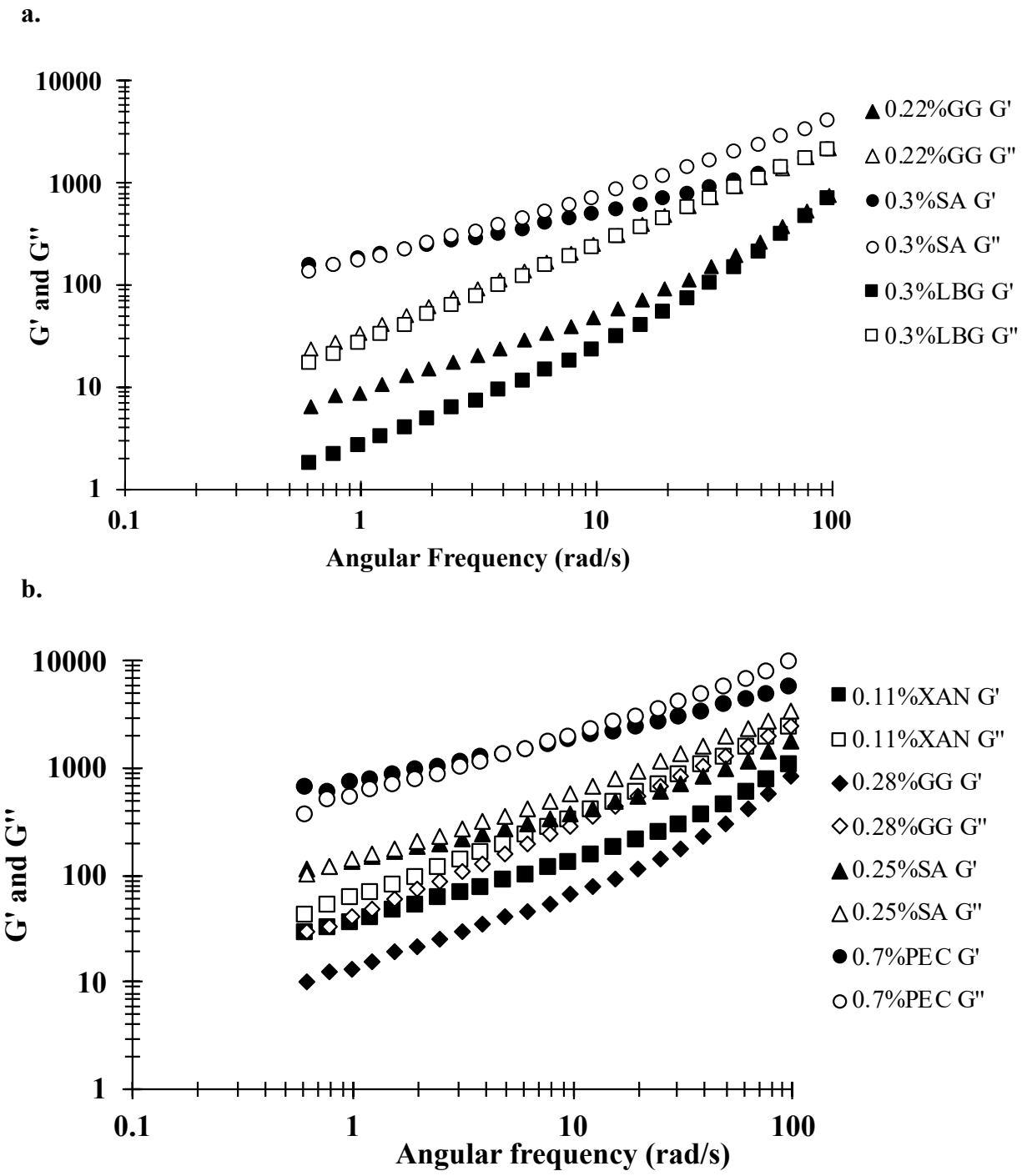

Figure 4.28 The frequency sweep of samples measured at -19.6˚C with (a) same flow rate index and (b) same apparent viscosity at 5 s^{-1} shear rate. GG: guar gum; SA: sodium alginate; LBG: locust bean gum; XAN: xanthan; PEC: pectin.

The unfrozen phase system containing locust bean gum and guar gum exhibited a phase separation phenomenon (**Figure 4.29**). This process occurred rapidly after sample preparation at room temperature, and once mixing stopped, phase separation developed within the system. Due to the high concentration of stabilizers, the distance between adjacent polysaccharide molecules is less than the size of the molecules themselves. This close proximity, along with the gradient of osmotic pressure, likely results in depletion flocculation between the two polysaccharides (Morrison, 2002). Another potential explanation for the phase separation is the occurrence of sugaring out in the concentrated galactomannan system. Initially, the galactomannan molecules form hydrogen bonds with water molecules. However, the addition of a large quantity of sucrose leads to the formation of sugar-water hydrogen bonds, causing the galactomannan to be pushed out and leading to phase separation (Dhamole et al., 2023).

This phase separation phenomenon may indicate that during the freezing process of the product, the unfrozen phase becomes increasingly concentrated due to water freezing into ice. The high polymer concentration may result in phase separation rather than a homogeneous unfrozen phase. Furthermore, during the melting of the sample, the dilution of water from the melted ice may not uniformly dilute the unfrozen phase, leading to variations in local viscosity and resulting in different local flow behaviors during liquid drainage.

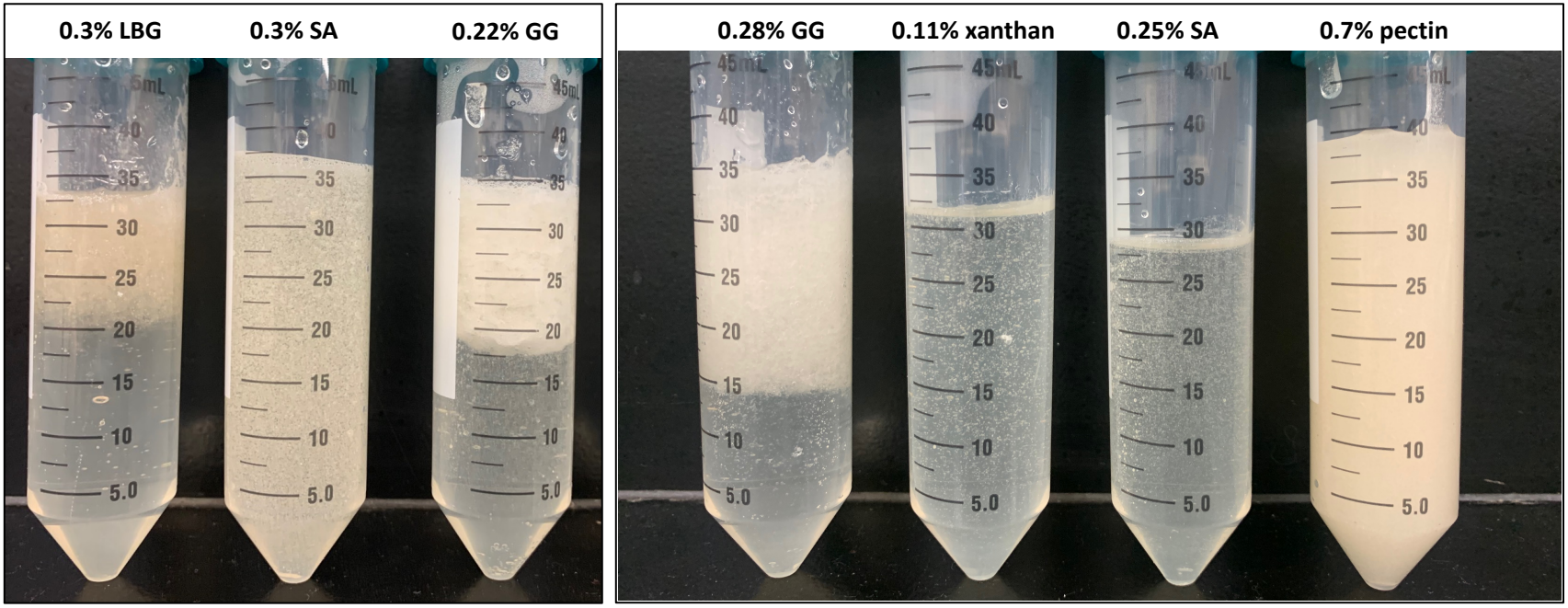

Figure 4.29 Images of unfrozen phase samples with same flow rate index (left) and same apparent viscosity (right).

4.2.8 Summary

The addition of polysaccharides to the sucrose model system exhibited surface-active properties, resulting in a decrease in surface tension within the range of 54 to 69 mN/m. Among the tested polysaccharides, neutral types such as guar gum and locust gum demonstrated the highest ability to decrease surface tension, while anionic polysaccharides such as xanthan and sodium alginate exhibited the lowest ability. The polysaccharides had a limited effect on both freezing point and ice crystal size.

Although no significant relationship was found between rheological properties and the meltdown rate, the type of polysaccharide had a significant impact on the meltdown rate in this sucrose model system. Anionic polysaccharides, for example, exhibited a faster meltdown rate than neutral polysaccharides like galactomannan. Additionally, locust bean gum showed a slower meltdown rate and a unique meltdown behavior compared to the other four polysaccharides, likely due to its ability to form a cryo-gel during freezing that could retain the internal structure and slow down drainage. The meltdown rate was also not associated with the rheological properties of the unfrozen phase, including viscosity and viscoelasticity.

4.3 The effect of rheological properties on meltdown behavior of aerated frozen sucrose system

To further understand the effects of rheological properties on meltdown in the sorbet system, air, at levels typically found in ice cream, was incorporated. Polysorbate 80, a typical emulsifier in ice cream and frozen desserts, was added to promote air incorporation in the frozen sucrose model system. Additionally, two levels of polysorbate 80 were introduced to achieve two overrun levels, allowing for comparison of the effects of both rheological properties and overrun on meltdown.

4.3.1 Rheology

Similarly to section **4.2**, two sets of experiments were designed to distinguish the impact of apparent viscosity and flow rate index, which denotes shear-thinning behavior. The two levels of overrun, 45% and 75%, were achieved by introducing 0.04% and 0.15% polysorbate 80, respectively. To investigate the effect of varying levels of hydrocolloids on meltdown, two different types, xanthan and guar gum, were employed, allowing for comparison between the rheological properties with same type of hydrocolloid. The power law model was fitted to calculate the flow rate index and the consistency.

Table 4.18 displays the rheological properties for two experimental sets, which includes flow rate index, apparent viscosity (measured at a 5 s^{-1} shear rate), and consistency coefficient. The experiments were conducted to achieve the same flow rate index (0.75 ± 0.01) and apparent viscosity (0.19 ± 0.01 Pa•s) for both sets. Despite the efforts made in this study to differentiate the rheological properties of apparent viscosity and shear-thinning behavior using various types of

hydrocolloids, a significant negative correlation was observed between apparent viscosity and flow rate index (r=-0.9102).

The addition of polysorbate 80, a low molecular weight surfactant, did not affect the apparent viscosity or shear-thinning behavior (data not shown). This is attributed to the reduced likelihood of entanglement and interaction among low-molecular weight surfactants within the system, resulting in minimal alteration of the rheological properties. Furthermore, by comparing samples containing the same type of hydrocolloid, an increase in the amount of hydrocolloid resulted in an increase in both apparent viscosity and consistency. Additionally, the samples exhibited more shear-thinning behavior, which aligned with the findings discussed in section **4.1**.

Table 4.18 Flow rate index, apparent viscosity at 5 s^{-1} shear rate, and consistency of samples with same flow rate index and same apparent viscosity. The standard deviation (±) refers to the variation among triplicate samples containing two levels of polysorbate 80.

Same flow rate index/shear-thinning behavior			
Sample	Flow rate index	Apparent viscosity at 5 s^{-1}(Pa•s)	Consistency coefficient (Pa•s)
0.014% xanthan (XAN)	0.76 ± 0.01	0.02 ± 0.00	0.03 ± 0.00
0.22% guar gum (GG)	0.74 ± 0.00	0.10 ± 0.00	0.17 ± 0.00
Same apparent viscosity at 5 s^{-1} (Pa•s)			
Sample	Flow index	Apparent viscosity at 5 s^{-1}(Pa•s)	Consistency coefficient (Pa•s)
0.11% xanthan (XAN)	0.47 ± 0.00	0.20 ± 0.00	0.47 ± 0.01
0.28% guar gum (GG)	0.67 ± 0.00	0.19 ± 0.00	0.35 ± 0.01

4.3.2 Freezing point

Given the utilization of a wide range of hydrocolloids, ranging from 0.014% xanthan to 0.28% guar gum, and the corresponding adjustment of water content, the freezing point was measured to compare the ice fraction formed during the freezing process. The freezing point for different formulations ranged from -2.75 to -2.91˚C, as shown in **Table 4.19**. The observed statistical differences among the samples are probably attributable to minor modifications made to the water content. Although the addition of polysorbate 80 (PS80) did not significantly affect the freezing point of the samples, a slight variation was observed between the samples with 0.04% PS80 and 0.15% PS80. No distinct correlation was identified between the amount of polysaccharide, which indirectly represented the water content, and the freezing point within this limited range.

Table 4.19 Freezing point (˚C) of the solution as measured by osmometer. The standard deviation (±) refers to the variation among triplication samples.

Same flow rate index*		
Sample	0.04%PS80	0.15%PS80
0.014% xanthan (XAN) 0.22% guar gum (GG)	-2.82 ± 0.15^{a} -2.80 ± 0.06^{a}	-2.75 ± 0.04^{a} -2.87 ± 0.08^{ab}
Same apparent viscosity at 5 s^{-1} (Pa•s)		
Sample	0.04%PS80	0.15%PS80
0.11% xanthan (XAN) 0.28% guar gum (GG)	-2.76 ± 0.14^{a} -2.81 ± 0.09^{a}	-2.84 ± 0.10^{ab} -2.91 ± 0.09^{b}

*Tukey's HSD test was performed for the significant difference at $P<0.05$
^{a,b} denote significant differences among samples with same level of polysorbate 80 (PS80)

4.3.3 Surface tension

Polysorbate 80, serving as a surfactant, primarily functions by rapidly adsorbing onto and fully coating the water-air interface, resulting in a reduction of surface tension at the interface. As shown in **Table 4.20**, the samples containing either 0.04% or 0.15% polysorbate 80 exhibited a reduction in surface tension to 41 mN/m. Its superior surface-active properties compared to hydrocolloids allowed the solution to approach quasi-equilibrium within 30 min. Considering the critical micelle concentration (CMC) range of 13-15 mg/L at 20-25˚C (Bąk & Podgórska, 2016; Kubbutat & Kulozik, 2021), the amount of polysorbate 80 used in this study greatly exceeded the CMC. As a result, increasing the quantity of polysorbate 80 had minimal impact on surface tension, instead influencing the rate at which it decreased during the initial stages of the measurement, as illustrated in (**Figure 4.30**). The surface tension measurements began at 52 mN/m for 0.04% polysorbate 80 and 46 mN/m for 0.15% polysorbate 80, both eventually reaching a similar surface tension of around 41 mN/m.

Table 4.20 Surface tension (mN/m) of the solution at 30 min. The standard deviation (±) refers to the variation among triplicate samples.

Same flow rate index*		
Sample	0.04%PS80	0.15%PS80
0.014% xanthan (XAN) 0.22% guar gum (GG)	$41.7 \pm 0.5^{a,A}$ $41.2 \pm 0.4^{a,A}$	$40.7 \pm 0.5^{a,B}$ $40.9 \pm 0.4^{a,A}$
Same apparent viscosity at 5 s^{-1} (Pa•s)		
Sample	0.04%PS80	0.15%PS80
0.11% xanthan (XAN) 0.28% guar gum (GG)	$41.4 \pm 0.4^{a,A}$ $41.1 \pm 0.7^{a,A}$	$41.0 \pm 0.5^{a,A}$ $40.7 \pm 0.5^{a,A}$

*Tukey's HSD test was performed for the significant difference at $P<0.05$
[a] denotes significant differences among samples with same level of polysorbate 80 (PS80)
[A,B] denote significant differences among samples with different level of polysorbate 80

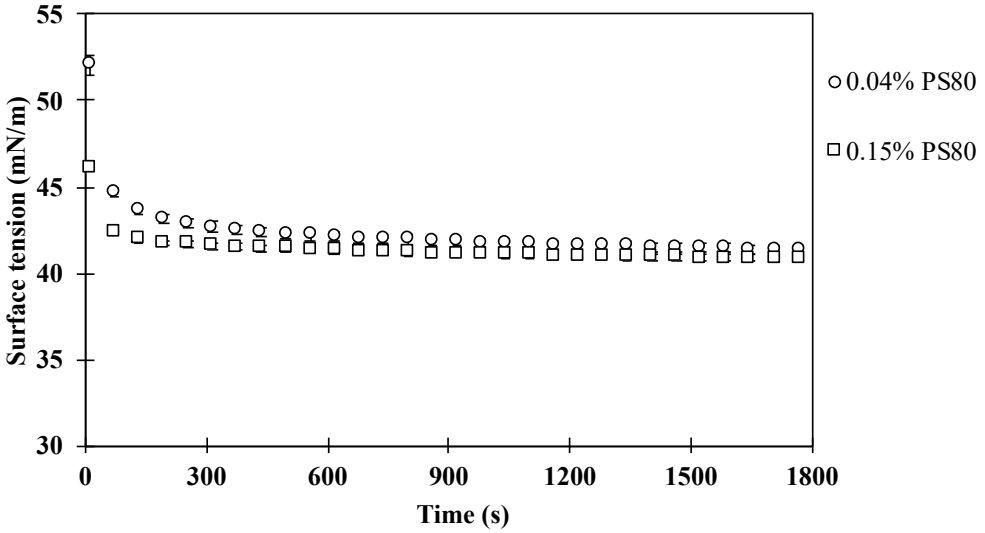

Figure 4.30 Surface tension of samples with two levels of polysorbate 80 (PS80) regardless of the type and amount of hydrocolloids usage. The error bars represent the standard deviation among the samples with same level of PS80 but varying hydrocolloids.

4.3.4 Dilatational rheology

During the melting process, the collapse of melted foam involves not only liquid drainage but also bubble collapse and disproportionation. Therefore, the viscoelastic properties of the film layer at the interface could potentially impact the stability of the foam. In this section, a preliminary study was conducted to examine whether the presence polysorbate 80 affected the viscoelastic behavior and its subsequent influence on the meltdown process.

An amplitude sweep was conducted to assess the presence of an in-plane structure at the interface. If such a structure exists, the interfacial microstructure may be affected by high deformation amplitudes (Wan et al., 2016). **Figure 4.31** demonstrates a slight increase in the complex modulus at higher deformations. However, when compared to previous findings in the literature (Wan et al., 2016; Yang et al., 2021), the dilatational modulus was observed to be

relatively low, with minimal changes. Furthermore, the addition of a higher quantity of surfactant resulted in a lower complex modulus in all samples, indicating that the surfactant enhanced the flexibility and mobility of the surface layer (**Figure 4.31**).

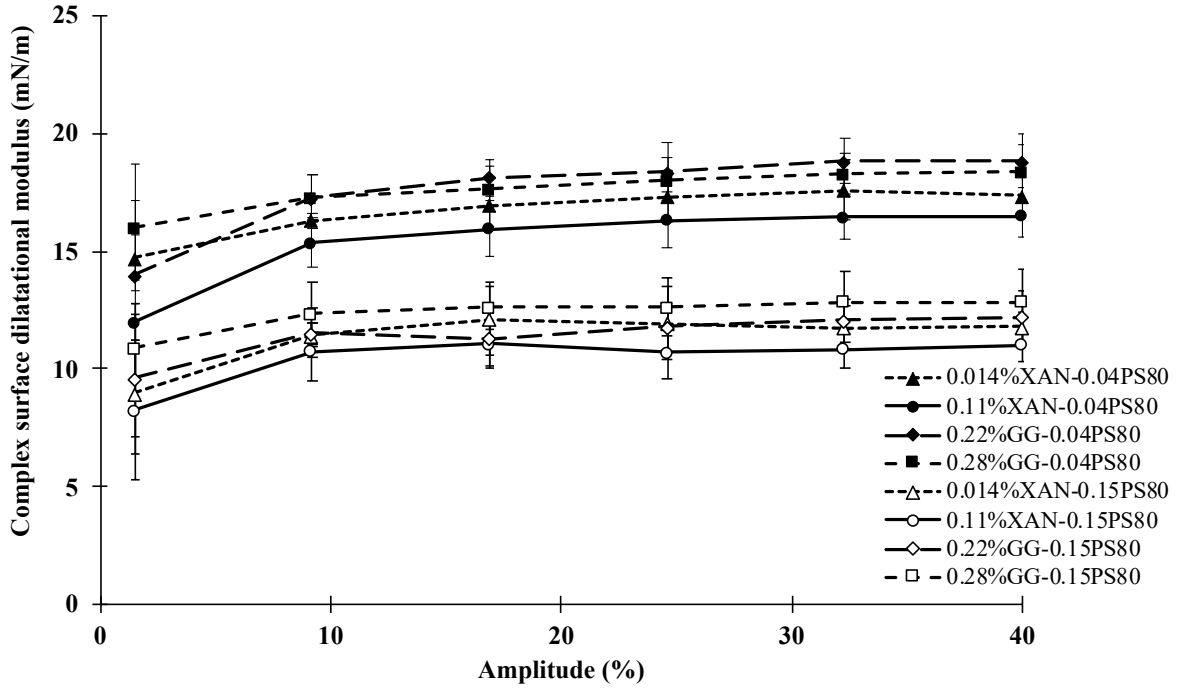

Figure 4.31 Complex surface dilatational modulus as a function of amplitude for air-water interfaces stabilized by mixture of hydrocolloids, either xanthan (XAN) or guar gum (GG), with two levels of polysorbate 80 (PS80) concentrations (0.04% and 0.15%). Frequency: 0.1 Hz; amplitude sweep: 1.5-40%. Closed symbol: 0.04% PS80; open symbol: 0.15% PS80.

A frequency sweep was conducted to gain deeper insights into the viscoelastic behavior of the interface. Across all frequencies (data not shown), the dilatational storage modulus (E') for all samples was slightly higher than the loss modulus (E''), indicating a weak elastic response of the interface at the measured frequencies. **Figure 4.32a** demonstrates a strong linear correlation between frequency and the complex surface dilatational modulus, independent of the quantity of polysorbate 80 and the hydrocolloid type. This indicates a high frequency-dependence of the interface. Additionally, a higher complex dilatational modulus was observed in systems with a

lower amount of polysorbate 80. No significant differences were found among systems with varying amounts/types of hydrocolloids.

To further analyze the frequency-dependent elastic behavior, **Figure 4.32b** illustrates the slope of a double logarithmic plot of the complex surface modulus as a function of frequency. A slope of 0 indicates a fully elastic response, suggesting that the surface-active molecules have formed a highly elastic film through self-assembly. A slope of 0.5 indicates that the dilatational elasticity is predominantly influenced by the rate of diffusional exchange of surfactants between the bulk phase and the interface, as described by the Lucassen van den Tempel model (Lucassen & Van Den Tempel, 1972). Typically, an interface stabilized by low-molecular-weight surfactants exhibits a slope value of 0.5, indicating that the molecules adsorb reversibly at the interface with the frequency change and the formation of a viscous layer at the interface.

As depicted in **Figure 4.32b**, the slope values ranged from 0.34 to 0.48, suggesting that the interface is predominantly stabilized by the low-molecular-weight surfactant (Chen et al., 2017). Moreover, an increase in the concentration of polysorbate 80 led to a significant rise in the slope, while xanthan exhibited a relatively higher slope compared to guar gum. This indicates that the increased amount of polysorbate 80 results in the formation of a highly viscous layer at the air/water interface, facilitating the exchange between the bulk phase and the interface.

a.

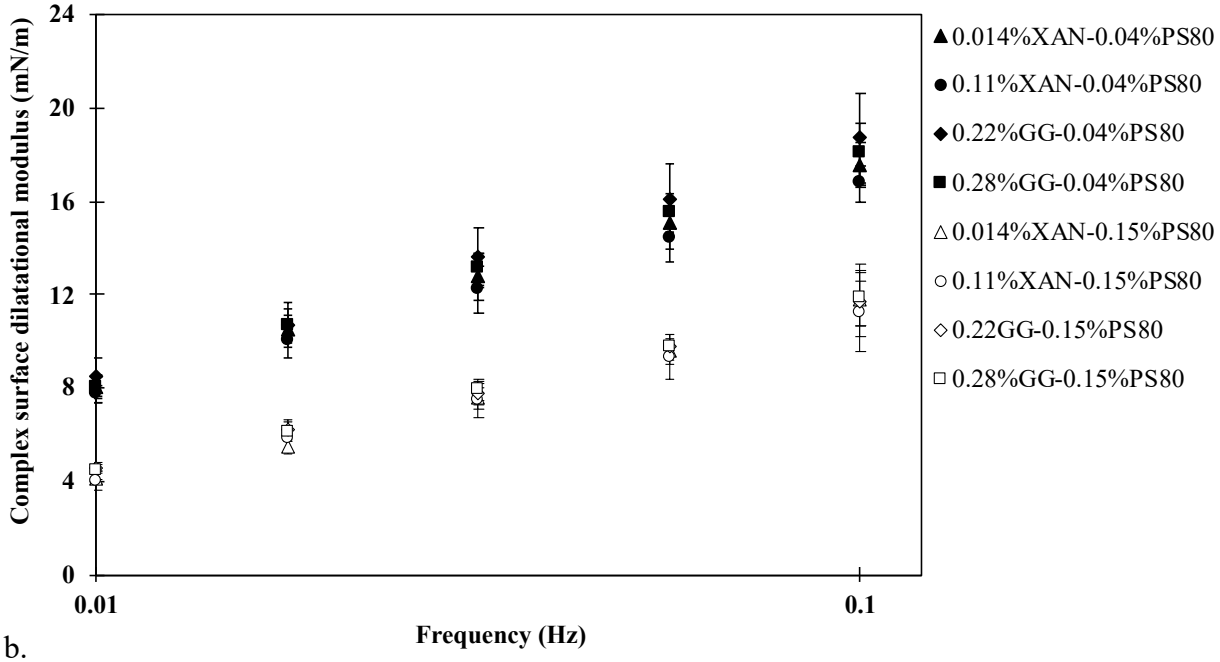

b.

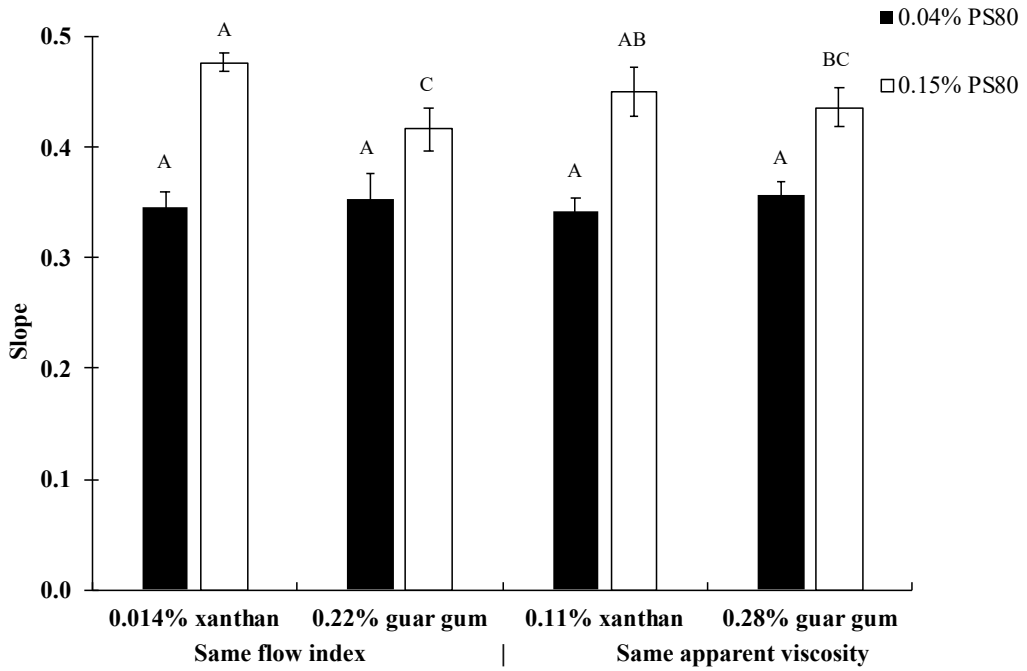

Figure 4.32 Complex surface dilatational modulus as a function of amplitude for air-water interfaces stabilized by mixture of hydrocolloids, either xanthan (XAN) or guar gum (GG), with two levels of polysorbate 80 (PS80) concentrations (0.04% and 0.15%) (a), and the slope of a double-logarithmic plot of the modulus versus frequency. Amplitude: 35%; frequency: 0.01-0.1 Hz. ^{A,B,C} indicate significant differences among samples with same level of polysorbate 80. Closed symbol: 0.04% PS80; open symbol: 0.15% PS80.

4.3.5 Ice crystal size

The average size of ice crystals ranged from 67.6 to 80.2 μm, as presented in **Table 4.21**. Representative images of ice crystals are displayed in **Figure 4.33**. Regardless of the rheological properties or the type of hydrocolloids, no significant trend was observed among the samples. While previous studies have suggested that nonionic surfactants can control ice crystal growth through the adsorption of polysorbate's hydroxyl group onto the ice crystal surface via Van der Waals interactions (Lv et al., 2022; Zhao et al., 2014), no significant correlation was observed between the amount of polysorbate 80 and the average ice crystal size. Note that this lack of correlation may be attributed to the limited storage time of the samples in the freezer.

Table 4.21 Mean ice crystal size (μm) of the frozen samples. The standard deviation (±) refers to the variation among triplicate samples.

Same flow rate index*		
Sample	45%OR	75%OR
0.014% xanthan (XAN) 0.22% guar gum (GG)	$67.6 \pm 8.9^{a,A}$ $75.3 \pm 7.8^{a,A}$	$70.5 \pm 4.7^{b,A}$ $79.7 \pm 6.5^{a,A}$
Same apparent viscosity at 5 s^{-1} (Pa•s)		
Sample	45%OR	75%OR
0.11% xanthan (XAN) 0.28% guar gum (GG)	$79.8 \pm 11.2^{a,A}$ $79.1 \pm 4.1^{a,A}$	$80.2 \pm 3.9^{a,A}$ $77.6 \pm 5.1^{ab,A}$

*Tukey's HSD test was performed for the significant difference at $P<0.05$
^{a,b} denote significant differences among samples with same level of overrun (OR)
^{A} denote significant differences among samples with different level of overrun

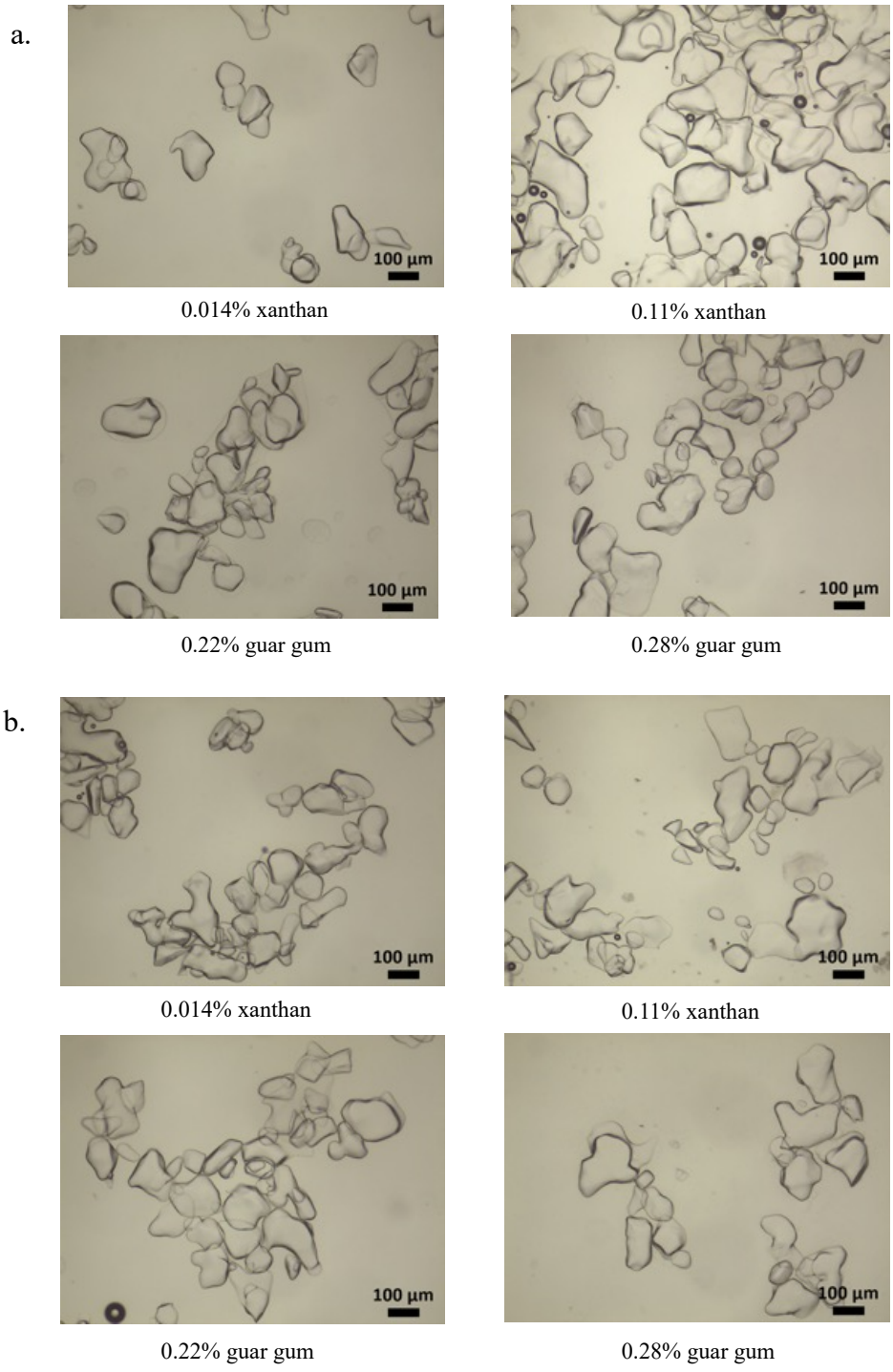

Figure 4.33 Example of ice crystals images for samples with the 45% overrun (a), and 75% overrun (b).

4.3.6 Air cell size

The average size of air cells ranged from 58.2 to 92.7 μm, as shown in **Table 4.22**, with corresponding representative images displayed in **Figure 4.34**. The wide variation in air cell size primarily results from the low churning speed of the bench-top batch freezer, which fails to uniformly break up the air bubbles. While some noticeable differences were observed among the samples, it is essential to acknowledge that the limited number of samples prevents drawing specific conclusions. Notably, an increase in the amount of polysorbate 80 generally decreased the air cell size, except for the 0.28% guar gum system, although not statistically significant due to the large variation. However, it is worth mentioning that no significant correlation between surface tension and air cell size was observed across all the samples (r=0.2). This decline in air cell size associated with the addition of polysorbate 80 could potentially be attributed to the increasing overrun, which leads to higher shear stress during the churning process (Sofjan & Hartel, 2004).

Table 4.22 Mean air cell size (μm) of the frozen samples. The standard deviation (±) refers to the variation among triplicate samples.

Same flow rate index*		
Sample	45%OR	75%OR
0.014% xanthan (XAN)	$65.9 \pm 15.5^{b,A}$	$58.2 \pm 3.8^{c,A}$
0.22% guar gum (GG)	$71.0 \pm 8.8^{b,A}$	$65.4 \pm 7.2^{bc,A}$
Same apparent viscosity at 5 s^{-1} (Pa•s)		
Sample	45%OR	75%OR
0.11% xanthan (XAN)	$92.7 \pm 4.5^{a,A}$	$85.9 \pm 4.7^{a,A}$
0.28% guar gum (GG)	$67.6 \pm 8.6^{b,A}$	$74.5 \pm 10.4^{ab,A}$

*Tukey's HSD test was performed for the significant difference at $P<0.05$
^{a,b,c} denote significant differences among samples with same level of overrun (OR)
^{A} denote significant differences among samples with different level of overrun

a.

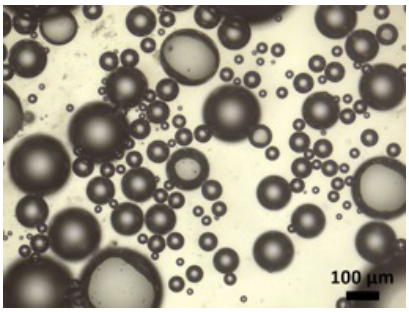

0.014% xanthan

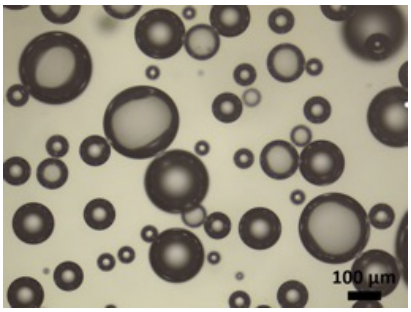

0.11% xanthan

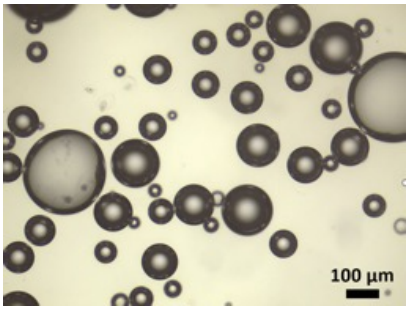

0.22% guar gum

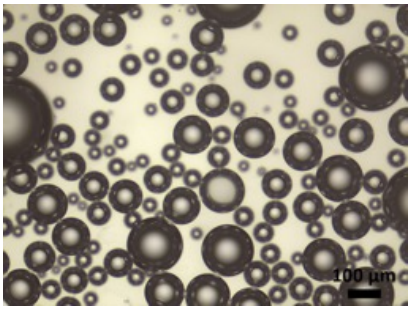

0.28% guar gum

b.

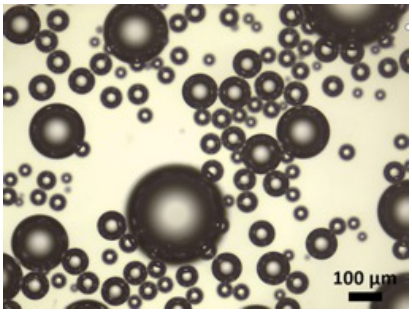

0.014% xanthan

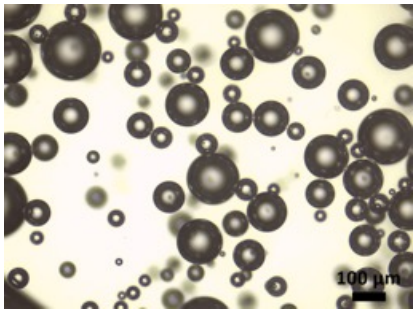

0.11% xanthan

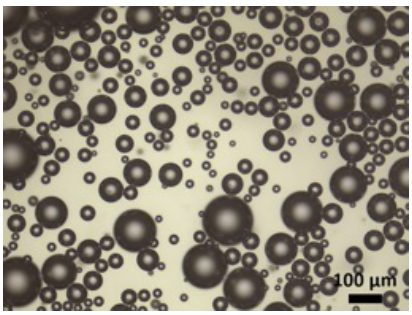

0.22% guar gum

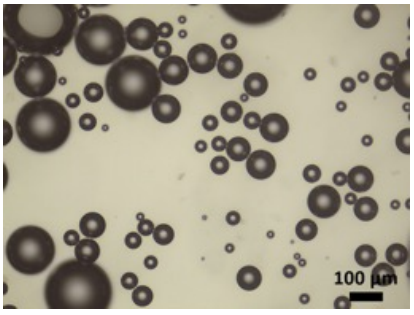

0.28% guar gum

Figure 4.34 Example of air cell images for samples with the 45% overrun (a), and 75% overrun (b).

4.3.7 Meltdown

Little structure was developed in this system, resulting in a narrow range of induction time and melting rate, ranging from 21.3 to 35.0 min and from 1.18 to 1.51 g/min, respectively (**Table 4.23**). All samples completely dripped through the mesh after a 120 min meltdown test. No strong correlations were found between ice crystal size and air cell size on induction time (air: r=0.5482; ice: r=0.5554) and melting rate (air: r=0.6383; ice: r=0.5909).

A strong positive correlation was observed between apparent viscosity and induction time when comparing all samples in both overruns (45% overrun: r=0.9864; 75% overrun: r=0.8141) (**Figure 4.35**), which supports the findings in section **4.1**. The increase in viscosity led to a more viscous melted liquid at the outer layers, slowing down the drainage process.

A strong negative correlation was observed between the flow rate index and induction time exclusively in the 45% overrun samples (r=-0.8028), whereas it was not apparent in the 75% overrun samples (r=-0.3377). These findings indicates that samples with more pronounced shear-thinning behavior display longer induction times. Interestingly, although a strong correlation was observed between apparent viscosity and shear-thinning behavior, the effect of shear-thinning on the induction time was not as significant as the observed impact on apparent viscosity at the 75% overrun level. This finding suggests that apparent viscosity may have a greater influence on the induction time compared to shear-thinning behavior.

The increase in overrun led to a decrease in induction time across all samples. This observation can be attributed to maintaining the same volume of samples, as opposed to the same mass as studied in section **4.1**. Samples with higher overruns had a lower mass and a reduced amount of ice available for melting, which likely contributed to the faster induction times.

A strong positive correlation was observed between apparent viscosity and melting rate at both overruns (45% overrun: r=0.9302; 75% overrun: r=0.8839), which contrasts with the findings in section **4.1**. The strong negative correlation observed during ice cream meltdown may be more closely related to the promotion of fat destabilization by higher shear forces in the more viscous ice cream mix product. Additionally, viscosity may have a greater impact on the movement of fat clusters and the formation of networks during the melting process, rather than directly affecting liquid dripping. In the simpler system designed for this study, where the liquid melted layer by layer from the outside without a tortuous travel path in the lamella inside the foam, there was no strong correlation observed between viscosity and melting rate.

A strong negative correlation was observed between the flow rate index and melting rate in the samples with 45% overrun (r=-0.9248), while this correlation was not apparent in the samples with 75% overrun (r=-0.4549). The solution with a more shear-thinning behavior exhibited a slower melting rate. Again, despite the strong correlation between apparent viscosity and shear-thinning behavior, the significant effect of apparent viscosity on the melting rate was not evident in the shear-thinning behavior.

Moreover, the significant effect of overrun on meltdown was only observed with xanthan gum and not with guar gum, as increasing overrun resulted in a slower melting rate. Notably, guar gum has a better surface-active property than xanthan gum. This variation based on hydrocolloid types may be due to the adsorption of hydrocolloids to the air interface, which consequently affects the stability and movement of air bubbles during drainage. Therefore, further study is needed to understand the impact of hydrocolloid types on meltdown in aerated frozen foam systems.

All samples exhibited a similar meltdown behavior, characterized by the gradual melting process starting from the outer layer and shrinking towards the core until all the melted liquid

dripped through the mesh. However, it is noteworthy that in the system containing 0.014% xanthan gum, which had a relatively lower concentration of hydrocolloids, the melting sample displayed a more foamy structure compared to the other samples (**Figure 4.36**).

Table 4.23 The induction time and melting rate of frozen samples. The standard deviation (±) refers to the variation among triplicate samples.

Same flow rate index*				
Sample	Induction time (min)		Melting rate (g/min)	
	45%OR	75%OR	45%OR	75%OR
0.014% xanthan	$29.4 \pm 2.5^{b,A}$	$21.3 \pm 2.2^{c,B}$	$1.38 \pm 0.03^{c,A}$	$1.18 \pm 0.02^{c,B}$
0.22% guar gum	$31.0 \pm 1.9^{b,A}$	$29.5 \pm 1.7^{ab,B}$	$1.39 \pm 0.02^{c,A}$	$1.39 \pm 0.02^{b,A}$
Same apparent viscosity at 5 s^{-1} (Pa•s)				
0.11% xanthan	$35.0 \pm 3.3^{a,A}$	$28.4 \pm 1.1^{b,A}$	$1.51 \pm 0.02^{a,A}$	$1.40 \pm 0.02^{b,B}$
0.28% guar gum	$34.8 \pm 2.2^{a,A}$	$31.8 \pm 2.3^{a,B}$	$1.47 \pm 0.01^{b,A}$	$1.47 \pm 0.03^{a,A}$

*Tukey's HSD test was performed for the significant difference at $P<0.05$
^{a,b,c} denote significant differences among samples with same level of overrun (OR)
^{A,B} denote significant differences among samples with different level of overrun

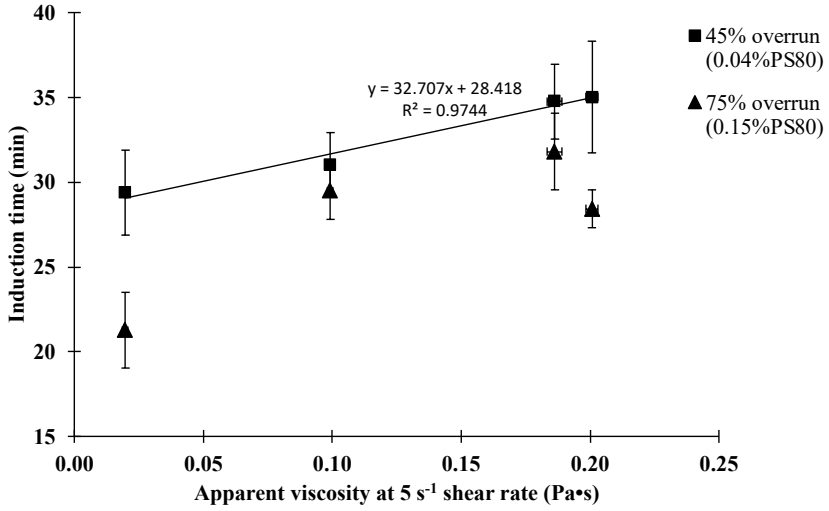

Figure 4.35 The correlation between apparent viscosity at 5 s^{-1} shear rate and induction time for samples with two levels of overrun (PS: polysorbate). The error bars represent the standard deviation of viscosity and induction time measured in triplicate.

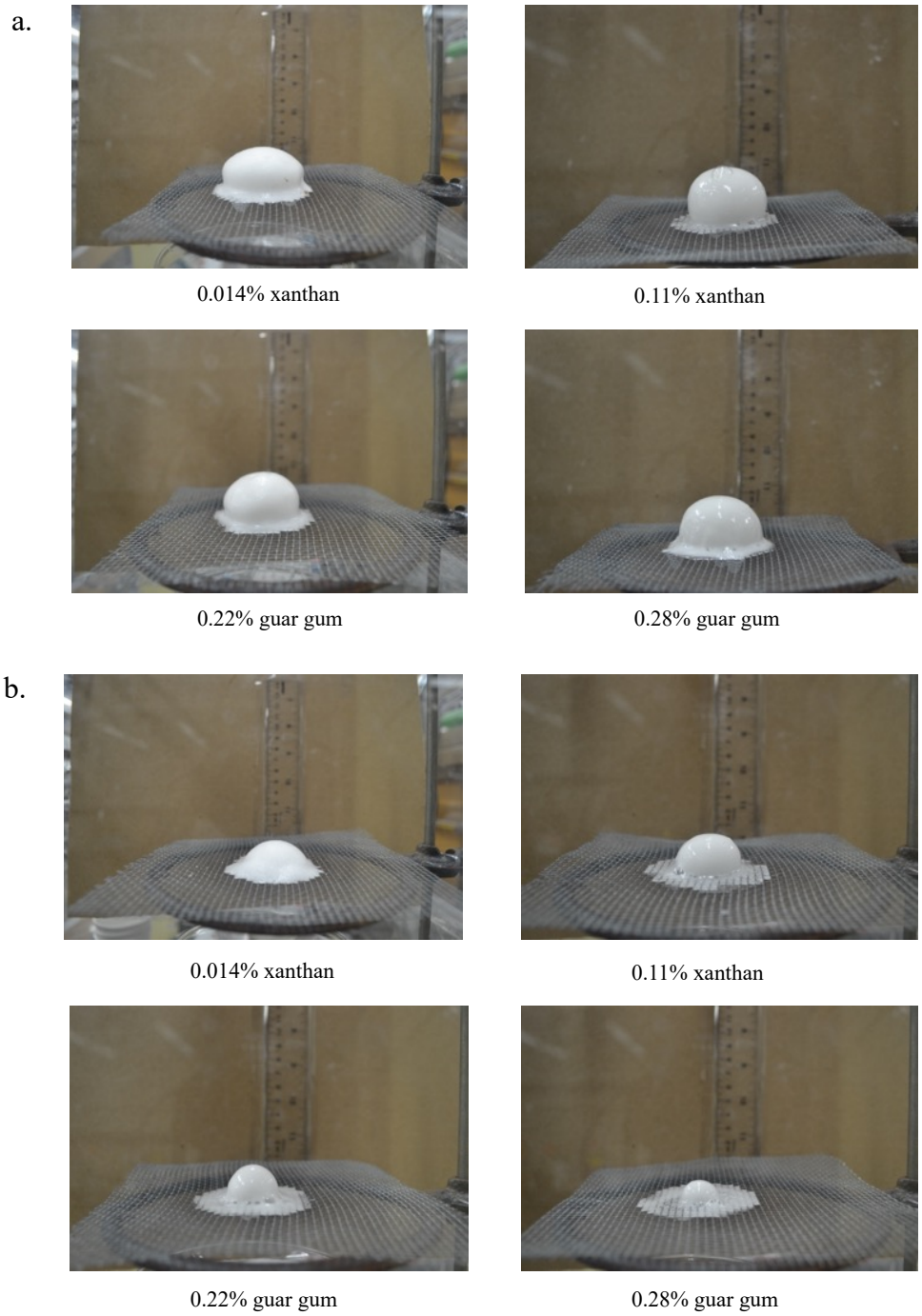

Figure 4.36 Meltdown images of samples on the screen with (a) 45% overrun/ 0.04% polysorbate 80, and (b) 75% overrun/ 0.15% polysorbate 80 at 90 min of the meltdown test.

4.3.9 Summary

The inclusion of polysorbate 80 in the sucrose-hydrocolloids system facilitated the incorporation of air, resulting in overruns of either 45% or 75% depending on the amount of polysorbate 80 added. It was observed that adding polysorbate 80 beyond the critical micelle concentration did not significantly affect the surface tension, but it did contribute to the formation of a more fluid-like viscous layer at the air-water interface. This suggests that higher concentrations of polysorbate 80 primarily influences the rheological properties of the interface rather than the surface tension.

The apparent viscosity demonstrated a positive impact on both the induction time and melting rate in both the 45% and 75% overrun systems, suggesting that a higher apparent viscosity led to a longer induction time but a faster melting rate. The conflicting findings regarding the relationship between apparent viscosity and melting rate can be attributed to the dominant influence of mix viscosity on destabilized fat mobility in the ice cream system.

In the 45% overrun samples, the shear-thinning behavior demonstrated a significant negative impact on both the induction time and melting rate, whereas this effect was not as prominent in the 75% overrun samples. Given the strong correlation between shear-thinning behavior and apparent viscosity, and considering that the effect of shear-thinning behavior on the meltdown process was not as significant as that of apparent viscosity, it can be concluded that apparent viscosity remains a better parameter for describing the meltdown process.

Additionally, the effect of overrun on the meltdown process was only observed in the xanthan gum samples and not in the guar gum samples. This suggests that the interaction between hydrocolloids and air may play a crucial role in the movement of air bubbles during liquid drainage.

4.4 The effect of protein-polysaccharides interaction on meltdown behavior of aerated frozen sucrose system

In this section, the protein-polysaccharide interaction, specifically the phase separation, was studied to gain an understanding of its impact on meltdown. Two types of galactomannans, guar gum and locust bean gum, commonly used in frozen desserts, were selected and added at two levels to alter the microscopic phase separation behavior across three milk protein levels. Furthermore, the effect of preventing phase separation on meltdown was investigated by adding *κ*-carrageenan, known for its ability to control phase separation.

4.4.1 Rheology of mix

Due to the controlled addition of hydrocolloids, the apparent viscosity and shear-thinning behavior, represented by the flow rate index, were not manipulated in this study. **Table 4.24** presents the rheological properties, including the apparent viscosity at a shear rate of 5 s^{-1}, flow rate index, and consistency. The apparent viscosity ranged from 0.02 to 0.46 Pa•s, while the flow rate index ranged from 0.62 to 0.89. In terms of consistency, the range observed was 0.03 to 0.84 Pa•s. The sample containing 4% milk protein and 0.05% locust bean gum exhibited the lowest viscosity, least shear-thinning behavior, and lowest consistency value. Conversely, the sample with 8% milk protein, 0.15% guar gum, and 0.015% κ-carrageenan displayed the highest apparent viscosity, most shear-thinning behavior, and highest consistency value.

Increasing protein content resulted in a significant increase in the apparent viscosity and consistency of all mixes. Protein also caused a greater shear-thinning behavior. Heating-induced denaturation of whey protein causes structural unfolding, leading to increased voluminosity of milk protein in the solution. This structural change, characterized by increased molecular

interactions and chain entanglement, further contributes to increased viscosity and enhanced shear-thinning behavior in the solution (Schmidt & Smith, 1992; Snoeren et al., 1981).

Likewise, increasing the concentration of hydrocolloids, such as galactomannans or κ-carrageenan, resulted in higher apparent viscosity, consistency, and a more pronounced shear-thinning behavior across all samples. The addition of hydrocolloid macromolecules increases voluminosity and facilitates molecular interactions, contributing to the enhanced viscosity and shear-thinning behavior observed in the solution.

At the same galactomannan concentration, particularly at 0.15%, guar gum demonstrated higher viscosity, consistency, and a more pronounced shear-thinning behavior compared to locust bean gum. This can be attributed to the superior solubility and hydration capacity of guar gum in solution, as well as its greater chain extension, which contributes to stronger solute-solvent interactions (Elfak et al., 1977).

Table 4.24 Apparent viscosity at 5 s^{-1} shear rate, flow rate index and consistency of samples with different protein levels, with and without 0.015% κ-carrageenan (carr), and different types and amounts of galactomannans (GG: guar gum; LBG: locust bean gum). The standard deviation (±) refers to the variation among triplicate samples.

	Apparent viscosity at 5 s^{-1} shear rate (Pa•s)*			
	0.05% LBG	**0.15% LBG**	**0.05% GG**	**0.15% GG**
4% protein	$0.02\pm0.00^{A,x,a,X}$	$0.10\pm0.00^{A,y,a,X}$	$0.03\pm0.00^{A,x,a,X}$	$0.13\pm0.00^{A,y,a,Y}$
6% protein	$0.04\pm0.00^{B,x,a,X}$	$0.19\pm0.01^{B,y,a,X}$	$0.04\pm0.00^{B,x,a,X}$	$0.20\pm0.00^{B,y,a,Y}$
8% protein	$0.08\pm0.00^{C,x,a,X}$	$0.38\pm0.01^{C,y,a,X}$	$0.08\pm0.00^{C,x,a,X}$	$0.40\pm0.03^{C,y,a,X}$
4% protein+carr	$0.05\pm0.00^{A,x,b,X}$	$0.14\pm0.00^{A,y,b,X}$	$0.05\pm0.00^{A,x,b,X}$	$0.19\pm0.00^{A,y,b,Y}$
6% protein+carr	$0.07\pm0.00^{B,x,b,X}$	$0.21\pm0.00^{B,y,b,X}$	$0.07\pm0.00^{B,x,b,X}$	$0.25\pm0.01^{B,y,b,Y}$
8% protein+carr	$0.11\pm0.00^{C,x,b,X}$	$0.41\pm0.04^{C,y,b,X}$	$0.12\pm0.00^{C,x,b,X}$	$0.46\pm0.01^{C,y,b,Y}$
	Flow rate index*			
	0.05% LBG	**0.15% LBG**	**0.05% GG**	**0.15% GG**
4% protein	$0.89\pm0.03^{A,x,a,X}$	$0.74\pm0.00^{A,y,a,X}$	$0.86\pm0.00^{A,x,a,Y}$	$0.70\pm0.01^{A,y,a,Y}$
6% protein	$0.84\pm0.03^{B,x,a,X}$	$0.70\pm0.01^{B,y,a,X}$	$0.82\pm0.01^{B,x,a,X}$	$0.67\pm0.00^{B,y,a,Y}$
8% protein	$0.76\pm0.01^{C,x,a,X}$	$0.64\pm0.01^{C,y,a,X}$	$0.76\pm0.00^{C,x,a,X}$	$0.65\pm0.02^{C,y,a,X}$
4% protein+carr	$0.76\pm0.01^{A,x,b,X}$	$0.70\pm0.00^{A,y,b,X}$	$0.79\pm0.00^{A,x,b,Y}$	$0.65\pm0.01^{A,y,b,Y}$
6% protein+carr	$0.75\pm0.00^{B,x,b,X}$	$0.67\pm0.01^{B,y,b,X}$	$0.78\pm0.01^{A,x,b,Y}$	$0.65\pm0.00^{A,y,b,Y}$
8% protein+carr	$0.74\pm0.01^{C,x,b,X}$	$0.61\pm0.01^{C,y,b,X}$	$0.73\pm0.01^{B,x,b,X}$	$0.62\pm0.01^{B,y,b,X}$
	Consistency (Pa•s)*			
	0.05% LBG	**0.15% LBG**	**0.05% GG**	**0.15% GG**
4% protein	$0.03\pm0.00^{A,x,a,X}$	$0.17\pm0.01^{A,y,a,X}$	$0.04\pm0.00^{A,x,a,Y}$	$0.23\pm0.01^{A,y,a,Y}$
6% protein	$0.06\pm0.00^{B,x,a,X}$	$0.32\pm0.02^{B,y,a,X}$	$0.06\pm0.00^{B,x,a,X}$	$0.35\pm0.01^{B,y,a,Y}$
8% protein	$0.13\pm0.00^{C,x,a,X}$	$0.72\pm0.01^{C,y,a,X}$	$0.13\pm0.01^{C,x,a,X}$	$0.71\pm0.05^{C,y,a,X}$
4% protein+carr	$0.07\pm0.00^{A,x,b,X}$	$0.23\pm0.01^{A,y,b,X}$	$0.07\pm0.00^{A,x,b,X}$	$0.35\pm0.01^{A,y,b,Y}$
6% protein+carr	$0.10\pm0.01^{B,x,b,X}$	$0.36\pm0.01^{B,y,b,X}$	$0.10\pm0.00^{B,x,b,X}$	$0.44\pm0.01^{B,y,b,Y}$
8% protein+carr	$0.17\pm0.01^{C,x,b,X}$	$0.77\pm0.06^{C,y,b,X}$	$0.18\pm0.01^{C,x,b,X}$	$0.84\pm0.04^{C,y,b,Y}$

*Tukey's HSD test was performed for the significant difference at $P<0.05$

^{A,B,C} denote significant differences among samples with different protein levels

^{x,y} denote significant differences between samples with two levels of hydrocolloids (0.05% and 0.15%)

^{a,b} denote significant differences between samples with and without κ-carrageenan

^{X,Y} denote significant differences between samples with same amount of guar gum and locust bean gum

4.4.2 Milk protein particle size analysis

The particle size of milk proteins was investigated using a particle size analyzer to observe changes in milk protein particle size resulting from phase separation, and how the size of milk proteins affected the structure of frozen samples. The particle size of milk protein ranged from 2.3 to 18.6 μm, as presented in **Table 4.25**. The sample containing 4% milk protein and 0.15% locust bean gum exhibited the largest particle size, while the sample with 8% milk protein and 0.05% guar gum had the smallest particle size. As a control, samples with protein concentrations of 4%, 6%, and 8% without the addition of hydrocolloids had an average particle size of 0.12 μm, which fell within the size range of casein micelles.

Across all the samples, a trend was observed where an increase in protein content resulted in a decrease in protein particle size, except for samples containing 0.05% locust bean gum with and without κ-carrageenan. The samples were adjusted to the same freezing point of -2.7˚C; however, the amount of sucrose varied depending on the milk protein content, with higher protein content corresponding to lower sucrose content. Examples of milk protein particle images observed under brightfield microscopy with three levels of protein content are shown in **Figure 4.37**. Previous research by Antipova and Semenova (1995) indicated that increasing sucrose content generally enhances the solubility of milk protein in a protein-polysaccharide system, but their study focuses on systems with the same protein amount but different sucrose content. In our study, due to the variations in both milk protein and sucrose content, it is difficult to establish a direct correlation.

Comparing the samples with 0.05% and 0.15% galactomannans, an increased amount of galactomannans generally led to larger particle sizes across the samples, except in the system containing 4% milk protein with κ-carrageenan and guar gum. Examples of milk protein particle

images observed under brightfield microscopy with two levels of galactomannans are shown in **Figure 4.38**. This can be attributed to two reasons. Firstly, the addition of galactomannans reduces the solvent quality, hindering the dissolution of milk protein in the solution (Schorsch et al., 1999). Secondly, the presence of additional galactomannans results in their exclusion from the space between casein micelles, leading to an increase in the local concentration of casein micelles. This increased local concentration can overcome the energy barrier and promote the aggregation of casein micelles (Bourriot et al., 1999). Spagnuolo et al. (2005) reported that the addition of κ-carrageenan in the range of 0-0.03% increased the diameter of casein micelles by adsorbing onto the micelle surface. However, in the present study, since only two levels of κ-carrageenan were used, no specific trend was observed in relation to κ-carrageenan concentration.

In general, the samples containing guar gum exhibited smaller particle sizes compared to those with locust bean gum, except for the 8% milk protein with 0.15% guar gum or locust bean gum, as well as the 4% milk protein with 0.05% galactomannans in the presence of κ-carrageenan. Examples of milk protein particle images observed under brightfield microscopy with guar gum and locust bean gum are shown in **Figure 4.39**. This observed trend could be attributed to the lower molecular weight of guar gum compared to locust bean gum. Cold water polymers, such as guar gum, typically have lower molecular weights than hot water polymers like locust bean gum (Gaisford et al., 1986). The lower molecular weight of guar gum may result in less incompatibility and depletion flocculation with milk protein, leading to better cosolubility with milk protein (Syrbe et al., 1998).

Table 4.25 Milk protein particle size (D[4,3]) of samples with different protein levels, with and without 0.015% κ-carrageenan (carr), and different types and amounts of galactomannans (GG: guar gum; LBG: locust bean gum). The standard deviation (±) refers to the variation among triplicate samples.

	Particle size (μm)*			
	0.05% LBG	**0.15% LBG**	**0.05% GG**	**0.15% GG**
4% protein	$6.0\pm1.2^{A,x,a,X}$	$18.6\pm1.5^{A,y,a,X}$	$4.8\pm0.4^{A,x,a,Y}$	$12.3\pm1.4^{A,y,a,Y}$
6% protein	$8.1\pm2.4^{A,x,a,X}$	$10.2\pm1.2^{B,x,a,X}$	$3.0\pm0.3^{B,x,a,Y}$	$8.6\pm1.5^{B,y,a,X}$
8% protein	$5.0\pm2.9^{A,x,a,X}$	$5.9\pm1.0^{C,x,a,X}$	$2.3\pm0.6^{B,x,a,Y}$	$7.3\pm2.6^{B,y,a,X}$
4% protein+carr	$5.6\pm1.8^{A,x,a,X}$	$18.1\pm2.1^{A,y,a,X}$	$16.5\pm3.0^{A,x,b,Y}$	$14.1\pm0.8^{A,y,b,Y}$
6% protein+carr	$8.8\pm2.3^{B,x,a,X}$	$12.5\pm2.1^{B,y,b,X}$	$3.8\pm1.1^{B,x,a,Y}$	$7.2\pm1.2^{B,y,a,Y}$
8% protein+carr	$8.2\pm1.5^{AB,x,b,X}$	$10.3\pm1.8^{B,x,b,X}$	$2.3\pm0.5^{B,x,a,Y}$	$5.6\pm0.7^{C,y,a,Y}$

*Tukey's HSD test was performed for the significant difference at $P<0.05$

^{A,B,C} denote significant differences among samples with different protein levels

^{x,y} denote significant differences between samples with two levels of hydrocolloids (0.05% and 0.15%)

^{a,b} denote significant differences between samples with and without κ-carrageenan

^{X,Y} denote significant differences between samples with same amount of guar gum and locust bean gum

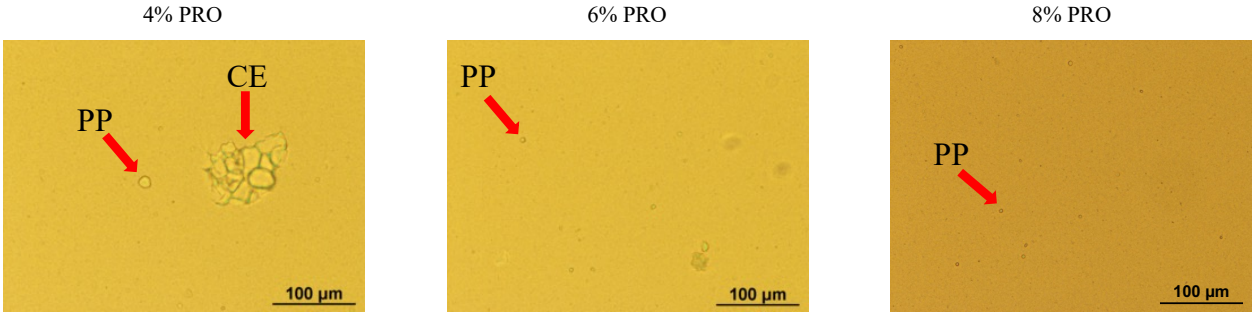

Figure 4.37 Examples of milk protein particle observed under brightfield microscopy in the samples with 0.15% guar gum and three levels of protein content. PP: undissolved protein particles; CE: cell structure from guar bean; PRO: milk protein.

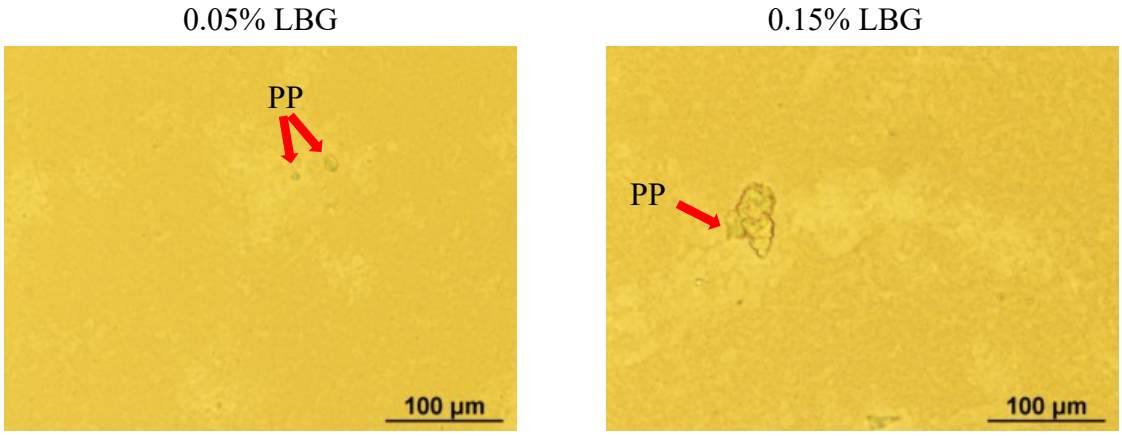

Figure 4.38 Example of milk protein particle observed under brightfield microscopy in the samples with 6% milk protein content, κ-carrageenan and two levels of locust bean gum. PP: undissolved protein particles; LBG: locust bean gum.

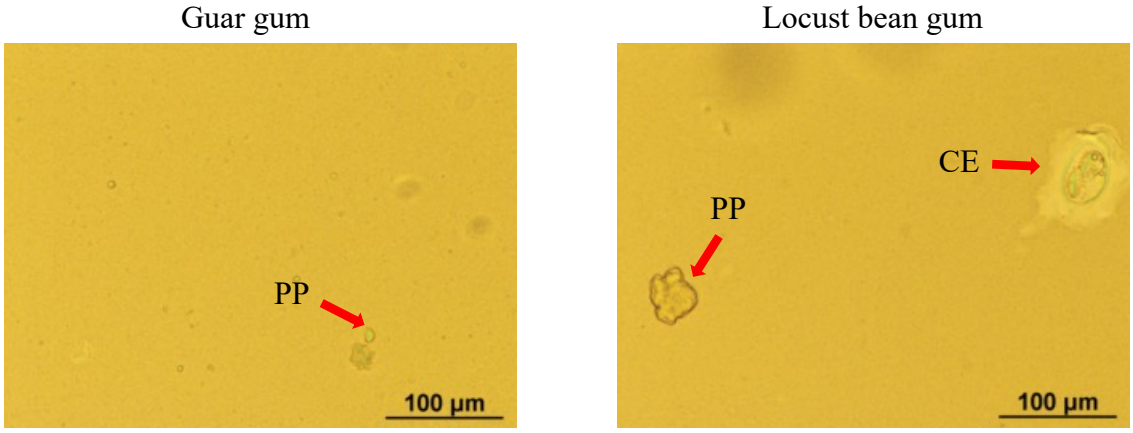

Figure 4.39 Example of milk protein particle observed under brightfield microscopy in the samples with 6% milk protein content and 0.05% of locust bean gum and guar gum. PP: undissolved protein particles; CE: cell structure from locust bean gum.

4.4.3 Overrun

The samples were frozen using a benchtop batch freezer, where air incorporation occurred naturally during the churning of the freezing slurry. No additional control measures were implemented, except for setting the draw temperature at -6˚C. The stabilization of the incorporated air was solely attributed to the presence of milk protein. The overrun values ranged from 62.4% to 124.1%. Specifically, the samples containing 8% milk protein and 0.15% locust bean gum in the presence of κ-carrageenan exhibited the lowest overrun, while the samples with 4% milk protein and 0.05% guar gum displayed the highest overrun (**Table 4.26**).

Table 4.26 Overrun (%) of samples with different protein levels, with and without 0.015% κ-carrageenan (carr), and different types and amounts of galactomannans (GG: guar gum; LBG: locust bean gum). The standard deviation (±) refers to the variation among triplicate samples.

	Overrun (%)*			
	0.05% LBG	**0.15% LBG**	**0.05% GG**	**0.15% GG**
4% protein	$106.3\pm3.9^{A,x,a,X}$	$122.4\pm4.3^{A,y,a,X}$	$124.1\pm2.3^{A,x,a,Y}$	$121.1\pm6.7^{A,x,a,X}$
6% protein	$87.9\pm4.1^{B,x,a,X}$	$101.1\pm2.3^{B,y,a,X}$	$108.5\pm7.2^{B,x,a,Y}$	$117.0\pm5.3^{A,y,a,Y}$
8% protein	$84.4\pm13.7^{B,x,a,X}$	$69.0\pm6.2^{C,y,a,X}$	$95.5\pm14.4^{C,x,a,X}$	$74.1\pm6.0^{B,y,a,Y}$
4% protein+carr	$77.7\pm1.5^{A,x,b,X}$	$108.1\pm4.7^{A,y,b,X}$	$121.0\pm5.3^{A,x,a,Y}$	$115.9\pm4.8^{A,y,a,Y}$
6% protein+carr	$75.3\pm3.4^{A,x,b,X}$	$89.7\pm14.3^{B,y,b,X}$	$88.2\pm8.2^{B,x,b,Y}$	$103.4\pm7.3^{B,y,b,Y}$
8% protein+carr	$75.3\pm11.3^{A,x,a,X}$	$62.4\pm2.2^{C,y,b,X}$	$81.5\pm9.4^{B,x,b,X}$	$87.5\pm8.5^{C,x,b,Y}$

*Tukey's HSD test was performed for the significant difference at $P<0.05$

^{A,B} denote significant differences among samples with different protein levels

^{x,y} denote significant differences between samples with two levels of hydrocolloids (0.05% and 0.15%)

^{a,b} denote significant differences between samples with and without κ-carrageenan

^{X,Y} denote significant differences between samples with same amount of guar gum and locust bean gum

Generally, increasing the protein content resulted in a decrease in overrun across the samples. This phenomenon can be attributed to the reduction in protein particle size within the protein-polysaccharide system. Notably, a positive correlation was observed between particle size and overrun in the samples containing locust bean gum with κ-carrageenan (r=0.7818), locust bean gum without κ-carrageenan (r=0.7691), and guar gum in the presence of κ-carrageenan (r=0.9723) (**Figure 4.40**). This correlation may be attributed to the behavior of the proteins in the system. Smaller proteins tend to migrate to the surface of the air bubbles, creating a viscoelastic layer that stabilizes the bubbles. On the other hand, larger proteins act as solid droplets, providing structural rigidity for air cell stabilization (Allen et al., 2008). In this case, the presence of large protein aggregates appears to be more effective in air incorporation.

The increased amount of galactomannans generally increased the overrun, except in the system with 8% milk protein. The higher viscosity resulting from the extra galactomannans generates a greater shear force, facilitating air incorporation. On the other hand, κ-carrageenan undergoes a helix-coil transition during freezing, forming a weak gel structure. Consequently, the system with additional κ-carrageenan exhibited a lower overrun due to the stiffness provided by the κ-carrageenan gel. This finding is consistent with the results of Cottrell et al. (1979), who reported that ice cream containing κ-carrageenan had a lower overrun compared to those containing locust bean gum or guar gum. Furthermore, in line with the observations of Cottrell et al. (1979), guar gum typically exhibited a higher overrun than locust bean gum, possibly attributable to the higher viscosity achieved by guar gum.

a.

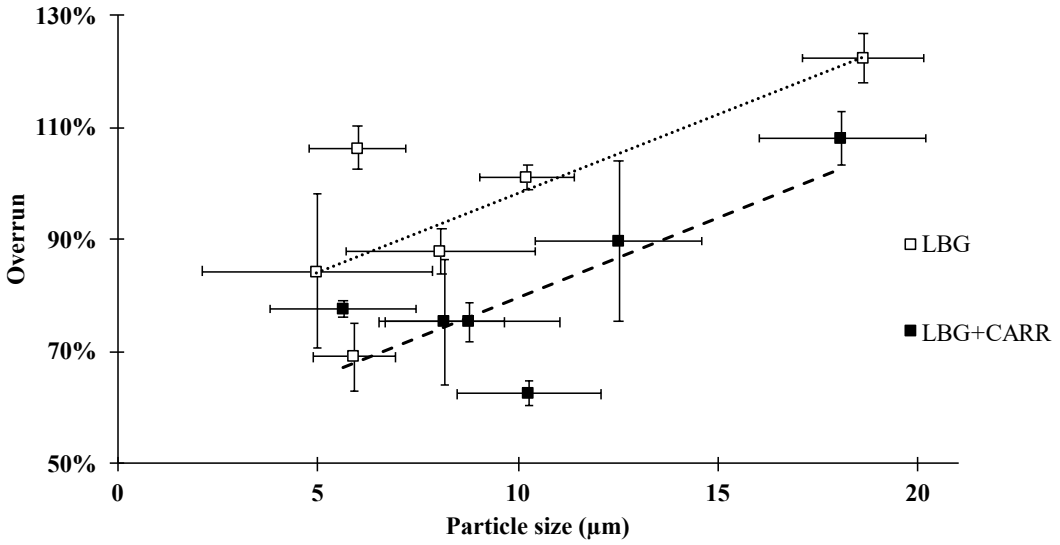

b.

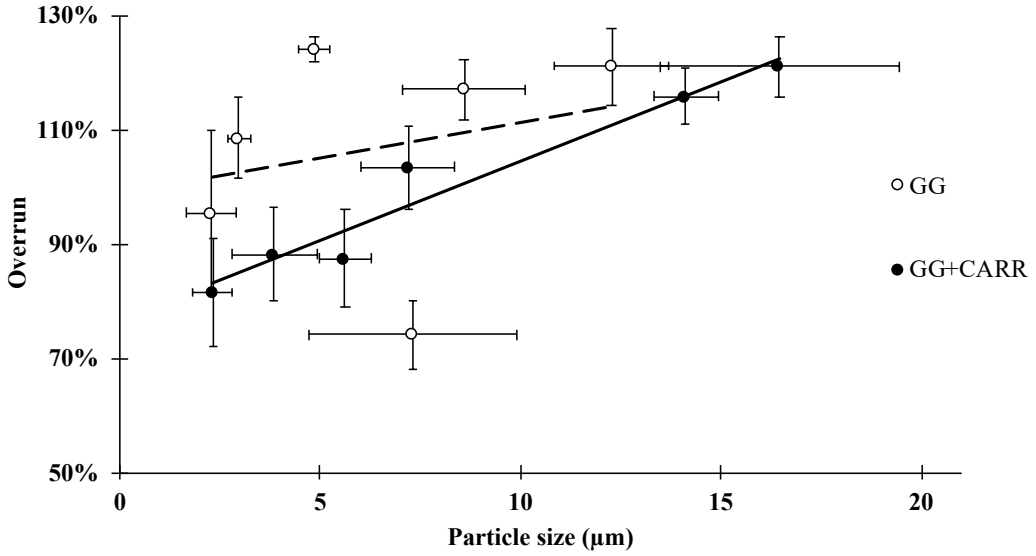

Figure 4.40 The correlation between particle size and overrun in (a) locust bean gum (LBG) system and (b) guar gum (GG) system. CARR: κ-carrageenan. Data includes all protein levels. R^2 for each regression line are: 0.5906 (LBG); 0.6167 (LBG+CARR); 0.0634 (GG); 0.9446 (GG+CARR).

4.4.4 Ice crystal size

The ice crystal size ranged from 52.8 to 66.1 μm, with the sample containing 4% milk protein and 0.15% locust bean gum exhibiting the smallest average ice crystal size, while the sample containing 8% milk protein and 0.15% locust bean gum in the presence of κ-carrageenan had the largest (**Table 4.27**). It is worth noting that, due to the use of a benchtop batch freezer, the overall ice crystal size in this study is larger compared to those produced using a continuous freezer or pilot plant scale batch freezer. Examples of ice crystal images are shown in **Figure 4.41**.

No significant correlation was observed between protein content, the amount/type of galactomannans, overrun, with and without κ-carrageenan, and the mean ice crystal size in this study. Typically, proteins and stabilizers do not play a significant role in ice crystal recrystallization, hence no discernible differences would be anticipated. The small differences in ice crystal size observed among the samples are unlikely to have an impact on the meltdown process.

Table 4.27 Mean ice crystal size (μm) of samples with different protein levels, with and without 0.015% κ-carrageenan (carr), and different types and amounts of galactomannans (GG: guar gum; LBG: locust bean gum). The standard deviation (±) refers to the variation among triplicate samples.

	Mean ice crystal size (μm)*			
	0.05% LBG	**0.15% LBG**	**0.05% GG**	**0.15% GG**
4% protein	$55.1\pm4.4^{A,x,a,X}$	$52.8\pm7.1^{A,x,a,X}$	$58.7\pm4.8^{A,x,a,X}$	$57.8\pm5.2^{A,x,a,X}$
6% protein	$55.8\pm2.4^{A,x,a,X}$	$59.2\pm4.7^{A,x,a,X}$	$56.3\pm5.8^{A,x,a,X}$	$59.6\pm1.2^{A,x,a,X}$
8% protein	$52.9\pm3.6^{A,x,a,X}$	$59.0\pm1.6^{A,x,a,X}$	$58.3\pm3.4^{A,x,a,X}$	$62.4\pm3.5^{A,x,a,X}$
4% protein+carr	$60.2\pm2.5^{A,x,a,X}$	$63.3\pm1.6^{A,x,a,X}$	$63.1\pm2.9^{A,x,a,X}$	$61.7\pm1.9^{A,x,a,X}$
6% protein+carr	$54.7\pm2.0^{A,x,a,X}$	$53.5\pm1.8^{B,x,a,X}$	$55.6\pm4.4^{A,x,a,X}$	$58.8\pm1.9^{A,x,a,Y}$
8% protein+carr	$57.5\pm5.3^{A,x,a,X}$	$66.1\pm2.7^{A,x,b,X}$	$61.0\pm3.6^{A,x,a,X}$	$64.1\pm4.0^{A,x,a,X}$

*Tukey's HSD test was performed for the significant difference at $P<0.05$

^{A,B} denote significant differences among samples with different protein levels

^{x} denotes significant differences between samples with two levels of hydrocolloids (0.05% and 0.15%)

^{a,b} denote significant differences between samples with and without κ-carrageenan

^{X,Y} denote significant differences between samples with same amount of guar gum and locust bean gum

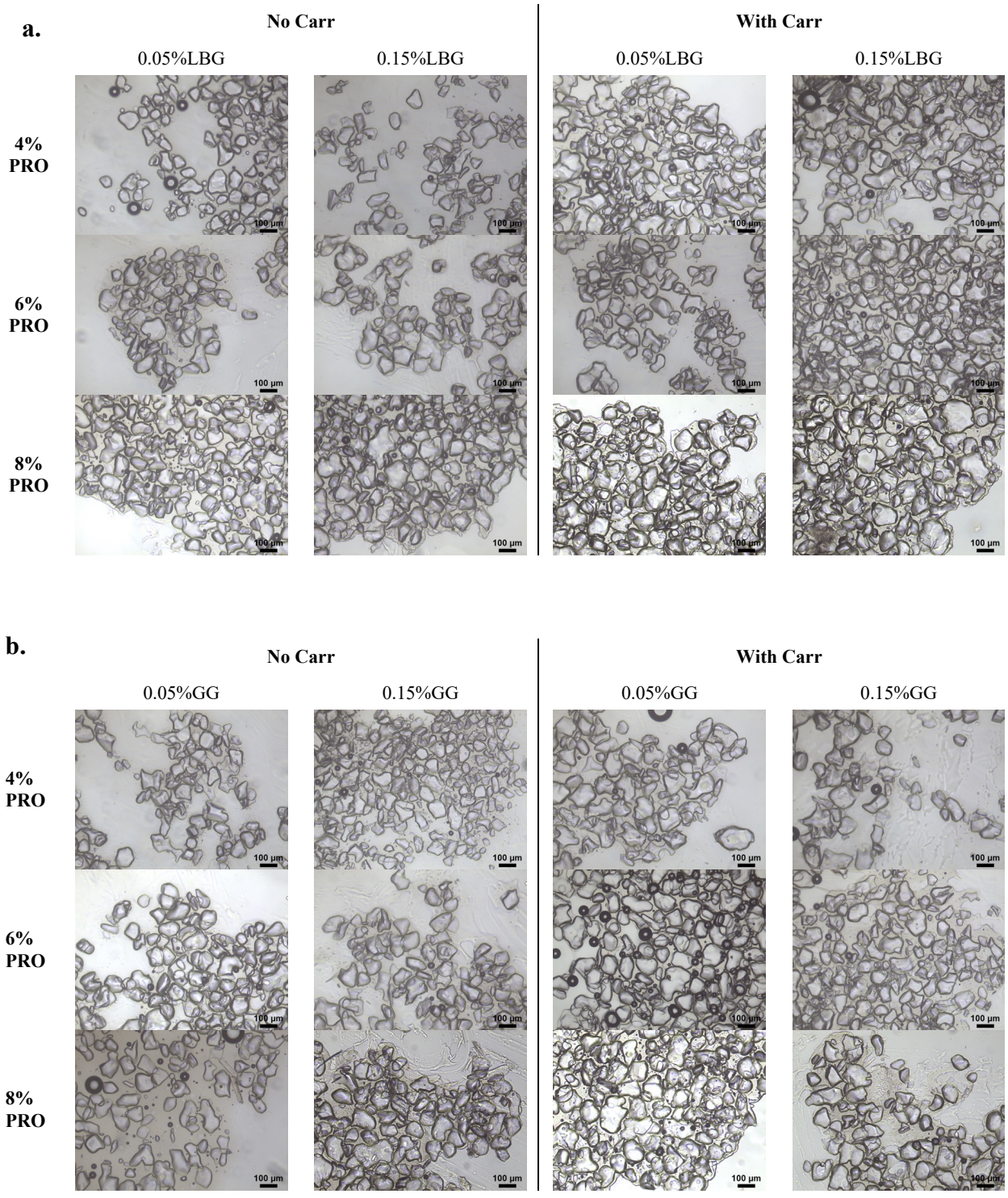

Figure 4.41 Examples of ice crystal images for samples with different protein content (PRO), with and without κ-carrageenan (Carr), in (a) locust bean gum system and (b) guar gum (GG) system.

4.4.5 Air cell size

The air cell size ranged from 40.6 to 51.4 μm (**Table 4.28**). The sample with 4% milk protein and 0.15% locust bean gum had the smallest average air cell size, while the sample with 4% milk protein and 0.05% locust bean gum in the presence of κ-carrageenan had the largest. It is noteworthy that the utilization of a benchtop batch freezer in this study resulted in a larger overall mean air cell size compared to ice cream produced using a continuous freezer or a pilot plant scale batch freezer. Examples of air cell images are shown in **Figure 4.42**.

No significant correlation was observed between protein content, the amount/type of galactomannans, overrun, with and without κ-carrageenan, and the mean air cell size in this study. Once again, proteins and stabilizers do not play a significant role in the growth of air cells; hence, no discernible differences would be anticipated. The small differences in air cell size observed among the samples are unlikely to have an impact on the meltdown process.

Table 4.28 Mean air cell size (μm) of samples with different protein levels, with and without 0.015% κ-carrageenan (carr), and different types and amounts of galactomannans (GG: guar gum; LBG: locust bean gum). The standard deviation (±) refers to the variation among triplicate samples.

	Mean air cell size (μm)*			
	0.05% LBG	**0.15% LBG**	**0.05% GG**	**0.15% GG**
4% protein	$45.6\pm1.9^{A,x,a,X}$	$41.1\pm4.2^{A,x,a,X}$	$40.6\pm4.4^{A,x,a,X}$	$45.1\pm4.7^{A,x,a,X}$
6% protein	$43.0\pm5.1^{A,x,a,X}$	$42.3\pm2.1^{A,x,a,X}$	$43.4\pm1.9^{A,x,a,X}$	$44.6\pm3.6^{A,x,a,X}$
8% protein	$47.5\pm1.3^{A,x,a,X}$	$47.4\pm3.6^{A,x,a,X}$	$45.7\pm3.4^{A,x,a,X}$	$44.9\pm1.0^{A,x,a,X}$
4% protein+carr	$51.4\pm6.9^{A,x,a,X}$	$48.9\pm5.4^{A,x,a,X}$	$44.5\pm1.4^{AB,x,a,X}$	$45.8\pm3.0^{A,x,a,X}$
6% protein+carr	$42.5\pm2.0^{A,x,a,X}$	$42.6\pm3.4^{A,x,a,X}$	$41.2\pm3.1^{B,x,a,X}$	$46.6\pm0.3^{A,y,a,X}$
8% protein+carr	$49.2\pm0.9^{A,x,a,X}$	$44.2\pm3.1^{A,x,a,X}$	$47.9\pm1.3^{A,x,a,X}$	$45.7\pm2.8^{A,x,a,X}$

*Tukey's HSD test was performed for the significant difference at $P<0.05$

^{A,B} denote significant differences among samples with different protein levels

^{x,y} denote significant differences between samples with two levels of hydrocolloids (0.05% and 0.15%)

^{a} denotes significant differences between samples with and without κ-carrageenan

^{X} denotes significant differences between samples with same amount of guar gum and locust bean gum

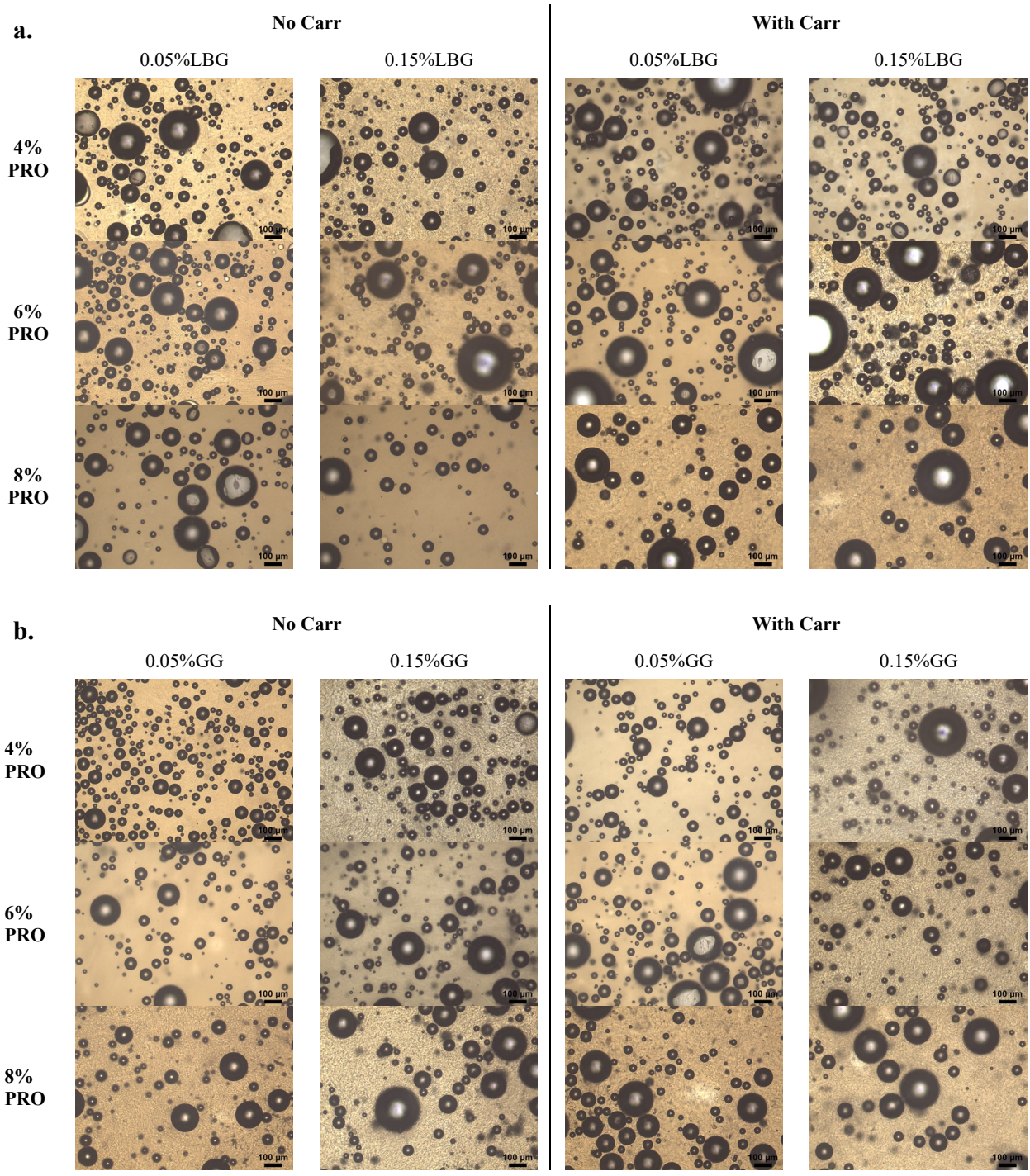

Figure 4.42 Examples of air cell images for samples with different protein content (PRO), with and without κ-carrageenan (Carr), in (a) locust bean gum system and (b) guar gum (GG) system.

4.4.6 Phase separation

The phase separation behavior was observed in both the microscopic and macroscopic images of mix and the drip-through samples collected after the meltdown test. This allowed the confirmation of the occurrence of phase separation and the observation of the type of phase separation behavior present in the samples.

4.4.6.1 Microscopic phase separation

Confocal laser scanning microscope (CLSM) images were captured to observe the microscopic phase separation. **Figure 4.43** and **Figure 4.44** display the CLSM images of the mix and drip-through samples with varying contents of galactomannans and milk protein, both with and without κ-carrageenan. In the case of guar gum and locust bean gum, phase separation occurs with milk protein, either due to thermodynamic incompatibility (Schorsch et al., 1999) or depletion-flocculation (Bourriot et al., 1999). Depending on the concentrations of both biopolymers, three main types of phase separation behavior can be identified: protein as the continuous phase, bi-continuous phase, and galactomannans as the continuous phase.

In both the guar gum and locust bean gum systems, an increase in protein or galactomannans content resulted in greater phase separation. This was evident through the enlargement of the protein area with increasing content and the transition from no phase separation to galactomannans as the continuous phase, to a bi-continuous phase, and to protein as the continuous phase. When κ-carrageenan was present, the CLSM images revealed aggregation between κ-carrageenan and casein micelles in the mix. The κ-carrageenan molecules adsorb to the surface of the casein micelle through electrostatic interaction, specifically between the negative charge of κ-carrageenan and the positively charged region of κ-casein (residues 97-112) (Dalgleish

& Morris, 1988). It is important to note that the amount of κ-carrageenan added to the system was below its critical gel formation concentration (0.03%; Schorsch et al., 2000), and therefore the formation of a weak gel by κ-carrageenan to trap the casein micelles did not occur in this case.

Hellebois et al. (2022) discovered that the galactomannans cryo-gel formed after freeze-thaw exhibited a spongy-like macroporous structure. Accompanying the cryo-gel formation in the locust bean gum system, microstructural changes were observed in the drip-through solution after the freezing-melting process. The CLSM images revealed a strand-like structure of locust bean gum in most samples, except for those with the highest concentration of milk protein and locust bean gum. However, no pore structure was observed, which could be attributed to the presence of a high amount of air that disrupted the cryo-gel structure. In the κ-carrageenan system, the aggregates were observed, but it was not possible to distinguish whether it was the aggregation between κ-carrageenan and casein micelles or the cryo-gel structure.

Variations in the phase separation behavior were observed in the CLSM images between the mix and the drip-through solution in the guar gum system, and these variations could be attributed to the sampling method. The drip-through samples were collected by pouring the samples collected in the beakers after the meltdown test, excluding the foamy layer. This exclusion may have altered the ratio between protein and guar gum content, thereby potentially influencing the phase separation behavior. Another possible explanation could be that during the melting process, proteins desorb from the destabilized air bubbles and become part of the drip-through fraction. Consequently, the increased protein content may alter the phase separation behavior in the drip-through liquid.

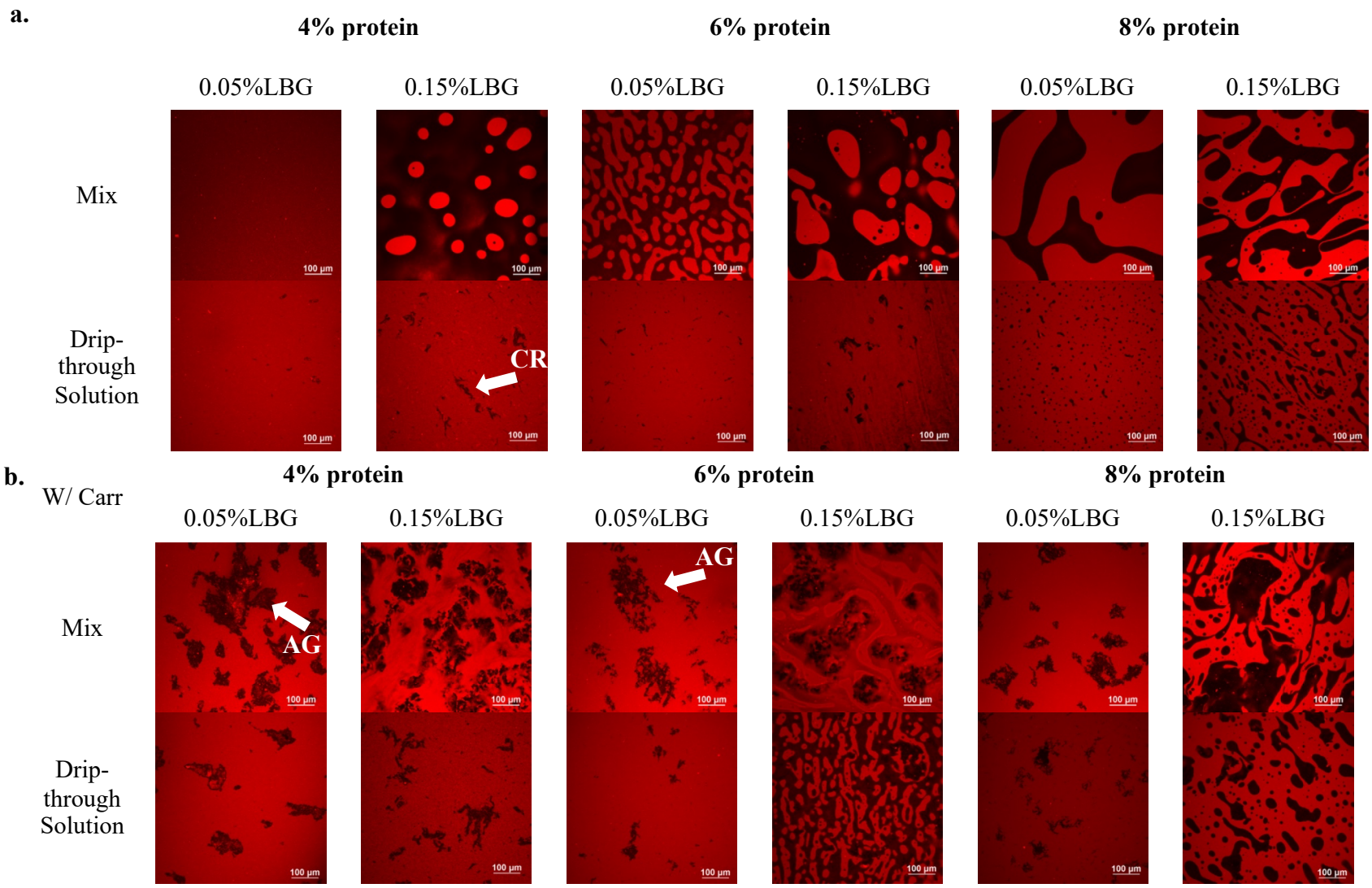

Figure 4.43 Confocal laser scanning microscopy (CLSM) images of mix and drip-through solution collected after meltdown test with locust bean gum and different amount of milk protein: (a) without κ-carrageenan and (b) with κ-carrageenan (Carr). AG: aggregation between κ-carrageenan and casein micelles; CR: cryo-gel structure.

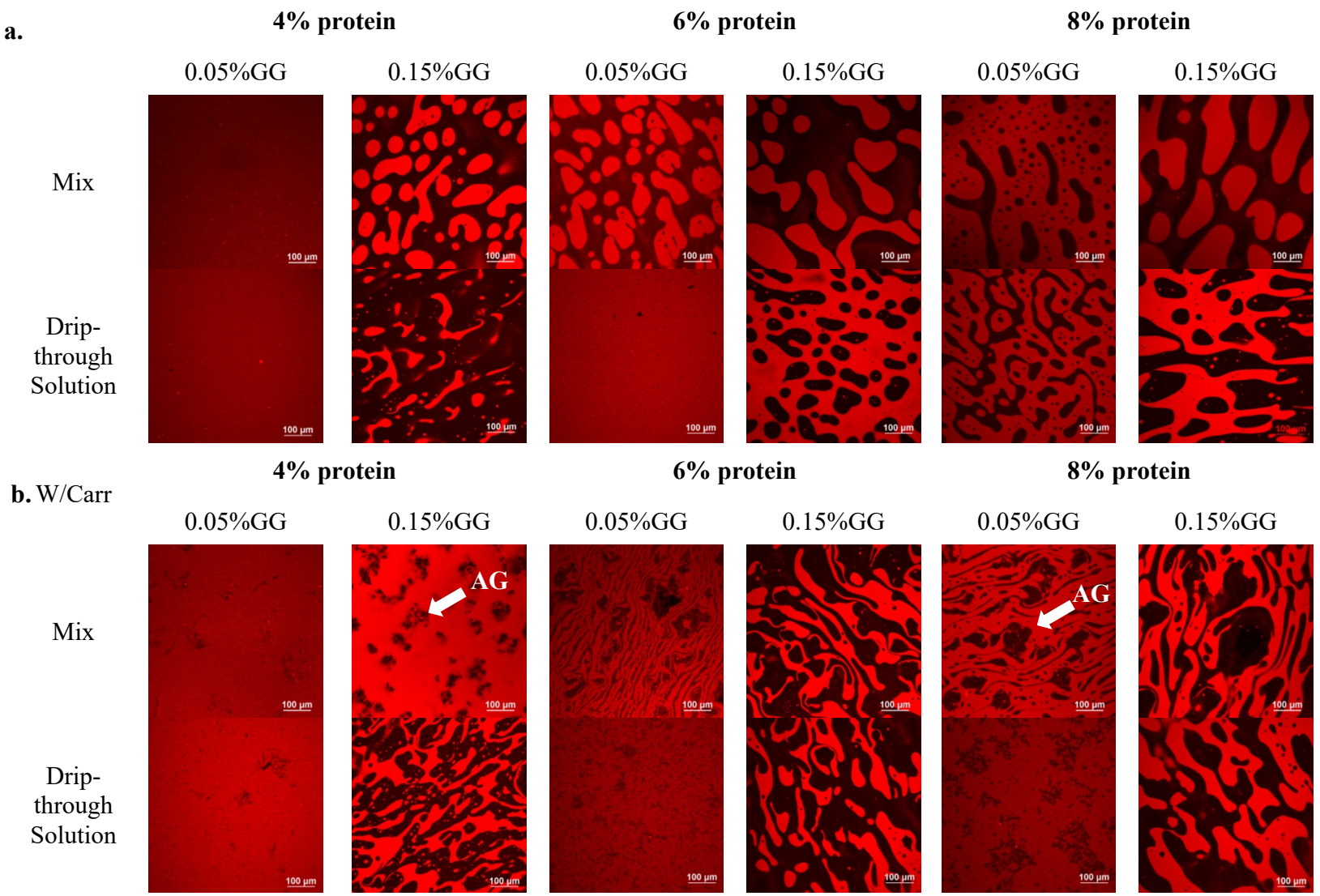

Figure 4.44 Confocal laser scanning microscopy (CLSM) images of mix and drip-through solution collected after meltdown test with guar gum and different amount of milk protein: (a) without κ-carrageenan and (b) with κ-carrageenan (Carr). AG: aggregation between κ-carrageenan and casein micelles.

4.4.6.2 Macroscopic phase separation

The macroscopic phase separation was observed by storing the mix or drip-through solution at 4˚C for 7 days, allowing sufficient time for phase separation to occur. All samples without κ-carrageenan exhibited phase separation, except for the sample with 4% milk protein and 0.05% guar gum or locust bean gum. When phase separation occurred, the top clear phase was enriched with galactomannans, while the bottom opaque phase was enriched with milk protein. Increasing the protein content resulted in a higher proportion of protein phase at the bottom, while increasing the amount of guar gum or locust bean gum led to a higher proportion of galactomannans phase at the top (**Figure 4.45** and **Figure 4.47**).

No phase separation was observed in the locust bean gum system in the presence of κ-carrageenan (**Figure 4.46**). However, in some of the guar gum samples, phase separation still occurred despite the presence of κ-carrageenan (**Figure 4.48**). It is worth noting that the boundary between the guar gum enriched phase and the protein phase in these samples was less distinct compared to those without κ-carrageenan.

It is interesting to note that, in the absence of κ-carrageenan, a stable phase was observed in the drip-through solution containing locust bean gum, except for the sample with the highest amount of protein and locust bean gum. This observation suggests that the cryo-gel formed during the freezing process can prevent phase separation upon melting. Although rheological testing did not detect a gel structure (data not shown), it is possible that the presence of a gel structure somehow diminishes the interaction between locust bean gum and protein. This could be explained by the structural changes that occur in locust bean gum, leading to altered interactions with proteins. In the presence of κ-carrageenan, a phase separation was observed in the drip-through solution of the sample containing 0.15% locust bean gum across three protein levels. This phase separation

could be attributed to the incompatibility between the cryo-gel and the protein-κ-carrageenan aggregates. Further investigation is needed to understand the mechanism underlying the interaction between the cryo-gel and the protein, as well as the protein-κ-carrageenan aggregates.

Since only the liquid portion of the drip-through solution was collected in the centrifuge tube, without including the floating foam layer where proteins are adsorbed to the air interface, the volume of the protein phase (bottom opaque phase shown in **Figure 4.47**) in the guar gum samples without κ-carrageenan generally appeared to be less than that of the original mix. In the case of guar gum samples with κ-carrageenan, it is interesting to observe that the samples with 0.15% guar gum and 4% or 6% milk protein exhibited a two-layered structure in the guar gum enriched phase, with the bottom layer displaying a more gel-like structure and the top layer having a more liquid-like structure. Further investigation is necessary to comprehend the changes in κ-carrageenan-protein aggregates in the presence of guar gum after the freezing-melting process.

By observing the phase separation at both microscopic and macroscopic scales, the confirmation of the phase separation seen under the CLSM indicates that it eventually undergoes macroscopic phase separation when sufficient storage time is provided. Furthermore, the CLSM images provide additional information regarding the type of phase separation behavior that is hard to distinguish in the macroscopic phase separation. Examples of phase separation observed both under CLSM and through the storage study are shown **Figure 4.49**.

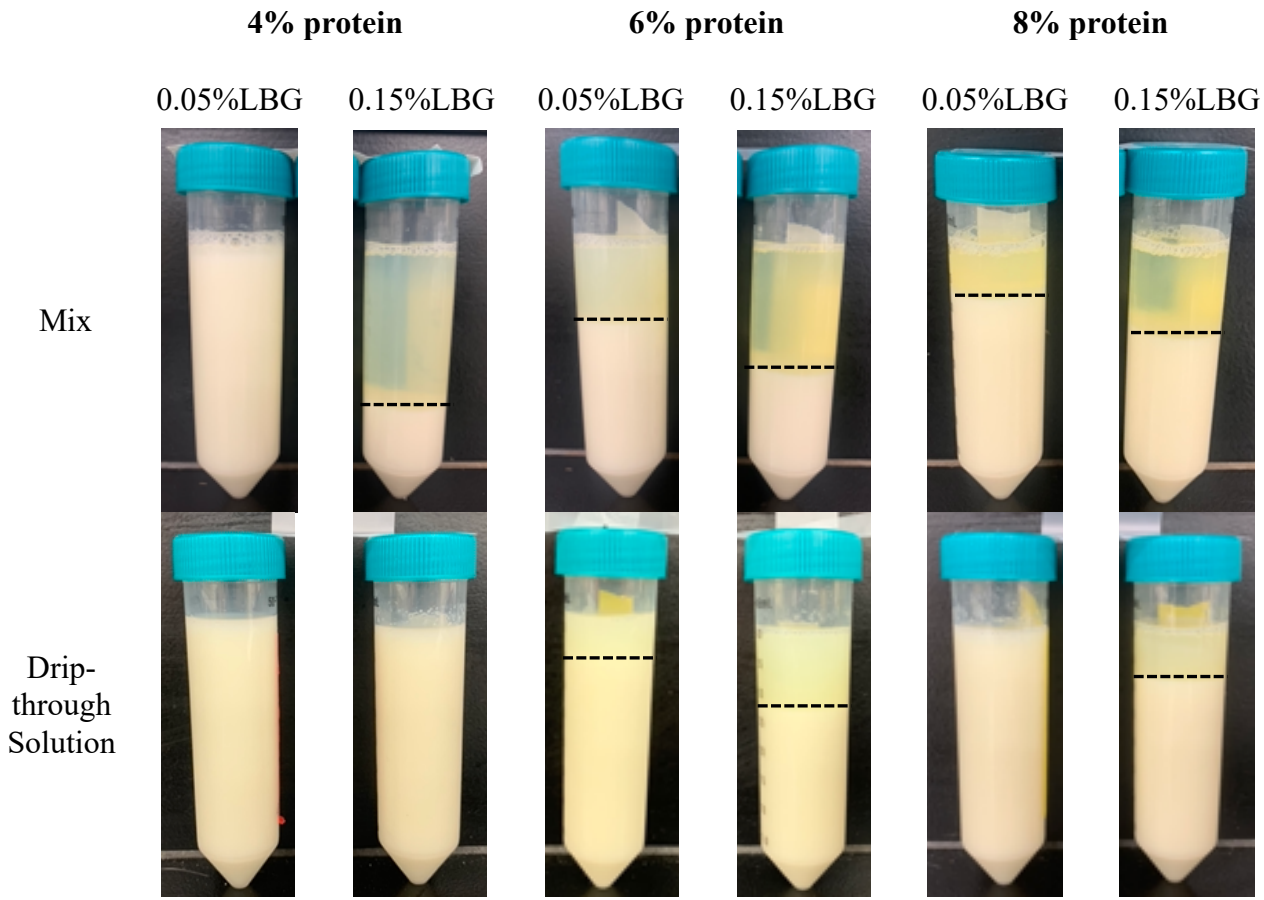

Figure 4.45 Images of locust bean gum mix and drip-through solution with different protein content after being stored in the refrigerator for 7 days. LBG: locust bean gum. The dashed line represents the separation boundary between the protein-enriched phase (bottom) and the hydrocolloids-enriched phase (top).

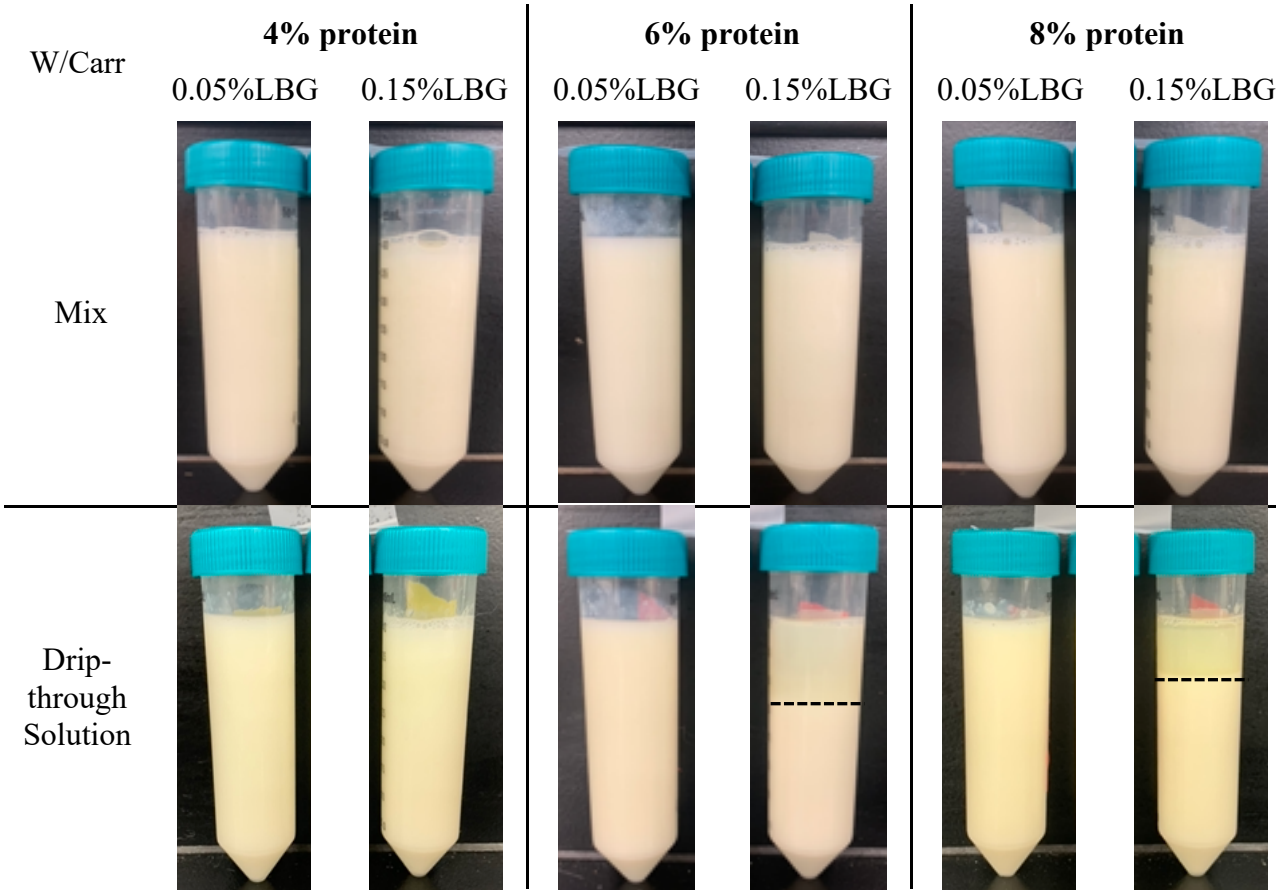

Figure 4.46 Images of locust bean gum + κ-carrageenan (Carr) mix and drip-through solution with different protein content after being stored in the refrigerator for 7 days. LBG: locust bean gum. The dashed line represents the separation boundary between the protein-enriched phase (bottom) and the hydrocolloids-enriched phase (top).

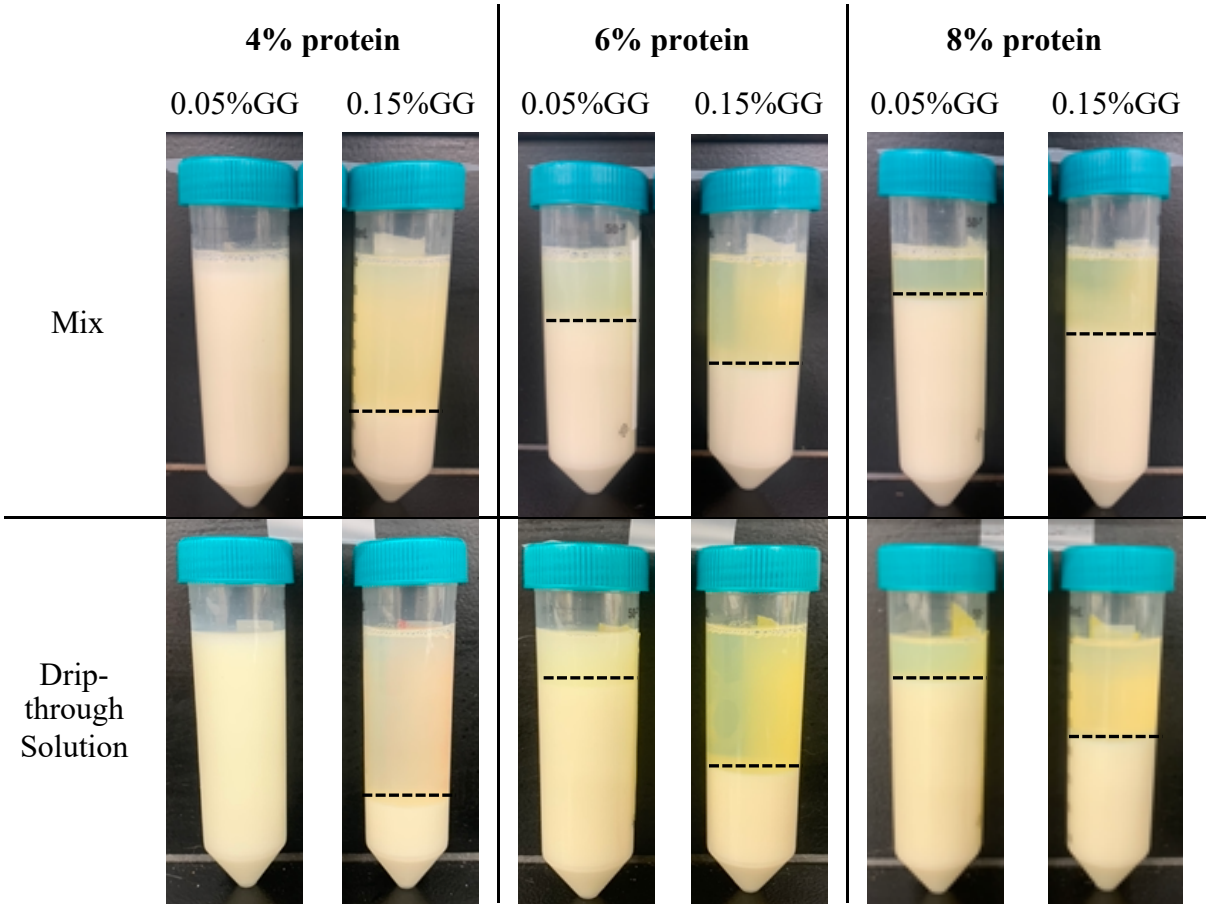

Figure 4.47 Images of guar gum solution and drip-through mix with different protein content after being stored in the refrigerator for 7 days. GG: guar gum. The dashed line represents the separation boundary between the protein-enriched phase (bottom) and the hydrocolloids-enriched phase (top).

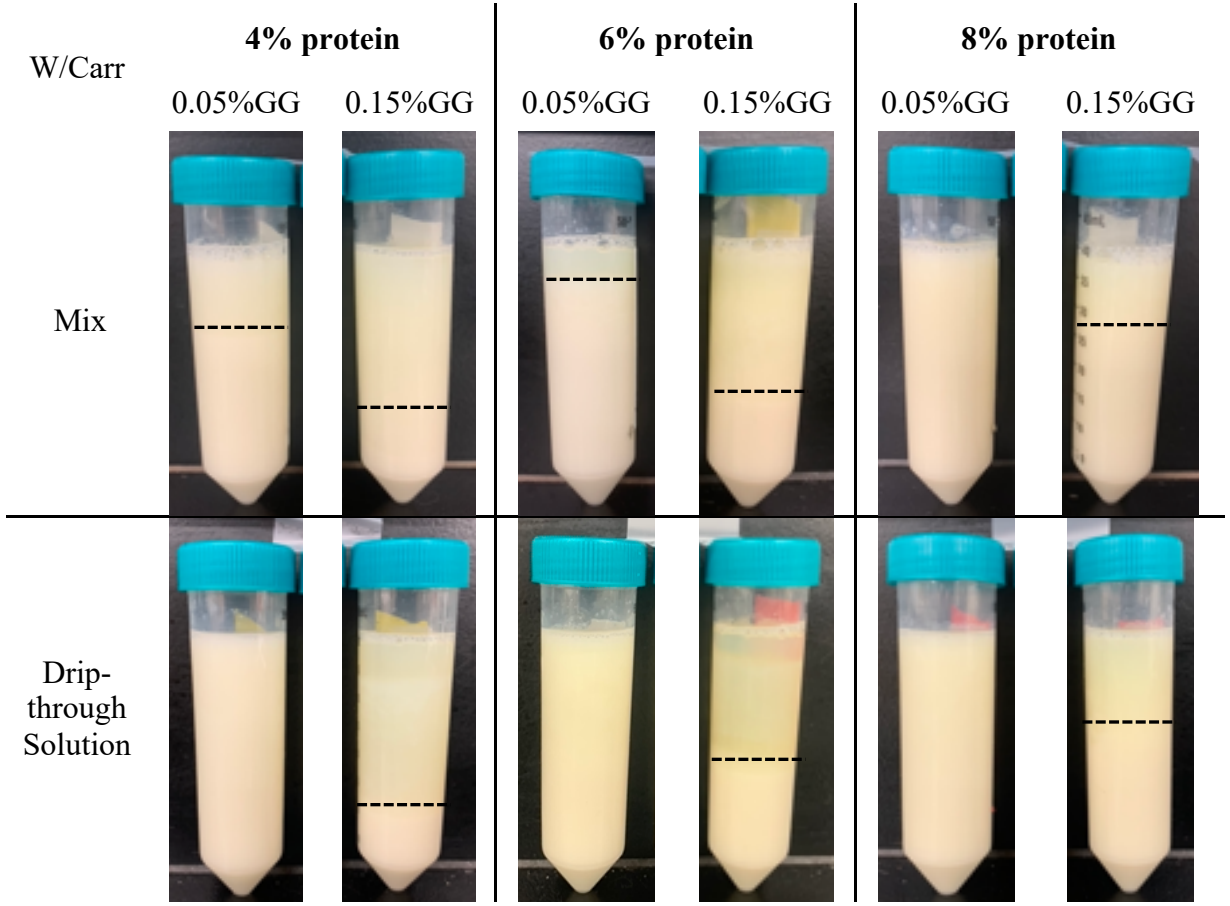

Figure 4.48 Images of guar gum + κ-carrageenan (Carr) mix and drip-through solution with different protein content after being stored in the refrigerator for 7 days. GG: guar gum. The dashed line represents the separation boundary between the protein-enriched phase (bottom) and the hydrocolloids-enriched phase (top).

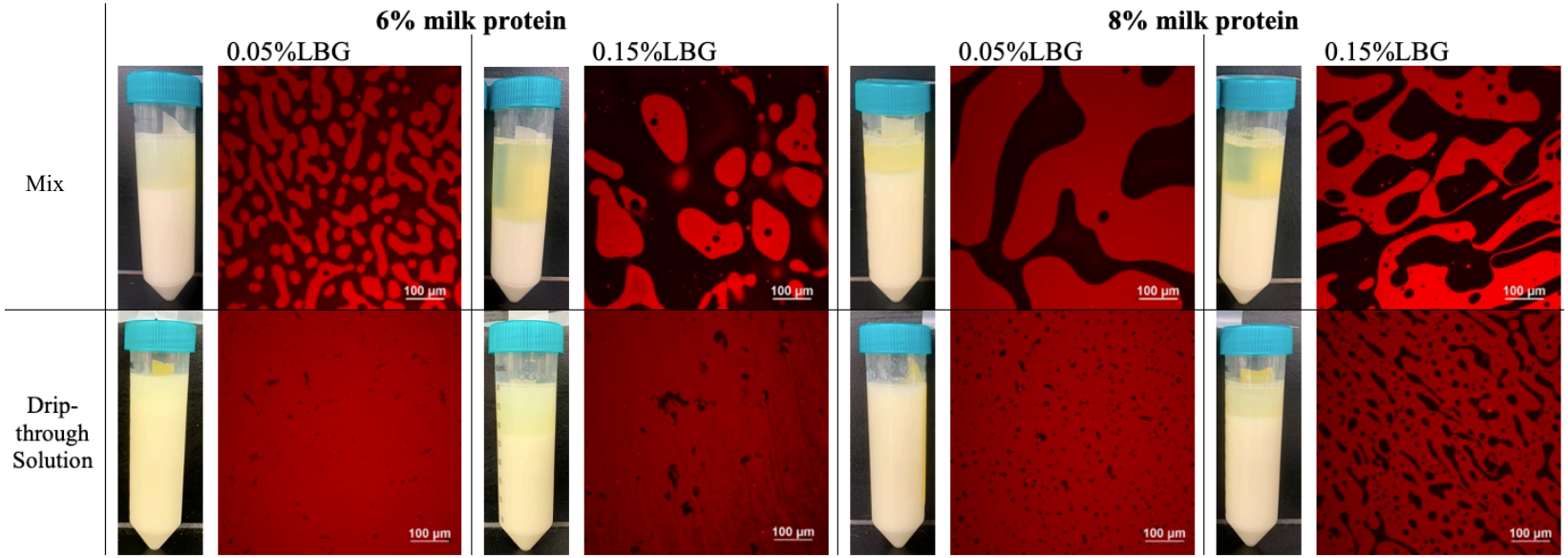

Figure 4.49 Examples of phase separation behavior observed both under CLSM and through the storage study.

4.4.7 Meltdown

In order to investigate phase separation during meltdown, two types of galactomannans, guar gum and locust bean gum, were chosen to induce phase separation with milk protein. The addition of κ-carrageenan to the system was aimed at controlling macroscopic phase separation, although microscopic phase separation was still observed. Depending on the type and amount of galactomannans used, two distinct meltdown behaviors were observed: complete drip-through or residual foam remaining on the mesh. This resulted in a wider range of melting rates compared to the findings in sections **4.2** and **4.3**.

The induction time was recorded when the first melted liquid started dripping through the mesh. Overall, the induction time ranged from 19.9 to 29.6 min (**Table 4.29**). Samples containing 6% milk protein and 0.15% guar gum exhibited the shortest induction time, while samples with 8% milk protein and 0.15% locust bean gum in the presence of κ-carrageenan had the longest induction time. No significant correlation was observed between protein content and induction time across all the samples.

An increase in the amount of locust bean gum generally resulted in a longer induction time, although this trend was not observed in the guar gum system. Furthermore, the addition of κ-carrageenan generally led to a longer induction time, except in the samples with 4% milk protein and 0.05% guar gum, and 8% milk protein with 0.15% guar gum. When comparing the types of galactomannans, guar gum generally exhibited a shorter induction time than locust bean gum. This difference may be attributed to the formation of a cryo-gel during freezing in the locust bean gum system, which tends to retain the internal structure and hinders drainage.

Table 4.29 Induction time (min) for melting of samples with different protein levels, with and without 0.015% κ-carrageenan (carr), and different types and amounts of galactomannans (GG: guar gum; LBG: locust bean gum). The standard deviation (±) refers to the variation among triplicate samples.

	Induction time (min)*			
	0.05% LBG	**0.15% LBG**	**0.05% GG**	**0.15% GG**
4% protein	$21.8\pm1.1^{A,x,a,X}$	$25.1\pm1.8^{A,y,a,X}$	$22.5\pm1.7^{A,x,a,X}$	$22.3\pm1.1^{AB,x,a,Y}$
6% protein	$22.4\pm1.1^{AB,x,a,X}$	$23.8\pm1.5^{A,y,a,X}$	$21.9\pm1.6^{A,x,a,X}$	$19.9\pm1.2^{A,y,a,Y}$
8% protein	$23.6\pm1.8^{B,x,a,X}$	$27.0\pm1.3^{B,y,a,X}$	$23.0\pm1.7^{A,x,a,X}$	$24.3\pm3.4^{B,x,a,Y}$
4% protein+carr	$25.1\pm1.3^{A,x,b,X}$	$27.0\pm2.4^{A,x,a,X}$	$22.1\pm1.6^{A,x,a,Y}$	$22.5\pm1.7^{A,x,a,Y}$
6% protein+carr	$25.5\pm0.9^{AB,x,b,X}$	$25.6\pm1.9^{A,x,b,X}$	$23.6\pm1.7^{A,x,b,Y}$	$21.2\pm2.3^{A,y,a,Y}$
8% protein+carr	$26.6\pm1.0^{B,x,b,X}$	$29.6\pm1.6^{B,y,b,X}$	$25.5\pm1.5^{B,x,b,X}$	$22.0\pm2.0^{A,y,a,Y}$

*Tukey's HSD test was performed for the significant difference at $P<0.05$

^{A,B} denote significant differences among samples with different protein levels

^{x,y} denote significant differences between samples with two levels of hydrocolloids (0.05% and 0.15%)

^{a,b} denote significant differences between samples with and without κ-carrageenan

^{X,Y} denote significant differences between samples with same amount of guar gum and locust bean gum

By conducting multivariate analysis on induction time, apparent viscosity, and flow rate index, irrespective of protein and galactomannans content, a strong positive correlation was observed between apparent viscosity and induction time in locust bean gum samples (**Figure 4.50**), both with κ-carrageenan (r=0.8746) and without κ-carrageenan (r=0.8813). Similarly, a strong negative correlation was identified between flow rate index and induction time in the locust bean gum samples, with (r=-0.8090) and without κ-carrageenan (r=-0.9097) (**Figure 4.51**). However, no significant correlation was detected between rheological properties and induction time in the guar gum system. These results imply that the association between induction time and rheological properties is highly dependent on the specific hydrocolloid utilized.

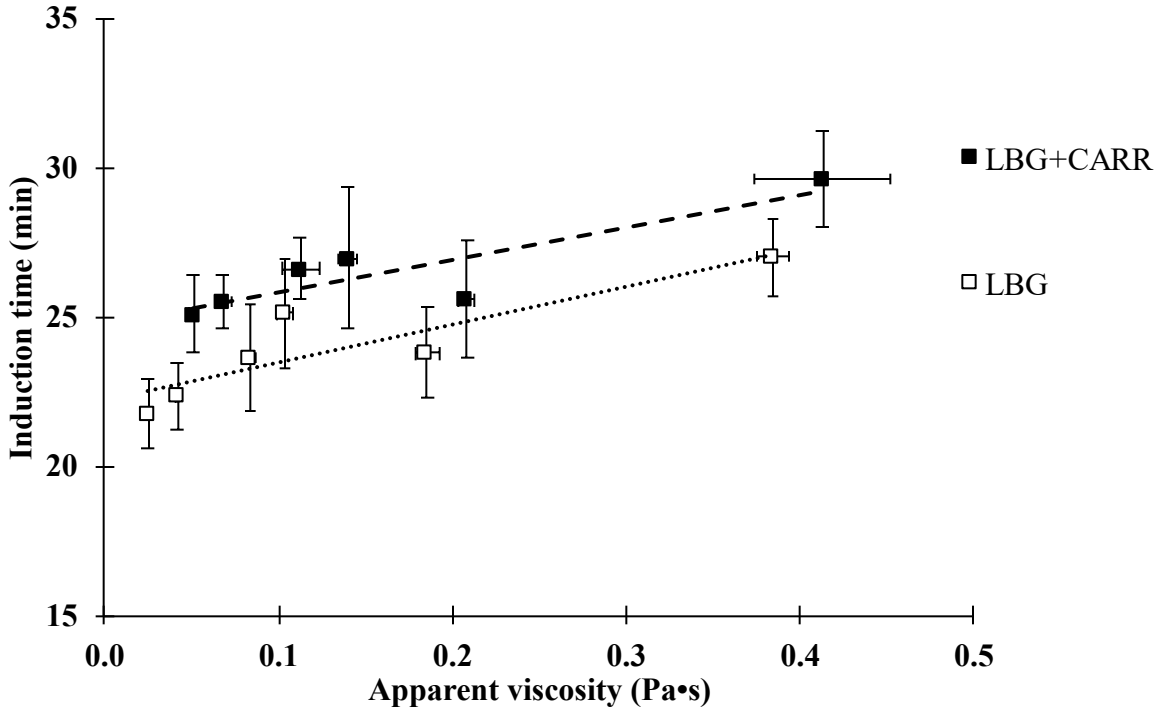

Figure 4.50 The correlation between apparent viscosity (at 5 s^{-1}) and induction time for melting in the locust bean gum (LBG) system. CARR: κ-carrageenan.

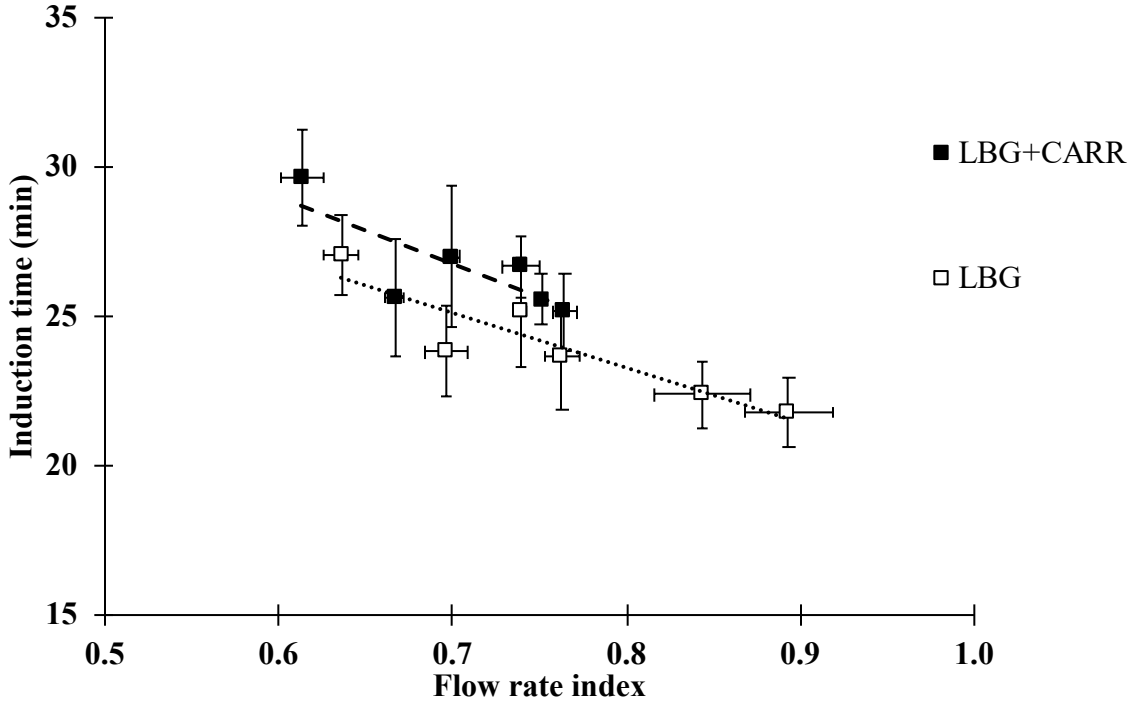

Figure 4.51 The correlation between flow rate index and induction time for melting in the locust bean gum (LBG) system. CARR: κ-carrageenan.

Upon closer examination of the CLSM images of the drip-through solutions for guar gum and locust bean gum (**Figure 4.43** and **Figure 4.44**), a potential explanation is proposed to account for the inconsistent correlation observed in the induction time. It appears that the phase separation behavior undergoes a change during the freezing and melting process. Specifically, in the case of locust bean gum, the drip-through solution predominantly existed as a single liquid phase. However, for guar gum, most of the samples exhibited a water-in-water phase separation behavior, suggesting the presence of nonhomogeneous liquids with potentially varying local viscosities. The inconsistent correlation observed between rheology and induction time in the guar gum samples is likely due to these variations in local viscosity. Nonetheless, the mechanisms through which the different types of hydrocolloid impact induction time remain unclear. A moderate correlation ($r=-0.6389$) was observed between overrun and induction time. However, no correlation was found between mean ice crystal size, air cell size, particle size, and induction time.

The melting rate was determined by calculating the slope of the linear portion of the meltdown curve. Across the samples, the melting rate ranged from 0.90 to 1.39 g/min. Notably, the samples containing 4% milk protein and 0.15% locust bean gum exhibited the slowest melting rate, while the samples with 8% milk protein and 0.15% locust bean gum in the presence of κ-carrageenan showed the fastest melting rate (**Table 4.30**). Furthermore, the samples containing 4% milk protein with locust bean gum, with and without κ-carrageenan, displayed the slowest melting rate. In these particular samples, instead of melting layer by layer in a hemispherical shape until fully dripping through, the melted foam accumulated at the bottom of the frozen samples, resulting in a gummy texture foam residue on the mesh after the meltdown test (**Figure 4.52**). This accumulation and residue formation contributed to the slower melting rate observed in comparison

to other samples. All guar gum samples melted in the same behavior, shrinking into a hemispherical shape, and fully dripping through the mesh (**Figure 4.53**).

Table 4.30 Melting rate (g/min) of samples with different protein levels, with and without 0.015% κ-carrageenan (carr), and different types and amounts of galactomannans (GG: guar gum; LBG: locust bean gum). The standard deviation (±) refers to the variation among triplicate samples.

	Melting rate (g/min)*			
	0.05% LBG	**0.15% LBG**	**0.05% GG**	**0.15% GG**
4% protein	$1.06\pm0.02^{A,x,a,X}$	$0.90\pm0.04^{A,y,a,X}$	$1.16\pm0.05^{A,x,a,Y}$	$1.23\pm0.02^{A,y,a,Y}$
6% protein	$1.26\pm0.02^{B,x,a,X}$	$1.28\pm0.03^{B,x,a,X}$	$1.23\pm0.02^{B,x,a,Y}$	$1.18\pm0.04^{A,y,a,Y}$
8% protein	$1.28\pm0.05^{B,x,a,X}$	$1.35\pm0.03^{C,y,a,X}$	$1.24\pm0.04^{B,x,a,X}$	$1.33\pm0.05^{B,y,a,X}$
4% protein+carr	$1.07\pm0.04^{A,x,a,X}$	$0.97\pm0.09^{A,y,b,X}$	$1.24\pm0.02^{A,x,b,Y}$	$1.17\pm0.04^{A,y,b,Y}$
6% protein+carr	$1.31\pm0.03^{B,x,b,X}$	$1.28\pm0.05^{B,x,a,X}$	$1.26\pm0.03^{AB,x,b,Y}$	$1.19\pm0.02^{A,y,a,Y}$
8% protein+carr	$1.32\pm0.05^{B,x,a,X}$	$1.39\pm0.04^{C,y,b,X}$	$1.30\pm0.08^{B,x,a,X}$	$1.25\pm0.05^{B,x,b,Y}$

*Tukey's HSD test was performed for the significant difference at $P<0.05$
^{A,B,C} denote significant differences among samples with different protein levels
^{x,y} denote significant differences between samples with two levels of hydrocolloids (0.05% and 0.15%)
^{a,b} denote significant differences between samples with and without κ-carrageenan
^{X,Y} denote significant differences between samples with same amount of guar gum and locust bean gum

Daw and Hartel (2015) observed that increasing the protein content from NFDM resulted in an increased melting rate in ice cream products, particularly from 4% to 6%, that was accounted to the decrease in fat destabilization. Similar trends were observed in this study, where the 4% milk protein samples exhibited significantly slower melting rates compared to the 6% and 8% samples, except in the 0.15% guar gum system, even in the absence of milk fat.

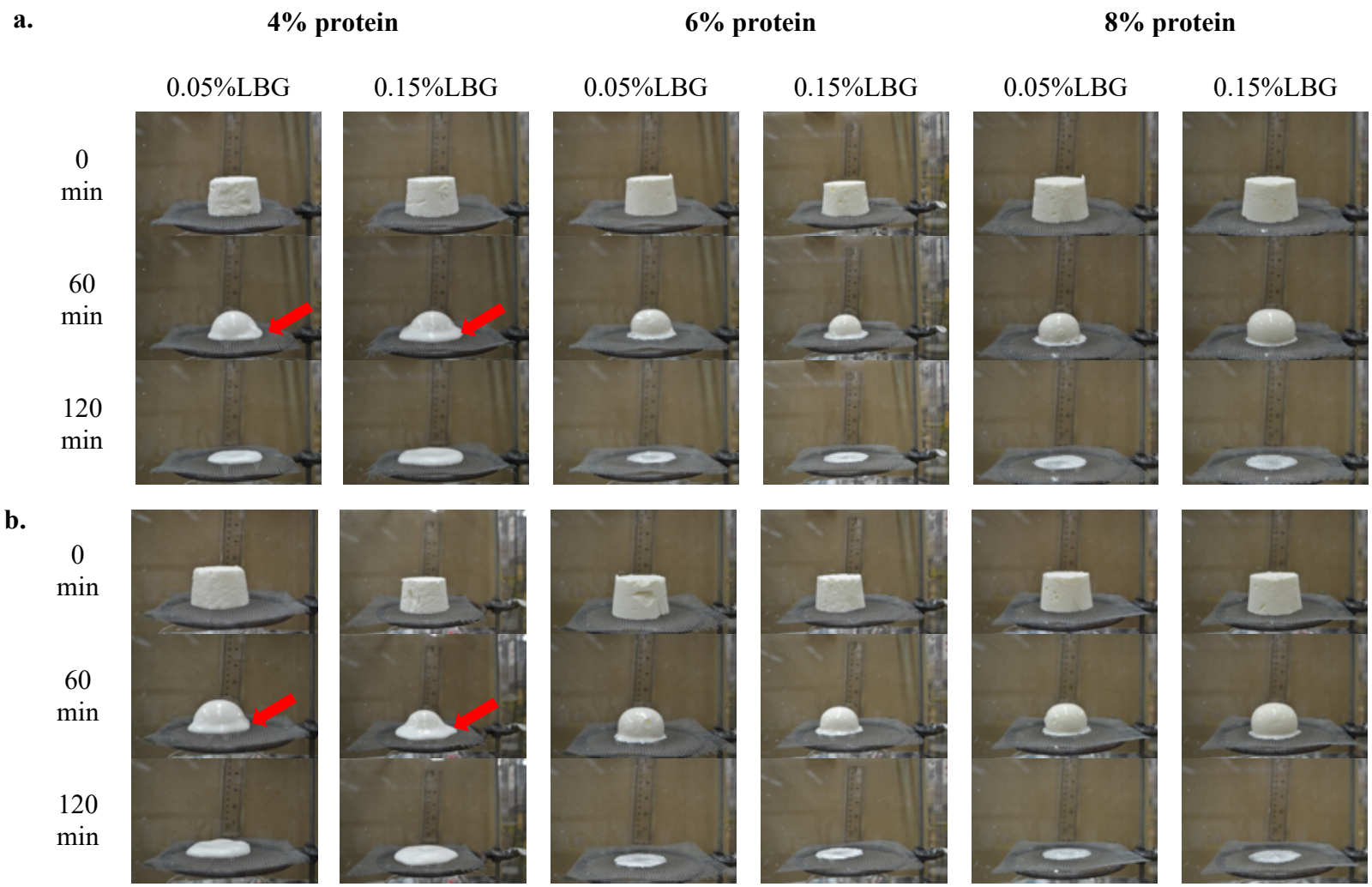

Figure 4.52 Meltdown test images for samples with locust bean gum and different protein content: (a) without κ-carrageenan and (b) with κ-carrageenan. The arrow points indicate the accumulation of melted liquid at the bottom of the frozen samples.

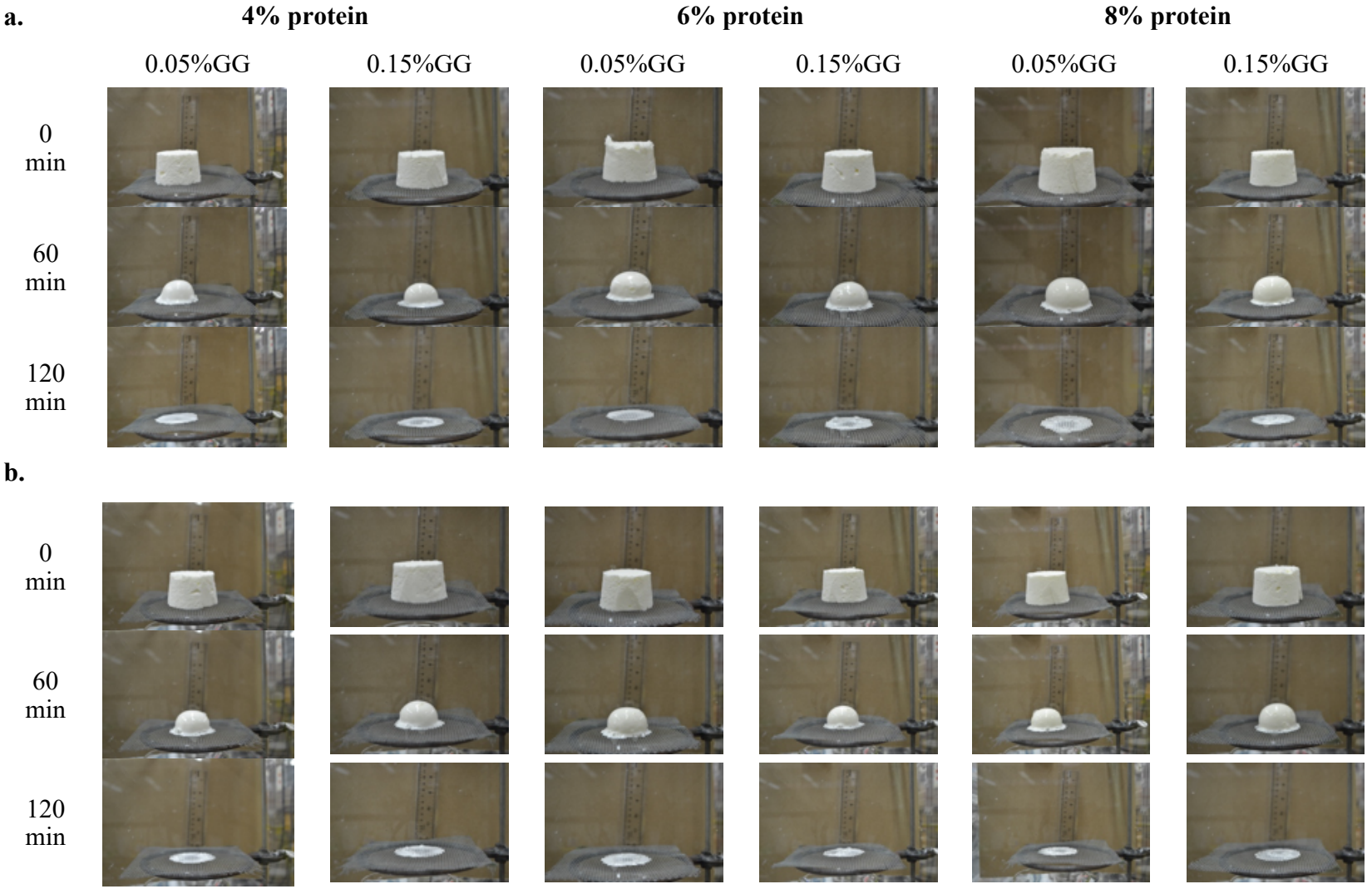

Figure 4.53 Meltdown test images for samples with guar gum and different protein content: (a) without κ-carrageenan and (b) with κ-carrageenan.

To further investigate the influence of protein content on melting rate, the different overruns achieved with varying protein content were analyzed for comparison. Multivariate analysis conducted across all samples, regardless of their protein and galactomannans content, revealed a strong negative correlation between overrun and melting rate (LBG: r=-0.8997; GG: r=-0.9078; LBG+κ-carr: r=-0.7747; GG+κ-carr: r=-0.7085). These correlations are illustrated in **Figure 4.54**. A general trend of decreasing melting rate with increasing overrun was observed across all samples. Specifically, a linear correlation was observed for the samples that fully dripped through, as well as for the samples with remnant foam on the mesh.

Although the correlation between overrun and meltdown rate was only observed in the samples without stabilizers in section **4.1**, the correlation seen here can be attributed to the absence of fat destabilization in these samples. Fat destabilization in ice cream impedes the drainage of liquid in the lamella and diminishes the impact of overrun on meltdown. In contrast, the absence of fat in this system allows for a clearer observation of the effect of overrun on meltdown.

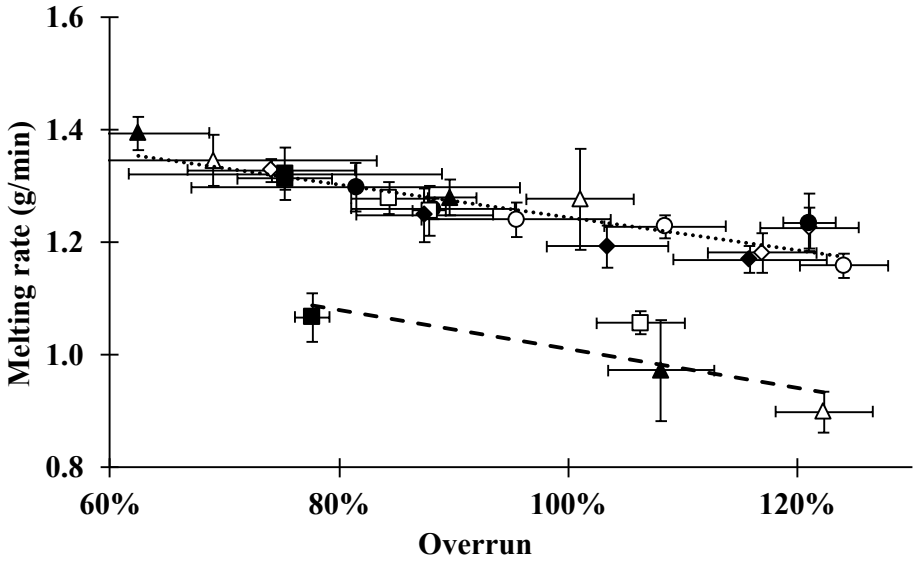

Figure 4.54 The correlation between melting rate and overrun. Square: 0.05% LBG (locust bean gum); triangle: 0.15% LBG; circle: 0.05% GG (guar gum); diamond: 0.15% GG. Hollow: without κ-carrageenan; filled: with κ-carrageenan.

The optical brightfield images (**Figure 4.55** and **Figure 4.56**) were captured for the melted foam samples obtained directly from the frozen samples. The images revealed a phase separation in the serum phase, characterized by two distinct liquid-liquid immiscible regions. The phase separation behavior observed in the melted foam was consistent with that in the drip-through solution observed under CLSM, except in the samples where remnant foam was present on the mesh. In these samples, the large particle structures observed in the melted foam were less prominent in the CLSM images because most of them did not drip through the mesh (**Figure 4.57**).

The air bubbles in this foam system are stabilized either by (1) a protein layer, which was observed in the guar gum system as a liquid phase surrounding the air bubbles and inferred to be a protein layer, (2) by the presence of locust bean gum cryo-gel structure resulting in protein depletion region or (3) the formation of κ-carrageenan and casein aggregates (as indicated in the arrows in **Figure 4.55** and **Figure 4.56**).

In the samples where air bubbles are stabilized by protein layers, the flow of the serum phase is influenced by the phase separation region. The presence of a protein-depleted region and a protein-rich region within this immiscible area may result in different flow speeds, thus affecting liquid drainage and the melting rate. On the other hand, in systems where air bubbles are stabilized by the cryo-gel structure or κ-carrageenan and casein aggregates, the mechanism of such structures might resemble the fat clusters found in ice cream systems. These structures not only provide rigidity in the lamella during drainage but also contribute to the stabilization of air bubbles. In both cases, it can be inferred that the presence of a substantial number of stabilized air bubbles hinders liquid drainage, which potentially explains the observed relationship between overrun and melting rate.

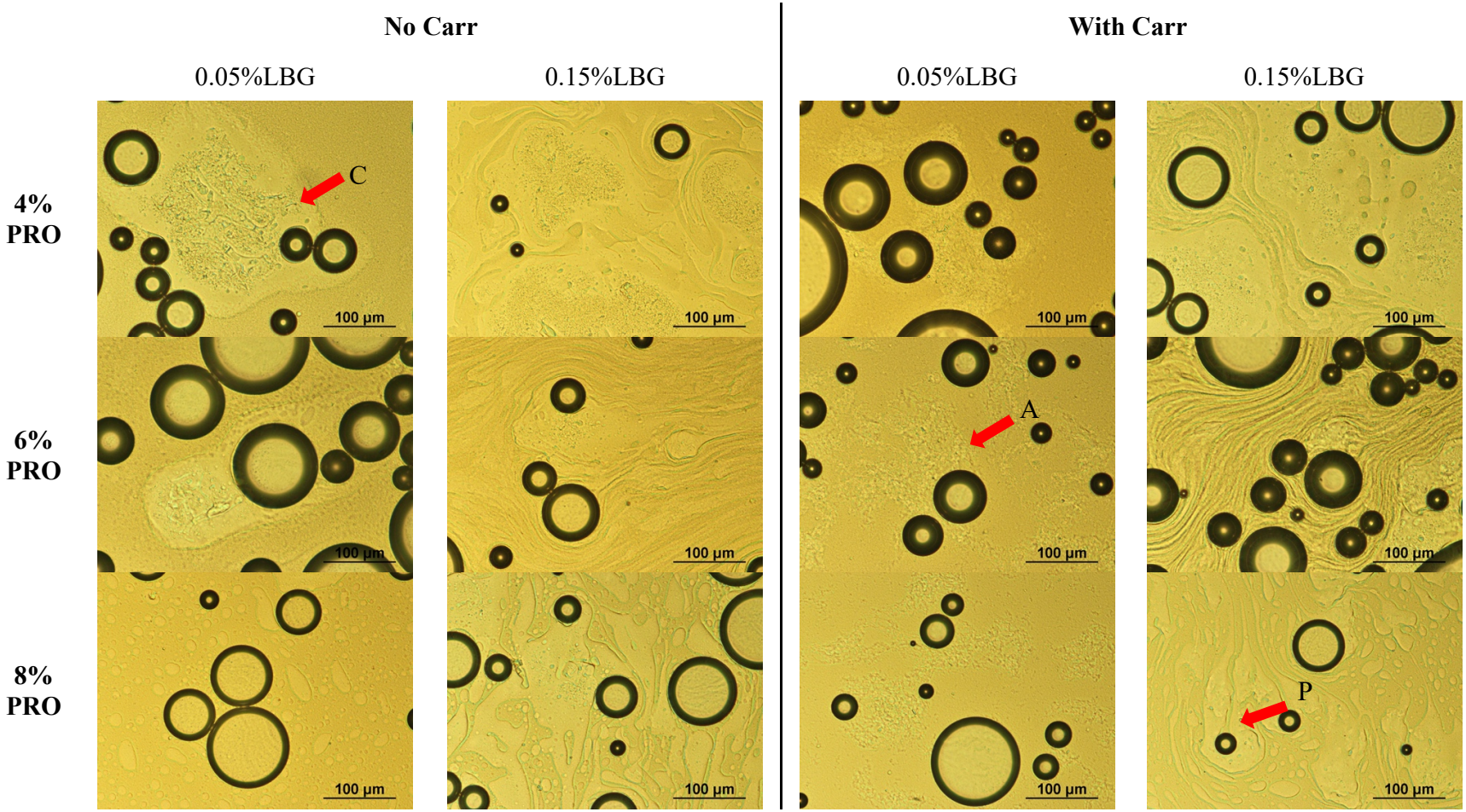

Figure 4.55 The brightfield images of melted foam containing locust bean gum (LBG). Carr: κ-carrageenan; PRO: milk protein; C: cryo-gel structure; A: κ-carrageenan and casein; P: protein layer. The presence of a protein layer is speculated due to its surrounding of the air cells and its indication of phase separation with the surrounding region.

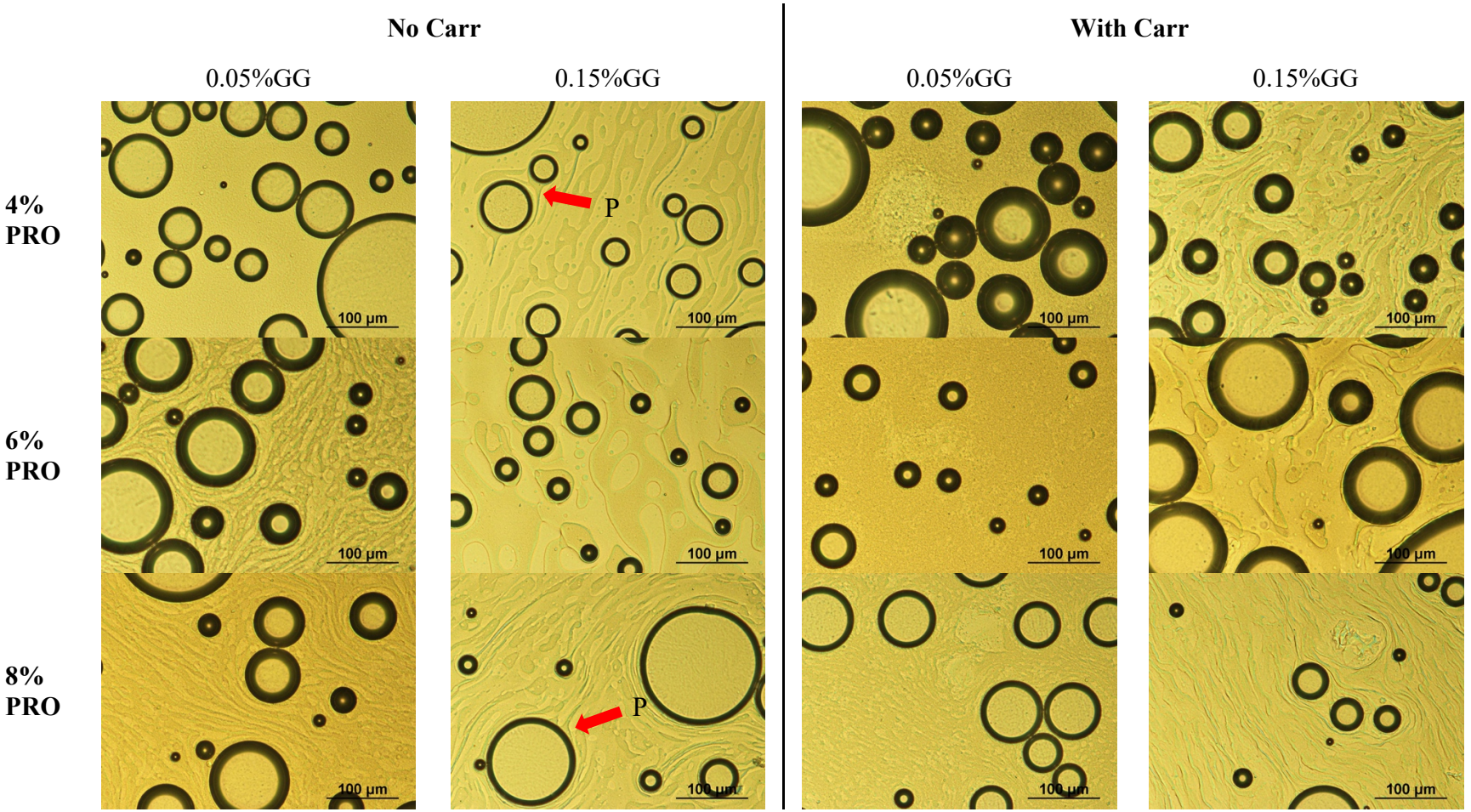

Figure 4.56 The brightfield images of melted foam containing guar gum (GG). Carr: κ-carrageenan; PRO: milk protein; P: protein layer. The presence of a protein layer is speculated due to its surrounding of the air cells and its indication of phase separation with the surrounding region.

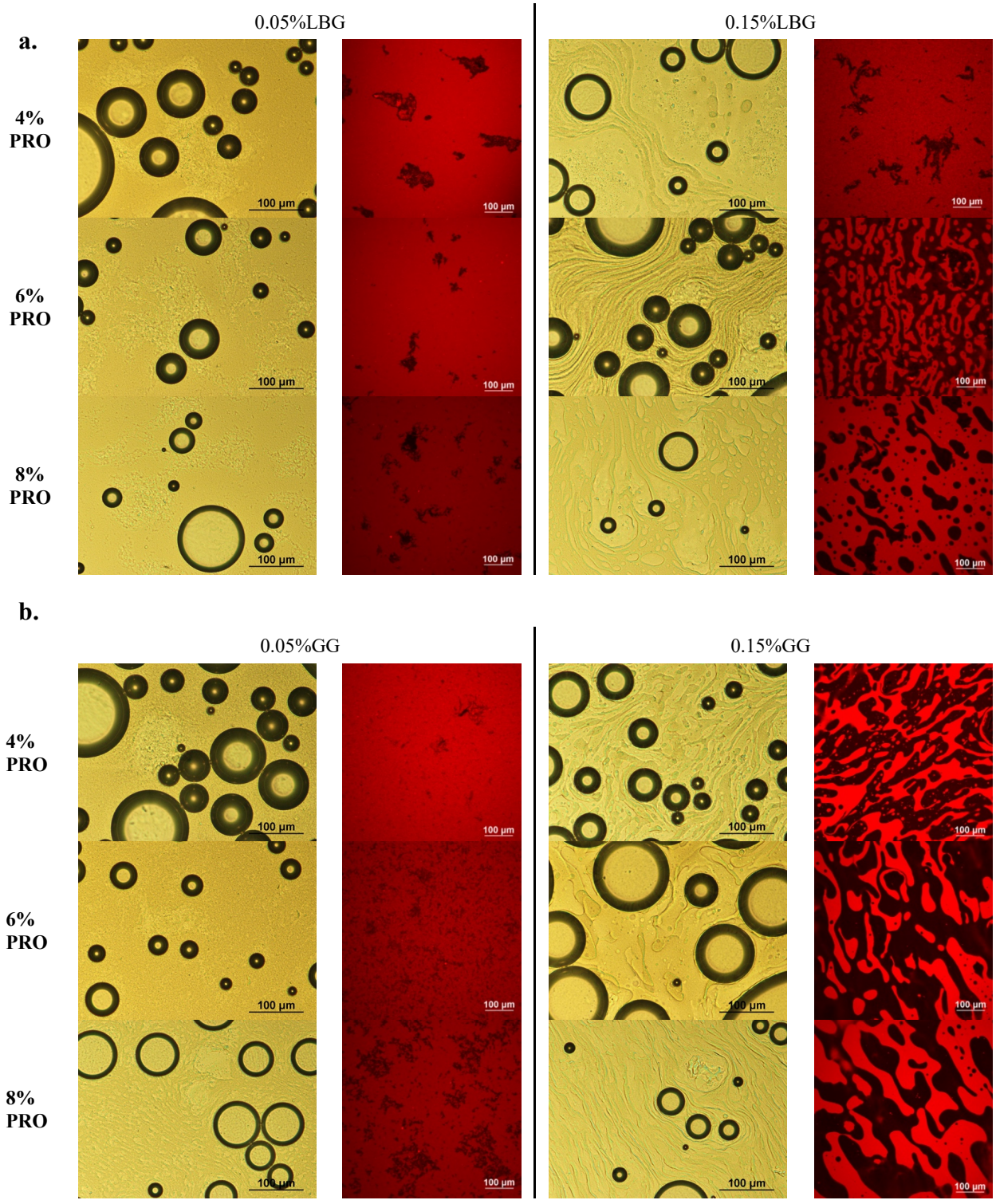

Figure 4.57 Examples of phase separation observed in the serum phase in the melted foam and in the drip-through solution under CLSM with the presence of κ-carrageenan: a. locust bean gum (LBG); b. guar gum (GG).

No discernible trend of melting rate was observed between 0.05% and 0.15% guar gum or locust bean gum. Additionally, no significant correlation was found between apparent viscosity, flow rate index, consistency, and melting rate. It is worth noting that the phase separation observed in the serum phase indicates that the measured rheological properties may not fully represent the local viscosity in either the protein phase or the protein-depletion phase. In certain instances of phase separation in the serum phase, one phase is in the form of a pocket or droplet embedded within the other phase. The interaction between these immiscible liquid phases may impact the liquid drainage process. In the guar gum system, when κ-carrageenan is present, the top phase volume, representing the hydrocolloids-enriched phase collected from the storage test, shows a linear correlation with the melting rate (**Figure 4.58**). A smaller top phase volume indicates reduced phase separation, leading to a higher melting rate. This is because the interaction between the immiscible regions decreases, accelerating the drainage. This correlation was not observed in the guar gum samples lacking κ-carrageenan, and further study is necessary to gain a better understanding of the influence of phase separation on meltdown.

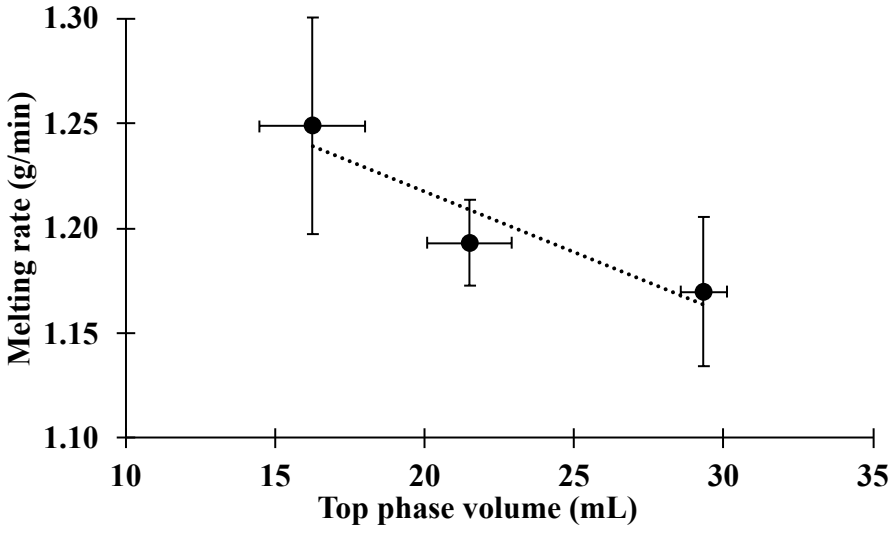

Figure 4.58 The linear correlation between top phase volume of hydrocolloid-enriched phase in the drip-through solution and melting rate of samples with κ-carrageenan in the guar gum system.

The addition of κ-carrageenan resulted in a slight increase in the melting rate across most of the samples, except for the 0.15% guar gum samples. When comparing samples with similar melting pattern between guar gum and locust bean gum, particularly those containing 6% and 8% milk protein, the guar gum samples generally exhibited a slower melting rate compared to locust bean gum. This observation suggests that the presence of phase separation, which is more likely to occur in guar gum samples, hinders the process of liquid drainage. One possible mechanism for this effect is the phase separation in the serum phase within the foam, which can disrupt the protein layer surrounding the air bubbles and contribute to a less stable foam (Parra et al., 2016).

Two distinct meltdown behaviors were observed: complete drip-through and the presence of collapsed melted foam on the mesh. The latter behavior was exclusively observed in samples with a 4% milk protein and locust bean gum system, regardless of the locust bean gum content or the presence of κ-carrageenan. This phenomenon can be attributed to the cryo-gel formation of locust bean gum during the freezing and melting process. The gel structure remains intact after melting, effectively holding the internal structure together and preventing drainage. This observation aligns with the findings in section **4.2**, where only locust bean gum and sucrose were present in the system. The additional milk protein induces phase separation, which causes the polysaccharide molecules to come closer together and form a stronger gel network (Goff et al., 1999). The absence of such a stable foam at higher protein content may be due to the disruptive effect of the increased milk protein, as evidenced by the larger protein region observed in the CLSM images compared to the 4% milk protein sample.

4.4.8 Summary

The designed milk protein-polysaccharide system not only affects phase separation but also influences the rheological properties of the solution, protein particle size, overrun of the frozen samples, and the meltdown process. Increasing the amount of biopolymers in the system, whether from milk protein or polysaccharide, generally resulted in higher apparent viscosity, consistency, and a more pronounced shear-thinning behavior in the solution due to increased voluminosity from the biopolymers.

The increase in protein content generally led to a decrease in particle size, primarily attributed to the variation in sucrose content among the systems with different protein concentrations. This change in sucrose content affected the solubility of milk protein, resulting in insufficient solubility at higher sucrose levels. Conversely, an increase in the amount of guar gum or locust bean gum resulted in larger particle sizes, mainly due to the depletion-flocculation effect that promoted the aggregation of casein micelles.

The increase in protein content decreased the overrun in the frozen sample. In samples with higher protein content, the smaller protein particles were more easily able to migrate to the air bubble surface and form a viscoelastic film layer. In contrast, the larger particles in samples with lower protein content tended to provide structural rigidity for air stabilization. Additionally, a higher amount of galactomannans generated a higher overrun by providing greater shear force, while the additional κ-carrageenan leaded to a lower overrun.

Microscopic phase separation was observed in all samples except for the system containing 4% milk protein and 0.05% guar gum or locust bean gum. While κ-carrageenan prevented macroscopic phase separation, microscopic phase separation was still observed. Interestingly, the freezing-melting process prevented phase separation in most of the locust bean gum samples,

primarily due to cryo-gel formation, which maintained the integrity of the internal structure. This phenomenon was not observed in the guar gum samples.

A higher induction time during the melting process was observed in samples with higher apparent viscosity and a more shear-thinning behavior in the locust bean gum system, while no clear trend was found in the guar gum samples. Additionally, a linear correlation was observed between overrun and melting rate. Two distinct melting behaviors were observed: complete drip-through and the presence of residual foam on the mesh. The latter behavior was specifically observed in samples containing 4% milk protein and locust bean gum. It is reasonable to speculate that this behavior may be associated with the formation of a cryo-gel structure at lower protein content, which allows for the formation of more junction zones among the locust bean gum molecules.

5. Conclusions and Recommendations

5.1 Conclusions

This study progressed from an ice cream system towards simplified model systems, with subsequent addition of structural components, aiming to gain insights into how these components affect the meltdown process in frozen desserts. Through formulation adjustments, different microstructures of ice cream were successfully achieved. By correlating the structural components with the data extracted from the entire meltdown curve, it was discovered that indicators such as the induction time, final drip-through weight, height change rate, and final height could be utilized to describe the melting behavior in addition to the melting rate. Notably, the height change curve offered supplementary information to distinguish between two distinct types of meltdown behavior.

Mix viscosity was identified as the dominant factor influencing the ice cream meltdown process, while fat destabilization and overrun were only factors in the ice cream with the lowest mix viscosity achieved by excluding stabilizers. However, the rheological properties were not found to be dominant in the non-aerated frozen sucrose system. Conversely, the type of polysaccharide was found to have a significant impact on the meltdown rate in the non-aerated system, with anionic polysaccharides generally melting faster than neutral ones, possibly due to their ability to achieve different surface tensions, which affected the size of the dripping drops. Additionally, locust bean gum exhibited a unique meltdown behavior, likely contributing to the formation of cryo-gel that helped retain the internal structure.

In the aerated frozen sucrose system, air was incorporated due to the inclusion of polysorbate 80. In this case, the mix viscosity demonstrated a positive influence on induction, with higher viscosity resulting in a longer induction time. However, higher mix viscosity also resulted in a faster melting rate, potentially due to the viscosity playing a more significant role in restricting

destabilized fat mobility in the ice cream system compared to this simplified system. Furthermore, the effect of overrun on the meltdown process was only observed in the xanthan gum samples, indicating that the interaction between air and hydrocolloids during bubble movement also influenced the melting and drainage rate.

The addition of milk protein to the system aimed to investigate the phase separation between milk protein and hydrocolloids and its effect on the meltdown process. It was observed that an increase in milk protein content resulted in a reduction in particle size and a decrease in overrun in the frozen samples. Furthermore, in the locust bean gum and milk protein samples, phase separation was prevented after the freezing-melting process. This effect was primarily attributed to the formation of a cryo-gel by the locust bean gum, which altered the structure of locust bean gum and influenced its interaction with milk protein.

In terms of the meltdown process, a higher induction time was observed in samples with higher apparent viscosity and shear-thinning behavior when locust bean gum was present. However, this trend was not observed in the guar gum samples, which may be attributed to the persistence of phase separation behavior in most of the guar gum melted samples. This suggests that the local rheological properties of the lamella could differ between the protein-enriched region and the guar gum-enriched region. Furthermore, a negative correlation was found between overrun and melting rate. Two melting behaviors were observed in this system: complete drip-through and the presence of residual foam on the mesh. The latter behavior was identified in samples with 4% milk protein and locust bean gum, suggesting a possible association with the formation of a cryo-gel from the locust bean gum, which helped retain the internal structure.

5.2 Recommendations

Considering the intriguing correlation observed between polysaccharide types and the meltdown process in both non-aerated and aerated frozen sucrose systems, as well as the demonstrated ability of polysaccharides to reduce surface tension, it would be intriguing to investigate whether this trend extends to ice cream. Additionally, exploring how polysaccharide types impact the meltdown process beyond their influence on drop size during dripping would provide further insights.

Furthermore, the observation of phase separation between milk protein and hydrocolloids highlights the potential significance of local viscosity variations over bulk viscosity. Therefore, future studies should focus on quantifying the local viscosity by measuring the viscosity for both the protein region and the hydrocolloid region after phase separation, and establishing correlations with the meltdown rate. This approach would be crucial in gaining a deeper understanding of the effects of phase separation and rheology on the meltdown process.

The change in phase separation behavior observed after the freezing-melting process indicates that the transformation of water and fat into ice and crystalline fat, followed by the reverse melting process into water and liquid fat, is not the sole factor at play. It suggests that the structure of the serum phase may also undergo changes depending on the types of stabilizers used. To gain further insights into the transformation of lamella before and after freezing-melting, future studies can employ techniques such as confocal laser scanning microscopy (CLSM) and cryo-scanning electron microscopy (cryo-SEM) to observe changes in both the ice cream mix and the resulting melted ice cream and drip-through liquid.

By addressing all the aforementioned aspects, a more comprehensive understanding of the influence of structural components on the meltdown process can be achieved. This, in turn, would aid in the development of healthier frozen dessert products with improved heat resistance.

6. Reference

Abd El-Rahman, A. M., Madkor, S. A., Ibrahim, F. S., & Kilara, A. (1997). Physical characteristics of frozen desserts made with cream, anhydrous milk fat, or milk fat fractions. *Journal of Dairy Science*, *80*(9), 1926–1935. https://doi.org/10.3168/JDS.S0022-0302(97)76133-2

Adhikari, B., Howes, T., Shrestha, A., & Bhandari, B. R. (2007). Effect of surface tension and viscosity on the surface stickiness of carbohydrate and protein solutions. *Journal of Food Engineering*, *79*(4), 1136–1143.

Adleman, R. (1998). *Effect of milk fat fractions and emulsifiers on processing of ice cream*. University of Wisconsin-Madison.

Ahmad, I., Khalique, A., Junaid, M., Shahid, M. Q., Imran, M., & Rashid, A. A. (2020). Effect of polyphenol from apple peel extract on the survival of probiotics in yoghurt ice cream. *International Journal of Food Science and Technology*, *55*, 2580–2588. https://doi.org/10.1111/ijfs.14511

Akalın, A. S., Kesenkas, H., Dinkci, N., Unal, G., Ozer, E., & Kınık, O. (2018). Enrichment of probiotic ice cream with different dietary fibers: Structural characteristics and culture viability. *Journal of Dairy Science*, *101*(1), 37–46. https://doi.org/10.3168/JDS.2017-13468

Allen, K. E., Murray, B. S., & Dickinson, E. (2008). Development of a model whipped cream: Effects of emulsion droplet liquid/solid character and added hydrocolloid. *Food Hydrocolloids*, *22*(4), 690–699. https://doi.org/10.1016/J.FOODHYD.2007.01.017

Alvarez, V. B., Wolters, C. L., Vodovotz, Y., & Ji, T. (2005). Physical properties of ice cream containing milk protein concentrates. *Journal of Dairy Science*, *88*(3), 862–871. https://doi.org/10.3168/JDS.S0022-0302(05)72752-1

Amador, J., Hartel, R., & Rankin, S. (2017). The effects of fat structures and ice cream mix viscosity on physical and sensory properties of ice cream. *Journal of Food Science*, *82*(8), 1851–1860. https://doi.org/https://doi.org/10.1111/1750-3841.13780

Antipova, A. S., & Semenova, M. G. (1995). Effect of sucrose on the thermodynamic incompatibility of different biopolymers. *Carhohydrare Polymers*, *28*, 9–365.

Ashley Wilson. (1989). *Foams: physics, chemistry, and structure* (1st edition). Springer London.

Bąk, A., & Podgórska, W. (2016). Interfacial and surface tensions of toluene/water and air/water systems with nonionic surfactants Tween 20 and Tween 80. *Colloids and Surfaces A: Physicochemical and Engineering Aspects*, *504*, 414–425. https://doi.org/10.1016/J.COLSURFA.2016.05.091

Ben-Yoseph, E., & Hartel, R. W. (1998). Computer simulation of ice recrystallization in ice cream during storage. *Journal of Food Engineering*, *38*(3), 309–329. https://doi.org/10.1016/S0260-8774(98)00116-2

Biasutti, M., Venir, E., Marino, M., Maifreni, M., & Innocente, N. (2013). Effects of high pressure homogenisation of ice cream mix on the physical and structural properties of ice cream. *International Dairy Journal*, *32*(1), 40–45. https://doi.org/10.1016/J.IDAIRYJ.2013.03.007

Bolliger, S., Goff, H. D., & Tharp, B. W. (2000). Correlation between colloidal properties of ice cream mix and ice cream. *International Dairy Journal*. https://doi.org/10.1016/S0958-6946(00)00044-3

Bolliger, S., Kornbrust, B., Goff, H. D., Tharp, B. W., & Windhab, E. J. (2000). Influence of emulsifiers on ice cream produced by conventional freezing and low-temperature extrusion processing. *International Dairy Journal*, *10*(7), 497–504. https://doi.org/10.1016/S0958-6946(00)00071-6

Bolliger, S., Wildmoser, H., Goff, H. D., & Tharp, B. W. (2000). Relationships between ice cream mix viscoelasticity and ice crystal growth in ice cream. *International Dairy Journal*, *10*(11), 791–797. https://doi.org/10.1016/S0958-6946(00)00108-4

Bourriot, S., Garnier, C., & Doublier, J. L. (1999). Phase separation, rheology and microstructure of micellar casein–guar gum mixtures. *Food Hydrocolloids*, *13*(1), 43–49. https://doi.org/10.1016/S0268-005X(98)00068-X

Brigham, J. E., Gidley, M. J., Hoffmann, R. A., & Smith, C. G. (1994). Microscopic imaging of network strands in agar, carrageenan, locust bean gum and kappa carrageenan/locust bean gum gels. *Food Hydrocolloids*, *8*(3–4), 331–344. https://doi.org/10.1016/S0268-005X(09)80345-7

Caniyilmaz, E., Uçarkuş, B., & Karaman, S. (2016). Optimization of formulation ingredients and aging time for ice cream processing using combined design approach. *Journal of Food Processing and Preservation*, *40*(6), 1325–1338. https://doi.org/10.1111/JFPP.12718

Chanamai, R., & McClements, D. J. (2002). Comparison of gum arabic, modified starch, and whey protein isolate as emulsifiers: Influence of pH, CaCl2 and temperature. *Journal of Food Science*, *67*(1), 120–125. https://doi.org/10.1111/J.1365-2621.2002.TB11370.X

Chang, Y., & Hartel, R. W. (2002a). Development of air cells in a batch ice cream freezer. *Journal of Food Engineering*, *55*(1), 71–78. https://doi.org/10.1016/S0260-8774(01)00243-6

Chang, Y., & Hartel, R. W. (2002b). Measurement of air cell distributions in dairy foams. *International Dairy Journal*. https://doi.org/10.1016/S0958-6946(01)00171-6

Chang, Y., & Hartel, R. W. (2002c). Stability of air cells in ice cream during hardening and storage. *Journal of Food Engineering*, *55*(1), 59–70. https://doi.org/10.1016/S0260-8774(01)00242-4

Chen, M., Sala, G., Meinders, M. B. J., van Valenberg, H. J. F., van der Linden, E., & Sagis, L. M. C. (2017). Interfacial properties, thin film stability and foam stability of casein micelle dispersions. *Colloids and Surfaces B: Biointerfaces*. https://doi.org/10.1016/j.colsurfb.2016.10.010

Chen, W., Liang, G., Li, X., He, Z., Zeng, M., Gao, D., Qin, F., Goff, H. D., & Chen, J. (2019). Effects of soy proteins and hydrolysates on fat globule coalescence and meltdown properties of ice cream. *Food Hydrocolloids*, *94*, 279–286. https://doi.org/10.1016/J.FOODHYD.2019.02.045

Cook, K. L. K., & Hartel, R. W. (2010). Mechanisms of ice crystallization in ice cream production. *Comprehensive Reviews in Food Science and Food Safety*, *9*(2), 213–222. https://doi.org/10.1111/J.1541-4337.2009.00101.X

Cottrell, J. I. L., Pass, G., & Phillips, G. O. (1979). Assessment of polysaccharides as ice cream stabilisers. *Journal of the Science of Food and Agriculture*, *30*(11), 1085–1088. https://doi.org/10.1002/JSFA.2740301111

Cottrell, J. I. L., Pass, G., & Phillips, G. O. (1980). The effect of stabilisers on the viscosity of an ice cream mix. *Journal of the Science of Food and Agriculture*, *31*(10), 1066–1070. https://doi.org/10.1002/JSFA.2740311015

Cropper, S. L., Kocaoglu-Vurma, N. A., Tharp, B. W., & Harper, W. J. (2013). Effects of locust bean gum and mono- and diglyceride concentrations on particle size and melting rates of ice cream. *Journal of Food Science*. https://doi.org/10.1111/1750-3841.12073

Dalgleish, D. G., & Morris, E. R. (1988). Interactions between carrageenans and casein micelles: electrophoretic and hydrodynamic properties of the particles. *Food Hydrocolloids*, *2*(4), 311–320. https://doi.org/10.1016/S0268-005X(88)80028-6

Davies, E., Dickinson, E., & Bee, R. (2000). Shear stability of sodium caseinate emulsions containing monoglyceride and triglyceride crystals. *Food Hydrocolloids*, *14*(2), 145–153. https://doi.org/10.1016/S0268-005X(99)00060-0

Davies, P. L. (2014). Ice-binding proteins: A remarkable diversity of structures for stopping and starting ice growth. *Trends in Biochemical Sciences*, *39*(11), 548–555. https://doi.org/10.1016/J.TIBS.2014.09.005

Daw, E., & Hartel, R. W. (2015). Fat destabilization and melt-down of ice creams with increased protein content. *International Dairy Journal*, *43*, 33–41. https://doi.org/10.1016/J.IDAIRYJ.2014.12.001

Dhamole, P. B., Joshi, N., & Bhat, V. (2023). A review of recent developments in sugars and polyol based soluting out separation processes. *Separation and Purification Technology*, *312*. https://doi.org/10.1016/J.SEPPUR.2023.123394

Docoslis, A., Giese, R. F., & Van Oss, C. J. (2000). Influence of the water–air interface on the apparent surface tension of aqueous solutions of hydrophilic solutes. *Colloids and Surfaces B: Biointerfaces*, *19*(2), 147–162. https://doi.org/10.1016/S0927-7765(00)00137-5

Donhowe, D. P., & Hartel, R. W. (1996). Recrystallization of ice in ice cream during controlled accelerated storage. *International Dairy Journal*, *6*(11–12), 1191–1208. https://doi.org/10.1016/S0958-6946(96)00029-5

Donhowe, D. P., Hartel, R. W., & Bradley, R. L. (1991). Determination of ice crystal size distributions in frozen desserts. *Journal of Dairy Science*, *74*(10), 3334–3344. https://doi.org/10.3168/JDS.S0022-0302(91)78521-4

Doublier, J. L., Garnier, C., Renard, D., & Sanchez, C. (2000). Protein-polysaccharide interactions. *Current Opinion in Colloid and Interface Science*, *5*(3–4), 202–214. https://doi.org/10.1016/S1359-0294(00)00054-6

Drewett, E. M., & Hartel, R. W. (2007). Ice crystallization in a scraped surface freezer. *Journal of Food Engineering*, *78*(3), 1060–1066. https://doi.org/10.1016/J.JFOODENG.2005.12.018

Eisner, M. D., Wildmoser, H., & Windhab, E. J. (2005). Air cell microstructuring in a high viscous ice cream matrix. *Colloids and Surfaces A: Physicochemical and Engineering Aspects*, *263*(1–3), 390–399. https://doi.org/10.1016/j.colsurfa.2004.12.017

Elfak, A. M., Pass, G., & Morley, R. G. (1977). The viscosity of dilute solutions of guar gum and locust bean gum with and without added sugars. *Journal of the Science of Food and Agriculture*, *28*(10), 895–899. https://doi.org/10.1002/JSFA.2740281005

Faydi, E., Andrieu, J., & Laurent, P. (2001). Experimental study and modelling of the ice crystal morphology of model standard ice cream. Part I: Direct characterization method and experimental data. *Journal of Food Engineering*, *48*(4), 283–291. https://doi.org/10.1016/S0260-8774(00)00168-0

Fernández, P. P., Martino, M. N., Zaritzky, N. E., Guignon, B., & Sanz, P. D. (2007). Effects of locust bean, xanthan and guar gums on the ice crystals of a sucrose solution frozen at high pressure. *Food Hydrocolloids*, *21*(4), 507–515. https://doi.org/10.1016/j.foodhyd.2006.05.010

Flores, A. A., & Goff, H. D. (1999a). Ice crystal size distributions in dynamically frozen model solutions and ice cream as affected by stabilizers. *Journal of Dairy Science*, *82*(7), 1399–1407. https://doi.org/10.3168/JDS.S0022-0302(99)75366-X

Flores, A. A., & Goff, H. D. (1999b). Recrystallization in ice cream after constant and cycling temperature storage conditions as affected by stabilizers. *Journal of Dairy Science*, *82*(7), 1408–1415. https://doi.org/10.3168/JDS.S0022-0302(99)75367-1

Gaisford, S. E., Harding, S. E., Mitchellt, J. R., Bradley, T. D., & Mitchell, J. R. (1986). A comparison between the hot and cold water soluble fractions of two locust bean gum samples. *Carbohydrate Polymers*, *6*, 423–442.

Garti, N., & Leser, M. E. (2001). Emulsification properties of hydrocolloids. *Polymer for Advanced Technologies*, *12*, 123–135.

Garti, N., & Reichman, D. (1994). Surface properties and emulsification activity of galactomannans. *Topics in Catalysis*, *8*(2), 155–173. https://doi.org/10.1016/S0268-005X(09)80041-6

Goff, H. D., Ferdinando, D., & Schorsch, C. (1999). Fluorescence microscopy to study galactomannan structure in frozen sucrose and milk protein solutions. *Food Hydrocolloids*, *13*(4), 353–362. https://doi.org/10.1016/S0268-005X(99)00017-X

Goff, H. D., Freslon, B., Sahagian, M. E., Hauber, T. D., Stone, A. P., & Stanley, D. W. (1995a). Structural development in ice cream—dynamic rheological measurements. *Journal of Texture Studies*, *26*(5), 517–536. https://doi.org/10.1111/J.1745-4603.1995.TB00801.X

Goff, H. D., Freslon, B., Sahagian, M. E., Hauber, T. D., Stone, A. P., & Stanley, D. W. (1995b). Structural development in ice cream—dynamic rheological measurements. *Journal of Texture Studies*, *26*(5), 517–536. https://doi.org/10.1111/J.1745-4603.1995.TB00801.X

Goff, H. D., & Hartel, R. W. (2013). *Ice cream* (seventh edition). Springer. https://doi.org/10.1007/978-1-4614-6096-1

Goff, H. D., Kinsella, J. E., & Jordan, W. K. (1989). Influence of various milk protein isolates on ice cream emulsion stability. *Journal of Dairy Science*, *72*(2), 385–397. https://doi.org/10.3168/JDS.S0022-0302(89)79120-7

Goh, K. K. T., Teo, A., Sarkar, A., & Singh, H. (2019). Milk protein-polysaccharide interactions. *Milk Proteins: From Expression to Food*, 499–535. https://doi.org/10.1016/B978-0-12-815251-5.00013-X

Goktas, H., Dikmen, H., Bekiroglu, H., Cebi, N., Dertli, E., & Sagdic, O. (2022). Characteristics of functional ice cream produced with probiotic Saccharomyces boulardii in combination with Lactobacillus rhamnosus GG. *LWT*, *153*, 112489. https://doi.org/10.1016/J.LWT.2021.112489

Hagiwara, T., & Hartel, R. W. (1996). Effect of sweetener, stabilizer, and storage temperature on ice recrystallization in ice cream. *Journal of Dairy Science*, *79*(5), 735–744. https://doi.org/10.3168/JDS.S0022-0302(96)76420-2

Hatakeyama, T., Naoi, S., Iijima, M., & Hatakeyama, H. (2005). Locust bean gum hydrogels formed by freezing and thawing. *Macromolecular Symposia*, *224*, 253–262. https://doi.org/10.1002/MASY.200550622

Hellebois, T., Gaiani, C., & Soukoulis, C. (2022). Freeze − thaw induced structuration of whey protein − alfalfa (Medicago sativa L.) galactomannan binary systems. *Food Hydrocolloids*, *125*, 107389. https://doi.org/10.1016/J.FOODHYD.2021.107389

Huang, J., Zeng, S., Xiong, S., & Huang, Q. (2016). Steady, dynamic, and creep-recovery rheological properties of myofibrillar protein from grass carp muscle. *Food Hydrocolloids*, *61*, 48–56. https://doi.org/10.1016/J.FOODHYD.2016.04.043

Hung, L. S., & Yao, S. C. (2002). Dripping phenomena of water droplets impacted on horizontal wire screens. *International Journal of Multiphase Flow*, *28*(1), 93–104. https://doi.org/10.1016/S0301-9322(01)00061-1

Hwang, J. Y., Shyu, Y. S., & Hsu, C. K. (2009). Grape wine lees improves the rheological and adds antioxidant properties to ice cream. *LWT - Food Science and Technology*, *42*(1), 312–318. https://doi.org/10.1016/J.LWT.2008.03.008

Ian D. Morrison, S. R. (2002). *Colloidal dispersions: suspensions, emulsions, and foams* (S. Ross & I. Morrison, Eds.). Wiley-Interscience.

Innocente, N., Biasutti, M., Venir, E., Spaziani, M., & Marchesini, G. (2009). Effect of high-pressure homogenization on droplet size distribution and rheological properties of ice cream mixes. *Journal of Dairy Science*, *92*(5), 1864–1875. https://doi.org/10.3168/JDS.2008-1797

Inoue, K., Ochi, H., Taketsuka, M., Saito, H., Sakurai, K., Ichihashi, N., Iwatsuki, K., & Kokubo, S. (2008). Modeling of the effect of freezer conditions on the principal constituent parameters of ice cream by using response surface methodology. *Journal of Dairy Science*, *91*(5), 1722–1732. https://doi.org/10.3168/JDS.2007-0796

Iwasaki, K., Uchida, H., Dobashi, Y., & Nishita, T. (2010). Fast particle-based visual simulation of ice melting. *Computer Graphics Forum*, *29*(7), 2215–2223. https://doi.org/10.1111/J.1467-8659.2010.01810.X

Jarpa-Parra, M., Tian, Z., Temelli, F., Zeng, H., & Chen, L. (2016). Understanding the stability mechanisms of lentil legumin-like protein and polysaccharide foams. *Food Hydrocolloids*, *61*, 903–913. https://doi.org/10.1016/J.FOODHYD.2016.07.017

Koxholt, M. M. R., Eisenmann, B., & Hinrichs, J. (2001). Effect of the fat globule sizes on the meltdown of ice cream. *Journal of Dairy Science*, *84*(1), 31–37. https://doi.org/10.3168/JDS.S0022-0302(01)74448-7

Kubbutat, P., & Kulozik, U. (2021). Interactions of sugar alcohol, di-saccharides and polysaccharides with polysorbate 80 as surfactant in the stabilization of foams. *Colloids and Surfaces A: Physicochemical and Engineering Aspects*, *616*, 126349. https://doi.org/10.1016/J.COLSURFA.2021.126349

Kurultay, Ş., Öksüz, Ö., & Gökçebaĝ, Ö. (2010). The Influence of different total solids, stabilizer and overrun levels in industrial ice cream production using coconut oil. *Journal of Food Processing and Preservation*, *34*(SUPPL. 1), 346–354. https://doi.org/10.1111/J.1745-4549.2009.00418.X

Li, Z., Marshall, R., Heymann, H., & Fernando, L. (1997). Effect of milk fat content on flavor perception of vanilla ice cream. *Journal of Dairy Science*, *80*(12), 3133–3141. https://doi.org/10.3168/JDS.S0022-0302(97)76284-2

Liu, X., Sala, G., & Scholten, E. (2022). Effect of fat aggregate size and percentage on the melting properties of ice cream. *Food Research International*, *160*, 111709. https://doi.org/10.1016/J.FOODRES.2022.111709

Livney, Y. D., Donhowe, D. P., & Hartel, R. W. (1995). Influence of temperature on crystallization of lactose in ice-cream. *International Journal of Food Science & Technology*, *30*(3), 311–320. https://doi.org/10.1111/J.1365-2621.1995.TB01380.X

Lobo, L. (2002). Coalescence during emulsification: 3. Effect of gelatin on rupture and coalescence. *Journal of Colloid and Interface Science*, *254*(1), 165–174. https://doi.org/10.1006/JCIS.2002.8561

Lucassen, J., & Van Den Tempel, M. (1972). Dynamic measurements of dilational properties of a liquid interface. *Chemical Engineering Science*, *27*(6), 1283–1291. https://doi.org/10.1016/0009-2509(72)80104-0

Lv, Y., Zhang, X., & Zou, L. (2022). Research progress on the effect of additives on ice slurry. *Heat and Mass Transfer*, *58*(8), 1279–1287. https://doi.org/10.1007/S00231-022-03174-6/METRICS

Masselot, V., Benkhelifa, H., Cuvelier, G., & Bosc, V. (2020). Rheological properties of stabilizers at low temperatures in concentrated sucrose solutions. *Food Hydrocolloids*, *103*. https://doi.org/10.1016/j.foodhyd.2020.105691

McClements, D. J. (2006). Non-covalent interactions between proteins and polysaccharides. *Biotechnology Advances*, *24*(6), 621–625. https://doi.org/10.1016/J.BIOTECHADV.2006.07.003

Méndez-Velasco, C., & Goff, H. D. (2011). Enhancement of fat colloidal interactions for the preparation of ice cream high in unsaturated fat. *International Dairy Journal*, *21*(8), 540–547. https://doi.org/10.1016/J.IDAIRYJ.2011.03.008

Méndez-Velasco, C., & Goff, H. D. (2012). Fat structures as affected by unsaturated or saturated monoglyceride and their effect on ice cream structure, texture and stability. *International Dairy Journal*, *24*(1), 33–39. https://doi.org/10.1016/J.IDAIRYJ.2011.11.009

Miller-Livney, T., & Hartel, R. W. (1997). Ice recrystallization in ice cream: interactions between sweeteners and stabilizers. *Journal of Dairy Science*, *80*(3), 447–456. https://doi.org/10.3168/JDS.S0022-0302(97)75956-3

Muse, M. R., & Hartel, R. W. (2004). Ice cream structural elements that affect melting rate and hardness. In *Journal of Dairy Science*. https://doi.org/10.3168/jds.S0022-0302(04)73135-5

Nickerson, T. A. (1962). Lactose crystallization in ice cream. IV. factors responsible for reduced incidence of sandiness. *Journal of Dairy Science*, *45*(3), 354–359. https://doi.org/10.3168/JDS.S0022-0302(62)89398-9

Patmore, J. V., Goff, H. D., & Fernandes, S. (2003). Cryo-gelation of galactomannans in ice cream model systems. *Food Hydrocolloids*, *17*(2), 161–169. https://doi.org/10.1016/S0268-005X(02)00048-6

Pintor-Jardines, A., Arjona-Román, J. L., Totosaus-Sánchez, A., Severiano-Pérez, P., González-González, L. R., & Escalona-Buendia, H. B. (2018). The influence of agave fructans on thermal properties of low-fat, and low-fat and sugar ice cream. *LWT*, *93*, 679–685. https://doi.org/10.1016/J.LWT.2018.03.060

Pinzer, B. R., Medebach, A., Limbach, H. J., Dubois, C., Stampanoni Bd, M., & Schneebeli, M. (2012). 3D-characterization of three-phase systems using X-ray tomography: tracking the microstructural evolution in ice cream †. *Soft Matter*, *8*, 4584–4594. https://doi.org/10.1039/c2sm00034b

Pronk, P., Hansen, T. M., Ferreira, C. A. I., & Witkamp, G. J. (2005). Time-dependent behavior of different ice slurries during storage. *International Journal of Refrigeration*, *28*(1), 27–36. https://doi.org/10.1016/J.IJREFRIG.2004.07.011

Regand, A., & Goff, H. D. (2002). Effect of biopolymers on structure and ice recrystallization in dynamically frozen ice cream model systems. *Journal of Dairy Science*, *85*(11), 2722–2732. https://doi.org/10.3168/jds.S0022-0302(02)74359-2

Regand, A., & Goff, H. D. (2003). Structure and ice recrystallization in frozen stabilized ice cream model systems. *Food Hydrocolloids*, *17*(1), 95–102. https://doi.org/10.1016/S0268-005X(02)00042-5

Roland, A. M., Phillips, L. G., & Boor, K. J. (1999). Effects of fat content on the sensory properties, melting, color, and hardness of ice cream. *Journal of Dairy Science*, *82*(1), 32–38. https://doi.org/10.3168/JDS.S0022-0302(99)75205-7

Russell, A. B., Cheney, P. E., & Wantling, S. D. (1999). Influence of freezing conditions on ice crystallisation in ice cream. *Journal of Food Engineering*, *39*(2), 179–191. https://doi.org/10.1016/S0260-8774(98)00161-7

Sakurai, K., Kokubo, S., Hakamata, K., Tomita, M., & Yoshida, S. (1996). Effect of production conditions on ice cream melting resistance and hardness. *Milchwissenschaft*.

Schmidt, K. A., & Smith, D. E. (1992). Rheological properties of gum and milk protein interactions. *Journal of Dairy Science*, *75*(1), 36–42. https://doi.org/10.3168/JDS.S0022-0302(92)77735-2

Schmidt, U. S., Schmidt, K., Kurz, T., Endreß, H. U., & Schuchmann, H. P. (2015). Pectins of different origin and their performance in forming and stabilizing oil-in-water-emulsions. *Food Hydrocolloids*, *46*, 59–66. https://doi.org/10.1016/J.FOODHYD.2014.12.012

Schorsch, C., Jones, M. G., & Norton, I. T. (1999). Thermodynamic incompatibility and microstructure of milk protein/locust bean gum/sucrose systems. *Food Hydrocolloids*, *13*(2), 89–99. https://doi.org/10.1016/S0268-005X(98)00074-5

Schorsch, C., Jones, M. G., & Norton, I. T. (2000). Phase behaviour of pure micellar casein/κ-carrageenan systems in milk salt ultrafiltrate. *Food Hydrocolloids*, *14*(4), 347–358. https://doi.org/10.1016/S0268-005X(00)00011-4

Segall, K. I., & Goff, H. D. (1999). Influence of adsorbed milk protein type and surface concentration on the quiescent and shear stability of butteroil emulsions. *International Dairy Journal*, *9*(10), 683–691. https://doi.org/10.1016/S0958-6946(99)00143-0

Sharqawy, M. H., & Goff, H. D. (2022). Effect of temperature variation on ice cream recrystallization during freezer defrost cycles. *Journal of Food Engineering*, *335*. https://doi.org/10.1016/J.JFOODENG.2022.111188

Silva, E. da, Silva, E. R. T. da, Muramatsu, M., & Lannes, S. C. da S. (2010). Transient process in ice creams evaluated by laser speckles. *Food Research International*, *43*(5), 1470–1475. https://doi.org/10.1016/J.FOODRES.2010.04.017

Smith, A. K., Goff, H. D., & Kakuda, Y. (2000). Microstructure and rheological properties of whipped cream as affected by heat treatment and addition of stabilizer. *International Dairy Journal*, *10*(4), 295–301. https://doi.org/10.1016/S0958-6946(00)00043-1

Snoeren, T. H. M., Damman, A. J., & Klok, H. J. (1981). The viscosity of skim-milk concentrate. *Zuivelzicht (Netherlands)*, *73*(42), 887–889. https://doi.org/10.3/JQUERY-UI.JS

Sofjan, R. P., & Hartel, R. W. (2004). Effects of overrun on structural and physical characteristics of ice cream. *International Dairy Journal*. https://doi.org/10.1016/j.idairyj.2003.08.005

Spagnuolo, P. A., Dalgleish, D. G., Goff, H. D., & Morris, E. R. (2005). Kappa-carrageenan interactions in systems containing casein micelles and polysaccharide stabilizers. *Food Hydrocolloids*, *19*(3), 371–377. https://doi.org/10.1016/J.FOODHYD.2004.10.003

Stanley, D. W., Goff, H. D., & Smith, A. K. (1996). Texture-structure relationships in foamed dairy emulsions. *Food Research International*, *29*(1). https://doi.org/10.1016/0963-9969(95)00063-1

Steffe, J. Freeman. (1996). *Rheological methods in food process engineering* (2nd ed.). Freeman Press.

Sung, K. K., & Goff, H. D. (2010). Effect of solid fat content on structure in ice creams containing palm kernel oil and high-oleic sunflower oil. *Journal of Food Science*, *75*(3). https://doi.org/10.1111/J.1750-3841.2010.01539.X

Syrbe, A., Bauer, W. J., & Klostermeyer, H. (1998). Polymer science concepts in dairy systems—an overview of milk protein and food hydrocolloid interaction. *International Dairy Journal*, *8*(3), 179–193. https://doi.org/10.1016/S0958-6946(98)00041-7

Tanaka, R., Hatakeyama, T., & Hatakeyama, H. (1998). Interaction between polymer molecules in locust bean gum-water systems during cooling and freezing process. In *Gums and Stabilisers for the Food Industry 9* (pp. 43–47). Woodhead Publishing. https://doi.org/10.1533/9781845698362.1.43

Tanaka, R., Hatakeyama2, T., & Hatakeyama3, H. (1998). Formation of locust bean gum hydrogel by freezing-thawing. *Polymer International*, *45*, 118–126. https://doi.org/10.1002/(SICI)1097-0126(199801)45:1

Tharp, B. W., Forrest, B., Swan, C., Dunning, L., & Hilmoe, M. (1997). Basic factors affecting ice cream meltdown. *International Dairy Federation Symposium on Ice Cream*.

Thiel, A. E., Hartel, R. W., Spicer, P. T., & Hendrickson, K. J. (2016). Coalescence behavior of pure and natural fat droplets characterized via micromanipulation. *JAOCS, Journal of the American Oil Chemists' Society*, *93*(11), 1467–1477. https://doi.org/10.1007/S11746-016-2896-4/FIGURES/8

Trgo, C., Koxholt, M., & Kessler, H. G. (1999). Effect of freezing point and texture regulating parameters on the initial ice crystal growth in ice cream. *Journal of Dairy Science*, *82*(3), 460–465. https://doi.org/10.3168/JDS.S0022-0302(99)75254-9

Tuinier, R., & Kruif, C. G. de. (1999). Phase behavior of casein micelles/exocellular polysaccharide mixtures: Experiment and theory. *The Journal of Chemical Physics*, *110*(18), 9296. https://doi.org/10.1063/1.478851

van Boekel, M. A. J. S., & Walstra, P. (1981). Stability of oil-in-water emulsions with crystals in the disperse phase. *Colloids and Surfaces*, *3*(2), 109–118. https://doi.org/10.1016/0166-6622(81)80071-6

VanWees, S. R., Rankin, S. A., & Hartel, R. W. (2020). The microstructural, melting, rheological, and sensorial properties of high-overrun frozen desserts. *Journal of Texture Studies*, *51*(1), 92–100. https://doi.org/10.1111/JTXS.12461

VanWees, S. R., Rankin, S. A., & Hartel, R. W. (2022). Shrinkage in frozen desserts. *Comprehensive Reviews in Food Science and Food Safety*, *21*(1), 780–808. https://doi.org/10.1111/1541-4337.12888

Wan, Z., Yang, X., & Sagis, L. M. C. (2016). *Nonlinear surface dilatational rheology and foaming behavior of protein and protein fibrillar aggregates in the presence of natural surfactant*. https://doi.org/10.1021/acs.langmuir.6b00446

Warren, M. M. (2015). *Understanding melt behavior of ice cream: influence of the microstructure and composition on drip-through rate of ice cream products*. University of Wisconsin-Madison.

Warren, M. M., & Hartel, R. W. (2014). Structural, compositional, and sensorial properties of United States commercial ice cream products. *Journal of Food Science*. https://doi.org/10.1111/1750-3841.12592

Warren, M. M., & Hartel, R. W. (2018). Effects of emulsifier, overrun and dasher speed on ice cream microstructure and melting properties. *Journal of Food Science*. https://doi.org/10.1111/1750-3841.13983

Wildmoser, H., Scheiwiller, J., & Windhab, E. J. (2004). Impact of disperse microstructure on rheology and quality aspects of ice cream. *LWT*, *37*(8), 881–891. https://doi.org/10.1016/J.LWT.2004.04.006

Williams, P. A., & Phillips, G. O. (2009). Handbook of hydrocolloids. In *Handbook of Hydrocolloids: Second Edition* (Second edition). Woodhead Publishing. https://doi.org/10.1533/9781845695873.1

Wu, Y., Cui, W., Eskin, N. A. M., & Goff, H. D. (2009). An investigation of four commercial galactomannans on their emulsion and rheological properties. *Food Research International*, *42*(8), 1141–1146. https://doi.org/10.1016/J.FOODRES.2009.05.015

Yadav, M. P., Manuel Igartuburu, J., Yan, Y., & Nothnagel, E. A. (2007). Chemical investigation of the structural basis of the emulsifying activity of gum arabic. *Food Hydrocolloids*, *21*(2), 297–308. https://doi.org/10.1016/J.FOODHYD.2006.05.001

Yan, L., Yu, D., Liu, R., Jia, Y., Zhang, M., Wu, T., & Sui, W. (2021). Microstructure and meltdown properties of low-fat ice cream: Effects of microparticulated soy protein hydrolysate/xanthan gum (MSPH/XG) ratio and freezing time. *Journal of Food Engineering*, *291*, 110291. https://doi.org/10.1016/J.JFOODENG.2020.110291

Yang, J., Waardenburg, L. C., Berton-Carabin, C. C., Nikiforidis, C. V., van der Linden, E., & Sagis, L. M. C. (2021). Air-water interfacial behaviour of whey protein and rapeseed oleosome mixtures. *Journal of Colloid and Interface Science*, *602*, 207–221. https://doi.org/10.1016/J.JCIS.2021.05.172

Zhang, Z., & Goff, H. D. (2005). On fat destabilization and composition of the air interface in ice cream containing saturated and unsaturated monoglyceride. *International Dairy Journal*, *15*, 495–500. https://doi.org/10.1016/j.idairyj.2004.08.014

Zhao, X. Z., Zhao, J., Ge, M. G., An, Q. S., Wang, F. B., & Gao, L. H. (2014). Control of ice crystal growth by different surfactants in ice slurries. *Applied Mechanics and Materials*, *694*, 193–199. https://doi.org/10.4028/WWW.SCIENTIFIC.NET/AMM.694.193